Studies of final state photon radiation at LEP

Morgan, Andrew Gordon

Studies of Final State Photon Radiation at LEP

Andrew Gordon Morgan
Department of Physics
University of Durham

A thesis submitted to the University of Durham
for the degree of Doctor of Philosophy
July 1994

This thesis is dedicated to my family,

to Mum, Dad, Paul

and Kelly.

I declare that the material presented in this thesis has not been submitted for a degree at this or any other university.

Much of the work in this thesis has been carried out in collaboration with Dr. E.W.N. Glover and Dr. Z. Bern, and has largely appeared in the following publications:

- E.W.N. Glover and A.G. Morgan, "Z boson decay into photons", Z. Phys. **C60** (1993) 175;
- E.W.N. Glover and A.G. Morgan, "Measuring the photon fragmentation function at LEP", Z. Phys. **C62** (1994) 311;
- Z. Bern and A.G. Morgan, "Supersymmetry relations between contributions to one loop gauge boson amplitudes", Phys. Rev. **D49** (1994) 6155;
- E.W.N. Glover and A.G. Morgan, "Soft gluon radiation in photon plus single jet events at LEP", Phys. Lett. **B324** (1994) 487;
- E.W.N. Glover and A.G. Morgan, "The Photon + 1 jet event rate with the cone algorithm in hadronic events at LEP", DTP-94-40 *to appear in* Phys. Lett. **B**.

Acknowledgments

Firstly and above all, I would like to thank Nigel Glover for his excellent supervision, encouragement and collaboration.

I offer my sincerest thanks to Zvi Bern of UCLA. Further I should like to acknowledge the kind hospitality of the UCLA Physics Department where much of Chapter 10 was completed.

To Mark Oakden and Matthew Reader I would like to say thanks for being stable and friendly office mates, good luck to you both!

I am grateful to Adrian Askew, David Barclay and David Summers for many stimulating insights and much useful discussion. To Ghadir Abu-Leil, Francisco Astorga-Saenz, Adnan Bashir, Jacques Bloch, Kirsten Buttner, Duncan Curtis, Aude De Ridder, Thomas Gehrmann, Ayse Kizilersu, Foster Langbein, Charles Lovett-Turner, David Miller, Ramon Munoz-Tapia, Jim Ohnemus, Jorge Portoles, Neil Shaban, Tim Stelzer, Peter Sutton, Bas Tausk and all the rest, my thanks for providing a great departmental atmosphere.

I would very much like to thank the following: John Thompson, Vincent Bertin, Mike Smith and Stan Thompson for much stimulating discussion concerning the ALEPH data; Jochum van der Bij for some useful discussion concerning Chapter 8; and Valery Khoze for clarifying several issues connected with soft gluon radiation patterns.

To the Particle Physics group of Durham University, Peter Collins, Alan Martin, Chris Maxwell, Mike Pennington and James Stirling, many thanks for giving me the opportunity to pursue a Ph.D. and providing such good facilities. I thank Mike Whalley for the many laughs we shared in keeping the computers up—good luck for the future!

I thank SERC/PPARC for the award of a research studentship.

Finally, I would like to thank Kelly Glover. Not least for her help in the preparation of this thesis (I never realised there was so much to a comma!) but mostly for her friendship.

Andrew Gordon Morgan

A thesis submitted to the University of Durham
for the degree of Doctor of Philosophy
July 1994

Studies of Final State Photon Radiation at LEP

Abstract

We consider two aspects of calculations involving the production of final state photons at LEP. The first addresses photons produced in association with hadrons. We motivate a measurement of the quark to photon fragmentation function and show how it can be used to account for isolated and non-isolated production rates. The second concerns the rare Z-decay to photons. We expose a subtle relationship between its various contributions. Following its investigation, we offer an improved method of calculation for weak processes at one loop.

Contents

Poets say science takes away from the beauty of the stars—mere globs of gas atoms.

I too can see the stars on a desert night, and feel them. But do I see less or more? The vastness of the heavens stretches my imagination—stuck on this carousel my little eye can catch million year old light. A vast pattern—of which I am a part... What is this pattern, or the meaning, or the *why*? It does not do harm to the mystery to know a little about it. For far more marvelous is the truth than any artists of the past imagined it. Why do the poets of the present not speak of it? What men are poets who can speak of Jupiter if he were a man, but if he is an immense spinning sphere of methane and ammonia must be silent?

—Richard P. Feynman. [1]

Chapter 1

Introduction

1.1 High energy physics

High energy physics is a study of high energy and small length scales. It is naturally an extreme where the theories of Special Relativity and Quantum Mechanics are paramount. A scale of distance and momentum at which *observation* and *interaction* are unified and inseparable.

All of the quantities given in this thesis, other than those in this chapter are given in the units that $\hbar = c = 1$, where $\hbar$ is the Plank Constant and c is the speed of light. These constants with dimensions of [Energy $\times$ Time] and [Length/Time] directly relate three dimensionful quantities. As a consequence we need only discuss dimensionful quantities in terms of one dimensionful scale. We shall usually do so in terms of an energy.

Within the scheme of these natural units the reciprocal relationship between length and energy is quite clear. The Compton wavelength for a particle,

$$\lambda = \frac{\hbar}{p} \tag{1.1}$$

defines the approximate length scale for a particle traveling with a momentum, p. This length defines the distance at which the particle can resolve structure with which to interact. As we raise the momentum so we shorten the length scale. A convenient terrestrial example of this inverse relation is the observation that radio waves ($\lambda \sim 100$m) are well reflected by wire netting, for which the spacing is $\sim$ 1cm. Such material is used in the construction of radio receiving dishes. Wire netting is, however, very poor at preventing the passage of shorter wavelength light—we can see through it!

By colliding particles whose relative momentum is very high (λ very small) we can examine their small scale structure. Probing with energies of a few keV using electron microscopes, we can resolve molecular structure. With electrons of MeV energies we can resolve the nuclear constituents of atoms. At the level of a few GeV we can see deeper into the sub-structure of individual nucleons. At this level a simple picture of elementary particles emerges, of spin-1/2 fermions: leptons; quarks; and neutrinos. The various interactions of these particles are mediated by spin-1 gauge bosons: the photon; gluon, $W^{\pm}$ and the Z.

This thesis documents a theoretical study centred around photons emitted in the final state at the Large Electron-Positron collider (LEP). This experiment is designed to collide electron and positron (anti-electron) beams at a centre of mass energy of around the rest-mass of the Z-boson, $\sim$ 91 GeV, per collision. In such collisions electrons and positrons annihilate and frequently their energy finds a form in the creation of a Z-boson. After but a small moment of time ($\sim 10^{-24}$ sec.), this unstable particle decays via the production of elementary particles. In the original work of this thesis we account for $\sim$ .05% of these

Z-decays, which currently corresponds to ~ 500 events.

1.2 An outline

The original work of this thesis is contained in the six chapters, 5 to 10, and can be neatly divided into two discrete studies. The former, is a phenomenological attempt at parameterising the collinear emission of photon radiation from quarks. The latter, a more formal study of the internal field symmetries of perturbative calculations which is motivated by the discovery of a simple relation between the fermionic and bosonic contributions to a *rare* Z-decay.

Phenomenologically, the former is more interesting as it represents an *observable* signal, but the latter has its own importance in exploring the more subtle aspects of perturbative calculation.

The order of presentation is as follows. In Chapter 2, we review the framework of Quantum Field Theory—the underlying tool of calculation for high energy physics. In Chapter 3, we introduce the *Standard Model of Particle Physics* which is currently the most popular theoretical model for elementary particle interaction. Chapter 4, contains a simple review of the relevant phenomenology at LEP that is assumed throughout the rest of the thesis.

In Chapter 5, we highlight the difficulties of the straightforward perturbative calculation of *collinear photon* emission in hadronic events at LEP and motivate a method of parameterising our *ignorance* of this problematic region. As a footnote to this chapter we review the measurement, made by the ALEPH collaboration, of the proposed *photon fragmentation function.* In Chapter 6, we discuss *isolated* photon emission in association with hadrons and

account for the apparently large variation in *radiative corrections* to the various definitions for photon isolation. In Chapter 7, we again discuss *isolated* photon production and use the ALEPH measurement of the *fragmentation function* to account for a previously measured rate.

With Chapter 8 we address the second theme of this thesis. Prompted by an apparent disagreement in the literature, we calculate the rate of decay of the Z-boson to three photons. In so doing we notice a curious similarity in the fermionic and bosonic contributions to the amplitudes. In Chapter 9, we introduce a novel technique for the calculation of fermionic internal loops in amplitudes; the *2nd Order Formalism.* Using this and the *Background Field Method* in Chapter 10, we once again perform the above calculation but this time *use* the internal *super*-symmetry present in such a calculation to optimise it. This symmetry is more apparent with the set of more *optimal* Feynman rules.

In Chapter 11 we summarise our main results and discuss some future applications.

The appendices listed at the end of the thesis contain many useful formulae and outline the methods used in the calculations of the main text. Appendix A contains the definitions for a number of special functions and some of their relevant identities. Appendix B reviews the relevant formalism for evaluating general loop integrals. Appendix C contains derivations for various phase space integrals in both $4-$ and $d-$dimensions. Appendix D contains a number of scalar loop integrals in integer and non-integer dimensions used in the text. Appendix E is a brief review of the Dirac equation and lists some useful identities for γ matrices. Appendix F covers the structure of $SU(n)$ groups.

1.3 Some definitions

The fine structure constant, α, as referred to throughout this thesis is the dimensionless constant defined,

$$\alpha = \frac{e^2}{4\pi}\frac{1}{\epsilon_0 \hbar c} \approx \frac{1}{137} \tag{1.2}$$

where, '$-e$' is the *natural* unit of charge as carried by the electron, and ϵ_0 is the permittivity of free space.

Throughout this thesis we refer to the metric, for this we mean the *flat* Minkowski metric of signature $(+,-,-,-)$.

Chapter 2

A Review of Quantum Field Theory

Quantum Field Theory (QFT) [2] is a generalisation of Quantum Mechanics (QM) [3] that includes, in a manner consistent with Special Relativity, the creation and annihilation of particles: the number of particles present in a state becomes just another quantum number.

In QM, we have the universal operator $\hat{x}$ that projects out the spatial position/distribution of a quantum state $|\psi\rangle$. QFT requires instead that we have separate position (density) operators for each species (*flavour*) of particle. Indeed we *construct* such operators from more fundamental *field* operators. In QM, the Hamiltonian (or equivalently the Lagrangian) is built from generalised position and momentum operators. In QFT, we construct Hamiltonian and Lagrangian (densities) from these elementary field operators. Individual terms in these densities give rise to the particle interactions and calculable transitions; not just in the exchange of energy but also of flavour.

Rather than addressing the evolution of initial states with respect to a prescribed Hamil-

tonian, it is the formulation of QM as hinted at by Dirac [4] and expanded by Feynman [5] that QFT has adopted. Namely an emphasis on the computation of transition amplitudes from some initial state (i) to a final state (f) by summing over *all possible* paths that one can construct between them. Each path is weighted according to how much energy is manipulated *in flight* (how great the Classical Action [6] would be for such a trajectory). Within the framework of QFT this corresponds to the sum over all spatial, and particle flavour, routes linking (i) and (f). These routes are merely constrained to lie along paths allowed by the Lagrangian (density) of the theory, and again are weighted by the size of the associated action.

The fields that build the Lagrangian density are of two types: *bosons* and *fermions*. The distinction between them being whether they permit more than one physical state to have identical quantum numbers (as is the case for bosons) or not (for fermions). In terms of the field operators, *bosonic* fields, $\hat{B}(x)$, are said to commute,

$$\left[\hat{B}(x), \hat{B}(y)\right] = \hat{B}(x)\hat{B}(y) - \hat{B}(y)\hat{B}(x) = 0 \tag{2.1}$$

and *fermionic* fields, $\hat{F}(x)$, are said to *anti-commute*,

$$\left\{\hat{F}(x), \hat{F}(y)\right\} = \hat{F}(x)\hat{F}(y) + \hat{F}(y)\hat{F}(x) = 0. \tag{2.2}$$

High Energy Theory in its phenomenological aspect finds its focus in the calculation of the S-matrix. This object is a Quantum Mechanical operator, $\hat{S}$, that operates on asymptotically free states (at a time well *before* any interaction) to project out each of its destinies (at a time well *after* any interaction). $\hat{S}$ is a unitary hermitian operator defined to satisfy,

$$\hat{S}|\mathrm{i}, t \to -\infty\rangle = \sum_{\mathrm{f}} s_{\mathrm{f}} |\mathrm{f}, \mathrm{t} \to \infty\rangle \tag{2.3}$$

where $\sum_f |s_f|^2 = 1$. As one might imagine the final state is often unchanged with respect to the initial state, so interest in $\hat{S}$ is especially focused on it's *transition* component, $\hat{T}$ defined by,

$$\hat{S} = 1 + i\hat{T}. \tag{2.4}$$

This simple rewriting has a very significant consequence that comes from the fact that $\hat{S}$ is required to be hermitian and unitary, namely,

$$\hat{S}^\dagger \hat{S} = 1 = 1 + i(\hat{T} - \hat{T}^\dagger) + \hat{T}^\dagger \hat{T} \tag{2.5}$$

or equivalently,

$$\hat{T}^\dagger \hat{T} = 2\ \mathrm{Im}(\hat{T}) \tag{2.6}$$

—a result that is fundamental to S-matrix theory and we shall return to an example of its consequences in Chapter 4.

2.1 Path integral quantisation and a representation for $\hat{S}$

The Path Integral approach to QFT builds on the Feynman formulation of Quantum Mechanics to include the notion of a field. His approach was to directly calculate transition amplitudes. The simplest of such objects is the *vacuum to vacuum* transition amplitude, $\langle 0, +\infty | 0, -\infty \rangle$. That is to say, the probability amplitude that the vacuum in the distant past will become the vacuum in the distant future. It seems quite reasonable to postulate that this occurs with probability 1, so we proceed by defining the arbitrary phase and set the *amplitude* to 1.

In the presence of an external source field, $\hat{J}$, this transition probability is not necessarily unity, so we define it to be,

$$Z[J] = \langle 0, +\infty | 0, -\infty \rangle^J = \frac{\int \mathcal{D}\phi \exp i \int d^4x \left(\mathcal{L}(\phi) + \phi J + \frac{i}{2}\phi^2 \epsilon \right)}{\int \mathcal{D}\phi \exp i \int d^4x \left(\mathcal{L}(\phi) + \frac{i}{2}\phi^2 \epsilon \right)} \tag{2.7}$$

which clearly satisfies $Z[0] = 1$. We are using a somewhat general notation where ϕ represents the set of fields in our field theory, and J a set of sources; one for each ϕ. The ϕ and J given here are *not* operator fields but rather what are termed classical (or *c-number*) fields; for each path of integration $|\phi, x\rangle$ as summed over with $\mathcal{D}\phi$ the $\phi(x)$ is really the expectation value of that field operator at the space-time point of integration x. For bosonic fields Eqn. (2.1) the *c-numbers* are simple commuting scalars, but for fermionic fields Eqn. (2.2) the *c-numbers* are anti-commuting scalars—elements of a Grassman algebra.

Eqn. (2.7) is inherently difficult to solve for an arbitrary Lagrangian density, $\mathcal{L}(\phi)$. However, it is in fact straight-forward in the simpler cases of *free* theories having no interactions (where $\hat{S} \equiv 1$). Writing $\mathcal{L} = \mathcal{L}_0 = -1/2\ \phi K_\phi \phi$, where K_ϕ is some differential operator acting on ϕ. The associated vacuum expectation value in the presence of a source is,

$$Z_0[J] = \exp\left(-\frac{i}{2} \int d^4x\ d^4y J(x) \Delta_\phi(x-y) J(y) \right) \tag{2.8}$$

here Δ_ϕ is the 2 point Green's function satisfying, $K_\phi \Delta_\phi(x-y) = -\delta^4(x-y)$. Using this result we can partially solve for $Z[J]$, where $\mathcal{L} = \mathcal{L}_0 + \mathcal{L}_{INT}$ to give,

$$Z[J] = \frac{\exp\left(i \int d^4x \mathcal{L}_{INT}\left(\frac{\delta}{i\delta J(x)} \right) \right) Z_0[J]}{\exp\left(i \int d^4x \mathcal{L}_{INT}\left(\frac{\delta}{i\delta J(x)} \right) \right) Z_0[J]\Big|_{J=0}}. \tag{2.9}$$

By expressing $Z[J]$ as a series expansion in J, it is seen to generate the n-point Green's

functions of the theory, i.e.

$$G^{(n)}(x_1,\ldots x_n) = \langle 0|\phi(x_1)\ldots\phi(x_n)|0\rangle = \frac{\delta^n}{i^n\delta J(x_1)\ldots\delta J(x_n)}Z[J]\bigg|_{J=0}. \tag{2.10}$$

Equivalently, we can define the *fourier transformed* Green's functions,

$$G^{(n)}(p_1,\ldots p_n) = \int\left(\prod_{i=1}^{n} d^4x_i\right) G^{(n)}(x_1,\ldots x_n)\exp i\sum_{j=1}^{n} p_j\cdot x_j. \tag{2.11}$$

For a completely self contained theory, $G_c^{(n)}(x_1,\ldots x_n)$ is translation invariant—it remains unchanged after the transformation $x_i \to x_i+\delta x$. As a consequence from the fourier integral given here we require that $\sum_i p_i\cdot\delta x = 0$, or that 4-momentum is conserved. Accordingly, $G^{(n)}(p_1,\ldots p_n)$ contains an implicit $(2\pi)^4\delta^4(\sum_i p_i^\mu)$ factor.

The fields, $\hat{\phi}$ also have fourier transformations. Writing the inverse of the above transformation to obtain $\hat{\phi}$ from its momentum space fields we have,

$$\hat{\phi}(x) = \int\frac{d^4k}{(2\pi)^4}\sum_\lambda e^{-ik\cdot x}\hat{a}_\phi^{(\lambda)}(k)f_\phi^{(\lambda)}(k). \tag{2.12}$$

Here $\hat{a}_\phi^{(\lambda)}(k)$ is an annihilation operator and $f_\phi^{(\lambda)}(k)$ a representation of the field's polarisation.

In order to avoid the existence of *negative energy* particle states, the $k^0 < 0$ contributions to $\hat{a}_\phi^{(\lambda)}(k)$ are taken to be *creation operators* for an anti-particle state of polarisation, $g_\phi^{(\lambda)}(-k) = f_\phi^{(\lambda)}(k)$, and conventionally we write,

$$\begin{aligned}\hat{\phi}(x) &= \int\frac{d^4k}{(2\pi)^4}\theta(k^0)\sum_\lambda\left\{e^{-ik\cdot x}\hat{a}_\phi^{(\lambda)}(k)f_\phi^{(\lambda)}(k) + e^{ik\cdot x}\hat{b}_\phi^{(\lambda)\dagger}(k)g_\phi^{(\lambda)}(k)\right\} &(2.13)\\ &= \hat{\phi}_+(x)+\hat{\phi}_-(x). &(2.14)\end{aligned}$$

It is the operators, $\hat{a}_\phi^{(\lambda)}$ and $\hat{b}_\phi^{(\lambda)}$, that carry the Bosonic (or Fermionic) nature of the fields,

i.e. they satisfy the (anti)commutation relations. They are defined such that they annihilate the vacuum,

$$\hat{a}_{\phi}^{(\lambda)} |0\rangle = 0 = \hat{b}_{\phi}^{(\lambda)} |0\rangle . \tag{2.15}$$

In the simple case of *hermitian* fields, $\hat{\phi}_i^{\dagger}(x) = \hat{\phi}_i(x)$, we see that $\hat{a}_{\phi,i}^{(\lambda)}(k) = \hat{b}_{\phi,i}^{(\lambda)}(k)$ and $f_{\phi,i}^{(\lambda)}(k) = g_{\phi,i}^{(\lambda)\dagger}(k)$.

These $G^{(n)}$ functions correspond to general amplitudes *connecting* unphysical states (i.e. they can be off mass-shell; their invariant mass is not equal to their rest mass) via interactions of the theory. By removing (*amputating*) the external propagators, placing the external states *on mass-shell* and attaching external (or asymptotically free—i.e. obeying the dynamics of the *free* lagrangian) field operators, $\hat{\phi}_{\rm in}$, we obtain the physical scattering matrix:

$$\hat{S} = \ : \left\{ \exp \int \hat{\phi}_{\rm in} K_{\phi} \frac{\delta}{\delta J(x)} \right\} : Z[J] \Big|_{J=0} . \tag{2.16}$$

The colons : ... : impose *normal ordering*, namely that the expansion of the operators contained within the colons, is performed such that their annihilation components act *before* their creation components. The term in the exponential generalises to the sum of such terms—one for each physical field of the Lagrangian density. We note that when the exponential is expanded the $1/n!$ factor neatly removes the potential over counting due to the $n!$ identical terms generated by $\delta^n/\delta J^n$.

2.2 Feynman diagrams and rules

A simplified method of calculation is arrived at through the use of *Feynman Diagrams*. These are a pictorial representation of the expansion of the exponential in Eqn. (2.9). Namely, the

coefficient of each term in $\mathcal{L}_{INT}$ is ascribed to a vertex and each factor of Δ_ϕ corresponds to a line (or *propagator*). The action of $\delta/i\delta J$ on $Z_0[J]$ gives rise to such a line truncated by a source field, J.

The essence of the simplification is that each Green's function is associated with a series of diagrams, the form of which can be readily determined. Taking each diagram in turn and using the *rules* for vertices and propagators, one can reconstruct the *mathematical* form of the Green's function. Over the laborious manipulation of Eqn. (2.9) the diagrams have an *intuitive* appeal that aids in their construction.

Indeed, in the everyday work of high energy physics it is diagrams and optimised versions of the rules that are used for calculation.

2.3 Building blocks of the S-matrix

Clearly Eqn. (2.16) includes the *no scattering* processes; the 1 of Eqn. (2.4). The interesting physics is associated with the transition part of $\hat{S}$. Of the remainder of the S-matrix there are two classes of contribution: those processes where all of the external states contribute to a single extended interaction; and those where two or more subsets of the external states are involved in simultaneous but factorisably independent interactions. In the former situation, the corresponding Green's functions are such that their (Feynman) diagrams have all lines connected. These functions are generated from the functional,

$$W[J] = -i \log Z[J]. \tag{2.17}$$

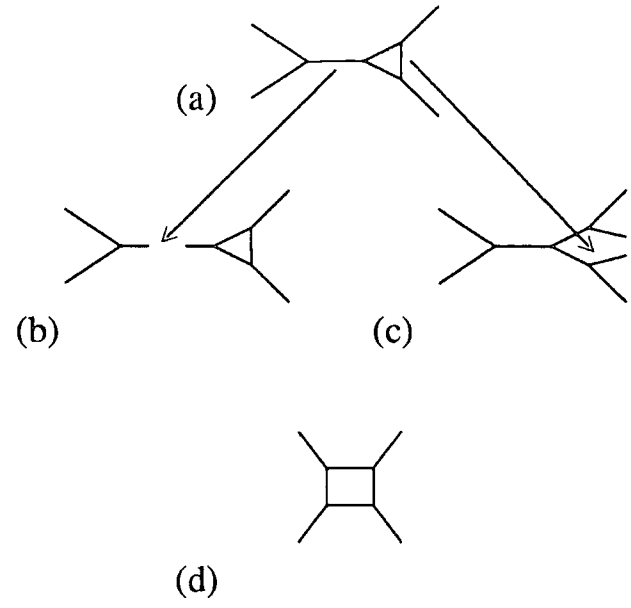

Figure 2.1: Diagrams representing the disection of a term from an n-point connected Green's function. (a) is the example Green's function term (in this case from a 4-point function of a "ϕ^3" theory), (b) cutting a line that breaks the diagram into *two* $m(\leq n)$-point diagrams, and (c) cutting an internal line that produces an $(n+2)$-point diagram. (d) is an example of a *one-particle-irreducible* contribution to the $n(=4)$-point connected Green's function.

They are named *connected* (or *irreducible*) Green's functions,

$$G_c^{(n)}(x_1, \ldots x_n) = \frac{\delta^n}{i^n \delta J(x_1) \ldots J(x_n)} W[J]\Big|_{J=0} . \tag{2.18}$$

In the latter case of factorisable sub-processes, the contribution to $\hat{S}$ is from *products* of lower point connected Green's functions.

A connected n-point Green's function can be represented diagrammatically by an infinite sum of diagrams each having n external lines (*legs*) and some number of internal lines. Consider one such diagram (see Figure 2.1a). We now notice the effects of *cutting* one internal line of this figure. Clearly in doing this we will either create a diagram of two separate $m(\leq n)$-point diagrams (Figure 2.1b) or create a single $(n+2)$-point diagram

(Figure 2.1c). It follows that amongst the infinite sum of diagrams (in other words *terms* in Eqn. (2.17)) associated with the connected n-point Green's function, there exist a sub-set of terms that *only* have the property associated with the cut of Figure 2.1c. For example that of Figure 2.1d. We note that since Figure 2.1a can be cut in both ways it will not itself be a member of this sub-set. The sum of such a sub-set is labeled the *one-particle-irreducible* n-point Green's function, $G^{(n)}_{1PI}$.

2.4 The Effective Action, $\Gamma[\phi]$

The connected Green's functions describe the interactions of the theory. We have shown that there is a more fundamental subset of these functions, namely the *one-particle-irreducible* functions $G^{(n)}_{1PI}$. It transpires that we can construct the connected functions from just the two-point connected function ($G^{(2)}_c$) and truncated $G^{(n)}_{1PI}$s, the so called *vertex functions*, $\Gamma^{(n)}(x_1, \ldots x_n)$. In other words the sum of all Feynman diagrams leading to a given $G^{(n)}_c$ can be built from trees of *vertices*, $\Gamma^{(n)}$, held together by $G^{(2)}_c$ propagators. To define the vertex functions we must reintroduce some representation of the field, since we have previously integrated it out (see Eqns. (2.10 and 2.18)). We define,

$$\phi(x, J) = \frac{\delta W[J]}{i\delta J(x)} \tag{2.19}$$

where we assume that this is invertible leading to $J(x, \phi)$ and we also note that for vanishing $G^{(1)}_c$, $J = 0 \Leftrightarrow \phi = 0$. In some sense this $\phi(x, J)$ is a generalisation of what is *removed* by the exponent in Eqn. (2.16) before it attaches an external field operator. Next we introduce

the *effective action*,

$$\Gamma[\phi] = -iW[J] - \int d^4x J(x)\phi(x) = -\log Z[J] - \int d^4x J(x)\phi(x). \tag{2.20}$$

which immediately leads to the relation,

$$J(x,\phi) = -\frac{\delta\Gamma[\phi]}{\delta\phi(x)}. \tag{2.21}$$

$\Gamma[\phi]$ is the generating functional for the so called vertex functions,

$$\Gamma^{(n)}(x_1,\ldots x_n) = \left.\frac{\delta^n\Gamma[\phi]}{\delta\phi(x_1)\ldots\delta\phi(x_n)}\right|_{\phi=0}. \tag{2.22}$$

By functionally differentiating Eqn. (2.19) once with respect to ϕ and taking the limit $\phi = J = 0$ we obtain the relation that,

$$\int d^4z \Gamma^{(2)}(y,z)G_c^{(2)}(z,x) = i\delta^4(x-y) \tag{2.23}$$

which in the *free* field theory, $G_0^{(2)} = G_c^{(2)} = i\Delta_\phi$ (see the paragraph containing Eqn. (2.8)), corresponds to $\Gamma^{(2)} = -K_\phi$.

Further differentiation of Eqn. (2.19) and the use of Eqn. (2.23) is seen to generate a relation between $G_c^{(n)}$ and a series of tree like structures having $\Gamma^{(m)}$ for each m-point vertex and a $G_c^{(2)}$ propagator linking them; Figure 2.2 illustrates this point. Note, that there are *no* explicit loops in such structures because that would over count contributions to the vertices.

$\Gamma[\phi]$ is termed the *effective action* because it is, in the interacting theory, a generalisation of the *action*, $S = \int d^4x\mathcal{L}$. As was indicated, in the free theory, $\Gamma_0^{(2)}$ (and correspondingly the simplest contribution to $\Gamma^{(2)}$ in the full interacting theory), is $\delta^2 S/\delta\phi^2$. Similarly, the simplest contributions to the higher point $\Gamma^{(n\geq 2)}$ vertices are terms of order ϕ^n in the coefficient of

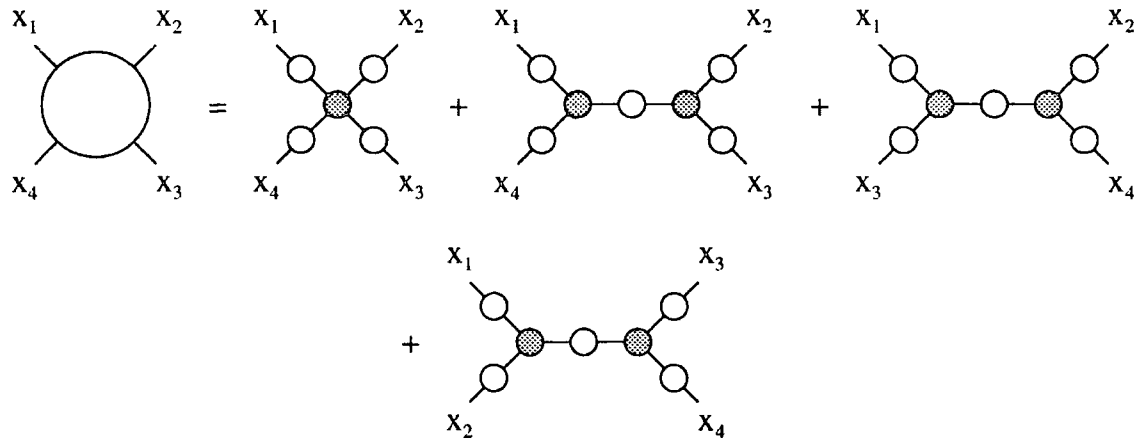

Figure 2.2: The 4−point connected Green's function, $G_c^{(4)}$, expanded in terms of the $n(\leq 4)$−point vertex functions, $\Gamma^{(n)}$ (shaded circles), and the full propagator, $G_c^{(2)}$ (empty circles).

the associated term in the $\mathcal{L}_{INT}$ part of the Lagrangian density. For example, the $\lambda\phi^3/3!$ term in the Lagrangian of a "ϕ^3" theory gives rise to a leading $\Gamma^{(3)}$ contribution of λ.

It is clear that vertices not present in the basic Lagrangian may come about at *higher orders* (i.e. as connected Green's functions containing at least one closed loop) and such a process is discussed in the latter chapters of this thesis.

We conclude this section with a description of the *full propagator*, $G_c^{(2)}(x_1, x_2)$. Following the discussion after Eqn. (2.10) we shall discuss the momentum space forms of $G_c^{(2)}$ etc. i.e. via Eqn. (2.11) we write $f(x_1, x_2) \rightarrow f(p_1, p_2) = f(p = p_1 = -p_2)$, where we have utilised the implicit δ function. We define the *self-energy*, $\Sigma(p)$, which arises from the modification that interactions make to the free theory by

$$\Gamma^{(2)}(p) = -K_\phi(p) + \Sigma(p). \tag{2.24}$$

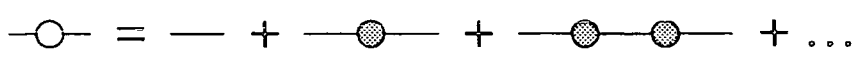

Figure 2.3: The *full propagator*, $G_c^{(2)}$ (with empty circle) is equivalent to the sum of free propagators, $G_0^{(2)}$ (straight lines), with all numbers of vertex functions, $\Gamma^{(2)}$ (shaded circles), inserted.

In momentum space for, $|\Sigma(p)| < |K_\phi(p)|$, Eqn. (2.23) leads to

$$\begin{aligned} G_c^{(2)}(p) &= \frac{i}{\Gamma^{(2)}(p)} = -\frac{i}{K_\phi(p)} \left\{ \frac{1}{1 - \frac{\Sigma(p)}{K_\phi(p)}} \right\} \\ &= -\frac{i}{K_\phi(p)} \left\{ 1 + \frac{\Sigma(p)}{K_\phi(p)} + \frac{\Sigma(p)^2}{K_\phi(p)^2} + \ldots \right\} \\ &= G_0^{(2)}(p) \left\{ 1 + i\Sigma(p) G_0^{(2)}(p) + \ldots + \left(i\Sigma(p) G_0^{(2)}(p) \right)^r + \ldots \right\} \end{aligned} \tag{2.25}$$

We have illustrated this series in Figure 2.3. In other words, the *full* propagator, $G_c^{(2)}$, is equivalent to an infinite sum of the free propagators, $G_0^{(2)}$, with all numbers of self-energy insertions, $\Sigma(p)$. Generically, we find that $\Gamma_0^{(2)}$ has the form, $p^2 - m^2$, so Σ gets its name *self-energy* because, due to ϕ's *interactions*, an effective modification is made to the mass, m, of the free theory.

2.5 Gauge symmetries

In considering a *typical* (term in a) Lagrangian density, $\hat{\phi}^\dagger \partial_\mu \partial^\mu \hat{\phi}$, where $\hat{\phi}$ is a multiplet of some fixed number of fields, we note that it is invariant under the *global* transformation,

$\hat{\phi} \rightarrow e^{i\theta}\hat{\phi}$, where θ may be expanded as[1]

$$\theta = \theta^a T^a \tag{2.26}$$

with respect to the generators, T^a, of some symmetry group, satisfying,

$$\left[T^a, T^b\right] = i f^{abc} T^c. \tag{2.27}$$

The structure constants of the group are labeled as f^{abc}.

The corresponding local (gauge) transformation is, [7]

$$\hat{\phi}(x) \rightarrow e^{i\theta(x)}\hat{\phi}(x), \tag{2.28}$$

where $\theta(x)$ is required to be small. Unfortunately, this is not a symmetry of the given Lagrangian (term). However, rather than reject this proposed symmetry transformation we find that it is more fruitful to replace the partial derivative with a modified *gauge covariant* partial derivative,

$$\hat{D}_\mu = \partial_\mu + ig\hat{A}_\mu(x) \tag{2.29}$$

and thus the contribution to the Lagrangian becomes

$$\mathcal{L} \sim \hat{\phi}^\dagger \hat{D}_\mu^\dagger \hat{D}^\mu \hat{\phi}. \tag{2.30}$$

We do this at the expense of invoking a new (Bosonic) *gauge field*, $\hat{A}_\mu$. Both $\theta(x)$ and $\hat{A}_\mu(x)$ can be expanded in terms of the generators, T^a, of the symmetry group; indeed it is the component fields, $\hat{A}^a_\mu(x)$, that commute with one another (are Bosonic see Eqn. (2.1)). The constant generators, which together with g define the coupling of $\hat{\phi}$ to the gauge field, tend

[1]Since we are presenting a summary, we give the general non-abelian gauge theory from the start.

to complicate the commutation relations of the multiplet field, $\hat{A}_\mu(x)$. The transformation of the gauge field with respect to $\theta(x)$ is constrained by requiring that $\hat{D}_\mu\hat{\phi}$ transforms in the same manner as $\hat{\phi}$. For small $\theta(x)$ this leads to,

$$\hat{A}^\theta_\mu(x) = \hat{A}_\mu(x) + i\left[\theta(x), \hat{A}_\mu(x)\right] - \frac{1}{g}\partial_\mu\theta(x). \tag{2.31}$$

We find that *mass* terms of the form, $m^2\hat{A}_\mu\hat{A}^\mu/2$, are not gauge invariant. It follows that we cannot arbitrarily put put masses into a Lagrangian without breaking its gauge symmetry.

If $\hat{A}_\mu$ is not to be an external field it must have a mode of propagation. This is facilitated by terms quadratic in the field. The antisymmetric *field strength* tensor is defined by,

$$\hat{F}_{\mu\nu}(x) = \frac{1}{ig}\left[\hat{D}_\mu, \hat{D}_\nu\right] = \left(\partial_\mu\hat{A}_\nu(x)\right) - \left(\partial_\nu\hat{A}_\mu(x)\right) + ig\left[\hat{A}_\mu(x), \hat{A}_\nu(x)\right] \tag{2.32}$$

The square of $\hat{F}$ is a gauge invariant quantity, under Eqn. (2.31), so it facilitates the required propagation term for a gauge invariant Lagrangian,

$$-\frac{1}{4}\hat{F}^a_{\mu\nu}\hat{F}^{a\,\mu\nu}. \tag{2.33}$$

In this general *non-abelian* theory, this term does not give rise to *free* propagation since it contains terms cubic and quartic in $\hat{A}_\mu$, instead it defines a self interacting field.

2.5.1 Abelian gauge theories

In the simplified case of an abelian gauge symmetry, with the f^{abc} of Eqn. (2.27) identically zero, two important results follow. The first is simply that self interactions are not present in Eqn. (2.32), so abelian fields when not coupled to fields $\hat{\phi}$ will *freely* propagate.

The second is that it becomes possible to define different gauge transformations for different (multiplet) fields. Given $\hat{\phi}$ and $\hat{\psi}$ say, we transform them as

$$\hat{\phi}(x) \rightarrow e^{iQ_\phi\theta(x)}\hat{\phi}(x) \qquad \text{and} \qquad \hat{\psi}(x) \rightarrow e^{iQ_\psi\theta(x)}\hat{\psi}(x). \tag{2.34}$$

The gauge covariant derivative is similarly altered,

$$\hat{D}^\phi_\mu = \partial_\mu + igQ_\phi\hat{A}_\mu(x) \qquad \text{and} \qquad \hat{D}^\psi_\mu = \partial_\mu + igQ_\psi\hat{A}_\mu(x), \tag{2.35}$$

but fortunately this leaves Eqn. (2.31), without the commutator term, unaffected. Eqn. (2.32) is modified to read,

$$\hat{F}_{\mu\nu}(x) = \frac{1}{igQ_\phi}\left[\hat{D}^\phi_\mu, \hat{D}^\phi_\nu\right] = \frac{1}{igQ_\psi}\left[\hat{D}^\psi_\mu, \hat{D}^\psi_\nu\right] = \left(\partial_\mu\hat{A}_\nu(x)\right) - \left(\partial_\nu\hat{A}_\mu(x)\right) \tag{2.36}$$

Correspondingly, the only terms in a general Lagrangian, that are not guaranteed to be gauge invariant are those that involve direct interactions between $\hat{\phi}$ and $\hat{\psi}$. Such terms are typically of the form

$$\sim \hat{\phi}^{\dagger r}\hat{\psi}^s \rightarrow \hat{\phi}^{\dagger r}\hat{\psi}^s \;\; e^{-i(Q_\phi r - Q_\psi s)\theta}. \tag{2.37}$$

Now, to actually be gauge invariant (for a small θ), we require $Q_\phi - s(Q_\psi/r) = 0$. In such a scenario $Q_\phi/s = Q_\psi/r$ defines a convenient *unit* of charge, which may be factored into a redefinition of the coupling, g. In summary, whilst it is possible for abelian gauge fields to couple with different strengths to different fields, these couplings are always in integer multiples of some more basic unit.

2.6 Ghosts

The gauge symmetry of a fully gauge invariant Lagrangian is a complete internal symmetry—a gauge choice does not manifest itself in any physical amplitude. Consequently, we must take care to treat it correctly in the Path Integral formalism. Having chosen a representation of $\hat{A}_\mu$ we have effectively selected a gauge. Thus in calculating the vacuum-to-vacuum transition amplitude we should not allow the path integral to wander over different gauges. Accordingly, we write the path integral over a *c-number* A^θ_μ (of Eqn. (2.31)) field as[2],

$$\int \mathcal{D}A^\theta_\mu \delta(\theta) \ldots \tag{2.38}$$

where the action of the delta function is to select the untransformed gauge. Equivalently, there is some gauge fixing function, $f(A^\theta)$, satisfying, $f(A) = 0$. Re-expressing the delta function Eqn. (2.38) becomes,

$$\int \mathcal{D}A^\theta_\mu \det\left(\left.\frac{\delta f^a}{\delta\theta^b}\right|_{\theta=0}\right) \delta\left(f(A^\theta_\mu)\right) \ldots = \int \mathcal{D}A_\mu \det\left(\left.\frac{\delta f^a}{\delta\theta^b}\right|_{\theta=0}\right) \delta\left(f(A_\mu)\right) \ldots \tag{2.39}$$

In reaching the right hand side we have used the delta function to constrain the integration region (much as we are able to write $\int_{-\infty}^{\infty} \delta(x^2) f(x) = \int_{-1}^{1} \delta(x^2) f(x)$). The determinant, as indicated, is with respect to the component indices of f and θ (see Eqn. (2.26)) and it is simply the Jacobian required to compensate for the change of argument to the delta function. Formally, the determinant can be rewritten in an exponential form. This is achieved by introducing a complex multiplet of Faddeev-Popov Ghost (FPG) *c-number* fields that are

[2]More formally we introduce an unrestricted path integral over all $\theta(x)$ (of Eqn. (2.28)) and show, by gauge invariance, the following treatment leads to an overall factor in both the numerator and denominator of Eqn. (2.7), thus leading to the same result.

fermionic (they anti-commute) [8]. That is to say,

$$\int \ldots \det(M_{ab}) \ldots = \int \mathcal{D}c\mathcal{D}c^\dagger \ldots \exp i \int \mathcal{L}_{\mathrm{FPG}} = \int \mathcal{D}c\mathcal{D}c^\dagger \ldots \exp i \int d^4x d^4y c_a^\dagger(x) M_{ab} c_b(y) \tag{2.40}$$

where $M_{ab} = \delta f^a / \delta \theta^b \big|_{\theta=0}$. It is also possible to write the *gauge fixing* delta function as an exponential,

$$\int \ldots \exp i \int \mathcal{L}_{\mathrm{GF}} = \int \ldots \exp -\frac{i}{2\xi} \int d^4x \{f(A(x))\}^2 \tag{2.41}$$

ξ is the *gauge parameter*. Although ξ can be thought of as just altering the normalisation of $f(A)$ hence contributing, via the determinant, an overall factor (to the numerator and denominator of Eqn. (2.7) and thus canceling), it does provide a convenient method of obtaining different gauges for a single type of function, $f(A)$. One of the favoured choices for gauge (and directly related to that used for all calculations in this thesis) are those known as *covariant* (or *lorentz*) gauges,

$$f(A) = \partial \cdot A. \tag{2.42}$$

This, and related choices, preserve the lorentz invariance of $\mathcal{L}$, which after absorbing Eqns. (2.40 and 2.41) becomes the *effective Lagrangian density*, $\mathcal{L}_{\mathrm{eff}} = \mathcal{L} + \mathcal{L}_{\mathrm{GF}} + \mathcal{L}_{\mathrm{FPG}}$.

Since the FPGs have been artificially introduced to rewrite the determinant of Eqn. (2.39), we do not expect them to be manifest as external fields. We do introduce an external source (a fermionic c-number field) for both of the ghost multiplets. However, in addition to setting these sources to zero when computing the Green's functions (cf. Eqns. (2.10 and 2.18) etc.) we also set c and $c^\dagger$ to zero too.

Another significant simplification, in the case of abelian gauge fields, is noted: from Eqn. (2.31) it follows that in lorentz gauges $\det(\delta f / \delta \theta)$ contains no terms in A^μ. Consequently, the effective Lagrangian does not couple the FPG fields to any others. Accordingly,

we may factor away the determinant and ignore ghost terms completely—they cannot contribute to any Green's functions in purely abelian gauge symmetric theories.

2.7 Gauge field polarisations

In lorentz gauges, the appropriate application of Eqn. (2.13) to massless gauge fields follows from the requirement that physical states, $|\alpha\rangle$, satisfy the weak gauge condition,

$$\partial \cdot \hat{A}_+ |\alpha\rangle = 0. \tag{2.43}$$

Where $\hat{A}_{+,\mu}$ is the annihilation component (see Eqn. (2.14)) of the expansion Eqn. (2.13). Since there are naively 4 orthogonal polarisation vectors for any gauge boson (in 4 dimensional space-time) and the two *physical* (or transverse) polarisations $\epsilon^{\pm}_{\mu}$, are orthogonal to the 4-momentum k, it follows that Eqn. (2.43) reduces to the requirement,

$$k^{\mu}\left(\epsilon^{0}_{\mu}\hat{a}^{0}_{A}(k) + \epsilon^{\parallel}_{\mu}\hat{a}^{\parallel}_{A}(k)\right)|\alpha\rangle = 0, \tag{2.44}$$

where we define ϵ^0 to be purely time-like, and $\epsilon^{\parallel}$ to be space-like and parallel to the 3-momentum of k. Since the time-like and space-like components of the Minkowski metric are of opposite sign we find that for a massless gauge field, $k^{\mu} \cdot \epsilon^0 = -k^{\mu} \cdot \epsilon^{\parallel}$ and consequently all physical states have an equal number of ϵ^0 and $\epsilon^{\parallel}$ polarisations:

$$\hat{a}^{0}_{A}(k)\,|\alpha\rangle = \hat{a}^{\parallel}_{A}(k)\,|\alpha\rangle \tag{2.45}$$

It can be shown that these states have opposite (in sign) contributions to the Hamiltonian (total energy) so they are unobservable.

Aside from the fact that mass terms for gauge fields are not by themselves gauge invariant, the modification for massive vector bosons is as follows. The introduction of mass, and thus a defined rest frame for the particle, gives rise to another space-like polarisation. Eqn. (2.43) is satisfied by a 4-vector, $\epsilon^{\parallel}$, parallel to the direction of motion of k, that transforms to $(0, \mathbf{k}/|\mathbf{k}|)$ as k is transformed to its rest frame. It follows that massive vector boson states, should they exist, have no time-like polarisations (the second term of the left-hand-side of Eqn. (2.44) is not present).

In summary, massless vector particles will have two transverse physical polarisations and massive vector particles will have three, all of which are space-like.

Chapter 3

The Standard Model

The most popular current model for elementary particles, enjoying the greatest success in describing High Energy Particle interaction data, has become known as the Standard Model (SM). It embeds the extremely successful theory of Quantum Electro-Dynamics (QED); a theory of *Weak Interactions* that predict the radioactive β-decay of nuclei; and Quantum Chromo-Dynamics (QCD), which successfully describes much hadronic experimental data. As yet, there is compelling evidence for the existence of all but one of the constituent fields[1] of the SM. It does however, not address all of nature's interactions, making no statements about the *gravitational* force, but in the face of an immense amount of high energy particle data, it does represent a formidable model for nature at its most elemental.

Before we describe the calculation of various physical processes—the topics of all the remaining chapters—we give the the Lagrangian density of the *Standard Model*, $\mathcal{L}_{SM}$, and

[1]The most recent particle to be *discovered* is the *heavy* Top quark [9].

Fermion, ψ	Left-handed	$Y_{\psi,L}$	Right-Handed	$Y_{\psi,R} = Q_\psi$
Leptons, l	$\begin{pmatrix}\nu_e\\ e\end{pmatrix}, \begin{pmatrix}\nu_\mu\\ \mu\end{pmatrix}, \begin{pmatrix}\nu_\tau\\ \tau\end{pmatrix}$	-1	$e, \quad \mu, \quad \tau$	-1
Quarks, q_i $N_f = 6$ and $N_c = 3$	$\begin{pmatrix}u_i\\ d_i\end{pmatrix}, \begin{pmatrix}c_i\\ s_i\end{pmatrix}, \begin{pmatrix}t_i\\ b_i\end{pmatrix}$	$+\frac{1}{3}$	$d_i, \quad s_i, \quad b_i$ $u_i, \quad c_i, \quad t_i$	$-\frac{1}{3}$ $+\frac{2}{3}$

Table 3.1: This is a table of Standard Model fermion *hypercharge*, Y_ψ—the factor governing the strength of the respective fermion's coupling to the $U(1)$ field, $\hat{B}_\mu$.

accompany it with some simple discussion.

3.1 The Standard Model Lagrangian

The SM is built from a system of 25 *physical* particle fields (i.e. observable directly or indirectly). Twelve of these are spin-1/2 fermionic fields, broken into their *left* and *right*-handed components (see Appendix E), that couple selectively to the 12 fields of three gauge symmetry groups $U(1) \times SU(2) \times SU(3)$. The remaining field is just one of the four real fields of a complex scalar doublet. It is the only visible remnant of a mechanism invoked to *give* masses to various fields of the theory, and also currently the only field for which no direct experimental evidence exists. Superficially, however, the SM Lagrangian contains mass terms for neither the fermions nor the gauge bosons; this is as required because it is explicitly devised to be gauge independent.

With respect to the fermionic fields given in Table 3.1 the Standard Model Lagrangian has the form,

$$
\begin{aligned}
\mathcal{L}_{SM} \;=\; & \\
& \sum_{l} \overline{L_l} \left(i\not{\partial}_\mu - g' \frac{Y_{l,L}}{2} \not{B}_\mu - g \not{W}_\mu \right) L_l + \sum_{l} \overline{R_l} \left(i\not{\partial}_\mu - g' Y_{l,R} \not{B}_\mu \right) R_l \\
& + \sum_{i,j=1}^{N_c} \sum_{q=1}^{N_f/2} \overline{L'_{q_i}} \left(\left(i\not{\partial}_\mu - g' \frac{Y_{q,L}}{2} \not{B}_\mu - g \not{W}_\mu \right) \delta^{ij} - g_s \not{G}_\mu^{ij} \right) L'_{q_j} \\
& + \sum_{i,j=1}^{N_c} \sum_{q=1}^{N_f} \overline{R_{q_i}} \left(\left(i\not{\partial}_\mu - g' Y_{q,R} \not{B}_\mu \right) \delta^{ij} - g_s \not{G}_\mu^{ij} \right) R_{q_j} \\
& - \frac{1}{4} B_{\mu\nu} B^{\mu\nu} - \frac{1}{4} W^i_{\mu\nu} W^{i\,\mu\nu} - \frac{1}{4} G^a_{\mu\nu} G^{a\,\mu\nu} \\
& - \sum_{l} h_{l,i} \left(\overline{L_l} \phi R_l + \overline{R_l} \phi^\dagger L_l \right) - \sum_{i=1}^{N_c} \sum_{q=1}^{N_f/2} h_{q,i} \left(\overline{L_{q,i}} \phi R_{q,i} + \overline{R_{q,i}} \phi^\dagger L_{q,i} \right) \\
& - \sum_{i=1}^{N_c} \sum_{q=1}^{N_f/2} h_{q+N_f/2,i} \left(\overline{L_{q,i}} \tilde{\phi} R_{q+N_f/2,i} + \overline{R_{q+N_f/2,i}} \tilde{\phi}^\dagger L_{q,i} \right) \\
& \left| \left(\partial_\mu + i g' \frac{Y_\phi}{2} B_\mu + i g W_\mu \right) \phi \right|^2 - \lambda (\phi^\dagger \phi)^2 + \mu^2 \phi^\dagger \phi .
\end{aligned}
\tag{3.1}
$$

For brevity we have neglected the operator hats on each of the fields. $\hat{B}_\mu$ is the $U(1)$ gauge field coupling to both fermions and the complex scalar doublet field, $\hat{\phi}$, proportional to their respective *hypercharge* value, Y_ψ. $\hat{W}_\mu$ is the $SU(2)$ gauge field that couples only to *left-handed* fermions and the complex scalar doublet field, $\hat{\phi}$. $\hat{G}_\mu$ is the $SU(3)$ gauge field of QCD. It is noticeable that neither the lepton nor the $\hat{\phi}$ (and its transformed variant, $\tilde{\phi}$) fields directly interact with $\hat{G}_\mu$; indeed, only particles carrying *colour* (the indices, i, of Table 3.1) feel this *gluonic field.* The tensors $\hat{B}_{\mu\nu}$, $\hat{W}_{\mu\nu}$ and $\hat{G}_{\mu\nu}$, are just the field strengths, $\hat{F}_{\mu\nu}$ of Eqn. (2.36) (for $\hat{B}$) and Eqn. (2.32) (for $\hat{W}$ and $\hat{G}$).

Both the left and right-handed fermionic fields couple equally to the $SU(3)$ gauge field, or in other words, QCD is a chirally invariant theory. It follows that, if the quarks are considered massless, then in the absence of $U(1) \times SU(2)$ or $\hat{\phi}$ couplings there is no mechanism for the different chiralities to interact: *massless* QCD is a chirally *independent* theory.

From Table 3.1, the *hypercharge*, Y_ψ, of a given flavour of fermion for the left and right-handed fermions is not generally the same. This differential coupling obeys gauge invariance because the $U(1)$ gauge field is an abelian one (see Section 2.5.1). Indeed, there is noticeably an absence of right handed *neutrino fields*, a point we shall address in Section 3.5. The *hypercharge* of the $\hat{\phi}$ field is

$$Y_\phi = 1. \tag{3.2}$$

We shall indicate the significance of the primes on the *left-handed* quark doublets in Section 3.6; they are linearly related to the un-primed doublets.

3.2 Spontaneous symmetry breaking

The process we describe in this section has become known as the *Higgs Mechanism* [10], it concerns the nature of the *Higgs doublet* field, $\hat{\phi}$.

We consider the case that $\hat{\phi}$ in its *un-excited* form is $\hat{\phi} = \phi_0$, for $\phi_0 \neq 0$. The excitations of $\hat{\phi}$ can be re-written as

$$\hat{\phi} = \phi_0 + \hat{\phi}'. \tag{3.3}$$

The first consequence of this is to ensure that the vacuum-expectation-value $\langle 0|\hat{\phi}|0\rangle = \langle 0|\phi_0|0\rangle$ is non-zero. This corresponds to quantum numbers belonging to the vacuum. To constrain ϕ_0 we require that rather than being zero, it *minimises* the last two terms of $\mathcal{L}_{SM}$ as it is presented in Eqn. (3.1); these last two terms are called the *Higgs potential.* Whilst $\phi_0 = 0$ clearly reduces this *potential* to zero, we find that, for $\mu^2 > 0$, the minimum of the

potential is at $\phi_0^\dagger \phi_0 = \mu^2/2\lambda$. Correspondingly we define,

$$\phi_0 = \begin{pmatrix} 0 \\ v/\sqrt{2} \end{pmatrix} \qquad \hat{\phi}' = \begin{pmatrix} \hat{\phi}^+ \\ (\hat{H} + i\hat{\chi})/\sqrt{2} \end{pmatrix} \tag{3.4}$$

with

$$v = \sqrt{\frac{\mu^2}{\lambda}}, \tag{3.5}$$

and the related field

$$\tilde{\phi} = i\tau_2 \hat{\phi}^* \tag{3.6}$$

or equivalently,

$$\tilde{\phi}_0 = \begin{pmatrix} v/\sqrt{2} \\ 0 \end{pmatrix} \qquad \tilde{\phi}' = \begin{pmatrix} (\hat{H} - i\hat{\chi})/\sqrt{2} \\ -\hat{\phi}^- \end{pmatrix}. \tag{3.7}$$

This choice of ϕ_0 is not unique, but all other choices are related to this one by an $SU(2)$ rotation. Since this is a globally selected choice for ϕ_0, we can view the generators of the rotation to another choice for ϕ_0 as the θ of Eqn. (2.26).

3.3 Masses for the fields

The Higgs potential does have a term quadratic in $\hat{\phi}$ but it has the wrong sign to be a mass term, cf. the text following Eqn. (2.25). We note, however, that the $\hat{H}$ component of $\hat{\phi}$ *develops* a mass type term of the correct form with respect to μ^2.

$$\begin{aligned} & -\lambda \left(\hat{\phi}^\dagger \hat{\phi}\right)^2 + \mu^2 \left(\hat{\phi}^\dagger \hat{\phi}\right) \\ = \; & -\frac{\mu^2}{v^2} \left(\phi_0^\dagger \phi_0 + \phi_0^\dagger \hat{\phi}' + \hat{\phi}'^\dagger \phi_0 + \hat{\phi}'^\dagger \hat{\phi}'\right)^2 + \mu^2 \left(\hat{\phi}'^\dagger \hat{\phi}' + \ldots\right) \end{aligned}$$

$$
\begin{aligned}
&= -\frac{\mu^2}{v^2}\left[2\frac{v^2}{2}\left(\hat{\phi}'^{\dagger}\hat{\phi}'\right) + \left(\phi_0^{\dagger}\hat{\phi}' + \hat{\phi}'^{\dagger}\phi_0\right)^2 + \ldots - v^2\left(\hat{\phi}'^{\dagger}\hat{\phi}' + \ldots\right)\right] \\
&= -\frac{\mu^2}{2}\left(\frac{\hat{H}+i\hat{\chi}}{\sqrt{2}} + \frac{\hat{H}-i\hat{\chi}}{\sqrt{2}}\right)^2 + \ldots \\
&= -\mu^2\hat{H}^2 + \ldots = -\frac{1}{2}m_H^2\hat{H}^2
\end{aligned}
\tag{3.8}
$$

where we have neglected terms not quadratic in a single component field. We see that it is *only* the $\hat{H}$ component that develops a mass in this manner. We now consider how the gauge bosons and fermions of the model *acquire* mass.

We shall find it useful to decompose the gauge field, $\hat{W}_\mu$, into its component fields in the basis defined by the Pauli matrices, τ_i, given in Section F.1. i.e.

$$
\hat{W}_\mu = \hat{W}_\mu^i\frac{\tau_i}{2}. \tag{3.9}
$$

From the covariant derivative squared terms for the Higgs doublet, we consider the gauge field interactions (see Eqns. (3.1 and 3.2)),

$$
\frac{1}{4}\hat{\phi}^{\dagger}\left(g'\hat{B}_\mu + g\hat{W}_\mu^i\tau_i\right)\left(g'\hat{B}_\mu + g\hat{W}_\mu^j\tau_j\right)\hat{\phi} \;=\; \frac{1}{4}\hat{\phi}^{\dagger}\left(g'^2\hat{B}\cdot\hat{B} + g^2\hat{W}_i\cdot\hat{W}_i + 2g'g\hat{B}\cdot\hat{W}_i\tau_i\right)\hat{\phi} \tag{3.10}
$$

where we have employed Eqn. (F.4). Concentrating on the ϕ_0^2 contribution (see Eqn. (F.1)) this becomes,

$$
\frac{v^2}{8}\left\{\left(g'\hat{B} - g\hat{W}_3\right)^2 + g^2\left(\hat{W}_1^2 + \hat{W}_2^2\right)\right\}. \tag{3.11}
$$

This is of a form that strongly suggests mass terms for three vector fields—the minus sign which we might expect to be preceding these bosonic terms is actually provided by the metric, since when acting on any physical state, the field contributes only space-like polarisations,

ϵ_μ, i.e. $\epsilon \cdot \epsilon < 0$.

With respect to the so called, *Weak Mixing Angle*, θ_W, satisfying

$$\sin\theta_W = \frac{g'}{\sqrt{g'^2+g^2}} \quad \text{and} \quad \cos\theta_W = \frac{g}{\sqrt{g'^2+g^2}}, \tag{3.12}$$

we define the transformed fields,

$$\begin{array}{rclcrcl} \hat{A}_\mu &=& \hat{B}_\mu\cos\theta_W + \hat{W}^3_\mu\sin\theta_W & & \hat{B}_\mu &=& \hat{A}_\mu\cos\theta_W - \hat{Z}_\mu\sin\theta_W \\ \hat{Z}_\mu &=& -\hat{B}_\mu\sin\theta_W + \hat{W}^3_\mu\cos\theta_W & \text{and} & \hat{W}^3_\mu &=& \hat{A}_\mu\sin\theta_W + \hat{Z}_\mu\cos\theta_W \\ \hat{W}^\pm_\mu &=& \frac{1}{\sqrt{2}}\left(\hat{W}^1_\mu \mp i\hat{W}^2_\mu\right) & & \hat{W}^1_\mu &=& \frac{1}{\sqrt{2}}\left(\hat{W}^+_\mu + \hat{W}^-_\mu\right) \\ &=& \hat{W}^{\mp\dagger}_\mu & & \hat{W}^2_\mu &=& \frac{i}{\sqrt{2}}\left(\hat{W}^+_\mu - \hat{W}^-_\mu\right). \end{array} \tag{3.13}$$

The *new* fields are mass eigenstates, the *Z-boson* field of mass,

$$M_Z = \frac{v\sqrt{g'^2+g^2}}{2}, \tag{3.14}$$

and the $W^\pm$*-bosons* of mass

$$M_W = M_Z\cos\theta_W. \tag{3.15}$$

The fourth of these transformed fields, $\hat{A}_\mu$, has no mass term.

We consider the fermionic terms that contain the v factor of Eqn. (3.5). The $\overline{L_\psi}\hat{\phi}R_\psi$ and $\overline{R_\psi}\hat{\phi}^\dagger L_\psi$ terms, the so-called *Yukawa couplings*, reduce to terms of the form,

$$-\frac{h_\psi v}{\sqrt{2}}\left(\overline{\psi_L}\psi_R + \overline{\psi_R}\psi_L\right) \tag{3.16}$$

which (cf. Section E.4) are chirality mixing mass terms for a fermion of flavour $\psi \in \{d_i, s_i, b_i\}$.

For the leptons of $\mathcal{L}_{SM}$, we see that this is the only included term giving rise to mass like

terms. Correspondingly, there would be no mixing of left and right handed *neutrino* states, even if we had included right-handed neutrino fields in Eqn. (3.1).

For the quarks, however, it is desirable for the u_i, c_i and t_i quarks to be massive. So, a transformation is made of $\hat{\phi}$ to $\tilde{\phi}$ (see Eqn. (3.6)) with which we obtain mass generating Yukawa terms (see Eqn. (3.16)) for the remaining quarks, $\psi \in \{u_i, c_i, t_i\}$.

3.4 Fixing a gauge

We find that the covariant derivative terms for the $\hat{\phi}$ field contribute awkward oscillation 2-point vertices for the $\hat{W}$, $\hat{B}$ (hence $\hat{A}$, $\hat{Z}$ and $\hat{W}^{\pm}$) and $\hat{\phi}'$ fields of the form,

$$\frac{ig'}{2}\hat{B}_\mu(\partial^\mu\hat{\phi}')\phi_0. \tag{3.17}$$

It has been found [11] that such terms can be eliminated by the following choice of gauge (see Section 2.6),

$$\begin{aligned} f^i_W(W) &= \partial^\mu W^i_\mu + \xi\tfrac{ig}{2}\left\{\phi'^\dagger\tau^i\phi_0 - \phi_0^\dagger\tau^i\phi'\right\} \\ f_B(B) &= \partial^\mu B_\mu + \xi\tfrac{ig'}{2}\left\{\phi'^\dagger\phi_0 - \phi_0^\dagger\phi'\right\}. \end{aligned} \tag{3.18}$$

Where ξ is the *gauge parameter*, and correspondingly, cf. Eqn. (2.41),

$$\mathcal{L}_{GF} = -\frac{1}{2\xi}\left\{f_W(W)^2 + f_B(B)^2\right\}. \tag{3.19}$$

Note, f^2 here refers to the straightforward square and *not* $f^\dagger f$.

The terms of the form Eqn. (3.17) are canceled by those from $\mathcal{L}_{GF}$ that are linear in $\hat{B}$(and $\hat{W}$). The terms quadratic in the gauge fields are simply the *normal* lorentz gauge

fixing condition, Eqn. (2.42).

The remaining terms in $\mathcal{L}_{GF}$ are quadratic in the un-physical component fields to ϕ'. They give rise to gauge dependent mass terms of the form, (see Eqns. (3.8 and 3.15))

$$-\xi M_W^2 \phi^- \phi^+ - \xi \frac{m_H^2}{2} \chi^2. \tag{3.20}$$

It is clear that the ϕ^+(and ϕ^-) and χ fields are deeply linked to the choice of gauge. It is for this reason that they are said to be *un-physical.* Indeed, by choosing $\xi \to \infty$ we can ensure that they are unable to propagate. This gauge is called the unitary gauge and contains only the physical fields.

3.5 The Electroweak theory

Firstly, we define the coupling,

$$e = g' \cos\theta_W = g \sin\theta_W. \tag{3.21}$$

The couplings of both the left-handed fermions and the $\hat{\phi}$ field to the $U(1) \times SU(2)$ gauge fields involve the generic contribution,

$$\partial_\mu + ig' \frac{Y_{\alpha,L}}{2} \hat{B}_\mu + ig \hat{W}_\mu = \partial_\mu + \frac{i}{2} \left(g' \hat{B}_\mu Y_{\alpha,L} \delta_{ab} + g \hat{W}_\mu^i \tau_{ab}^i \right) \tag{3.22}$$

where $\hat{\alpha}$ is the appropriate field type. Expanding in terms of the transformed fields, Eqn. (3.13),

and with Eqn. (3.21) this becomes, [12]

$$\partial_\mu + \frac{ie}{2}\begin{bmatrix} (Y_{\alpha,L}+1)\hat{A}_\mu + \frac{2}{\sin 2\theta_W}(\cos^2\theta_W - Y_{\alpha,L}\sin^2\theta_W)\hat{Z}_\mu & \frac{\sqrt{2}}{\sin\theta_W}\hat{W}^+_\mu \\ \frac{\sqrt{2}}{\sin\theta_W}\hat{W}^-_\mu & (Y_{\alpha,L}-1)\hat{A}_\mu - \frac{2}{\sin 2\theta_W}(\cos^2\theta_W + Y_{\alpha,L}\sin^2\theta_W)\hat{Z}_\mu \end{bmatrix}. \tag{3.23}$$

Applying this to the fermionic sector we see that the flavour conserving interactions are with the $\hat{A}_\mu$ and $\hat{Z}_\mu$ fields, since they form the diagonal of the matrix in Eqn. (3.23). We note that the strength of the $\hat{A}_\mu$ couplings to the fermions is one unit of e larger for the upper member of the left-handed doublet (ν_e, u', etc.) than for the lower member (e, d', etc.).

Concentrating on the $\hat{W}^\pm$ fields, we find that they couple the two flavours of fermion in a single doublet, since they form the diagonal components of the matrix. As we have said, this transition corresponds to a change of e in the $\hat{A}_\mu$ coupling—in a real sense it is the $\hat{W}^\pm_\mu$ that carries this difference. We note also that the $\hat{W}^\pm_\mu$ couple identically to all doublets independently of the hypercharge: the $\hat{W}^\pm_\mu$ fields are blind to the leptonic or quark nature of the fermions. This is entirely as we would expect since the transformation of fields for them has just been a rotation in $SU(2)$ and they remain purely non-abelian (cf. Section 2.5.1). Another consequence of the non-abelian nature of the $SU(2)$ field is that it gives rise to self-interaction (see the discussion following Eqn. (2.32)). It is the $\hat{W}^3$ component of $\hat{A}$ and $\hat{Z}$ that cause $\hat{W}^\pm$ to interact with them. The fact that $\hat{B}$ and $\hat{W}^3$ are mutually abelian means that they do not interact without simultaneously coupling to two charged fields—$\hat{A}$ cannot interact without the presence of a charge.

The right-handed fermions do not couple to the $SU(2)$ field. Instead, their covariant derivative to the $U(1) \times SU(2)$ sector is,

$$\partial_\mu + ig'Y_{\alpha,R}\hat{B}_\mu = \partial_\mu + ieY_{\alpha,R}\left[\hat{A}_\mu - \tan\theta_W\hat{Z}_\mu\right]. \tag{3.24}$$

We define eQ_α to be the value of the coupling for fermion $\hat{\alpha}$ to the field $\hat{A}_\mu$, from Table 3.1 we observe that,

$$Q_{\alpha,L} = Q_{\alpha,R} = Y_{\alpha,R}. \tag{3.25}$$

Since, $Q_{e,L} = Q_{\nu_e,L} - 1$, it follows via this relationship that $Y_{\alpha,R} = 0$. This justifies our exclusion of right handed neutrinos from $\mathcal{L}_{SM}$ (Eqn. (3.1)).

The $\hat{A}$ field is identified with the 4-vector potential for the classical **E** and **B** 3-vector Electromagnetic fields, and e with the fundamental unit of charge as defined by the electron having $e \times (-1)$. Historically, it was the knowledge of e and the relative charges of the fermions, $Q_{\alpha,R}(= Q_{\alpha,L})$, that enabled the hypercharges to be deduced. Indeed, with the benefit of hindsight, the choice $3e = g' \cos\theta_W = g \sin\theta_W$ for Eqn. (3.21), might have been more natural—in this way all particles would have had integer charges, n e. The massless external states of the field $\hat{A}_\mu$ are called *photons*; particles of light.

We are now in the position to appreciate the significance of the choice Eqn. (3.4). The covariant derivative for the Higgs doublet has the form,

$$-\hat{\phi}^\dagger \left(\partial^2 - \frac{1}{4} \begin{bmatrix} \left(g'\hat{B} + g\hat{W}^3\right) & 0 \\ 0 & \left(g'\hat{B} - g\hat{W}^3\right) \end{bmatrix}^2 + \ldots \right) \hat{\phi} \tag{3.26}$$

where we have neglected the $\hat{W}^1$ and $\hat{W}^2$(equivalently $\hat{W}^\pm$) contributions. This leads to the following terms expressed with respect to $\hat{\phi}$'s component fields,

$$\begin{aligned} &-\hat{\phi}^- \left(\partial^2 - \left(e\hat{A} + \frac{e}{\tan 2\theta_W} \hat{Z} \right)^2 \right) \hat{\phi}^+ \\ &\quad - \frac{1}{2} H \left(\partial^2 - \frac{e^2}{\sin^2 2\theta_W} \hat{Z}^2 \right) H - \frac{1}{2} \chi \left(\partial^2 - \frac{e^2}{\sin^2 2\theta_W} \hat{Z}^2 \right) \chi. \end{aligned} \tag{3.27}$$

We note that none of the lower components to $\hat{\phi}$ couple to the $\hat{A}_\mu$ field. That is to say, the $\hat{\phi}$

field has no charge, either in its unexcited (*vacuum*) state or with a *physical* excitation, $\hat{H}$.

The $\hat{Z}_\mu$ and $\hat{W}^\pm_\mu$ fields are those of the *Weak* force. The charged interactions, involving the $\hat{W}^\pm_\mu$ fields and left-handed fermions, are *flavour changing*; $\nu_e \leftrightarrow e$ and $u' \leftrightarrow d'$ etc. to each of which it couples equally. The $\hat{Z}_\mu$ field couples to both the left and right handed fermions, but *differentially*. This gives rise to the so-called $V-A$ (Vector-minus-Axial-vector) coupling of the $\hat{Z}_\mu$ to fermions.

Multiplying Eqns. (3.23 and 3.24) by γ^μ we can write the general fermion, $\hat{\alpha}$, to $\hat{Z}_\mu$ interaction vertex as,

$$ie\hat{Z}_\mu \left(c_L \overline{\hat{L}_\alpha} \gamma^\mu \hat{L}_\alpha + c_R \overline{\hat{R}_\alpha} \gamma^\mu \hat{R}_\alpha \right) \tag{3.28}$$

where $c_{L(R)}$ are the left(right) couplings. Substituting Eqn. (E.19) into this expression we can write the overall coupling as,

$$ie\hat{Z}_\mu \left(\overline{\alpha} \gamma^\mu \alpha v_\alpha - \overline{\alpha} \gamma^\mu \gamma_5 \alpha a_\alpha \right) \tag{3.29}$$

where,

$$v_\alpha = \frac{c_L + c_R}{2} \quad \text{and} \quad a_\alpha = \frac{c_L - c_R}{2} \tag{3.30}$$

—A *vector* – *axial vector* current, cf. Section E.4. For the fermions whose left-handed component is the *upper* member of a $SU(2)$ doublet these coupling factors have the following forms,

$$v_\alpha = +\frac{1 - (1 + Y_{\alpha,L} + 2Y_{\alpha,R}) \sin^2 \theta_W}{2 \sin 2\theta_W} \qquad a_\alpha = +\frac{1 - (1 + Y_{\alpha,L} - 2Y_{\alpha,R}) \sin^2 \theta_W}{2 \sin 2\theta_W}, \tag{3.31}$$

and for the lower members,

$$v_\alpha = -\frac{1 - (1 - Y_{\alpha,L} - 2Y_{\alpha,R}) \sin^2 \theta_W}{2 \sin 2\theta_W} \qquad a_\alpha = -\frac{1 - (1 - Y_{\alpha,L} + 2Y_{\alpha,R}) \sin^2 \theta_W}{2 \sin 2\theta_W}. \tag{3.32}$$

3.6 No flavour changing neutral currents

The use of $L'_{q,i}$, in $\mathcal{L}_{SM}$ (Eqn. (3.1)), indicates that it is modified left handed doublets that couple to the $SU(2)$ gauge field. They are related to $L_{q,i}$ by,

$$L'_{d,i} = \begin{pmatrix} u \\ d' \end{pmatrix}, \qquad L'_{d,i} = \begin{pmatrix} c \\ s' \end{pmatrix}, \qquad L'_{d,i} = \begin{pmatrix} t \\ b' \end{pmatrix}, \tag{3.33}$$

where the primed quarks are related to the unprimed ones by,

$$\begin{pmatrix} d' \\ s' \\ b' \end{pmatrix} = U_{CKM} \begin{pmatrix} d \\ s \\ b \end{pmatrix}. \tag{3.34}$$

U_{CKM} is the unitary Cabibbo-Kobayashi-Maskawa [13] mixing matrix. The non-diagonal form of U_{CKM} ensures that the quark mass eigenstates of the Lagrangian (terms containing $h_{q,i}$) are not the same as those participating in interactions with the $SU(2)$ field. This transformation is global and unitary so the $U(1)$ and $SU(2)$ *couplings* are unaffected.

We have established the fact that $\hat{W}^{\pm}$ interaction is associated with flavour change: for example, a vertical transition will occur in Eqn. (3.33). The fact that the lower components to these doublets are *not* the mass eigenstates prompts us to investigate whether an interaction with the neutral fields, $\hat{A}$ and $\hat{Z}$, can result in a horizontal transition. Assuming some neutral combination, $\hat{N}_\mu \sim \hat{A}_\mu + \beta \hat{Z}_\mu$, for the fermionic fields, $\hat{\psi} \in \{\hat{d'}_i, \hat{s'}_i, \hat{b'}_i\}$ and $\hat{f} \in \{\hat{d}_i, \hat{s}_i, \hat{b}_i\}$, we have a combined series of interaction terms of the form,

$$\sim \sum_{\psi} \hat{\overline{\psi}} \hat{N}_\mu \hat{\psi} = \sum_{\psi, f} \hat{\overline{f}} \left(U^{\psi f}_{CKM} \right)^{-1} \hat{N}_\mu U^{\psi f}_{CKM} \hat{f}. \tag{3.35}$$

Since $\hat{N}_\mu$ is diagonal with respect to U_{CKM}, we can commute U_{CKM} through it to cancel against U_{CKM}^{-1}. Thus, the neutral currents do *not* give rise to flavour changing interactions. [14]

3.7 The Strong interaction

The Higgs field, $\hat{\phi}$, is not coupled to the *gluonic* gauge field, $\hat{G}_\mu$, in $\mathcal{L}_{SM}$. Thus, the $SU(3)$ field is not broken by the Higgs mechanism. Consequently, $\hat{G}_\mu$ remains massless and only couples to quarks and itself. Having generated masses for the quarks, we write the $SU(3)$ relevant part of Eqn. (3.1) as,

$$\mathcal{L}_{QCD} = \sum_{i,j}^{N_c} \hat{\overline{q}}_i \left[\left(i\hat{\not\partial} - m_q \right) \delta_{ij} - g_s T^a_{ij} \hat{\not G}^a_\mu \right] \hat{q}_j - \frac{1}{4} \hat{G}^a_{\mu\nu} \hat{G}^{a\,\mu\nu}. \tag{3.36}$$

The quark fields are, with respect to the gluons, each resolved into a triplet of fields, q_i, which couple to the 8 gluonic fields via the $SU(3)$ generators T^a_{ij} and with a strength g_s. These generators, and the fact that $\hat{G}^a_{\mu\nu}\hat{G}^{a\,\mu\nu}$ contains cubic and quartic, $\hat{G}^a$, *self* couplings are what distinguish QCD from QED. An algebra for these generators is discussed in Section F.2.

Chapter 4

Simple Phenomenology for LEP

A convenient *phenomenology* of the Standard Model is generated with respect to a perturbative expansion in the couplings, e and g_s. It is based on the assumption that these quantities are *small*. Within this framework, the appropriate free Lagrangian density is taken to be the $(e, g_s) \rightarrow 0$ limit of the full Standard Model Lagrangian, Eqn. (3.1). In this limit one establishes the propagators for the free theory, Eqn. (2.8). The interaction Lagrangian is simply the difference of the full and free Lagrangians and naturally leads to the Feynman rules for the vertices of the theory. The Green's functions and hence the scattering amplitudes of the theory can then be evaluated to some power in the couplings by expanding the exponentials in Eqns. (2.9 and 2.16).

The success of this perturbative approach, in terms of making accurate predictions based on the Standard Model Lagrangian, rides on an ability to identify physical quantities for which these small coupling limits are a valid approximation.

The basic process at LEP is the collision of a beam of electrons with a beam of anti-electrons (*positrons*) at a centre of mass energy for each particle collision equal to that of the Z-boson at rest. Before addressing the high energy collision at the Z-mass we shall cover collisions at lower energies. This will give us an opportunity to review some simple QED and also indicate the need for *renormalisation* in a consistent picture of High energy behaviour.

4.1 Parameters of the Standard Model

World average values for the masses of the massive weak gauge fields and the leptons of the Standard Model are as follows [15]. The weak gauge fields: the Z-boson is 91.173 ± 0.020 GeV; and the W-boson is 80.22 ± 0.26 GeV. This combination leads to a value for $\sin^2\theta_W$ of 0.226 ± 0.005, the error here is dominated by the uncertainty in the mass of the W. The masses of the leptons are very well known and have the values: $m_e = 0.51099906 \pm 0.00000015$ MeV; $m_\mu = 105.658389 \pm 0.000034$ MeV; and $m_\tau = 1784.1^{+2.7}_{-3.6}$ MeV. The masses of the quarks are by comparison not well known because they are only observed in bound states—as hadrons. For convenience, Table 4.1 contains approximate numerical values used in this chapter for all of the fermions of the SM.

4.2 $e^+e^- \to f\overline{f}$

We consider the $2 \to 2$ particle process of,

$$e^+(p_1) + e^-(p_2) \to f(p_3) + \overline{f}(p_4). \tag{4.1}$$

Fermion	Q_f	v_f	a_f	Mass [MeV]
e	-1	-0.048	-0.594	0.5
μ	-1	-0.048	-0.594	100
τ	-1	-0.048	-0.594	1800
ν_e	0	0.594	0.594	0
ν_μ	0	0.594	0.594	0
ν_τ	0	0.594	0.594	0
d	$-1/3$	-0.412	-0.594	5
s	$-1/3$	-0.412	-0.594	5
b	$-1/3$	-0.412	-0.594	5000
u	$2/3$	0.230	0.594	5
c	$2/3$	0.230	0.594	1500
t	$2/3$	0.230	0.594	170000

Table 4.1: A table of relevant properties for the fermions of the Standard Model. Containing the electric charges, Q_f, the vector (v_f) and axial (a_f) couplings, evaluated with respect to a weak mixing angle satisfying, $\sin^2\theta_W = 0.23$, and the approximate masses.

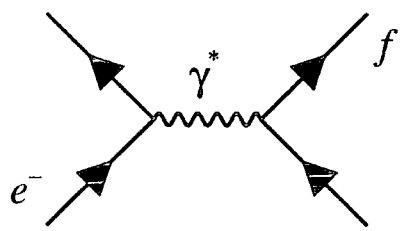

Figure 4.1: The Feynman diagram for the creation of a fermion-antifermion pair from the annihilation of an electron-positron pair via a virtual photon.

That is to say, the annihilation of a electron-positron pair leading to the production of a fermion-anti-fermion pair via a virtual photon.

With respect to a perturbative expansion in the coupling constant, e, the leading contribution to the probability amplitude for this process can be deduced from the single appropriate Feynman diagram, Figure 4.1, as

$$\mathcal{M}_{eeff} = \overline{v}_e(p_1)\,(+ie\gamma^\mu)\,u_e(p_2)\frac{-i}{q^2}\left(g_{\mu\nu} - (1-\xi)\frac{q_\mu q_\nu}{q^2}\right)\overline{u}_f(p_3)\,(-ieQ_f\gamma^\nu)\,v_f(p_4). \qquad (4.2)$$

The 4-momenta, p_i, are defined in Eqn. (4.1) and, respectful of 4-momentum conservation, we define

$$q = p_1 + p_2 = p_3 + p_4. \tag{4.3}$$

In Eqn. (4.2), we have explicitly included the gauge dependence of the photon propagator. The simplest choice for the gauge parameter would be $\xi = 1$, the Feynman gauge. However, in this case it is simple to use the on-shell condition for the electron, Eqn. (E.14), to show explicitly that the gauge dependent, $\frac{q_\mu q_\nu}{q^2}$, contribution vanishes.

The generic two particle cross-section for incoming particle momenta, p_1 and p_2, and with invariant masses, m_1 and m_2, is,

$$\sigma_{2\to 2} = \frac{(\text{sym})}{4\sqrt{(p_1.p_2)^2 - m_1^2 m_2^2}} \int dLips_{2\to n} \left(\overline{\mathcal{M}^\dagger \mathcal{M}}\right)_{event}. \tag{4.4}$$

Here, $\mathcal{M}$ is the matrix element for the $2 \to n$ process and $(\overline{\mathcal{M}^\dagger \mathcal{M}})_{event}$ is the matrix element squared, which is averaged over degenerate initial states and summed over indistinguishable final states. The factor, (sym), is a symmetry factor for averaging over identical *bosons* in the final state. It is usually of the form $1/j!$, where j is the number of identical bosons. The appropriate symmetry factor for this process is 1. We shall take the limit that $m_e \to 0$. We are not to observe the initial or final state polarisations, so we shall sum over the final states and average over the initial ones. In this way,

$$\left(\mathcal{M}^\dagger \mathcal{M}\right)_{eeff} = \frac{e^4 Q_f^2}{4q^4} \mathrm{Tr}\left\{\not{p}_1 \gamma^\mu \not{p}_2 \gamma^\nu\right\} \mathrm{Tr}\left\{\not{p}_3 \gamma_\mu \not{p}_4 \gamma_\nu - m_f^2 \gamma_\mu \gamma_\nu\right\}. \tag{4.5}$$

The product of the traces can be evaluated from the identities in Section E.1 to be,

$$32\left((p_1 \cdot p_2)m_f^2 + (p_1 \cdot p_3)^2 + (p_2 \cdot p_3)^2\right) \tag{4.6}$$

where we have also employed the momentum conservation of Eqn. (4.3). In the centre of mass frame we can specialise to the following representation for the momenta of the process,

$$\begin{array}{lll} p_1 = (E, \mathrm{p}_1, 0, 0) & & p_3 = (E, \mathrm{p}_3\cos\theta, \mathrm{p}_3\sin\theta, 0) \\ p_2 = (E, -\mathrm{p}_1, 0, 0) & q = (2E, 0, 0, 0) & p_4 = (E, -\mathrm{p}_3\cos\theta, -\mathrm{p}_3\sin\theta, 0) \end{array} . \tag{4.7}$$

With respect to this choice, the cross-section for the production of an $f\overline{f}$ pair becomes,

$$\begin{aligned} \sigma_{e^+e^-\to f\overline{f}} &= \frac{1}{8E^2}\frac{1}{16\pi E}\frac{e^4Q_f^2}{16Eq^2}\sqrt{1-\frac{m_f^2}{E^2}}\theta(E-m_f) \\ &\times \int_0^\pi d\theta \sin\theta \left\{64E^2\left((E^2+m_f^2)+(E^2-m_f^2)\cos^2\theta\right)\right\}. \end{aligned} \tag{4.8}$$

Substituting the $2 \to 2$ phase space integral for massive final state particles, Eqn. (C.10), we evaluate the total cross-section to be,

$$\sigma_{e^+e^-\to f\overline{f}} = \frac{4\pi\alpha^2Q_f^2}{3q^2}\left\{1+\frac{2m_f^2}{q^2}\right\}\sqrt{1-\frac{4m_f^2}{q^2}}\theta\left(\sqrt{q^2}-2m_f\right). \tag{4.9}$$

Here, we have replaced e by the fine structure constant, $\alpha = e^2/4\pi$. Based on this formula the total cross-section, σ_{TOT}, for the rate of production for all fermions (excluding the electron) is plotted in Figure 4.2. The quarks have a colour degree of freedom, so they appear to contribute 3 times the cross-section that a single fermion of the corresponding charge would—in other words, with respect to QED there are 3 types of each quark. Note from this expression that $\sigma_{e^+e^-\to f\overline{f}}$ drops off sharply with increasing energy. This dramatic *shrinking* of the effective target size is a common feature of high energy cross-sections (it is driven by the force-mediating *propagator* contribution).

Plotting Eqn. (4.9) in the form of Figure 4.2 does show the general prediction for the cross-section as a function of the beam energy (half the centre of mass energy). It gives some indication of the c quark, the τ-lepton and the b-quark thresholds, but these are

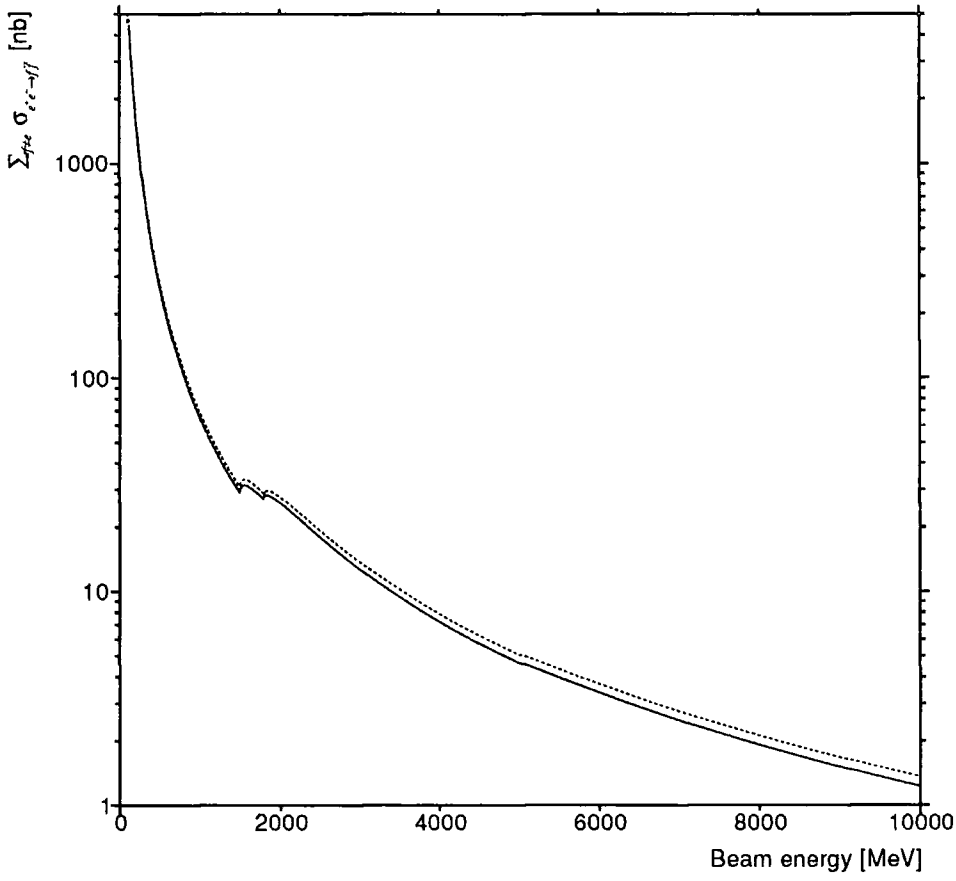

Figure 4.2: The total cross-section for $e^+e^- \to f\overline{f}$ verses half the centre of mass energy: at leading order (full) and after renormalisation of the charge (dotted). To create this graph, we have summed over all final state fermions, excluding the electron, with rest-masses below 10 GeV. The c-quark and τ-lepton thresholds can be seen at 1.5 and 1.8 GeV respectively. The b-quark threshold is barely visible at 5.0 GeV—its contribution to σ_{TOT} is suppressed because of its small electric charge.

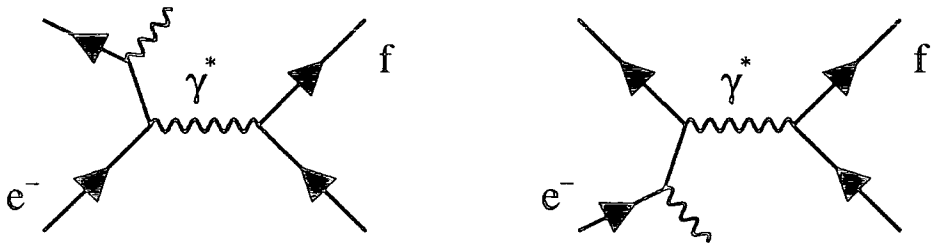

Figure 4.3: Two of the contributions at next-to-leading order (in α) that contribute to the *observed* process $e^+e^- \to f\overline{f}$.

mostly swamped by the $1/q^2$ damping. The experimental cross-section is actually larger than this simple calculation would suggest. This is principally due to large corrections from initial state photon radiation.

4.3 Ratios: more stable predictions

Extending the calculation of the process in Eqn. (4.1) to the next order in the coupling, α, we must at least include the processes illustrated in Figure 4.3. This corresponds to an additional photon being radiated off the incoming particles. For the inclusive $f\overline{f}$ cross-section, where we sum over all additional particles in the final state, all such photons contribute to the observable cross-section. Even when we attempt to exclusively measure the cross-section for this process, such photons can significantly affect the rate. The *observed* final state is that of a $f\overline{f}$ pair in any of the following situations: if the photon carries too little energy to show up in an experimental measurement; or it travels so close to one of the fermions that the two particles seem to be one and the same; or, as is most likely, it escapes detection by accompanying the spectator electrons/positrons in the incident beams *down the beam pipe*. Despite the fact that the radiation of a photon *costs* a power of α, such radiative processes involving un-resolved particles can, in some cases, alter the observed cross-section

considerably. In this case the effect of radiating an initial state photon reduces the q^2 of the virtual photon and (see Figure 4.2) significantly enhances the apparent cross-section.

A more stable calculation, i.e. one that is more likely to compare well at leading order in the perturbative expansion with an experimental measurement, arises from calculating the ratio of two processes with similar radiative corrections. One such observable is the ratio

$$R_{TOT} = \frac{\sum_{f \neq e} \sigma_{e^+e^- \to f\bar{f}}}{\sigma_{e^+e^- \to \mu^-\mu^+}}. \tag{4.10}$$

With respect to Eqn. (4.9), this ratio and the ratio with just quarks in the numerator (R_{HAD}) are plotted in Figure 4.4. The correction (often referred to as the K-factor) associated with un-resolved radiation, such as that of Figure 4.3, is present in both the numerator and the denominator of Eqn. (4.10) and cancels. We therefore expect the computed value to compare with the experimental one. The measured contribution to R_{TOT} from the strongly interacting quarks (R_{HAD}) is larger than this. At higher energies this is principally due to large $\mathcal{O}(\alpha_s)$ corrections. Over most of the area of this graph, however, it can be understood in terms of resonances associated with the production of quark-bound states (hadrons).

It is interesting to note that once we are clearly above each of the threshold regions ($q^2 \gg 4m_f^2$) this quantity, R_{TOT}, reduces to the sum of the squared charges for all *active* fermions,

$$R_{TOT} \approx \sum_{f \neq e} Q_f^2. \tag{4.11}$$

Since we are going to be interested in such ratios, we shall explicitly try to calculate only the final state contribution to the cross-section, and not include the complication of the incoming e^+e^- state. We shall consider a quantity *like* the decay rate of a virtual photon, corresponding to the diagram of Figure 4.5. We shall *sum* over the 3 helicities of the virtual

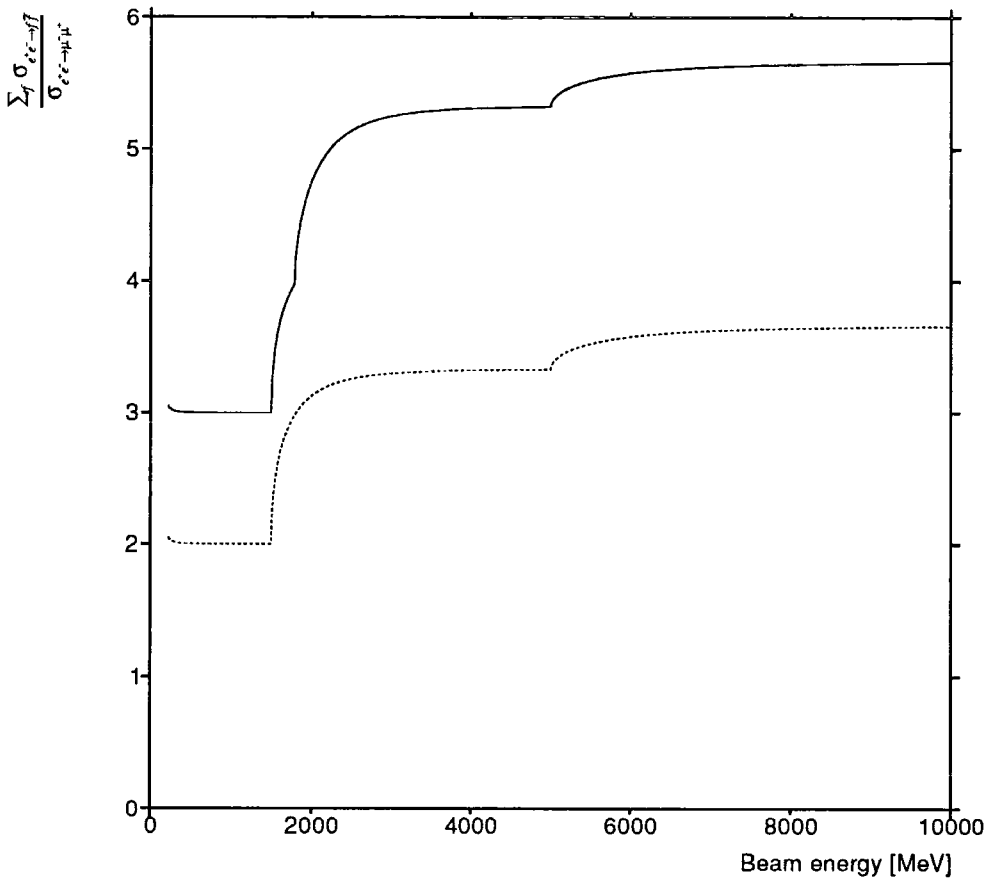

Figure 4.4: The ratio, R_{TOT}, is shown as a full line and the purely hadronic (just quarks) R_{HAD}-ratio is shown dotted. Away from thresholds, these curves take the value of the sum of the squared charges for the corresponding included fermions. Initial state radiation, being similar for the cross-sections in the numerator and denominator of these quantities, makes a comparison with experiment more meaningful.

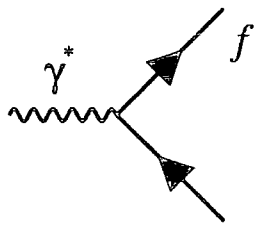

Figure 4.5: A Feynman diagram representing the decay of a virtual photon.

photon as if it were an on shell massive vector boson, using

$$\sum_i \varepsilon_i^{\mu\dagger}\varepsilon_i^{\nu} = -g^{\mu\nu} + \frac{q^\mu q^\nu}{q^2}. \tag{4.12}$$

As was the case with the gauge dependent part of the propagator, a *vector* current will cancel against the $q^\mu q^\nu$ contribution to this sum.

Correspondingly, the matrix element for this process is,

$$\mathcal{M}_0 = \overline{u}_f(p_3)\left(-ieQ_f\gamma^\mu\right)v_f(p_4)\varepsilon_\mu. \tag{4.13}$$

Which leads to the squared matrix element of the form,

$$\begin{aligned}\mathcal{M}_0^\dagger\mathcal{M}_0 &= -e^2Q_f^2\mathrm{Tr}\left\{\not{p}_3\gamma^\mu\not{p}_4\gamma^\nu - m_f^2 g^{\mu\nu}\right\}g_{\mu\nu} \\ &= 4e^2Q_f^2q^2\left\{1+\frac{2m_f^2}{q^2}\right\}.\end{aligned} \tag{4.14}$$

Integrating over the two particle final state phase space (see Eqn. (C.10)) we obtain

$$\mathcal{F}_0(q^2) = \int Dlips_{1\to 2}\mathcal{M}_0^\dagger\mathcal{M}_0 = 2\alpha Q_f^2 q^2\left(1+\frac{2m_f^2}{q^2}\right)\sqrt{1-\frac{4m_f^2}{q^2}}\theta\left(\sqrt{q^2}-2m_f\right), \tag{4.15}$$

which, apart from the factor $2\pi\alpha/3q^4$, has the same form as the total cross-section, Eqn. (4.9). Clearly, a computation for the ratio of e^+e^- cross-sections R_{TOT} (see Figure 4.4), based on

$\mathcal{F}_0$ instead of Eqn. (4.9) will yield the same result.

The generic n-particle decay width for an un-stable particle of a given invariant mass, M, is given by,

$$\Gamma_{1\to n} = \frac{(\text{sym})}{2M} \int Dlips_{1\to n} \left(\overline{\mathcal{M}^\dagger \mathcal{M}}\right)_{decay}. \tag{4.16}$$

As was the case for the cross-section, the factor (sym) is the symmetry factor for averaging over identical bosons in the final state.

The quantity $\mathcal{F}_0$ would simply be the decay-width for the virtual photon if we divided by twice the invariant mass of this photon and a further factor 3 for each its independent polarisations.

4.4 The self-energy of the photon

At the same order in e (or equivalently α) as the initial state radiative corrections associated with Figure 4.3, there is another form of correction. This arises from the purely internal process of $\gamma^* \to f\overline{f} \to \gamma^*$ and can be viewed as a modification to the photon propagator.

Guided by the non-perturbative expansion of Eqn. (2.25), we evaluate the leading contribution to the photon self-energy,

$$i\Sigma_{\mu\nu}(q) = -(e\mu^\epsilon)^2 \sum_f Q_f^2 \int \frac{d^d k}{(2\pi)^d} \frac{\text{Tr}\left\{(\not{q} + \not{k} + m_f)\gamma_\mu(\not{k} + m_f)\gamma_\nu\right\}}{((k+q)^2 - m^2 + i\varepsilon)\,(k^2 - m^2 + i\varepsilon)} \tag{4.17}$$

which corresponds to the Feynman diagram in Figure 4.6. The various contributions to this equation require some explanation.

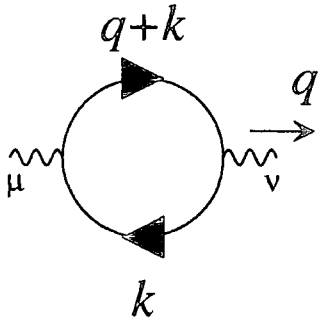

Figure 4.6: The photon self-energy or vacuum polarisation diagram. The virtual photon splits into a virtual fermion-antifermion pair which then annihilate to re-form the photon.

Anticipating problems evaluating the integral in 4 space-time dimensions, we have expressed Eqn. (4.17) as a d-dimensional integral. By making a variable of the number of dimensions over which we perform a divergent (in 4 dimensions) integral, it is possible to parameterise the divergence as a function of the number of dimensions, *dimensional transmutation* [16]. This method is just one of a number of ways to *regulate* divergent integrals [17]. These methods are known as *regularisation* procedures and the one we adopt is that of *Dimensional Regularisation* (DR). It has proved popular because it can regulate both Infra-red (IR) and Ultra-violet (UV) divergences with a single parameter. It also preserves many of the symmetries of a physical Lagrangian, such as gauge invariance and translational invariance.

Whilst we shall be altering the number of space-time dimensions, it is desirable to keep the Action dimensionless. Since each term in the Lagrangian is thus required to have four mass dimensions it becomes necessary to make the coupling e *dimensionful.* Rather than do so implicitly, we introduce an arbitrary parameter, μ, with the dimensions of mass. As we have indicated in Eqn. (4.17), the generalisation of e is thus $e\mu^{\epsilon}$ where we define,

$$\epsilon = \frac{4-d}{2}. \tag{4.18}$$

The vanishingly small ε term in the denominators is defined to be positive and is a technical device to keep track of which side of a branch cut the integrand is positioned. The momentum q, as in Section 4.2, is defined to be the momentum carried by the virtual photon. The *free* momentum, k, that flows around the loop takes all values for its components. When performing the trace we shall be using the convention that $\mathrm{Tr}\{1\} = d$. With this convention the numerator of the integrand in Eqn. (4.17) becomes,

$$d\left(\left(q_\mu + k_\mu\right)k_\nu + k_\mu\left(q_\nu + k_\nu\right) - g_{\mu\nu}(q+k)\cdot k + m_f^2 g_{\mu\nu}\right). \tag{4.19}$$

It is clear that separating each of these terms will lead to a sum of separately divergent integrals; going as k^2 or $\log(k^2)$ in the UV limit ($k^2 \to \infty$).

By evaluating the integral with respect to a well defined regularisation scheme, we are effectively able to quantify the form of each divergence in the integrals. In this way, we can *cancel* one divergence with respect to another and establish how divergent the total integral *really* is. Having done this, we can set about compensating for it: *Renormalisation.*

Using the method of Form Factor Reduction (See Appendix B.4 and [18]) we can re-write Eqn. (4.17) in the form,

$$\begin{aligned} i\Sigma_{\mu\nu}(q) &= (e\mu^\epsilon)^2 \sum_f Q_f^2 \frac{d}{2(d-1)}\left(\frac{q_\mu q_\nu}{q^2} - g_{\mu\nu}\right) \\ &\quad \times \left(\left((d-2)q^2 + 4m_q^2\right) B_0\left(q, m_q, m_q\right) - 2(d-2)A_0\left(m_q\right)\right) \qquad (4.20) \\ &= i\left(\frac{q_\mu q_\nu}{q^2} - g_{\mu\nu}\right)\Sigma(q^2). \qquad (4.21) \end{aligned}$$

Here the scalar functions $A_0(q)$ and $B_0(q, m_f, m_f)$ are defined in Eqn. (D.2) and Appendix D.2.2 respectively.

The photon propagator function for the free theory in the Lorentz gauge (as used in

Eqn. (4.2)) is,

$$G^{(2)}_{0\,\mu\nu}(q) = \frac{i}{q^2}\left(\frac{q_\mu q_\nu}{q^2} - g_{\mu\nu}\right) - i\xi\frac{q_\mu q_\nu}{q^4}. \tag{4.22}$$

Now, since $(q_\mu q_\nu/q^2 - g_{\mu\nu})q^\nu = 0$, it follows that the approximation of the connected (or full) propagator (cf. Eqn. (2.25)) that results from Eqn. (4.20) is,

$$G^{(2)}_{c\,\mu\nu}(q) = \frac{-i}{q^2 + \Sigma(q^2)}\left(g_{\mu\nu} - \frac{q_\mu q_\nu}{q^2}\right) - i\xi\frac{q_\mu q_\nu}{q^4}. \tag{4.23}$$

As is clear from this expression, the choice $\xi = 1$ is no longer the Feynman gauge. However, this is not a problem since the gauge dependent terms, $\sim q_\mu q_\nu$, cancel when contracted into a fermionic vector current.

Substituting for A_0 and B_0 in Eqn. (4.20) we have,

$$\Sigma(q^2) = -\sum_f \frac{e^2Q_f^2}{8\pi^2}\Gamma(1+\epsilon)\left(\frac{4\pi\mu^2}{m_f^2}\right)^\epsilon \frac{2-\epsilon}{\epsilon(3-2\epsilon)}\left(2m_f^2(1-\mathcal{I}_\epsilon) - q^2\mathcal{I}_\epsilon(1-\epsilon)\right). \tag{4.24}$$

$\mathcal{I}_\epsilon$ is defined in Appendix D.2.2.

The physical limit ($d \to 4$) of this expression diverges, since this is the $\epsilon \to 0$ limit and $\Sigma(q^2) \sim 1/\epsilon$. This represents the *total* UV divergence of $i\Sigma_{\mu\nu}$ as it is defined in Eqn. (4.17). With respect to a series expansion in ϵ, however, there are a number of *finite* terms, $\sim \epsilon^0$. It is these finite factors, and notably those which depend on q^2, that contain the *physics* of this expression.

To what extent we expand the various factors as a series in ϵ, is a matter of convention. There are two popular choices: that of Minimal Subtraction (MS), where all contributions containing the ϵ parameter are expanded; and the Modified Minimal Subtraction ($\overline{\text{MS}}$) approach where the ubiquitous factor $(4\pi)^\epsilon\Gamma(1+\epsilon)$ is not expanded. The divergence

of Eqn. (4.24) in these two schemes is thus,

$$\begin{aligned} \text{MS} \qquad & \sum_f \tfrac{e^2Q_f^2}{12\pi^2} q^2 \tfrac{1}{\epsilon} \\ \overline{\text{MS}} \quad q^2\Sigma_0 \;\; &= \;\; \sum_f \tfrac{e^2Q_f^2}{12\pi^2} q^2 \left(\tfrac{1}{\epsilon} + \log(4\pi) - \gamma_E + \mathcal{O}(\epsilon)\right). \end{aligned} \tag{4.25}$$

In the $\overline{\text{MS}}$ term we have, for the purpose of comparison, expanded the factor $\Gamma(1+\epsilon)$ (using Eqn. (A.7)). Because it is more efficient, we shall adopt $\overline{\text{MS}}$ when regularisation is required. We define,

$$q^2\Sigma'(q^2) = \Sigma(q^2) - q^2\Sigma_0. \tag{4.26}$$

The finite correction to the self-energy $\Sigma'(q^2)$, is well behaved in $\epsilon \to 0$ limit. In this limit it takes the form,

$$\Sigma'(q^2) = \sum_f \frac{e^2Q_f^2}{12\pi^2}\left(\left(1 + \frac{2m_f^2}{q^2}\right)\mathcal{J} + \log\left(\frac{\mu^2}{m_f^2}\right) - \frac{5}{6}\right) \tag{4.27}$$

where, we define $\mathcal{J} = (\mathcal{I}_\epsilon - 1)/\epsilon$. We note that in the small q^2 limit, the term in $\mathcal{J}$ actually converges and the above expression reduces to a constant.

Writing $Z = 1/(1+\Sigma_0)$, the full propagator, $G^{(2)}_{c\,\mu\nu}(q)$, can be written in the following manner,

$$G^{(2)}_{c\,\mu\nu}(q) = \frac{-iZ}{q^2(1+Z\Sigma'(q^2))}\left(g_{\mu\nu} - \frac{q_\mu q_\nu}{q^2}\right) - i\xi\frac{q_\mu q_\nu}{q^4}. \tag{4.28}$$

Recalling that whenever we *use* a propagator it is always to join two vertices which each contribute a coupling, e. We see that this Z in both the numerator and the denominator is always accompanied by a factor e^2. Accordingly, we can redefine (*renormalise*) the coupling by replacing it with $e_R^2 = Ze^2$. The full propagator becomes,

$$G^{(2)}_{R\,\mu\nu}(q) = \frac{-i}{q^2(1+\Sigma'_R(q^2))}\left(g_{\mu\nu} - \frac{q_\mu q_\nu}{q^2}\right) - \frac{i\xi}{Z}\frac{q_\mu q_\nu}{q^4} \tag{4.29}$$

with respect to an effective set of Feynman rules that are valid to 1-loop, and have a coupling of strength, e_R. The value of e_R is determined by our *arbitrary* choice for μ (of Eqn. (4.17)) and an experimental measurement at one q^2. As was the case with e in the more naive first order identification of Section 3.5, we identify the $q^2 \to 0$ limit (in fact we choose the space-like point; $q^2 = -m_e^2$) with the classical coulomb law,

$$\frac{e_R^2}{1 + \Sigma'_R(-m_e^2)} = 4\pi\alpha. \tag{4.30}$$

The fact that $\Sigma'(q^2)$ reduces to a constant in the $q^2 \to 0$ limit, implies that the photon remains *massless* even after renormalisation.

An alternative, but equivalent interpretation of Eqn. (4.28), is to say that the coupling *runs* with q^2. Conventionally, we define $\alpha_R = e_R^2/4\pi$ and use a *normal* propagator (Eqn. (4.22)) with a *varying* coupling constant,

$$\alpha(q^2) = \left| \frac{\alpha_R}{1 + \Sigma'_R(q^2)} \right|^{1/2}. \tag{4.31}$$

In the large $|q^2|$ limit, this expression is found to reduce to the following simple form,

$$\alpha(q^2) = \frac{\alpha_R}{1 - \frac{\alpha_R}{3\pi} \sum_f Q_f^2 \log\left(\frac{|q^2|}{\mu^2}\right)}. \tag{4.32}$$

It is natural, in such a limit, to say that $\alpha_R = \alpha(\mu^2)$, that is to say μ is the *renormalisation scale.*

For *all* of the charged quarks in the SM, we have plotted this running coupling constant over the full range up to the LEP energy; Figure 4.7. We observe that $\alpha((M_Z = 91\ \text{GeV})^2) \approx 1/128$. The evolution is most sensitive to the masses of the lightest quarks—reducing their masses from 5 to 1 MeV increases $\alpha(M_Z^2)$ to $\approx 1/127$. The contribution from the extremely

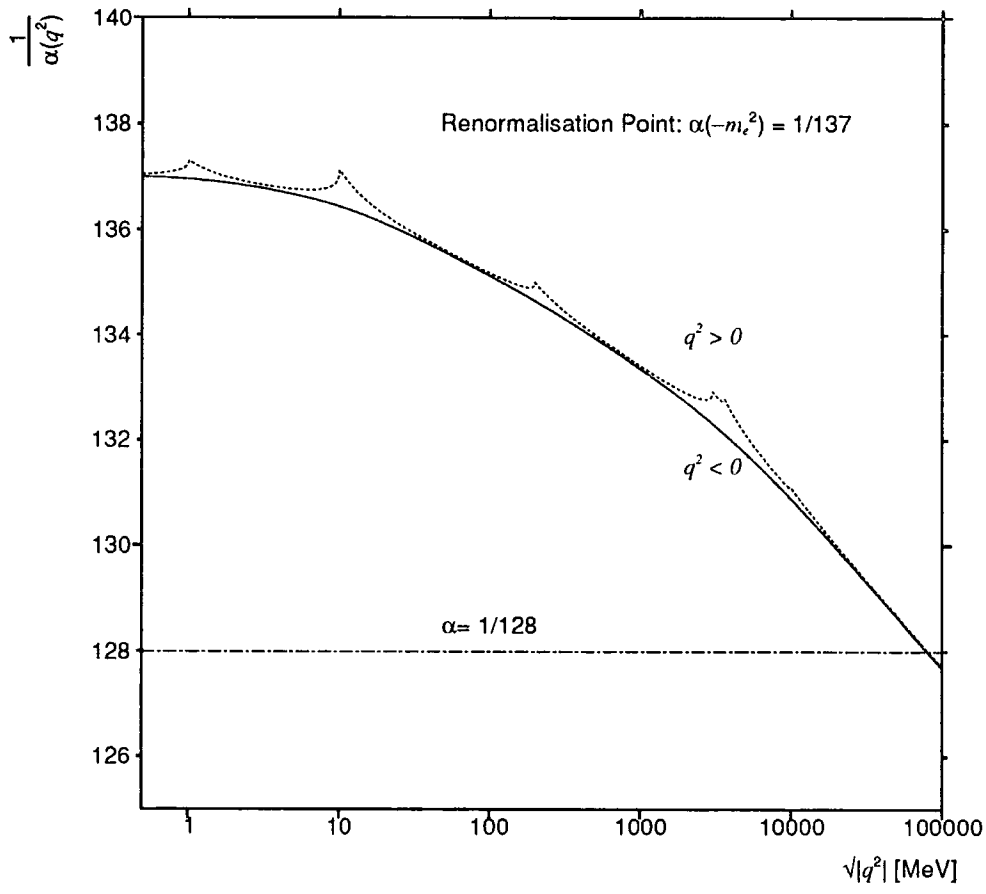

Figure 4.7: The running coupling $\alpha(q)$ plotted as a function of $\sqrt{|q^2|}$ for both time-like (dotted) and space-like virtual photons (full). The two lines differ principally at the threshold regions for $f\overline{f}$ production.

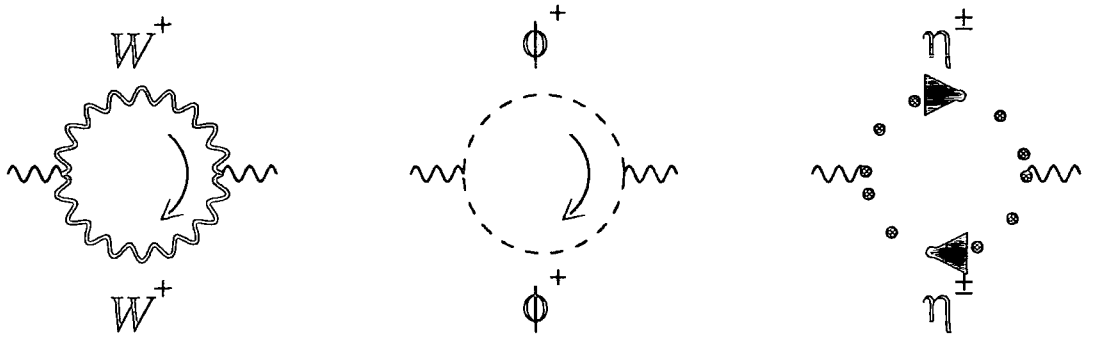

Figure 4.8: The Electroweak modification to the self-energy of the photon. The ghost loops (there are two of these diagrams) contain an implicit minus sign because the ghosts are fermionic.

heavy *top* quark is negligible; $< .01\%$ at M_Z.

Further, using the rules developed in Chapter 10, we can evaluate the $W^{\pm}$ contribution to the self-energy, as represented in Figure 4.8—this corresponds to the extension of QED to the full Electroweak theory. The corresponding contribution can be written as a modification to the photon self energy, Eqns. (4.25 and 4.27), of the form,

$$\overline{\text{MS}} \qquad \Sigma_0^W = -\frac{7e^2}{16\pi^2}(4\pi)^\epsilon\Gamma(1+\epsilon)\frac{1}{\epsilon} \qquad \Sigma'_W(q^2) = -\frac{7e^2}{16\pi^2}\left(\left(1+\frac{4M_W^2}{7q^2}\right)\mathcal{J} + \log\frac{\mu^2}{M_W^2}\right). \tag{4.33}$$

This contribution, like that of the top quark, is negligible in the range of energies accessible to LEP. In the space-like region ($q^2 = -M_Z^2$) it *decreases* the effective coupling by $\sim 0.1\%$. This is also true of the time-like contribution at energies well above twice the mass of the W-boson. However, below the W^+W^- threshold, which occurs at $q^2 = 4M_Z^2\cos^2\theta_W$, there is a small tail to the resonance in Σ'_W that actually increases the value of $\alpha(q^2 = M_Z^2)$: the resonance is of the same type as the fermionic ones, but enters with a relative minus sign. The level of this effect is $\sim 0.1\%$, and is insufficient to change the value $\alpha(M_Z^2)$ from $\approx 1/128$.

4.5 The optical theorem

We return to the unitary property of the S-matrix as it was expressed in Eqn. (2.6). In matrix element language, contracted between two identical states, $|\alpha\rangle$, it corresponds to the expression,

$$\langle\alpha|\hat{T}^\dagger\hat{T}|\alpha\rangle = \sum_\beta \left|\langle\beta|\hat{T}|\alpha\rangle\right|^2 = 2\mathrm{Im}\langle\alpha|\hat{T}|\alpha\rangle, \tag{4.34}$$

where the sum is over all physical *states*, $|\beta\rangle$. This relation is known as the *optical theorem.* We shall give an example of its validity related to the virtual photon of the previous sections and then, in the next section, use it to motivate some Z-particle phenomenology.

If $|\alpha\rangle$ is a *virtual* photon state decaying as in Figure 4.5, then this expression may be rewritten in terms of the decay-like quantity $\mathcal{F}_0$ (of Eqn. (4.15)),

$$\mathcal{F}_0(q^2) = 2\mathrm{Im}\left(-g^{\mu\nu}\Sigma_{\mu\nu}(q)\right). \tag{4.35}$$

The imaginary contribution to $\Sigma_{\mu\nu}(q)$ is all from the finite contribution to the self-energy and accordingly is not divergent with respect to ϵ. Applying $-g^{\mu\nu}$ to the $(q_\mu q_\nu/q^2 - g_{\mu\nu})$ part of $\Sigma_{\mu\nu}$ can be seen to give a factor of $(d-1)$. This equals the number of independent *helicities* of the virtual photon. The consequence of this is that the *imaginary part* of the propagator's denominator is directly proportional to the *decay width* for the propagating particle. With reference to the definition of a particle's decay width (Eqn. (4.16)) we see that

$$\mathrm{Im}\ \Sigma(q^2) = \sqrt{q^2}\ \Gamma_{TOTAL}. \tag{4.36}$$

4.6 The Breit-Wigner propagator and the Z resonance

At higher energies the process $e^+e^- \to f\overline{f}$ receives a significant contribution from the intermediate creation of a Z-boson. For the massive Z-boson, the argument of Section 4.4 is modified. The *free* Z-propagator (cf. that for the photon, Eqn. (4.22)) is,

$$G^{(2)Z}_{0\,\mu\nu}(q) = \frac{-i}{q^2 - M_Z^2}\left(g_{\mu\nu} - (1-\xi)\frac{q_\mu q_\nu}{q^2 - \xi M_Z^2}\right). \tag{4.37}$$

This function is apparently singular at the point $q^2 = M_Z^2$. Neglecting the gauge dependent terms (for a recent discussion of this part see [19]), the same analysis as before leads to a full propagator with a denominator of the form,

$$q^2 - M_Z^2 + \Sigma_Z(q^2). \tag{4.38}$$

In this case it is the *mass* that we renormalise. By absorbing *all* of the real component of $\Sigma_Z(q^2)$, which includes the divergences, we create a *running* renormalised mass for the Z-boson, $M_Z(q^2)$. The renormalisation point for this mass is taken to be the experimental mass of the particle; $M_{Z,expt} = M_Z(M^2_{Z,expt})$. The experimental mass is determined from the position of the peak in the $e^+e^- \to f\overline{f}$ cross-section, which is associated with the vanishing of the real contribution to this denominator—its resonance[1]. Here this denominator reduces to the pure imaginary component of $\Sigma_Z(q^2)$.

In the previous section, we established that the imaginary component is nothing other than the decay width of the propagating Z. So we can formally re-write the above denomi-

[1] Unfortunately, radiative corrections of the type in Figure 4.3 can shift the resonance peak to higher energies; we shall not address that complication here.

nator in the region of the resonance, as

$$q^2 - M^2_{Z,expt} + iM_{Z,expt}\Gamma_{TOTAL}. \tag{4.39}$$

With this denominator we obtain the so called *Breit-Wigner* form for the Z propagator.

We can calculate the decay rate for the Z boson. It is the sum of the partial decays of the Z to fermions lighter than $M_Z/2$. The process is pictorially the same as that of Figure 4.5 but with a Z-boson instead of a virtual photon. The matrix element is given by,

$$\mathcal{M}_{Z\to f\bar{f}} = \overline{u}(p_3)\; ie\gamma^\mu\left(v_f - a_f\gamma_\mu\right)\; v(p_4)\varepsilon_\mu. \tag{4.40}$$

Taking the square and *averaging* over the three initial polarisations of the Z (with reference to Eqn. (4.12) and Section E.1), the mean squared amplitude has the form,

$$\left(\overline{\mathcal{M}^\dagger\mathcal{M}}\right)_{Z\to f\bar{f}} = \frac{4}{3}e^2(v_f^2 + a_f^2)q^2\left(1 + \frac{2m_f^2}{q^2}\right) - 8e^2a_f^2m_f^2. \tag{4.41}$$

The axial contribution does not cancel against the $(q^\mu q^\nu)$ part of the helicity sum, leading to a modification of the simple vector result for the virtual photon decay, Eqn. (4.14). To a good approximation, however, this additional term is negligible as it is suppressed by a factor of m_f^2/q^2 (which is $\sim 3\times10^{-3}$ for the largest of the included quarks—the b). Indeed, to a very good approximation we can neglect the fermion masses completely. In this limit the partial decay width at the Z-resonance ($q^2 = M^2_{Z,expt}$) is simply, (see Eqns. (4.16 and C.10))

$$\Gamma_{Z\to f\bar{f}} = \frac{M_{Z,expt}\alpha(M^2_{Z,expt})}{3}\left(v_f^2 + a_f^2\right). \tag{4.42}$$

Substituting the values contained in Table 4.1 yields the following statistics,

Fermion type	Decay-width in GeV	Branching ratio in %
quarks, q	1.69	69
neutrinos, ν	0.50	21
leptons, l	0.25	10
all fermions	2.45	100

(4.43)

It is interesting to note that 21% of the decays are to neutrinos, which are massless and without electric charge; they are extremely difficult to detect giving rise to an *unseen* decay. They only reveal themselves in their contribution to the propagator; namely, in a reduction of the resonant cross-section. The experimental measurements agree well with these numbers, except for the hadronic width (decay via quarks) for which the observed width is 1.735 ± 0.011 GeV [15]. We shall see that this can be explained in terms of a $\mathcal{O}(\alpha_s)$ correction to the hadronic decay width.

To give some idea of the enhancement in the cross-section for $e^+e^- \to f\overline{f}$, we have plotted the cross-section in the region of the Z resonance using the theory reviewed in this chapter; Figure 4.9. It includes both γ and Z-exchange for the coupling, $\alpha(M_Z) = 1/128$. We indicate the unseen neutrino contribution to the total cross-section. As was the case previously, this cross-section receives significant modifications when initial state photon radiation is included. It has the effect of modifying the Z peak: moving it to higher energies, reducing its height and broadening it. The experimental cross-section reflects this.

By running the LEP collider at a centre of mass energy equal to the rest-mass of the Z, a large number of events have been observed. By far the largest number of these events ($\sim 90\%$) have been via quark production.

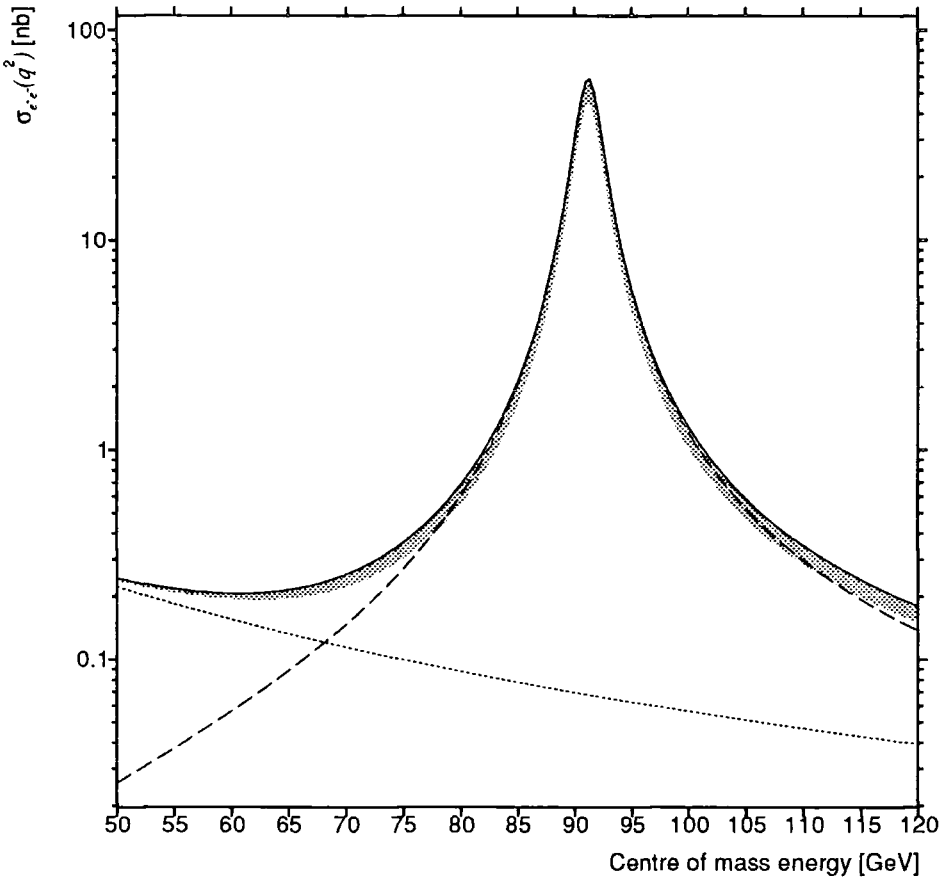

Figure 4.9: The Z-resonance. Here we plot the total cross-section for $e^+e^- \rightarrow f\overline{f}$ (again we exclude the electron). The three contributions are plotted: all channels (full); just γ-exchange (dotted); just Z-exchange (dashed). The shaded region indicates the *unseen* neutrino component to the total cross-section.

4.7 Quarks and hadrons

The form of the W-loop contribution to the self-energy of the photon is given in Eqn. (4.33). Although small, it is interesting from the point of view that it has the opposite sign to that of the fermionic contribution, Eqn. (4.25). This is characteristic of non-abelian (self-coupling) theories and leads to *weakening* contributions in the running of the effective coupling with increased energy.

It follows in those theories where there are sufficient *flavours* of gauge boson, with respect to the number of active fermions, that the *overall* sign accompanying the self-energy contribution is *positive*. Such theories are said to be *asymptotically free* because with higher and higher energies their constituent fields behave increasingly as if they *are* free particles. QCD, with eight gluons and six quarks, is believed to be of this type. [20]

In spatial terms, this leads to the notion of *confinement*—when left unexcited, the strongly interacting gluons and quarks, each possessing colour, *freeze* themselves into *colourless* (colour *singlet*) combinations known as *hadrons*. It is only with respect to small distance scales (large *probing* momenta) that it becomes a good approximation to say that the quarks and gluons behave as almost free particles. In such extremes, the first few terms of a perturbative expansion in the (effective) coupling can be used to calculate observable interaction probabilities. If we attempt to separate such particles, then they begin to interact/radiate more strongly—to the point that they can confine themselves again with *new* particles created from the resource of their enormous binding energy. The method of perturbative calculation, at fixed order in the appropriate coupling, g_s, is insufficient to describe this *hadronisation*. For this reason, it is often said to be a *non*-perturbative process.

Whilst the dynamics of such a process is not currently understood, two important features

of this *fragmentation* are assumed to hold true. (a) Momentum conservation is obeyed, and (b) *fragmentation* can be considered a *late* time phenomena—it is a process governed by relatively long distances (small $|q^2|$). These two notions lead to the observation that at sufficiently high energy, the coloured quarks and gluons (*partons*) dictate the subsequent *hadronic* momentum flow *after* hadronisation. In effect, for high enough energies the *hard* process that underlies the formation of hadrons is nothing other than a simple partonic event.

The experimental observation is that of *jets* of hadrons often in well collimated cones. These jets are felt to be the footprint of their hard parton initiators. To some extent, softer calculated partons will dictate the distributions of momentum with respect to the predominant direction of the leading jets in an event. Complete fixed order calculations are currently limited by technical difficulty to just three partons in the final state at next-to-leading order[2]. This can be compared with twenty or more final state hadrons in a typical event at LEP. By leading order, we mean that each parton separately leads to a jet in the final state and by next-to-leading order that one of the calculated partons does not form a jet—it is not *resolved* in the final state. The definition of what constitutes a jet in an individual event is conveniently made with respect to a *jet algorithm*. We shall elaborate on two of the more popular choices for these algorithms at LEP in the next chapters.

The difficulty of many parton calculations has led to the construction of hadronisation models. These are models inspired by aspects of perturbative QCD calculations, but are sufficiently flexible so as to produce realistic numbers of final state particles that can be tuned to mimic experimental distributions. Such models provide a good working description of the products of hadronisation and have become a valuable tool in high energy physics.

[2]Recently, progress has been made to the level of calculating *five* parton processes at next-to-leading order [21, 22, 23]. But as yet, these calculations are for all massless external states which excludes them from use in four-particle final state calculations at LEP.

[24]

The notion that at the heart of high energy hadronic interactions there is a governing hard partonic event leads to a *factorisation* in the method of calculation. The interaction of hadrons, in sufficiently energetic configurations, can be *factored* into probability distributions describing the partonic content of the participating hadrons and a series of hard underlying partonic interactions. The philosophy underlying this approach being that the hard partonic process occurs over a characteristically short time period and is insensitive to the softer physics of the hadron.

With respect to the initial state, we speak of parton (probability) density functions, $f_{a/h}(x)$, which each correspond to the probability of finding a given parton, a, in a given hadron, h. The quantity x is related to the fraction of h's momentum that is carried by a. For a recent set of such functions for the proton, as constrained by world data, we refer the reader to [25]. For the final state, the relationship is reversed and the probability densities are termed *fragmentation functions*[3], $D_{a\to h}(x)$, where this represents the probability that a parton, a, will become a hadron, h.

At LEP, incoming *elementary* particles, e^+e^-, interact overwhelmingly via the mediation of a Z-boson and generally there is little need to introduce parton densities. At other energies, the interaction of high energy bremsstrahlung photons that radiate off the incoming electrons can provide a significant contribution to the observed cross-section. In such cases, these photons can often be considered to be *like* neutral mesons and correspondingly they can be parameterised in terms of *parton densities*, $f_{a/\gamma}(x)$ or the associated function F_2^γ. For a recent review we refer the reader to [26].

As for the hadronic final states, based on the fact that all hadronic final states must

[3]The notation $D_{h/a}(x)$ is also used.

initiate from $q\overline{q}$ production, we can just consider the total hadronic cross-section where we implicitly sum over all possible fragmentations, i.e. multiply by one! This is addressed in the next section. More challenging is the calculation of *jet* production rates. With next-to-leading-order calculations, where we begin to calculate the substructure of jets, the energy distributions amongst such jets can also be calculated. [27, 28]

4.8 The total hadronic width at next-to-leading-order

The leading order hadronic decay width has been calculated above (see 4.43) and represents $\sim$ 70% of the total decay rate. In this section, we calculate the leading, $\mathcal{O}(\alpha_s = g_s^2/4\pi)$, correction to this, with respect to the radiation of a single gluon. In this calculation, justified by our previous results, we treat the final state particles as massless. In such a limit there is no difference in the *form* of the decay rate of a virtual photon and a Z-boson, so we shall concern ourselves with the virtual photon decay only.

The Feynman diagrams for the amplitudes we require are given in Figure 4.10. The first four diagrams are for the 2-particle final states and have potential interferences. The remaining two diagrams are for the 3-particle final state, involving the *real emission* of a final state gluon.

We first address the two diagrams with fermion self-energy loops, Figures 4.10c and 4.10d. These figures contain factors of the form,

$$\sim \overline{u}_i(p_q)\gamma^\mu \frac{\not{p}_q + \not{k}}{(p_q+k)^2 + i\varepsilon}\gamma_\mu = (2-d)\left(B_0(p_q) + B_1(p_q)\right)\overline{u}_i(p_q)\not{p}_q, \tag{4.44}$$

where B_0 and B_1 are lorentz invariant scalar functions of p_q^2 (see Eqns. (B.24, D.3 and E.6)).

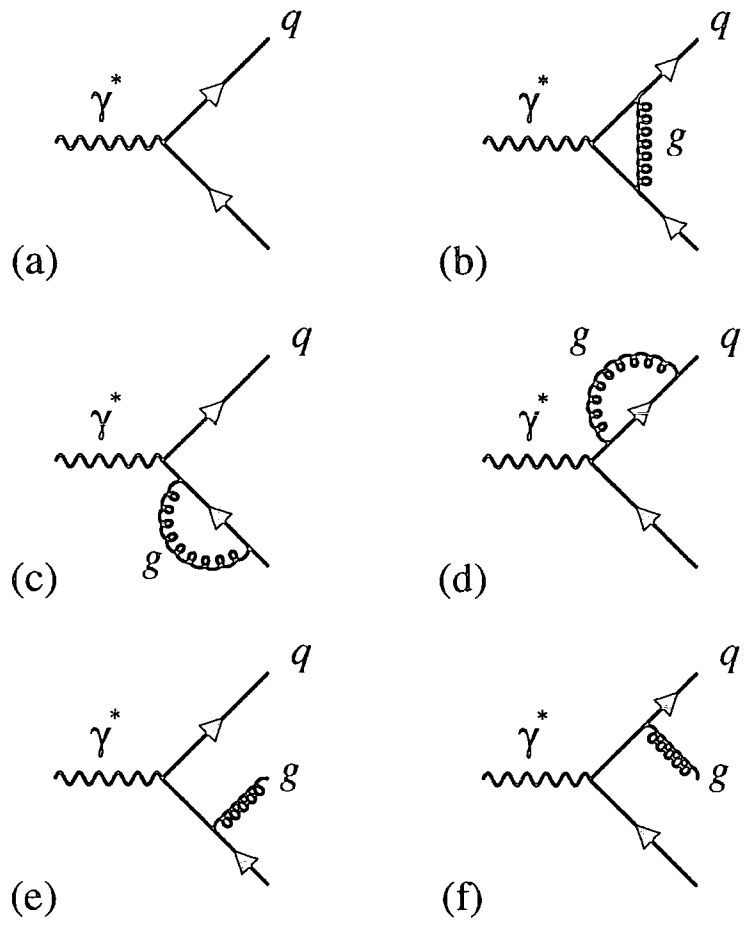

Figure 4.10: The Feynman diagrams required for the calculation of the $\mathcal{O}(\alpha_s)$ hadronic decay width.

Since the quarks are taken to be massless, these two amplitudes identically vanish.

It is the *interference* between the two diagrams 4.10a and 4.10b, and the squared sum of 4.10e and 4.10f that contribute to the $\mathcal{O}(\alpha_s)$ correction to the inclusive decay width. Except for Figure 4.10a, each of these diagrams is divergent over some region of its integrated phase-space. Unlike the divergences of Sections 4.4 and 4.6, these divergences are of the IR variety. They correspond to the regions of phase-space where the invariant mass of the quark(or antiquark) and gluon *combined* vanishes. As a consequence of the Bloch-Nordsiek [50] and Kinoshita-Lee-Nauenberg [29] theorems, the divergences will be seen to be an artifact of our method of calculation and in fact there is no overall divergence at each order in the coupling. These theorems basically say that, if a calculated observable is insensitive to the IR limits, then its complete calculation at each order in perturbation theory must be finite.

Because of the divergences, we shall calculate in $(4-2\epsilon)$-dimensions. The leading order amplitude is, (cf. Eqn. (4.13))

$$\mathcal{M}_0^\epsilon(q) = -i(e\mu^\epsilon)Q_q\ \overline{u_i}(p_q)\not{\epsilon}_\gamma v_j(p_{\overline{q}})\ \delta_{ij}, \tag{4.45}$$

where we have explicitly written out the colour indices for the quarks, (ij). In $(4-2\epsilon)$ dimensions, Eqns. (C.6, E.6 and E.7), the squared matrix element integrated over the final state phase-space is

$$\mathcal{F}_0^\epsilon(q^2) = \alpha Q_q^2 q^2 N \left(\frac{4\pi\mu^2}{q^2}\right)^\epsilon \frac{\Gamma(1-\epsilon)}{\Gamma(1-2\epsilon)} \frac{(2-\epsilon)(1-\epsilon)}{(1-2\epsilon)}. \tag{4.46}$$

$\mathcal{F}_0^\epsilon(q^2)$ is the decay-like quantity we introduced previously, but calculated here for massless quarks in $(4-2\epsilon)$ dimensions. It can be compared with Eqn. (4.15) in the $m_f \to 0$ limit.

The correction to this vertex, Figure 4.10b, in the Feynman gauge ($\xi = 1$) is given by,

$$\mathcal{M}_2^\epsilon(q) = -(e\mu^\epsilon)Q_q\,(g_s\mu^\epsilon)^2 \int \frac{d^dk}{(2\pi)^d}\overline{u_i}(p_q)\gamma^\mu \frac{\not{k}+\not{p}_q+\not{p}_{\overline{q}}}{(k+p_q+p_{\overline{q}})^2+i\varepsilon}\not{\epsilon}_\gamma \frac{\not{k}}{k^2+i\varepsilon}\gamma_\mu v_j(p_{\overline{q}})\,T^a_{ik}T^a_{kj}. \tag{4.47}$$

It corresponds to the emission and re-absorption of a virtual gluon across the photon vertex, i.e. *between* the quark and anti-quark. This amplitude can be reduced (see Section B.4 and Eqn. (F.13)) to the following form,

$$\mathcal{M}_2^\epsilon(q) = +i(g_s\mu^\epsilon)^2\frac{N^2-1}{2N}\left((3+2\epsilon)B_0(p_q+p_{\overline{q}}) + 2q^2C_0(p_q,p_{\overline{q}})\right)\mathcal{M}_0^\epsilon(q) \tag{4.48}$$

For a complex number, $\mathcal{C}$, we note that $|1+ig_s^2\mathcal{C}|^2 = 1 - 2g_s^2\mathrm{Im}\mathcal{C} + \mathcal{O}(g_s^4)$. We write $(-1)^\epsilon = \exp(\pm i\pi\epsilon)$ and contract over the polarisations of the virtual photon with Eqn. (4.12) to give the $\mathcal{O}(\alpha_s = g_s^2/4\pi)$ integrated amplitude squared,

$$\begin{aligned}\mathcal{F}_2^\epsilon(q) \;=\; & \left(1 - \frac{\alpha_s}{2\pi}\frac{N^2-1}{2N}\left(\frac{4\pi\mu^2}{q^2}\right)^\epsilon \frac{\Gamma(1+\epsilon)\Gamma^2(1-\epsilon)}{\Gamma(1-2\epsilon)}\cos(\pi\epsilon)\left\{\frac{3+2\epsilon}{\epsilon(1-2\epsilon)}+\frac{2}{\epsilon^2}\right\}\right)\mathcal{F}_0^\epsilon(q^2) \\ & +\mathcal{O}(\alpha_s^2),\end{aligned} \tag{4.49}$$

where the suffix 2 indicates that this is the $\mathcal{O}(g_s^2)$ improved $\mathcal{F}_0^\epsilon$. The term of $\mathcal{O}(\alpha_s)$ is the *interference* of Figures 4.10a and 4.10b.

Next, we turn our attention to the pair of three final state particle amplitudes of Figures 4.10e and 4.10f (which do not interfere with the previous two particle ones). The matrix elements for the two processes sum to give,

$$\mathcal{M}_3^\epsilon(q) = i(e\mu^\epsilon)Q_q\,(g_s\mu^\epsilon)\,\overline{u_i}(p_q)\left[\not{\epsilon}_\gamma\frac{\not{p}_{\overline{q}}+\not{p}_g}{(p_{\overline{q}}+p_g)+i\varepsilon}\not{\epsilon}_g - \not{\epsilon}_g\frac{\not{p}_q+\not{p}_g}{(p_q+p_g)+i\varepsilon}\not{\epsilon}_\gamma\right]v_j(p_{\overline{q}})\,T^a_{ij}. \tag{4.50}$$

The helicity sum for massless gauge bosons in the lorentz gauge is,

$$\sum_i \varepsilon_i^{\mu\dagger}\varepsilon_i^{\nu} = -g^{\mu\nu}. \tag{4.51}$$

Using this and expressing the result in terms of the dimensionless invariants,

$$y_{rs} = \frac{(p_r + p_s)^2}{q^2} = \frac{2p_r \cdot p_s}{q^2}, \tag{4.52}$$

the matrix element squared and summed over the helicities of the particles is,

$$4(e\mu^\epsilon)^2 Q_q^2\,(g_s\mu^\epsilon)^2\,\frac{N^2-1}{2}(2-\epsilon)(1-\epsilon)\left\{\frac{2y_{q\bar{q}}}{y_{qg}y_{\bar{q}g}} + (1-\epsilon)\left[\frac{y_{qg}}{y_{\bar{q}g}} + \frac{y_{\bar{q}g}}{y_{qg}}\right]\right\}. \tag{4.53}$$

We have neglected some $\mathcal{O}(\epsilon)$ terms from this expression. It is safe to do this because they do not accompany any invariants in the denominator, and consequently they cannot contribute finite terms in the limit, $\epsilon \to 0$.

We perform the phase space integrals to obtain the following expression for the integrated amplitude squared (for reference this is via: Eqns. (C.15 and 4.46), a change of variables $x = y_{qg}$ with $z = y_{\bar{q}g}/(1-y_{qg})$ and repeated use of Eqn. (A.10)),

$$\mathcal{G}_2^\epsilon(q^2) = \left(\frac{\alpha_s}{2\pi}\frac{N^2-1}{2N}\left(\frac{4\pi\mu^2}{q^2}\right)^\epsilon \frac{\Gamma^2(1-\epsilon)}{\Gamma(1-3\epsilon)}\left\{2\frac{1-\epsilon}{1-3\epsilon}\left(\frac{1}{\epsilon^2} - \frac{1-\epsilon}{\epsilon(2-3\epsilon)}\right)\right\}\right)\mathcal{F}_0^\epsilon(q^2) \tag{4.54}$$

The divergences, as can be seen from Eqn. (4.53), correspond to the limits that y_{qg} and $y_{\bar{q}g}$ vanish.

Using the expansion for the function $\Gamma(1+z)$ given in Eqn. (A.7), we find that

$$\frac{\Gamma(1-2\epsilon)}{\Gamma(1+\epsilon)\Gamma(1-3\epsilon)} = \exp\left\{-\frac{6}{2}\zeta(2)\epsilon^2 + O(\epsilon^3)\right\}. \tag{4.55}$$

and since $\zeta(2) = \frac{\pi^2}{6}$ we have,

$$\frac{1}{\Gamma(1-3\epsilon)} = \frac{\Gamma(1+\epsilon)}{\Gamma(1-2\epsilon)}\cos(\pi\epsilon) + O(\epsilon^3). \tag{4.56}$$

Thus we can add $\mathcal{F}_2^\epsilon$ and $\mathcal{G}_2^\epsilon$ to obtain the total, $\mathcal{O}(\alpha_s)$, hadronic decay rate,

$$\begin{aligned}\mathcal{H}_2^\epsilon(q^2) &= \mathcal{F}_2^\epsilon(q^2) + \mathcal{G}_2^\epsilon(q^2) \\ &= \left(1 + \mathcal{K}^\epsilon\left[2\frac{1-\epsilon}{1-3\epsilon}\left(\frac{1}{\epsilon^2} - \frac{1-\epsilon}{\epsilon(2-3\epsilon)}\right) - \left(\frac{3+2\epsilon}{\epsilon(1-2\epsilon)} + \frac{2}{\epsilon^2}\right)\right]\right)\mathcal{F}_0^\epsilon(q^2),\end{aligned} \tag{4.57}$$

where,

$$\mathcal{K}^\epsilon = \frac{\alpha_s}{2\pi}\frac{N^2-1}{2N}\left(\frac{4\pi\mu^2}{q^2}\right)^\epsilon \frac{\Gamma(1+\epsilon)\Gamma^2(1-\epsilon)}{\Gamma(1-2\epsilon)}\cos(\pi\epsilon). \tag{4.58}$$

Expanding the contents of the square brackets of Eqn. (4.57) as a series in ϵ, we find that all the negative powers in ϵ *cancel.* Indeed,

$$\mathcal{H}_2^\epsilon(q^2) = \left(1 + \mathcal{K}^\epsilon\left[\frac{3}{2} + \mathcal{O}(\epsilon)\right]\right)\mathcal{F}_0^\epsilon(q^2). \tag{4.59}$$

Since no negative powers remain in this expression, we can safely take the $(\epsilon \to 0)$ limit and find (for $N = 3$ of QCD)

$$\frac{\mathcal{H}_2(q^2)}{\mathcal{F}_0(q^2)} = 1 + \frac{3\alpha_s}{4\pi}\frac{N^2-1}{2N} = 1 + \frac{\alpha_s}{\pi}. \tag{4.60}$$

In summary this correction represents an enhancement to the hadronic width of the Z-boson. Reconciling the leading order calculation above for the decay rate and the experimentally observed rate with this expression gives a value for $\alpha_s(M_Z^2) \approx 0.1$.

4.9 IR finiteness and factorisation

As required, the $\mathcal{O}(\alpha_s)$ correction to the total hadronic decay rate is finite, whereas the individual terms in its calculation are not. In physical terms, this really says that a *simplistic* picture of individual asymptotically free particles as described by the external legs of individual feynman diagrams is not a good approximation in some parts of phase-space. By summing over these regions and combining the result with other terms of the same perturbative order, we cancel the ambiguity of what is a virtual, *force-mediating*, vector boson and what can be considered a *free* gauge field. We sum over oppositely divergent terms to obtain a finite result: the real gluon emission is divergently *positive* and the virtual gluon *negatively* so.

Attempting to resolve particles in these regions leads to difficulties: experiments find large backgrounds when they look for fixed numbers of particles in confined regions; and calculations run up against divergences. With regard to the latter, they are unable to include the natural perturbative antidote—the appropriate virtual correction—as this by definition does not contain the required particle in the final state.

As indicated above, real gluon divergences correspond to the regions of phase-space where the invariant mass of the gluon with respect to the quark (or anti-quark) vanishes. With regard to the quark this means,

$$y_{qg} = \frac{(p_q + p_g)^2}{q^2} = \frac{2E_q E_g}{q^2}(1 - \cos\theta_{qg}) \to 0, \tag{4.61}$$

where E_r is the energy of parton r and θ_{qg} is their angular separation. That is to say, the gluon is *soft* ($E_g \to 0$), or the gluon is collinear with the quark—we define the soft quark limit to be part of this region because the qg composite has the quantum numbers of a quark.

In terms of the experimentally observed *hadronisation*, probing these regions is equivalent to resolving the sub-structure of jets and since *non*-perturbative effects actually dominate here we might expect a fixed order description to break-down. Extensions of perturbation theory into these regions are attempted via *Resummation* techniques and the reader is directed to the literature for more information [30]. In QED, an analogous break-down occurs that corresponds to the probability for multiple photon emission to increase in collinear and soft regions of phase space. The finite resolution of experiment justifies the need to sum over these problematic regions. [31]

Despite these problems, it is desirable to test theory more stringently than by calculating total event rates. A solution is to define what are called *IR-finite* observables. These are insensitive to the softer particles in an event. The *number* of jets in the large resolution limit is one such observable. Here the soft and collinear particles cannot make jets by themselves: they are not *resolved* and it is therefore possible to include different numbers of final state particles in a single calculation which allows for the type of IR cancellation discussed in the previous section.

Unresolved emission of partons, as characterised by the invariant mass of the unresolved cluster, is necessarily a *late-time* effect. This causes problems with the factorisation of calculations involving non-perturbative distribution functions. The assumptions used to factorise the process were based on the distinct time-scales for the two factors: prompt for the hard part and delayed for the soft part. With unresolved emission, the *hard* partonic process extends its intrinsic time scale into that of the soft physics of the hadron. The remedy to this overlap is to *renormalise* the non-perturbative function by absorbing the IR divergence into it. This is possible because, in the unresolved limits, the partonic sub-process factors into a *hard* but finite piece and a *soft* but divergent piece.

4.10 Summary

It has been the purpose of this chapter to review some simple phenomenology of the Standard Model with respect to the calculation of observables at LEP. The bias has been deliberately weighted in favour of introducing the approximations assumed throughout this thesis. These can be summarised in the following way: in general it is a good approximation to treat quarks as massless; the overwhelming phenomenology at LEP can be derived from Z-decay, or equivalently, after a modification of couplings, from the decay of an off-shell photon; and that perturbative divergences can be canceled in a meaningful manner to yield stable phenomenological predictions.

Chapter 5

Measuring the photon fragmentation function at LEP

Using an algorithm that treats photons and hadrons democratically, we discuss how the quark to photon fragmentation function, $D_{q\to\gamma}$, might be measured in 'photon' + jet events at LEP. Simple analytic results are given at lowest order. The possibility of determining the gluon to photon fragmentation function, $D_{g\to\gamma}$, in 'photon' + 2 jet events is also discussed, however, the prospects for doing so seem bleak.

5.1 Introduction

High energy hadronic events in e^+e^- annihilation are observed to contain sprays or clusters of approximately co-moving hadrons. With the aid of a suitable jet algorithm, it is possible to resolve the rather messy hadronic final state into a cleaner skeleton of vectors or jets along which the majority of the observed energy flows. Events are then defined by the number of jets they contain. This jet structure is a result of the high energy perturbative nature of QCD and one can in principle calculate $1, 2, 3 \ldots n$ jet rates using perturbative QCD. Although the quarks and gluons are not directly observed, the jet energy and jet axis is well modeled by a shower of partons. It is thus possible to match theoretical parton level calculations to experimental hadronic jet rates by subjecting both parton and hadron momenta to the same impartial jet algorithm, generally characterised by some invariant cut $y_{\rm cut}$.

In a small fraction of events one may observe an energetic photon in addition to the jets of hadrons [32, 33]. This photon may have originated early in the development of the parton shower, thus reflecting the electric charge of the parent quark. These 'direct' or 'internal' photons are generally well separated from the hadronic debris formed by the quark shower. Alternatively, the photon may have been radiated somewhat later during the hadronisation process which includes both photon emission collinear with the quark and genuine non-perturbative effects. Physical quantities are necessarily finite and the collinear divergence may be factorised into the photon fragmentation function [34]. Such 'non-prompt' photons are usually not isolated from the other hadrons in the event and generally suffer from large experimental backgrounds.

Former studies of photon + jet events at LEP have focused on almost isolated photons [35], (thus reducing the fragmentation contribution) with a view to extracting the electroweak couplings of the quarks [36]. To identify the photon, a cone-type algorithm has been applied

where photon candidates are required to have few hadronic tracks within a cone centred on the electromagnetic cluster. The photon is then removed from the event and a jet algorithm applied to the remaining hadrons. Theoretical studies [37, 38, 39] for the photon + 1,2 and 3 jet rates agree reasonably well at large $y_{\rm cut}$ with experimental results [40, 41, 42, 43] even though the corrections are rather large for the 1 jet rate. As expected, the measured quark couplings are in agreement with the standard model predictions [40].

It is the purpose of this chapter to advocate an alternative approach to the analysis of such final states where the contribution from the photon fragmentation function is not suppressed. Provided the experimental difficulties in identifying non-isolated photons can be overcome, one can then in principle *measure* the photon fragmentation function. LEP offers a very clean environment for such a measurement since there are relatively few hadrons in the event. The necessary formulae for measuring the photon fragmentation function at LEP using both the inclusive photon data and the cone-type photon definition were presented in [39]. However, since the fragmentation function depends on the fraction of the parent parton energy carried by the photon z, it is potentially more useful to formulate the cross section in terms of z rather than the energy of the photon, E_γ. A photon with a given energy can have a range of values of z depending on whether or not it is associated with a group of hadrons. It therefore makes sense to keep track of the amount of hadronic energy associated with the photon. Although this can be done within the context of the cone-type algorithm, in order to make comparisons with purely hadronic data more straightforward we introduce a somewhat different photon definition than that discussed in [39], so that photons and hadrons are grouped together democratically into potentially mixed electromagnetic/hadronic clusters. The precise algorithm for doing this can be any of those commonly used in the analysis of hadronic data such as the JADE/E0 [44] or Durham [45] schemes. The fraction z is then the fraction of electromagnetic energy in the cluster.

An additional advantage of analysing the photon data in terms of the number of clusters or jets in the event is that it enhances the non-perturbative part of the fragmentation function that we wish to measure. In the leading log approximation, the fragmentation function grows as $\sim \log(p_T^2/\Lambda_{QCD}^2)$ due primarily to a kinematic evolution in transverse photon momentum with respect to its charged (quark) source. Within this approximation, the lower limit of integration is set as the appropriate mass scale for the quarks, Λ_{QCD}. As discussed in [32], this leading log behaviour is a perturbative (i.e. *calculable*) one and breaks down in the limit that the photon is emitted collinear to the quark (as $|p_T| \to \Lambda_{QCD}$). The non-perturbative (i.e. *incalculable*) hadronic component (characterised above by Λ_{QCD}) resides in this collinear region corresponding to the delayed emission of the photon from within a boosted jet of hadrons. The jet or cone-type algorithm limits the allowed p_T of the photon thus exposing the non-perturbative contribution. In particular, photon + 1 jet events will allow the measurement of the quark to photon fragmentation function $D_{q\to\gamma}(z,\mu_F)$ since it is present at the first non-trivial order. This would then serve as an input to other calculations in much the same way as measurements of the proton structure function are measured in deep inelastic scattering and used in $p\overline{p}$ collisions. Particularly interesting is the application to single [46] and double prompt photon [47] production at the Fermilab TEVATRON where theoretical calculations appear to disagree with the data at small transverse momentum [48, 49].

The structure of this chapter is as follows. In Section 5.2 we review the way in which the photon fragmentation function enters in the n jet + photon cross section. We then propose a suitable photon definition (Section 5.3) and show in Section 5.4, with simple analytic calculations, how the quark to photon fragmentation function might be measured in photon + one jet events at LEP. The possibilities for extracting the gluon to photon fragmentation function from photon + two jet events are briefly discussed in Section 5.5. Our main results are summarised in Section 5.6 while the relevant analytic formulae for the photon + one jet

cross section are collected in an appendix at the end of this chapter.

5.2 The n jet + photon cross section

Let us consider the $e^+e^- \to n$ jet + photon cross section, fully differential in all quantities, which at lowest order is given by,

$$d\sigma^{LO}(n \text{ jets} + \text{“}\gamma\text{”}) = \Theta \; d\hat{\sigma}_0(n\; p + \gamma). \tag{5.1}$$

The n parton + photon cross section $d\hat{\sigma}_0(n\; p+\gamma)$ is evaluated in the tree approximation and Θ represents the experimental jet and photon definition cuts. In this way the theoretical cross section can be matched onto the specific experimental details. At this order, however, each parton is identified as a jet and the photon as a photon.

At next-to-leading order[1], the situation is rather more complicated, since in addition to QCD corrections to n parton processes including a photon, we admit the possibility of a parton fragmenting into a photon,

$$\begin{aligned} d\sigma^{NLO}(n \text{ jets} + \text{“}\gamma\text{”}) = \Theta \; \Big\{ & \; d\hat{\sigma}_1(n\; p + \gamma) + \int d\hat{\sigma}_0((n+1)\; p + \gamma) \\ & + \sum_a \frac{d\hat{\sigma}_0((n+1)\; p)}{dE_a} dE_a dz dE_\gamma \delta(E_\gamma - zE_a) D_{a\to\gamma}(z) \Big\}. \end{aligned} \tag{5.2}$$

The first term in this equation represents the one loop virtual corrections to the n parton + photon process while the second describes the tree level emission of an additional parton.

[1]By leading order we mean that each parton (which includes the photon) is separately resolved. For next-to-leading-order up to two partons maybe un-resolved and appear as a single hadronic jet.

In both cases, a 'prompt' photon is produced in the hard process. The third contribution is from the lowest order $n+1$ parton process where one of the partons fragments into a photon and transfers a fraction z of the parent momentum to the photon. Each type of parton, a, contributes according to the parton to photon fragmentation functions $D_{a\to\gamma}$ and the sum runs over all partons.

Although the physical cross section is finite, the individual contributions are divergent. The virtual graphs contain singularities due to soft gluons or collinear partons which cancel against similar poles from the bremsstrahlung process once the phase space of the additional parton is integrated out. The correct treatment of infra-red divergences is well known [50, 29] and has been discussed widely in the literature. In order to make the cancellation of poles explicit, we use the approach of [28] to remove the divergent part of the bremsstrahlung phase space and include it with the virtual graphs. Nevertheless, after the purely QCD infra-red poles have canceled, there remain quark-photon singularities as the quark and photon become collinear. These mass singularities are factorisable and can be absorbed by a redefinition of the fragmentation function so that,

$$d\sigma^{NLO}(n \text{ jets} + \text{“}\gamma\text{”}) = \Theta \left\{ d\hat{\sigma}_1^R(n\ p+\gamma) + \int d\hat{\sigma}_0^R((n+1)\ p+\gamma) + \sum_a \frac{d\hat{\sigma}_0((n+1)\ p)}{dE_a} dE_a dz dE_\gamma \delta(E_\gamma - zE_a)\mathcal{D}_{a\to\gamma}(z) \right\}, \quad (5.3)$$

where each term is now finite[2]. The resolved parton cross sections, $d\hat{\sigma}^R$, are given by $d\hat{\sigma}$ where the poles are regulated by $s_{ij} = (p_i + p_j)^2 > s_{\min}$. In other words, the partons are "resolved". A more precise definition of the resolved parton cross sections is given in refs. [28, 37]. Here, we will first focus on the next-to-leading order effective quark fragmentation function $\mathcal{D}_{q\to\gamma}$ for a quark of electric charge e_q which in $4-2\epsilon$ dimensions is related to the lowest order

[2]The strong coupling constant is renormalised to remove the ultra-violet poles

(bare) fragmentation function by,

$$\mathcal{D}_{q\to\gamma}(z) = D_{q\to\gamma}(z) - \frac{1}{\epsilon}\left(\frac{4\pi\mu^2}{s_{\min}}\right)^{\epsilon}\frac{1}{\Gamma(1-\epsilon)}\left(\frac{\alpha e_q^2}{2\pi}\right)[z(1-z)]^{-\epsilon}P_{q\to\gamma}(z), \tag{5.4}$$

where,

$$P_{q\to\gamma}(z) = \frac{1+(1-z)^2-\epsilon z^2}{z}. \tag{5.5}$$

The second term in Eqn. (5.4), is the contribution where the photon is collinear with quark a such that $s_{a\gamma} < s_{\min}$ [28]. It is conventional to factorise the explicit $1/\epsilon$ divergence into the bare fragmentation function $D(z)$ at the factorisation scale μ_F such that in the $\overline{MS}$ scheme (see Section 4.4, Eqn. (A.7) and [34, 39]),

$$D_{q\to\gamma}(z) = D_{q\to\gamma}(z,\mu_F) + \frac{1}{\epsilon}\left(\frac{4\pi\mu^2}{\mu_F^2}\right)^{\epsilon}\frac{1}{\Gamma(1-\epsilon)}\left(\frac{\alpha e_q^2}{2\pi}\right)\left(\frac{1+(1-z)^2}{z}\right), \tag{5.6}$$

so that,

$$\mathcal{D}_{q\to\gamma}(z) = D_{q\to\gamma}(z,\mu_F) + \left(\frac{\alpha e_q^2}{2\pi}\right)\left(\left(\frac{1+(1-z)^2}{z}\right)\log\left(\frac{s_{\min}z(1-z)}{\mu_F^2}\right)+z\right). \tag{5.7}$$

It is worth noting that $\mathcal{D}$ should be independent of the unphysical factorisation scale, since the factorisation scale dependence only arises through a shuffling of terms between the fragmentation function D and the perturbative contribution to $\mathcal{D}$. This implies that at this order $D(z,\mu_F)$ satisfies an evolution equation determined by the perturbative content of $\mathcal{D}$,

$$\frac{\partial D_{q\to\gamma}(z,\mu_F)}{\partial\log(\mu_F^2)} = \left(\frac{\alpha e_q^2}{2\pi}\right)\left(\frac{1+(1-z)^2}{z}\right). \tag{5.8}$$

A measurement at a given factorisation scale can thus be related to a measurement at a different scale. So far, we have ignored perturbative QCD effects which alter the z dependence of the fragmentation function, however, as higher and higher orders are included, more and more perturbative terms will appear in the effective fragmentation function $\mathcal{D}(z)$, thus

modifying the evolution equation for $D(z, \mu_F)$.

We see that in the $\overline{MS}$ scheme, an artificial pole as $z \to 1$ is introduced in the perturbative correction to $\mathcal{D}(z)$. This is entirely due to the way soft and collinear poles are regulated in dimensional regularisation. For practical purposes, this means that $D(z, \mu_F)$ in the $\overline{MS}$ scheme must contain a similar logarithmic divergence so that $\mathcal{D}(z)$ is well behaved as $z \to 1$. We note that different factorisation schemes such as the DIS_γ scheme of ref. [51] can remove this singularity.

We also note that the effective quark fragmentation function, $\mathcal{D}$, depends on the unphysical parton resolution parameter $s_{\min}$. For physical cross sections this cannot be the case, and indeed, as we will show in the next section for an explicit example, when the fragmentation contribution is combined with the resolved $(n+1)$ parton + photon cross section, any dependence on $s_{\min}$ cancels provided $s_{\min}$ is chosen to be small and terms of $\mathcal{O}(s_{\min})$ can be neglected.

At this order, the effective gluon fragmentation function receives no correction, since there is no gluon-photon collinear singularity,

$$\mathcal{D}_{g\to\gamma}(z) = D_{g\to\gamma}(z). \tag{5.9}$$

However, at higher orders, the gluon fragmentation function becomes coupled with the quark fragmentation function (through $g \to q \to \gamma$ splittings) and has a similar dependence on the factorisation scale. It is thus conventional to use the factorised form, $D_{g\to\gamma}(z, \mu_F)$ even at lowest order. The first process that this fragmentation function enters is "photon" + 2 jet production. As with the quark fragmentation function, this can in principle be measured at LEP.

5.3 Photon definition

In previous analyses of photon + jet events at LEP, the observed "photon" has been almost completely isolated from the hadronic debris. This attempts to eliminate the fragmentation contribution by requiring that,

$$z > 1 - \delta, \tag{5.10}$$

with δ very close to zero[3]. What we propose here is experimentally more difficult, since the backgrounds for non-isolated photons are much greater. However, a measurement of the fragmentation functions may be possible. The essence of the algorithm is to treat hadrons and "photon" candidates democratically and to cluster them according to a standard jet algorithm. After clustering, one of the clusters will contain the electromagnetic shower and can be deemed a "photon" if the fraction of electromagnetic energy in the cluster is larger than some experimentally determined value $z_{\rm cut}$,

$$z = \frac{E_{EM}}{E_{EM} + E_{HAD}} > z_{\rm cut}. \tag{5.11}$$

Equivalently, one can require that the hadronic energy in the cluster is smaller than some fraction $\epsilon_{\rm cut}$ of the electromagnetic energy,

$$\frac{E_{HAD}}{E_{EM}} < \epsilon_{\rm cut} = \frac{1 - z_{\rm cut}}{z_{\rm cut}}. \tag{5.12}$$

An additional advantage of such an algorithm is that comparisons between jet and photon+jet rates are rather more straightforward.

There are several distinct jet algorithms in use at LEP and here we will focus on the

[3] δ cannot be zero either experimentally, due to finite detector resolution, or theoretically since a completely isolated photon is not infra-red safe.

JADE/E0 [44] (which we shall generally refer to as E0) and Durham [45] algorithms. The essence of these algorithms is that a test variable d_{ij} is constructed for all possible momenta p_i and p_j in the event. The pair with the smallest d_{ij} are then combined to form a pseudo-particle with four momentum $p_i^\mu + p_j^\mu$ *provided* d_{ij} is less than the jet resolution parameter $y_{\rm cut}$. This process is then repeated until no further clusterings occur and the number of jets in the event and their momenta are then given by the remaining pseudo-particles. In the E0 scheme at a centre-of-mass energy $\sqrt{s}$,

$$d_{ij} = y_{ij} = \frac{s_{ij}}{s} = \frac{(p_i + p_j)^2}{s}, \tag{5.13}$$

while in the Durham or D scheme,

$$d_{ij} = \min\left(\frac{E_i}{E_j}, \frac{E_j}{E_i}\right) y_{ij}. \tag{5.14}$$

This latter scheme is preferred on the grounds that the soft gluon contributions exponentiate [52].

5.4 The photon + 1 jet rate

There is no $e^+e^- \to \gamma + 1$ parton process, so the lowest order cross section defined by Eqn. (5.1) and the first term in Eqn. (5.2) both vanish. As a consequence, the first non trivial contribution comes from $e^+e^- \to q\overline{q}\gamma$ and $e^+e^- \to q\overline{q}$ where one of the quarks fragments into a photon. In this way, the fragmentation function is effectively present at leading order rather than at next-to-leading order. This makes the photon + 1 jet rate especially sensitive to $D_{q\to\gamma}$.

Rather than the full e^+e^- cross-section, we shall consider the ratio of single photon production in association with hadrons and the total hadronic rate. The contribution from the $e^+e^- \to q\bar{q}\gamma$ process to the photon + 1 jet rate can be obtained by integrating the differential cross section (for massless quarks of charge e_q),

$$\frac{1}{\sigma_0}\frac{d^2\sigma}{dxdx'} = \left(\frac{\alpha e_q^2}{2\pi}\right)\frac{x^2+x'^2}{(1-x)(1-x')}, \tag{5.15}$$

where the quark energy-fractions are given by $x = 2E_q/\sqrt{s}$, $x' = 2E_{\bar{q}}/\sqrt{s}$ and $x_\gamma = 2-x-x'$. In terms of these energy fractions, the scaled pair invariant masses are given by,

$$y_{q\gamma} = 1-x', \quad y_{\bar{q}\gamma} = 1-x, \quad y_{q\bar{q}} = 1-x_\gamma. \tag{5.16}$$

Up to an overall coupling and the replacement $\gamma \leftrightarrow g$, Eqn. (5.15) is just Eqn. (4.53) in the $\epsilon \to 0$ limit. Note that *all* $y_{ij} > s_{\min}/s = y_{\min}$ so that the singularities in the matrix elements along $x = 1$ and $x' = 1$ are regulated by the parton resolution cut $y_{\min}$. Therefore, the three-particle contribution to the one jet rate will depend on $y_{\min}$. However, when combined with the fragmentation contribution all $y_{\min}$ dependence must vanish in the small $y_{\min}$ limit.

If we work in the E0 jet algorithm with a jet resolution parameter $y_{\rm cut} \leq 1/3$ then, for a photon cluster electromagnetic energy fraction greater than $z_{\rm cut}$, the 1 jet region is defined by the following three regions of phase space,

$$\begin{aligned}
1: &\quad y_{q\bar{q}} < y_{q\gamma}, y_{\bar{q}\gamma};\ \text{and}\ y_{q\bar{q}} < y_{\rm cut} \\
2: &\quad y_{q\gamma} < y_{\bar{q}\gamma}, y_{q\bar{q}};\ y_{q\gamma} < y_{\rm cut};\ \text{and}\ \frac{E_\gamma}{E_\gamma+E_q} > z_{\rm cut} \\
3: &\quad y_{\bar{q}\gamma} < y_{q\bar{q}}, y_{q\gamma};\ y_{\bar{q}\gamma} < y_{\rm cut};\ \text{and}\ \frac{E_\gamma}{E_\gamma+E_{\bar{q}}} > z_{\rm cut}.
\end{aligned} \tag{5.17}$$

The corresponding Dalitz plot is shown in Figure 5.1 for $y_{\rm cut} = 0.1$ and $z_{\rm cut} = 0.7$. In region 1, the quark and antiquark combine to form the jet, while in regions 2 (3), the photon

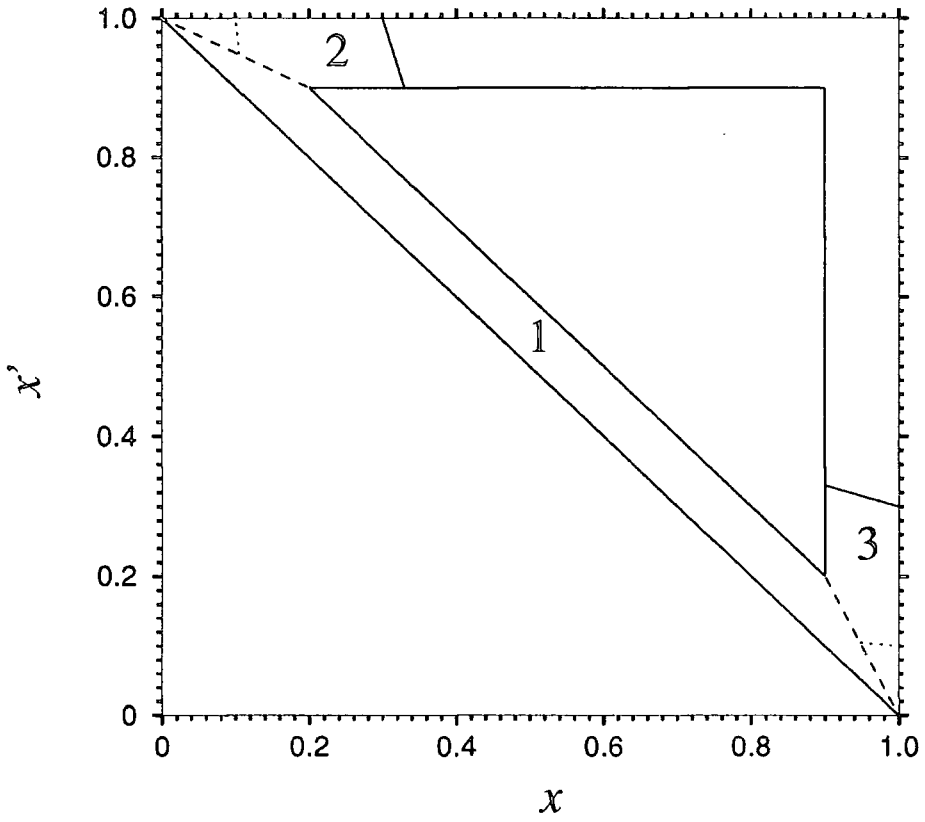

Figure 5.1: Dalitz plot for the $q\overline{q} + \gamma$ final state in terms of the quark and antiquark energy fractions x and x'. The regions 1, 2 and 3 show the photon + one jet phase space for $y_{\rm cut} = 0.1$ and $z_{\rm cut} = 0.7$ in the E0 scheme. The dotted lines show regions 2 and 3 for $z_{\rm cut} = 0.9$. Region 1 where the quark-antiquark combine to form a jet is separated from the regions where the quark (antiquark) combines with the photon by a dashed line.

coalesces with a quark (antiquark) to form a mixed electromagnetic/hadronic cluster.

In the Durham scheme, again with $y_{\rm cut} \leq 1/3$, the 1 jet region is defined by,

$$\begin{aligned}
1: &\quad \min\left(\frac{x}{x'}, \frac{x'}{x}\right) y_{q\overline{q}} < y_{\rm cut}, \\
2: &\quad \min\left(\frac{x}{x_\gamma}, \frac{x_\gamma}{x}\right) y_{q\gamma} < y_{\rm cut} \quad \text{and} \quad \frac{E_\gamma}{E_\gamma + E_q} > z_{\rm cut}, \\
3: &\quad \min\left(\frac{x_\gamma}{x'}, \frac{x'}{x_\gamma}\right) y_{\overline{q}\gamma} < y_{\rm cut} \quad \text{and} \quad \frac{E_\gamma}{E_\gamma + E_{\overline{q}}} > z_{\rm cut}.
\end{aligned} \tag{5.18}$$

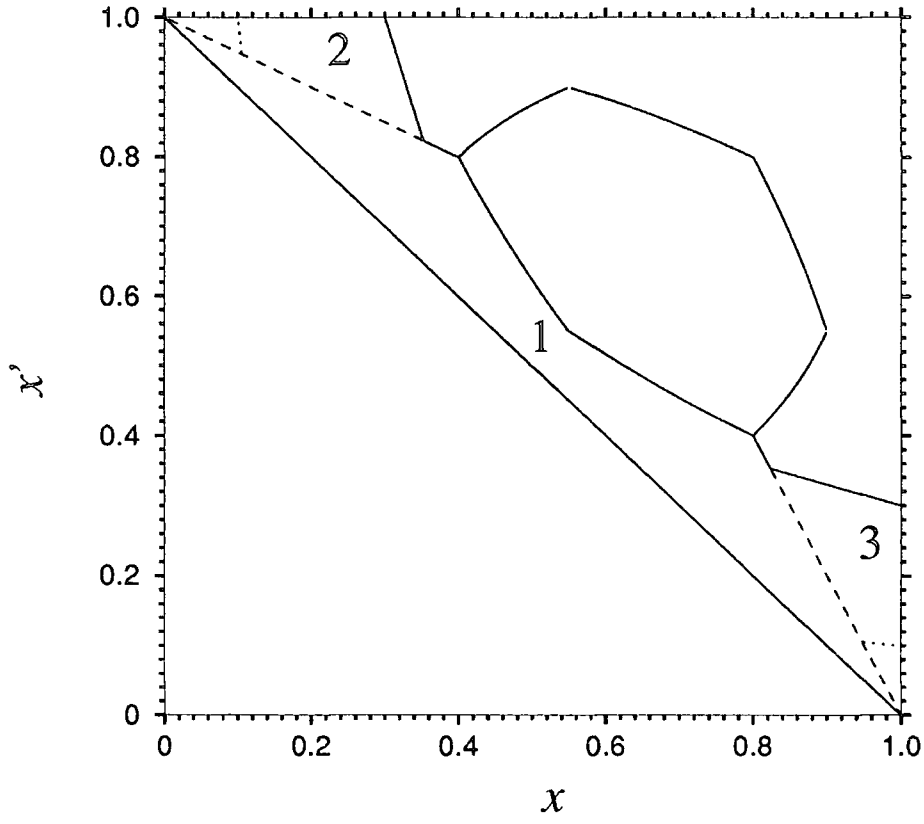

Figure 5.2: Dalitz plot for the $q\overline{q}+\gamma$ final state in terms of the quark and antiquark energy fractions x and x'. The regions 1, 2 and 3 show the photon + one jet phase space for $y_{\rm cut}=0.1$ and $z_{\rm cut}=0.7$ in the Durham scheme. The dotted lines show regions 2 and 3 for $z_{\rm cut}=0.9$. Region 1 where the quark-antiquark combine to form a jet is separated from the regions where the quark (antiquark) combines with the photon by a dashed line.

The rather more complicated Dalitz plot is shown in Figure 5.2 for $y_{\rm cut}=0.1$ and $z_{\rm cut}=0.7$. As before, in region 1, the quark and antiquark combine to form the jet, while in regions 2 (3), the photon coalesces with a quark (antiquark) to form a mixed electromagnetic/hadronic cluster.

In the region of phase space where the quark and photon combine (regions 2 and 3), the

fraction of electromagnetic energy in the cluster, z, is related to x and x' by,

$$z = \frac{2 - x - x'}{2 - x'}, \tag{5.19}$$

in region 2 and by Eqn. (5.19) with $x \leftrightarrow x'$ in region 3. By integrating over either x or x' it is straightforward to obtain the 1 jet + photon cross section as a function of z in scheme $S = E0,\ D$,[4]

$$\begin{aligned}\frac{1}{\sigma_0}\frac{d\sigma^S(1\text{ jet} + \text{“}\gamma\text{”})}{dz} &= 2\ D_{q\to\gamma}(z,\mu_F) + \left(\frac{\alpha e_q^2}{\pi}\right)\left[\frac{\left(1+(1-z)^2\right)}{z}\log\left(\frac{s}{\mu_F^2}\right)\right] \\ &+ \frac{1}{\sigma_0}\frac{d\hat{\sigma}^S(1\text{ jet} + \text{“}\gamma\text{”})}{dz} + R_\Delta^S\,\delta(1-z) + \mathcal{O}(s_{\min}).\end{aligned} \tag{5.20}$$

Here the dependence on the scale μ_F has been made explicit, while the quantity R_Δ^S represents the contribution to the cross section where quark and antiquark combine, thus leaving the photon completely isolated. In this case, the photon cluster has $z = 1$. An explicit form for R_Δ^S in the two schemes is given in the Appendix. The scale independent contribution is given by,

$$\begin{aligned}\frac{1}{\sigma_0}\frac{d\hat{\sigma}^S(1\text{ jet} + \text{“}\gamma\text{”})}{dz} &= \left(\frac{\alpha e_q^2}{\pi}\right)\left[\frac{\left(1+(1-z)^2\right)}{z}\log\left(y^S z(1-z)\right) + z\right. \\ &- \frac{1+(1-z)^2}{1-z}\left(\frac{zy^S}{1-z} + \frac{y^S(y^S-2)}{2} + \frac{(1-2z)^2}{z(1-z)^2}\log\left(\frac{z\left(1+y^S\right)-y^S}{z}\right)\right) \\ &\left.- 4(1-z)y^S - 4\log\left(\frac{z(1+y^S)-y^S}{z}\right)\right],\end{aligned} \tag{5.21}$$

where y^{E0} and y^D are determined by the lower boundaries of either the x or x' integration,

$$\begin{aligned} y^{E0} &= \min\left(y_{\text{cut}}, \frac{1-z}{1+z}\right), \\ y^D &= \frac{1-z}{1+z} \quad \textbf{if} \quad z > z_0 = \frac{1-y_0}{1+y_0}, \end{aligned} \tag{5.22}$$

[4]We have made the natural assumption, $D_{\bar{q}\to\gamma}(z,\mu_F) = D_{q\to\gamma}(z,\mu_F)$.

$$= \frac{z y_{\rm cut}}{1-z} \quad \textbf{otherwise}, \tag{5.23}$$

with,

$$y_0 = \frac{\sqrt{y_{\rm cut}^2 + 8y_{\rm cut}} - y_{\rm cut}}{4}. \tag{5.24}$$

As expected, the logarithmic dependence on $s_{\rm min}$ has canceled and the limit $s_{\rm min} \to 0$ can be safely taken. We note that as $z \to 1$, $y \to \frac{1-z}{1+z}$ and therefore, the perturbative contribution grows as $\log((1-z)^2)$. A similar behaviour is observed with other photon definitions such as the cone-type algorithm.

In order to turn this analytic form into a physical cross section, it is necessary to know the process independent fragmentation function, $D_{q\to\gamma}(z,\mu_F)$ in the $\overline{MS}$ scheme. The general form of the fragmentation function which satisfies the evolution equation is,

$$D_{q\to\gamma}(z,\mu_F) = A\left(z, \frac{\mu_F^2}{\mu_0^2}\right) + B(z,\mu_0). \tag{5.25}$$

Here the scale μ_0 and the associated function $B(z,\mu_0)$ are nothing more than the constants of integration. However, a more physical interpretation of μ_0 could be the scale below which the physics is *non*-perturbative. As discussed above and in Section 5.2, in the $\overline{MS}$ scheme, the perturbative contribution to $\mathcal{D}$ contains a logarithmic singularity as $z \to 1$. This should be balanced by a similar behaviour in D.

To give some idea of the possible size of the 1 jet + photon cross section, we consider two over simplified choices for the fragmentation function,

$$D^I_{q\to\gamma}(z,\mu_F) = 0, \tag{5.26}$$

$$D^{II}_{q\to\gamma}(z,\mu_F) = \left(\frac{\alpha e_q^2}{2\pi}\right)\frac{1+(1-z)^2}{z}\log\left(\frac{\mu_F^2}{\mu_0^2(1-z)^2}\right). \tag{5.27}$$

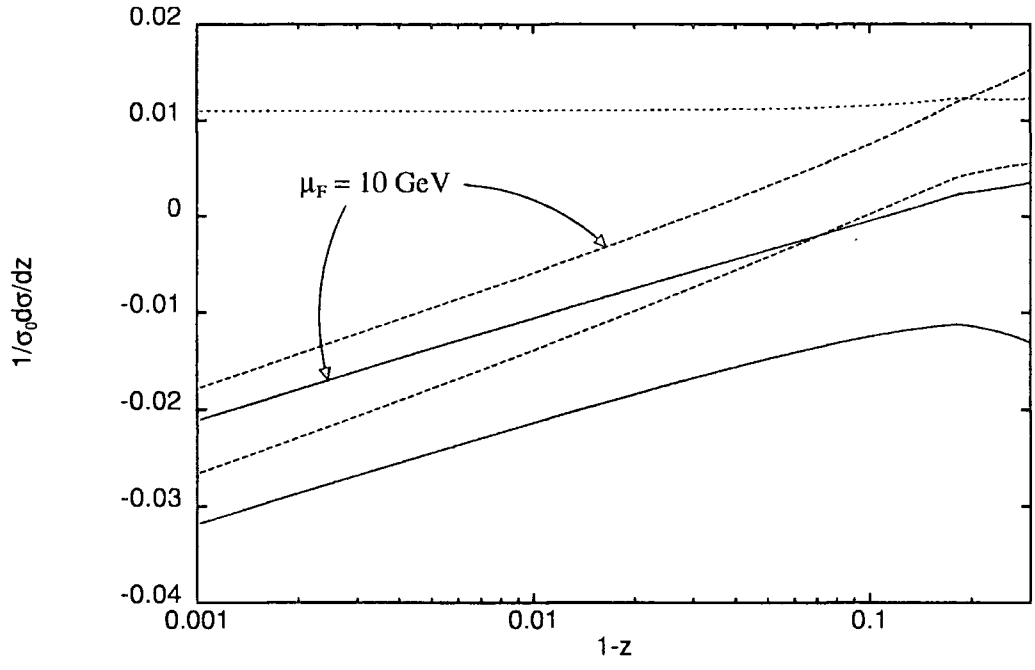

Figure 5.3: The differential cross section in the E0 scheme, $1/\sigma_0 d\sigma/dz$, for a single quark of unit charge for $D_{q\to\gamma} = 0$ with $\mu_F = 10$ and 100 GeV and $y_{\rm cut} = 0.1$. The scale independent rate for the D^{II} fragmentation function with $\mu_0 = 10$ GeV is shown dotted, while the dashed lines show the D^{III} rate for $\mu_F = 10$ and 100 GeV.

The first of these fragmentation functions is clearly unphysical and exhibits only the perturbative contribution to the cross section. The result therefore depends strongly on μ_F and becomes negatively *divergent* as $z \to 1$. This is shown for the E0 scheme in Figure 5.3 for a single quark with unit charge and $\mu_F = 10$ and 100 GeV. We see that there is a change in slope at $1 - z = \frac{2y_{\rm cut}}{1+y_{\rm cut}} \sim 0.18$ because events with $y_{q\gamma} > y_{\rm cut}$ are identified as "photon" + 2 jet events where the photon cluster has $z = 1$.

On the other hand, the second fragmentation function is an exact solution of the leading order evolution equation Eqn. (5.8), and therefore the factorisation scale dependence is eliminated. Furthermore, the $\log(1-z)$ behaviour is canceled so that, as shown in Figure 5.3, the differential cross section is positive for all values of z. Although this fragmentation

function satisfies the leading order evolution equation it is not intended as a substitute for an experimental determination of $D_{q\to\gamma}$.

As a final example, we take the large μ_F solution of the next-to-leading order evolution equations obtained by ref. [53], consistent with its use in [47],

$$D^{III}_{q\to\gamma}(z,\mu_F) = \left(\frac{\alpha}{2\pi}\right)\left(e_q^2\frac{2.21-1.28z+1.29z^2}{1-1.63\log(1-z)}z^{0.049}+0.002(1-z)^2z^{-1.54}\right)\log\left(\frac{\mu_F^2}{\Lambda^2_{QCD}}\right), \tag{5.28}$$

where $\Lambda_{QCD} = 0.2$ GeV. As shown in Figure 5.3, there is a significant scale dependence, since this solution contains perturbative contributions that are not included in our calculation. It is also interesting to note that as $z \to 1$, this fragmentation function does not appear to nullify the explicit $\log(1-z)$ appearing in the leading order perturbative contribution and the rate becomes negative. We therefore drop this fragmentation function from further consideration.

However, at present we do not know the fragmentation function and the purpose of this chapter is to motivate such a measurement at LEP. Of course, at LEP, both up- and down-type quarks are produced so that, in principle, the combination,

$$D^{\rm LEP}_{q\to\gamma}(z,\mu_F) = \frac{2\,(v_u^2+a_u^2)D_{u\to\gamma}(z,\mu_F)+3\,(v_d^2+a_d^2)D_{d\to\gamma}(z,\mu_F)}{2\,(v_u^2+a_u^2)+3\,(v_d^2+a_d^2)}, \tag{5.29}$$

where v_q and a_q are the vector and axial vector couplings of quark q with the Z boson, can be determined in photon + 1 jet events.

The fragmentation function must contribute with respect to some scale μ_F. Unlike deep inelastic scattering, there is no obvious choice for this scale, and the best one can do is to choose μ_F of the order of a few GeV. We will take $\mu_F = 10$ GeV and 100 GeV to be representative choices. Measurements at different scales are related through the evolution

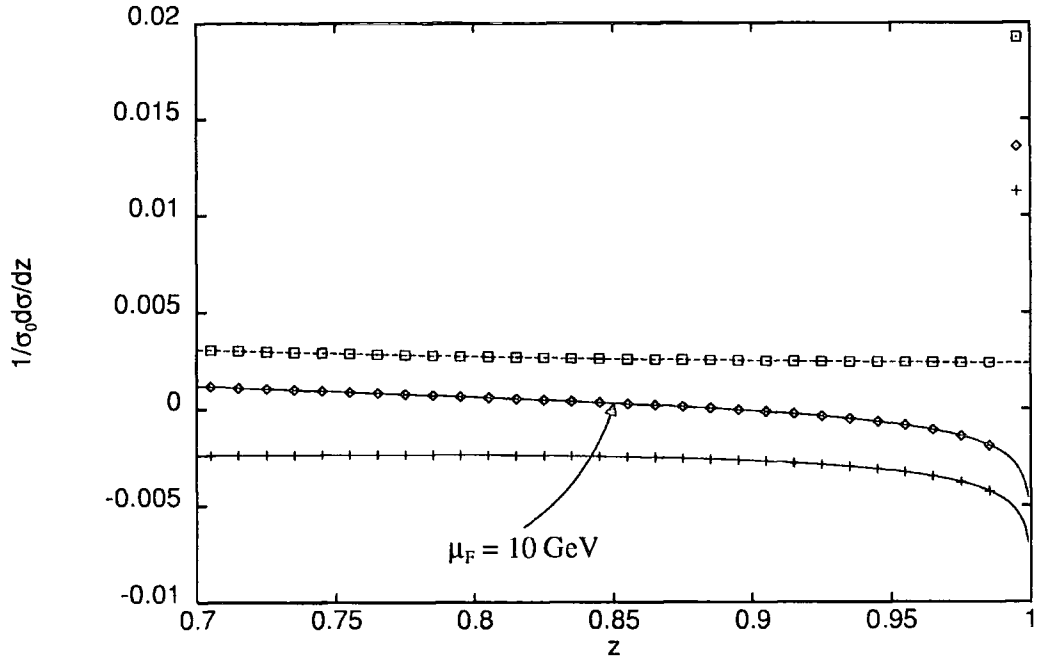

Figure 5.4: The differential cross section, $1/\sigma_0 d\sigma/dz$, for $D_{q\to\gamma} = 0$ with $\mu_F = 10$ and 100 GeV and $y_{\rm cut} = 0.1$. The data points show the distribution in bins 0.01 wide, while the solid lines show the analytic result. The open square data points shows the distribution for the D^{II} fragmentation function with $\mu_0 = 10$ GeV.

equation and in principle should yield identical results. Once a factorisation scale has been chosen, the difference between the data $\sigma^{\rm EXP}$ and Eqn. (5.20) with $D_{q\to\gamma} = 0$ provides a lowest order measurement of the fragmentation function,

$$D^{\rm LEP}_{q\to\gamma}(z,\mu_F) = \frac{1}{2}\left(\frac{1}{\sigma_0}\frac{d\sigma^{\rm EXP}(1\text{ jet} + \text{“}\gamma\text{”})}{dz}(z) - \frac{1}{\sigma_0}\frac{d\sigma(1\text{ jet} + \text{“}\gamma\text{”})}{dz}(z,\mu_F)|_{D_{q\to\gamma}=0}\right). \quad (5.30)$$

In Figure 5.4, we show the z distribution in the Durham scheme for the appropriate mixture of up- and down-type quarks normalised to the total hadronic cross section for e^+e^- collisions at $\sqrt{s} = M_Z$ with $\mu_F = 10$ GeV and 100 GeV. The smooth curve is the analytic distribution of Eqn. (5.20), while the data points show the differential cross section integrated

over bins 0.01 wide. As expected, this unphysical distribution depends strongly on μ_F and is negative for quite a wide range of z. The divergent behaviour as $z \to 1$ is clearly seen. These effects are reflected in the highest bin of the histogram centred at $z = 0.995$, where the R_Δ contribution from the quark combining with the antiquark is added to the integral of the distribution from $z = 0.99$ to 1. Even though one would expect the end bin to be insensitive to the fragmentation contribution, because of the way the $\overline{MS}$ scheme treats the $z \to 1$ region, there appears to be a sizable effect. This is largely due to cancellations that should take place between D and the perturbative part of $\mathcal{D}$. In a different scheme, such as the DIS_γ scheme [51], this effect may be reduced. To give some idea of what a physical z distribution might look like, we also show the rate for the D^{II} fragmentation function, again with $\mu_0 = 10$ GeV. There is a sizable increase in the end bin because the $\log(1-z)$ behaviour of the perturbative contribution in $\mathcal{D}$ is canceled by that of the fragmentation function.

In the E0 scheme, the z distribution looks rather similar, however there are two main differences. First, at small z the cross section is slightly reduced due to the different definition of y^S. This occurs for $z < \frac{1-y_{\rm cut}}{1+y_{\rm cut}} = 0.82$ and reduces the differential cross section by 0.0004 at $z = 0.7$ independently of the scale. Second, the quantity R_Δ is much larger in the Durham scheme as can be deduced from the Dalitz plots shown in Figures 5.1 and 5.2. Once again, the difference between the two schemes is scale invariant and decreases the distribution in the end bin by 0.0043.

It is also straightforward to integrate over the allowed values of z to obtain the one jet fraction,

$$\begin{aligned}
\frac{\sigma^S(1 \text{ jet} + \text{“}\gamma\text{”})}{\sigma_0} &= \int_{z_{\rm cut}}^1 \frac{1}{\sigma_0}\frac{d\sigma(1 \text{ jet} + \text{“}\gamma\text{”})}{dz} \\
&= 2\int_{z_{\rm cut}}^1 D_{q\to\gamma}(z,\mu_F)\,dz + F^S + R_\Delta^S \\
&+ \left(\frac{\alpha e_q^2}{\pi}\right)\left\{\left(\frac{1-z_{\rm cut}^2}{2} - 2(1-z_{\rm cut}) - 2\log(z_{\rm cut})\right)\log\left(\frac{s}{\mu_F^2}\right)\right\}. \quad (5.31)
\end{aligned}$$

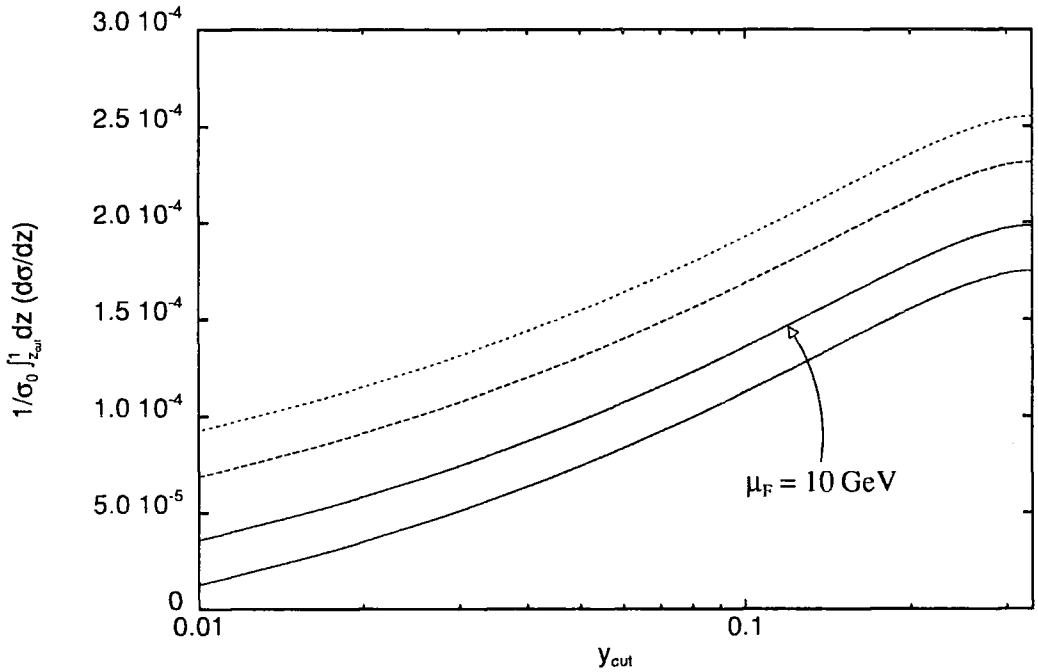

Figure 5.5: Photon + 1 jet rate in the Durham scheme as a function of the jet separation parameter $y_{\rm cut}$ for $z_{\rm cut} = 0.99$ with $D_{q\to\gamma} = 0$ and $\mu_F = 10$ and 100 GeV. The dashed line show R^D_Δ in the Durham scheme while the rate for the D^{II} fragmentation function with $\mu_0 = 10$ GeV is shown dotted.

The scale independent function F^S is somewhat lengthy and is given in the Appendix. We see that the scale dependence is the same for all schemes, reflecting the fact that it originates in a subtraction in the collinear limit. The one jet fraction normalised to the total hadronic cross section is shown in Figure 5.5 for the Durham scheme as a function of $y_{\rm cut}$ for $D_{q\to\gamma} = 0$ with $z_{\rm cut} = 0.99$. As in the z distribution shown in Figure 5.4, even for this very restricted range of z, the cross section does depend strongly on the factorisation scale. At small $y_{\rm cut}$, the cross section diverges logarithmically in both schemes,

$$\frac{\sigma^S(1 \text{ jet} + \text{“}\gamma\text{”})}{\sigma_0} \to \left(\frac{\alpha e_q^2}{\pi}\right)\left\{\left(\frac{1-z_{\rm cut}^2}{2} - 2(1-z_{\rm cut}) - 2\log(z_{\rm cut})\right)\log\left(y_{\rm cut}\right)\right\}, \qquad (5.32)$$

with a coefficient determined by $z_{\rm cut}$. For comparison, we show the scale independent R_Δ contribution which tends to zero at small $y_{\rm cut}$. Once again, we also show the total cross section for the D^{II} fragmentation function. Even for $z > 0.99$, the total rate is sensitive to the form of the fragmentation function due partly to the $\log(1-z)$ behaviour of the perturbative part of $\mathcal{D}$, but also to the additional $\log(1-z)$ term from the boundary of phase space.

At large $z_{\rm cut}$, the cross section simplifies dramatically,

$$\frac{\sigma^S(1 \text{ jet} + \text{“}\gamma\text{”})}{\sigma_0} \to R_\Delta^S, \qquad (5.33)$$

which is simply the contribution when the quark and antiquark combine to form the cluster. Figure 5.6 shows the one jet rate in the Durham scheme normalised to the total hadronic cross section for fixed $y_{\rm cut}$ as a function of $z_{\rm cut}$. As expected, the unphysical prediction ($D_{q\to\gamma} = 0$) depends strongly on the choice of scale. The difference between the data and solid curves with $\mu_F = 10$ or 100 GeV therefore represents a lowest order measurement of the integral of the fragmentation function at that scale provided that the non-prompt π^0 background has been correctly subtracted. As expected, we see that as $z_{\rm cut} \to 1$, the rate

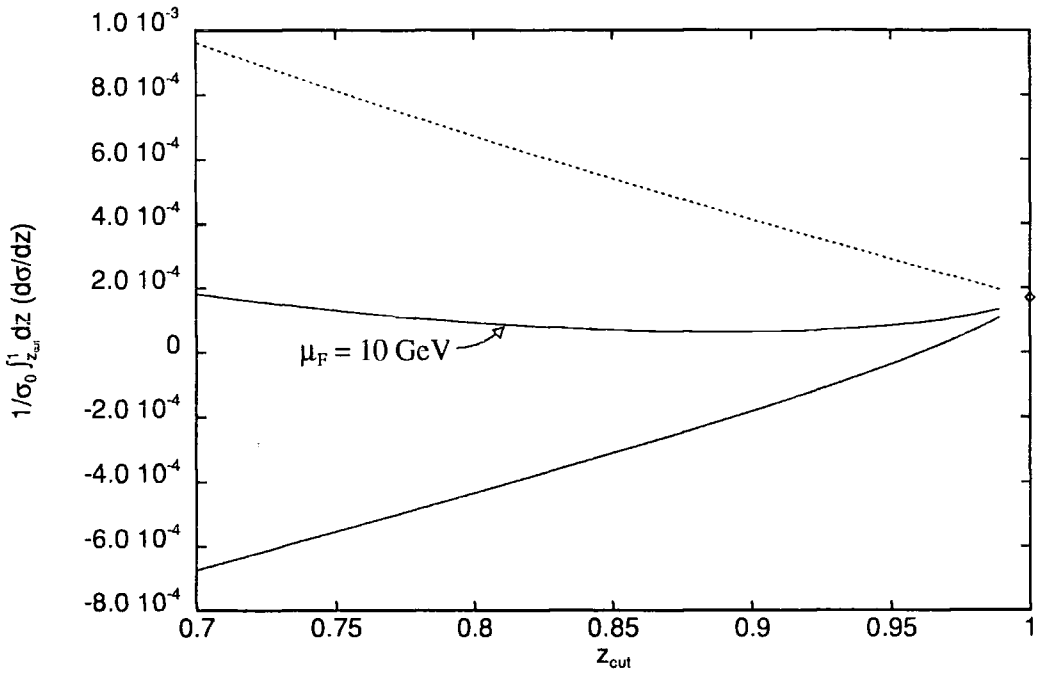

Figure 5.6: Photon + 1 jet rate in the Durham scheme as a function of the electromagnetic energy fraction $z_{\rm cut}$ with $D_{q\to\gamma} = 0$ for $\mu_F = 10$ and 100 GeV and $y_{\rm cut} = 0.1$. R^D_Δ is shown as a point on the right hand axis. The rate for the D^{II} fragmentation function with $\mu_0 = 10$ GeV is shown dotted.

becomes independent of the choice of fragmentation function as described by Eqn. (5.33). This is also true for the more physical D^{II} fragmentation function.

5.5 The photon + 2 jet rate

Unlike the previous case, the $e^+e^- \to \gamma + 2$ parton process does not vanish and therefore, the fragmentation function which appears at next-to-leading order is suppressed in the total cross-section. The cross section is thus dominated by the lowest order contribution which occurs at $z = 1$. On the other hand, the fragmentation function contribution comes from the lowest order $e^+e^- \to q\overline{q}g$ process and is potentially sensitive to the gluon fragmentation contribution. In fact, the two jet rate depends on a combination of quark and gluon fragmentation functions,

$$\alpha_s \left(2\ D^{LEP}_{q\to\gamma}(z,\mu_F) + D_{g\to\gamma}(z,\mu_F)\right),$$

so that in addition to the particular combination of quark fragmentation functions as measured at LEP, a knowledge of the strong coupling constant is also required to have any chance of extracting the gluon fragmentation function.

It is straightforward to compute the full next-to-leading order QCD corrections to this process. The necessary resolved parton one loop $q\overline{q}\gamma$ and bremsstrahlung $q\overline{q}\gamma g$ matrix elements have been described in [28, 37] and can be directly implemented in a Monte Carlo program along with the fragmentation process as described by Eqns. (5.3 and 5.6). The resulting z distribution in the Durham scheme is shown in Figure 5.7 for $z < 0.99$ and $y_{\rm cut} = 0.1$. As in the one jet case, the predictions with the unphysical choice $D_{q\to\gamma} = 0$ show a dependence on the factorisation scale which should be compensated by a more physical

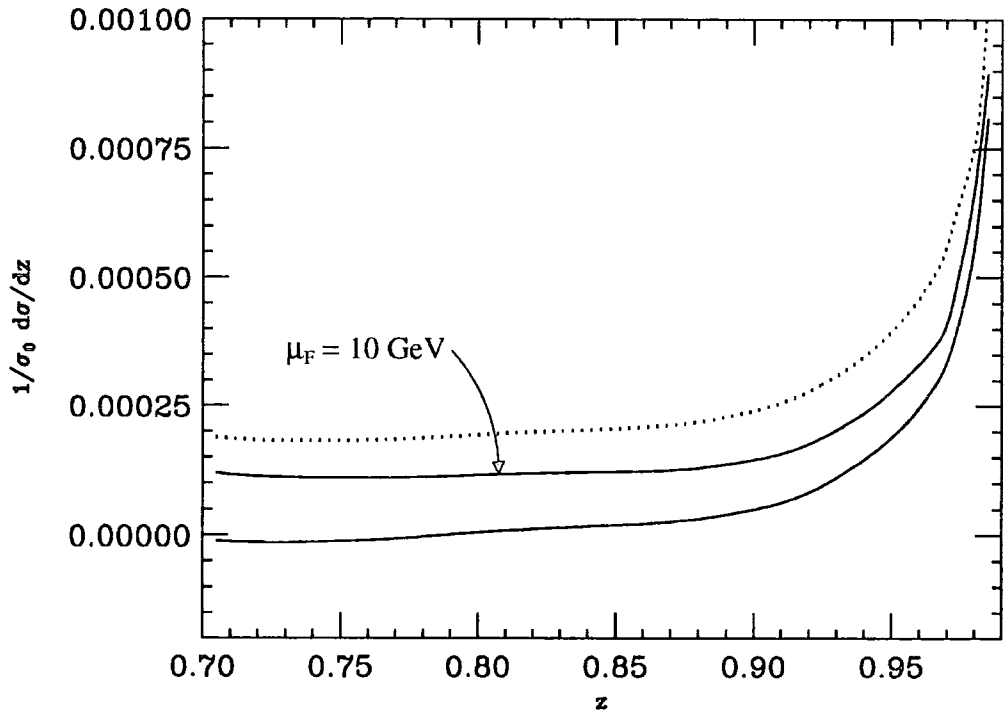

Figure 5.7: The differential cross section in the Durham scheme, $1/\sigma_0 d\sigma/dz$, for photon + 2 jet events for $D_{q\to\gamma} = D_{g\to\gamma} = 0$ with $\mu_F = 10$ and 100 GeV (dashed) and $y_{\rm cut} = 0.1$. The dotted line shows the distribution for the D^{II} fragmentation function with $\mu_0 = 10$ GeV.

choice such as that given by Eqn. (5.27). Nevertheless, the variation of the two jet rate with the factorisation scale is rather small,

$$\delta\left(\frac{1}{\sigma_0}\frac{d\sigma^{NLO}(2\text{ jets} + \text{“}\gamma\text{”})}{dz}\right) = \frac{4\alpha_s}{3\pi}\frac{\sigma^{LO}(2\text{ jets} + \text{“}\gamma\text{”})}{\sigma_0}\left(\frac{1+(1-z)^2}{z}\right)\log\left(\frac{\mu_1^2}{\mu_2^2}\right). \quad (5.34)$$

This indicates that even with a physical fragmentation function, the two jet rate for $z < 0.99$ is small. It is important to note that, once the fragmentation function $D_{q\to\gamma}^{LEP}$ has been established using the one jet data, it can be directly applied to estimate the two jet rate.

So far we have not discussed the gluon fragmentation function, which at lowest order does not exhibit factorisation scale dependence and is merely a function of z. In principle one can hope to make a determination of the lowest order gluon fragmentation function at LEP,

$$\begin{aligned} D_{g\to\gamma}(z) &= \frac{3\alpha}{4\alpha_s}\frac{2e_u^2(v_u^2+a_u^2)+3e_d^2(v_d^2+a_d^2)}{2(v_u^2+a_u^2)+3(v_d^2+a_d^2)}\frac{\sigma_0}{\sigma^{LO}(2\text{ jets} + \text{“}\gamma\text{”})} \\ &\times \left(\frac{1}{\sigma_0}\frac{d\sigma^{\mathrm{EXP}}(2\text{ jet} + \text{“}\gamma\text{”})}{dz}(z) - \frac{1}{\sigma_0}\frac{d\sigma^{NLO}(2\text{ jet} + \text{“}\gamma\text{”})}{dz}(z)|_{D_{g\to\gamma}=0}\right), \quad (5.35) \end{aligned}$$

where the measured quark fragmentation function is used as an input in σ^{NLO} and σ^{EXP} represents the measured data. In practice, however, the event rate is rather small and it is unlikely that such a measurement can be meaningfully carried out.

Because the lowest order process contributes at $z = 1$, as expected the $z > 0.99$ region completely dominates the cross section. This is clearly seen in Figure 5.8 where the total two jet + photon cross section at next-to-leading order for $z > z_{\mathrm{cut}}$ is shown in the Durham scheme as a function of z_{cut} for $y_{\mathrm{cut}} = 0.1$. The lowest order cross section, $\sigma^{LO}(2\text{ jets} + \text{“}\gamma\text{”})/\sigma_0$, is 0.0004. The bulk of the cross section, (81% for the D^{II} fragmentation function), exists at $z > 0.99$. While for smaller z_{cut}, the integrated rate is extremely flat reflecting the rather small $d\sigma/dz$ distribution shown in Figure 5.7.

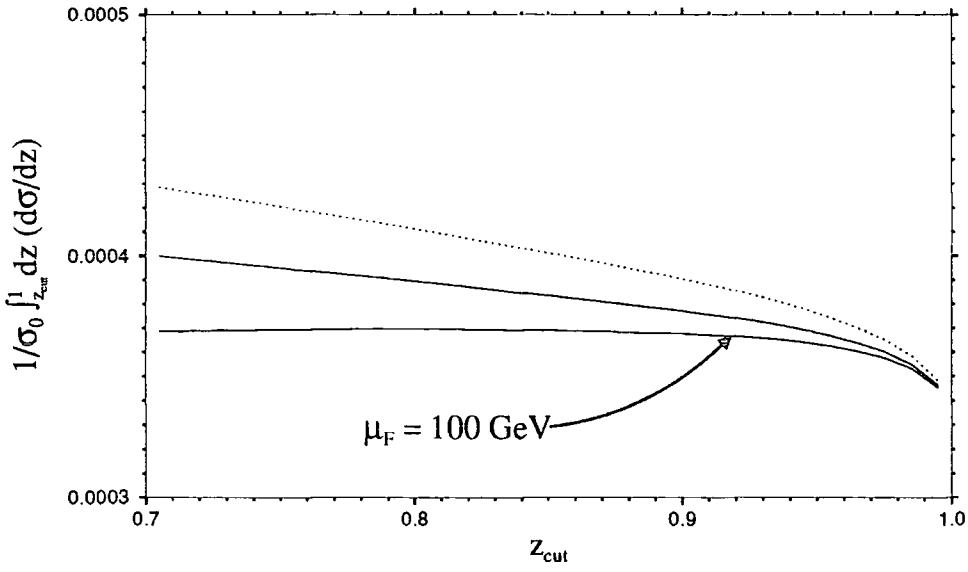

Figure 5.8: The photon + 2 jet rate in the Durham scheme as a function of the electromagnetic energy fraction $z_{\rm cut}$ with $D_{q\to\gamma} = 0$ and $D_{g\to\gamma} = 0$ for $\mu_F = 10$ and 100 GeV and $y_{\rm cut} = 0.1$. The factorisation scale independent rate for the D^{II} quark fragmentation function is shown dotted.

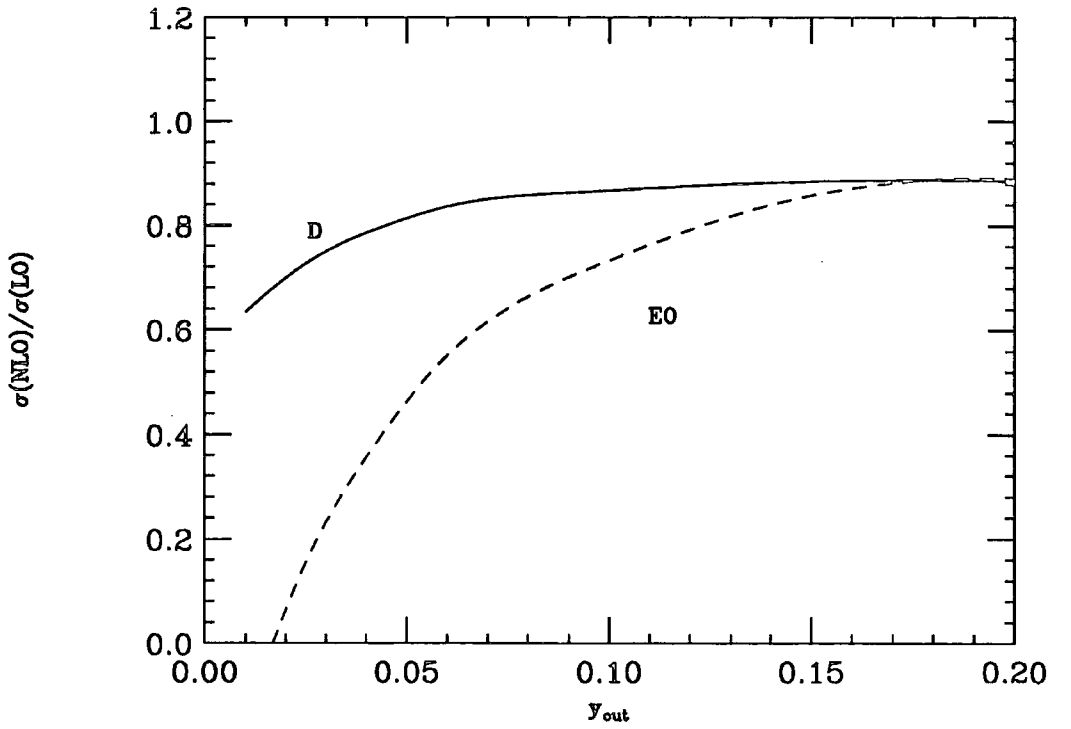

Figure 5.9: The next-to-leading order photon + 2 jet rate for $\alpha_s = 0.1087$ divided by the leading order rate in the Durham (solid) and E0 (dashed) schemes as a function of the jet separation parameter $y_{\rm cut}$ for $z_{\rm cut} = 0.99$.

We also see that as $z_{\rm cut} \to 1$, the contribution of the fragmentation function is extremely small, since the scale dependence almost vanishes. In other words, the nearly isolated photon cross section is insensitive to the fragmentation function in the two jet case and can be safely used to determine the quark electroweak charges [36, 40, 41]. For such purposes it is instructive to compare the relative size of the next-to-leading order corrections compared to lowest order. In Figure 5.9, we show this ratio for $z > 0.99$ as a function of $y_{\rm cut}$. In the Durham scheme with $\alpha_s = 0.1087$, the correction amounts to about -12% at large $y_{\rm cut}$, eventually exceeding -50% at $y_{\rm cut} = 0.005$. For larger values of α_s, the corrections are relatively more negative. On the other hand, in the E0 scheme, the corrections are much larger and imply that higher order corrections are necessary to have any reasonable prediction of the two jet rate in this scheme for almost the whole range of $y_{\rm cut}$.

It is interesting to compare the size of these corrections with the two step cone algorithm used in previous analyses. Here the photon is required to be isolated within a cone typically of half angle 15°. It is then removed from the event and the remaining hadrons clustered according to a jet algorithm. Of course, the photon is not completely isolated and can have 200-500 MeV of hadronic energy within the cone. This is approximately the same as requiring $z > 0.99$. The radiative corrections in this scheme for the E0 algorithm are relatively small [37]. However, we now see that in the "democratic" E0 algorithm, the corrections are large and negative. This is because the gluon is more often clustered with the photon since the effective cone size is larger. The requirement of little hadronic energy in the cluster then eliminates more events, thus reducing the cross section. Despite the fact that the "democratic" E0 scheme suffers large corrections, the "democratic" Durham scheme seems perturbatively stable for a reasonable range of $y_{\rm cut}$. We note that in all algorithms, as $y_{\rm cut}$ decreases the correction becomes large since the gluon is resolved as an additional jet thus reducing the two jet rate.

5.6 Summary

Throughout this chapter we have focused on photon production where the "photon" carries a large fraction of hadronic energy. This necessarily involves the photon fragmentation functions, $D_{q\to\gamma}$ and $D_{g\to\gamma}$. In photon + one jet events at LEP, the quark fragmentation function enters effectively at lowest order. Such events can potentially provide an experimental determination of the fragmentation function at large z. With the aid of simple analytic results, we have shown how the fragmentation function might be extracted at leading order for a "democratic" algorithm where photons and hadrons are treated equivalently. It is important to note that the fragmentation function measured with such a democratic algorithm should

be identical to that obtained from a cone-type definition. Furthermore, the fragmentation function should not depend on the value of $y_{\rm cut}$ at which it is determined. This provides a cross check on the measurement.

The gluon fragmentation function $D_{g\to\gamma}$ enters into the "photon" + two jet rate. However, it does so only at next-to-leading order. As a result, the cross section is only weakly sensitive to the gluon fragmentation function and it seems unlikely that a useful measurement can be made. On the other hand, the large z or almost isolated "photon" + two jet rate is largely insensitive to either quark or gluon fragmentation function and it should be possible to use these events to determine the quark electroweak charges.

We have seen that the next-to-leading order corrections to the photon + two jet rate are quite large and negative in the democratic algorithm. For cone-type algorithms, the corrections to the one jet rate are larger than for the two jet rate. One might expect that they might be important here as well and should be investigated.

The most important question to answer, however, is whether or not it is experimentally possible to observe the non-isolated photon signal at LEP. The main background is from π^0 decay into two photons. By requiring large z, the number of π^0's in the cluster can be reduced, however it is still a significant experimental problem to resolve two almost collinear photons from π^0 decay when the cluster energy is close to $M_Z/2$. This is a detector dependent issue and requires much study. Nevertheless, provided that the non-prompt background from π^0 decay can be experimentally controlled, events containing a single jet give an unparalleled opportunity to measure $D_{q\to\gamma}$. This may then be used as an input to other calculations such as the inclusive photon spectrum at the Fermilab TEVATRON where the theoretical uncertainty will be reduced. A determination of the small x gluon structure function may then be possible.

5.7 Postscript

Following the work contained in this chapter, the ALEPH collaboration have measured the photon fragmentation function at LEP. With respect to Eqn. (5.25), they find a parameterisation of the form

$$D^{\aleph}_{q\to\gamma}(z,\mu_F) = \left(\frac{\alpha e_q^2}{2\pi}\right)\left\{\frac{1+(1-z)^2}{z}\log\left(\frac{\mu_F^2}{\mu_0^2(1-z)^2}\right)+B\right\}, \tag{5.36}$$

is consistent with their data, where $\mu_0 = 0.16 \pm 0.2$ GeV and $B = -12.9 \pm 2.9$. This function has been measured for a democratic photon definition and the Durham clustering algorithm in the region $0.7 < z < 0.95$. With respect to their fit, the preferred values for these parameters are $\mu_0 = 0.2$ GeV and $B = -12.4$. [58]

For comparison with Figure 5.4, we include graphs of this fit plotted with respect to the ALEPH data, Figure 5.10, as it appeared in Ref. [58]. It is clear that our approach gives a consistent description of the available data. Note the rise of the data over the fit for all but the smallest value of $y_{\rm cut}$ shown. Following an analysis with the two hadronisation models ARIADNE and HERWIG [24], ALEPH conclude that this rise is due to *large* hadronisation corrections in this region. This point is illustrated by Figure 5.11, which is a comparison of the z values for 1-jet + photon events at the parton level and then at the hadron level as given by ARIADNE. In reaching the hadron level, they observe a significant fraction of 'isolated' parton level events populate the $0.95 < z < .99$ bin. This spilling over of events is noted to increase with $y_{\rm cut}$. For $y_{\rm cut} = 0.1$ there is a $\approx 20\%$ migration of events.

Accordingly, ALEPH choose to define 'isolated' 1-jet + photon events as those events with $z > .95$ and a comparison of the data to the full calculation, including the above parameterisation for the photon fragmentation function, is shown in Figure 5.12. Whilst

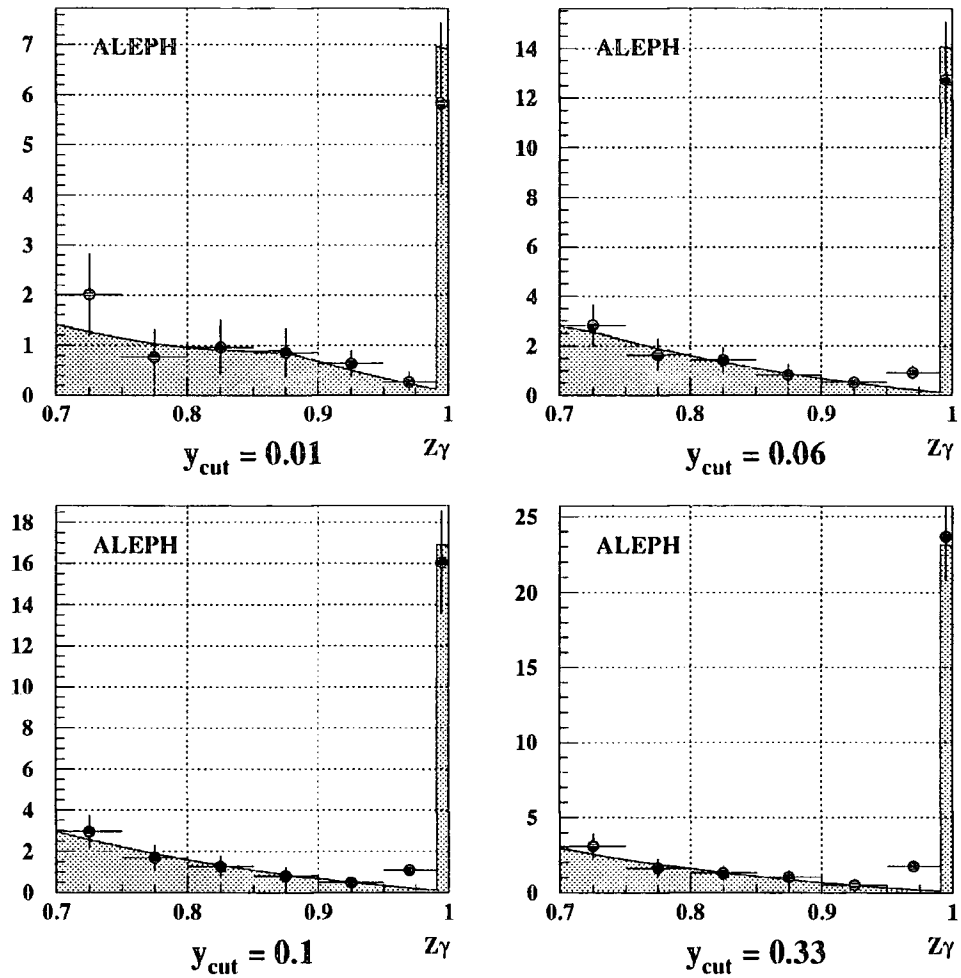

Figure 5.10: Comparison between the 1-jet + "photon" data and the full calculation including the ALEPH preferred fit for the photon fragmentation function. The large contribution to the $0.99 < z < 1$ bin is essentially the R_Δ contribution. The graphs are for four different values of $y_{\rm cut}$. The quantity represented on the vertical axis is $10^3 \times 1/\sigma_{HAD}\, d\sigma(\text{1-jet + "photon"})/dz$.

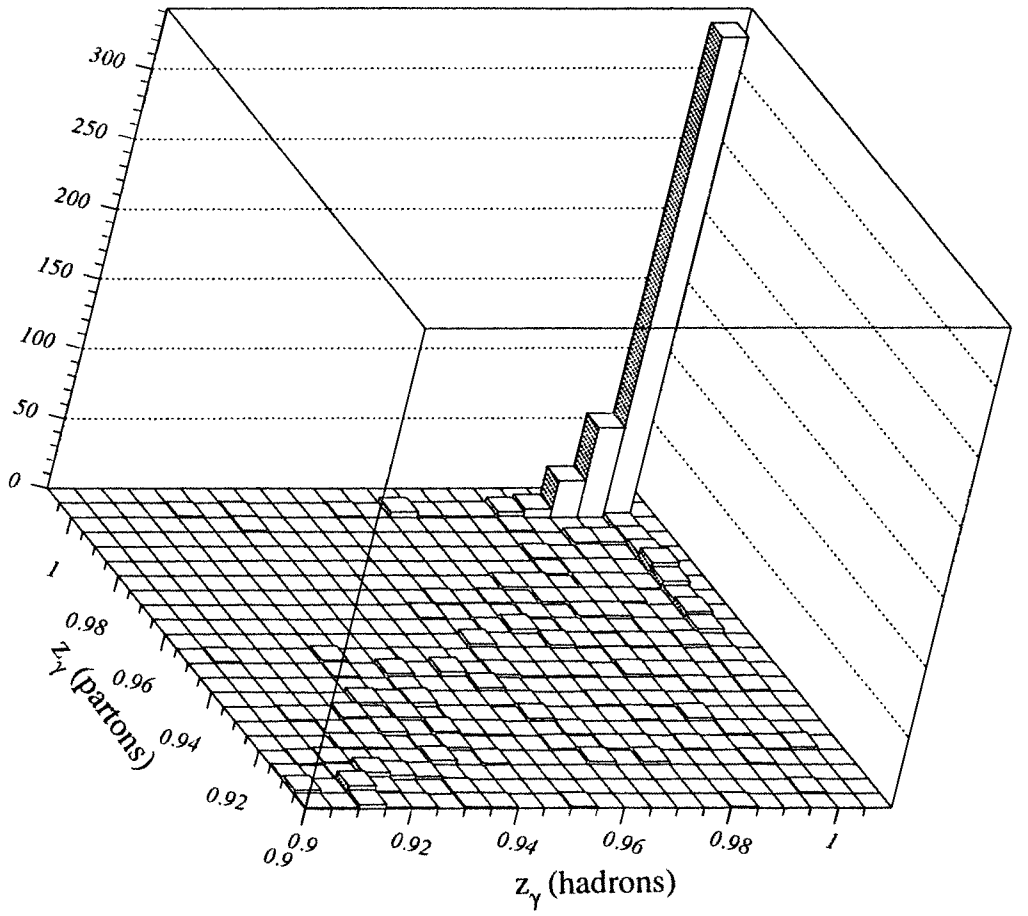

Figure 5.11: A comparison of parton level and hadron level z fractions for a selection of ARIADNE events at $y_{cut} = 0.1$. There is a distinct smearing of isolated partonic events into non-isolated hadronic events.

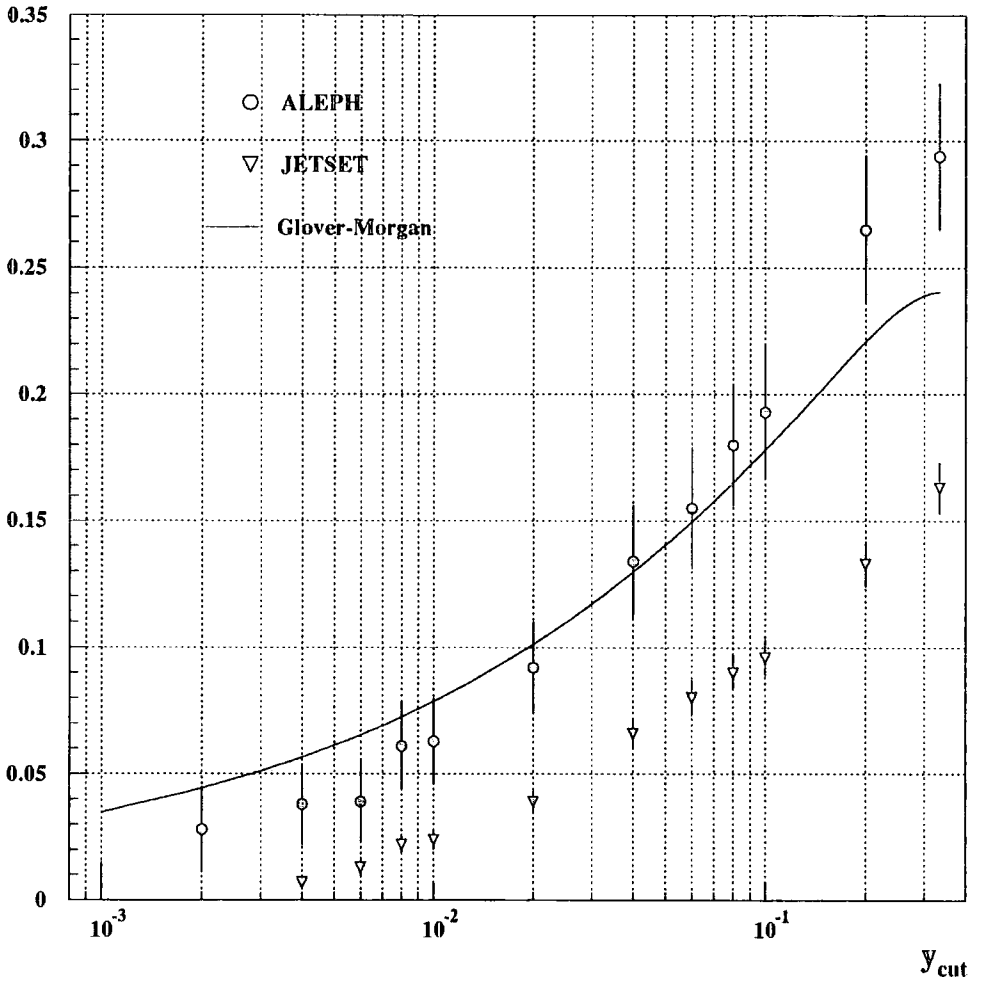

Figure 5.12: The 'isolated' 1-jet + photon rate plotted as a function of $y_{\rm cut}$. This graph shows the dependence of the "isolated" rate as a function of the jet resolution parameter $y_{\rm cut}$. Good agreement between the calculation of this chapter and the ALEPH data is observed in the central region of this plot. The vertical axis is $10^3 \times 1/\sigma_{HAD} \int_{0.95}^{1}[d\sigma(\text{1-jet + "photon"})/dz]\,dz$.

good agreement over the central range of $y_{\rm cut}$ is observed, taking the data as a whole it would appear that the overall slope is steeper in $y_{\rm cut}$ than the calculation would suggest. It is hoped that extending the calculation to the next order will address this difference.

The 2-jet + photon events (with a soft photon cut of $E_\gamma > 5$ GeV) are observed to be mostly insensitive to the fragmentation process, as might be expected since the leading order process is non-zero. For completeness, we show a comparison between the experimental rate and the predicted rate which includes the fragmentation function as measured in 1-jet + photon events. It is soft gluons that give the gentle slope to the high z region of the graphs, but the isolated, $z = 1$, leading order ($q\overline{q}\gamma$) contribution to the cross-section dominates the end bin. The effect of a rise in the cross-section from the collinear $q\gamma$ region appears to be suppressed over the whole range of z plotted.

The treatment of the asymptotic solution to the fragmentation function $D^{III}(z, \mu_F)$ of Eqn. (5.28) [53], in the main text of this chapter was based on its apparent use in a calculation of direct photon production [47]. Perhaps a more appropriate use of this function is as follows: for a suitable choice of scale, μ_F, chosen to characterise the size of a photon jet, we can hope to obtain from $D^{III}(z, \mu_f)$ the fraction of all hadronic final states that contain a photon of energy fraction z. In Figure 5.14, we have plotted the differential distribution in z of the 1-jet rate for $y_{\rm cut} = 0.1$. We include the ALEPH data and a number of curves. The full line is the calculation documented above using the ALEPH fragmentation function. The dotted curve is $2 \times D^{III}(z, \mu^2 = M_Z^2)$ and as is to be expected this lies well above the observed rate. The dashed curve is interesting in that it is simply the ALEPH measured fragmentation function $2 \times D^{\rm N}(z, \mu^2 = y^D M_Z^2/3)$, where y^S is the z dependent dimensionless invariant describing the size of the quark-photon jet (it is defined in Eqn. (5.23)). The factor 1/3 is inserted by hand and approximates the value of the non-logarithmic remainder to the complete calculation. The agreement of this curve with the full calculation suggests $\mu_F^2 = y^D M_Z^2/3$

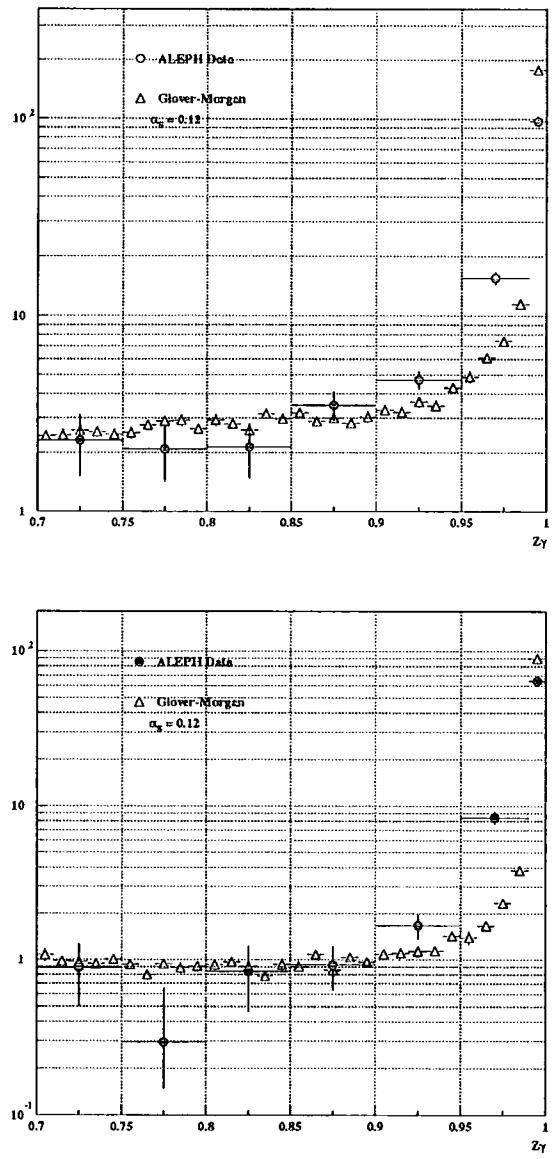

Figure 5.13: Comparison between the 2-jet + "photon" data and an $\mathcal{O}(\alpha\alpha_s)$ monte-carlo calculation (small triangles) including the ALEPH preferred fit for the photon fragmentation function. The graphs are for two values of $y_{\rm cut}$: 0.01 (upper) and 0.04 (lower). The quantity represented on the vertical axis is $10^3 \times 1/\sigma_{HAD}\ d\sigma(\text{2-jet + "photon"})/dz$.

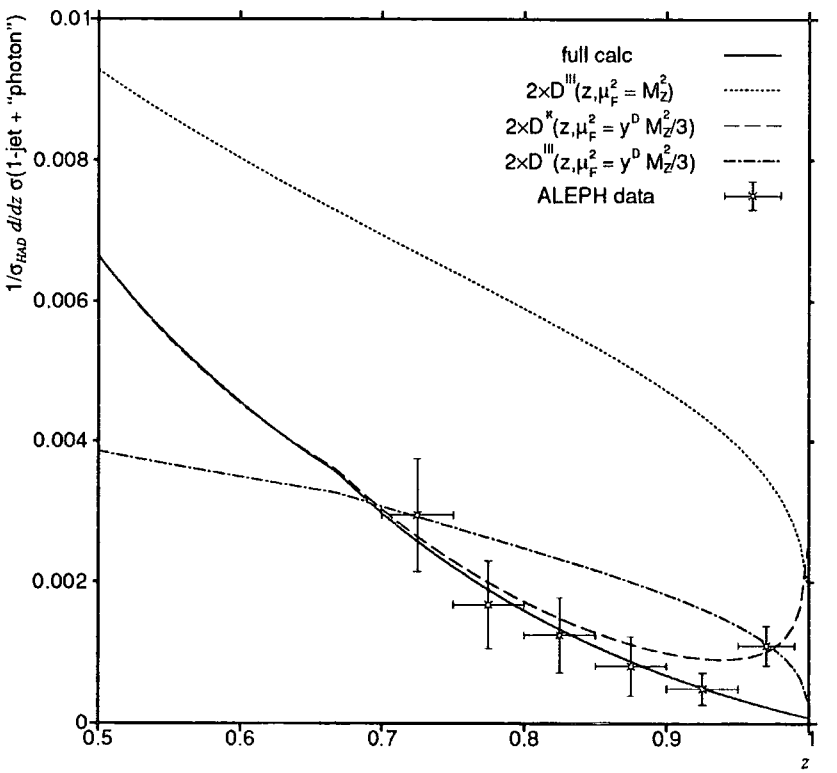

Figure 5.14: A comparison of the ALEPH data (at $y_{\rm cut} = 0.1$) with a more intuitive use of the D^{III} and $D^{\aleph}$ fragmentation functions.

is an appropriate choice. The remaining (dash-dotted) curve is $2 \times D^{III}(z, \mu^2 = y^D M_Z^2/3)$. Whilst the normalisation of this curve seems about right, it does appear to be somewhat flatter than the data would suggest. Figure 5.15 is the same as the previous graph but for a smaller jet resolution parameter, $y_{\rm cut} = 0.01$. Again, $2 \times D^{III}(z, \mu^2 = y^D M_Z^2/3)$ does not compare well with the data.

Appendix

In this appendix we give explicit formulae for the integrated cross-sections for the one jet plus photon events in various regions of phase space (see Figures 5.1 and 5.2).

The quantity R_Δ is the contribution from the region where the quark and antiquark combine to form a jet. For the two schemes considered here we find that (for a quark of charge e_q),

$$\begin{aligned} R_\Delta^{E0} &= \left(\frac{\alpha e_q^2}{2\pi}\right) \int_0^{y_{\rm cut}} dy_{q\bar{q}} \int_{y_{q\bar{q}}}^{1-2y_{q\bar{q}}} dy_{\bar{q}\gamma} \frac{(1-y_{\bar{q}\gamma})^2 + (y_{q\bar{q}} + y_{\bar{q}\gamma})^2}{(1-y_{q\bar{q}} - y_{\bar{q}\gamma})\, y_{\bar{q}\gamma}} \\ &= \left(\frac{\alpha e_q^2}{\pi}\right) \Bigg[-2{\rm Sp}(1-y_{\rm cut}) - 2{\rm Sp}(2\,y_{\rm cut} - 1) + \frac{3y_{\rm cut}}{4}(2y_{\rm cut} - 1) + \frac{\pi^2}{6} \\ &+ \log(1-2y_{\rm cut}) \left(\frac{5}{8} - 2\log(2-2y_{\rm cut})\right) + \log\left(\frac{y_{\rm cut}}{1-2y_{\rm cut}}\right) \left(y_{\rm cut} + \frac{y_{\rm cut}^2}{2}\right) \Bigg], \end{aligned} \tag{5.37}$$

and,

$$\begin{aligned} R_\Delta^D &= R_\Delta^{E0} + \left(\frac{\alpha e_q^2}{\pi}\right) \int_{y_{\rm cut}}^{y_0} dy_{q\bar{q}} \int_{y_{q\bar{q}}}^{\frac{y_{\rm cut} - y_{q\bar{q}}^2}{y_{\rm cut} + y_{q\bar{q}}}} dy_{\bar{q}\gamma} \frac{(1-y_{\bar{q}\gamma})^2 + (y_{q\bar{q}} + y_{\bar{q}\gamma})^2}{(1-y_{q\bar{q}} - y_{\bar{q}\gamma})\, y_{\bar{q}\gamma}} \\ &= \left(\frac{\alpha e_q^2}{\pi}\right) \Bigg[-\Big(8y_{\rm cut} - 9y_0 - 5 - 4(2+y_0)\log(y_0)\Big)\frac{y_0}{4} + \left(\frac{5}{8} - \log(4)\right)\log(1-2y_0) \\ &+ \log\left(\frac{1-y_{\rm cut}}{(y_{\rm cut} - {y_0}^2)\,(1-2y_0)}\right) \left(2\log(1-y_0) + \frac{(2+y_0)y_0}{2}\right) \end{aligned}$$

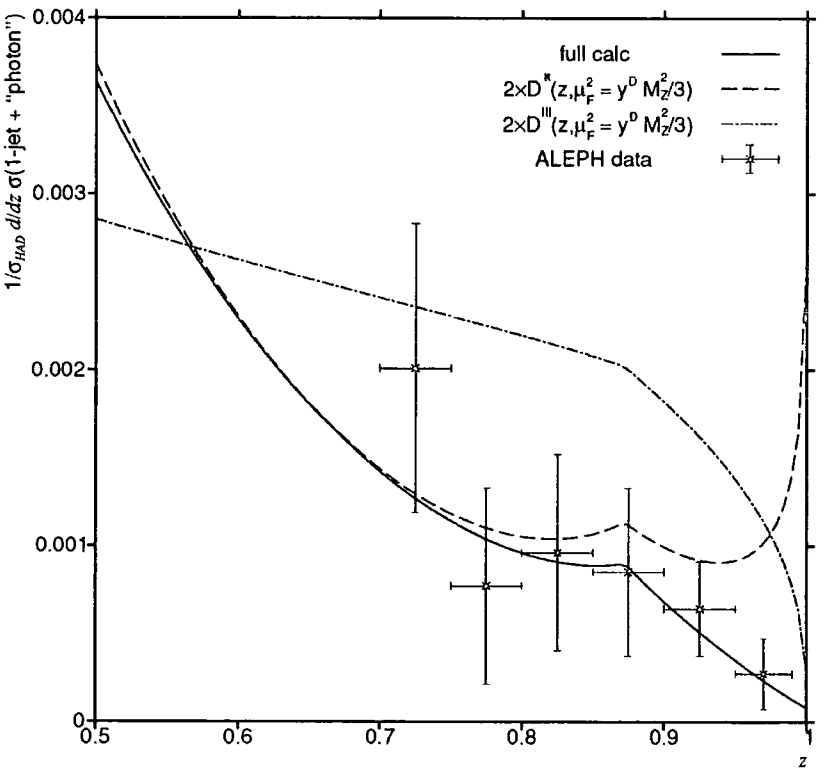

Figure 5.15: A comparison of the ALEPH data (at $y_{\rm cut} = 0.01$) with a more intuitive use of the D^{III} and $D^{\aleph}$ fragmentation functions.

$$
\begin{aligned}
&- \left(2\log\left(\frac{y_{\rm cut}+y_0}{2y_{\rm cut}}\right)+\frac{5}{4}\right)y_{\rm cut}\,(1-y_{\rm cut}) - \frac{(3+2\log(y_{\rm cut}))\,y_{\rm cut}}{4} \\
&+ \log\left(\frac{\sqrt{y_{\rm cut}}-y_0}{1-\sqrt{y_{\rm cut}}}\right)\left(\sqrt{y_{\rm cut}}+\frac{y_{\rm cut}}{2}\right) - 2{\rm Sp}\left(\frac{y_0-\sqrt{y_{\rm cut}}}{1-\sqrt{y_{\rm cut}}}\right) - 2\log^2(1-\sqrt{y_{\rm cut}}) \\
&- \log\left(\frac{\sqrt{y_{\rm cut}}+y_0}{1+\sqrt{y_{\rm cut}}}\right)\left(\sqrt{y_{\rm cut}}-\frac{y_{\rm cut}}{2}\right) - 2{\rm Sp}\left(\frac{\sqrt{y_{\rm cut}}+y_0}{1+\sqrt{y_{\rm cut}}}\right) - 2\log^2(1+\sqrt{y_{\rm cut}}) \\
&+ 2\log(1-\sqrt{y_{\rm cut}})\log(\sqrt{y_{\rm cut}}-y_0) + 2\log(1+\sqrt{y_{\rm cut}})\log(\sqrt{y_{\rm cut}}+y_0) \\
&- 2{\rm Sp}(2y_0-1) - 4{\rm Sp}(1-y_0) + {\rm Sp}(1-y_{\rm cut}) + \frac{\pi^2}{3}\Bigg],
\end{aligned}
\tag{5.38}
$$

where,

$$
y_0 = \frac{1}{4}(\sqrt{y_{\rm cut}^2+8y_{\rm cut}}-y_{\rm cut}).
$$

The Spence function, Sp, is given in Eqn. (A.14).

Where the photon and the quark (antiquark) combine to form a cluster with electromagnetic energy fraction greater than $z_{\rm cut}$, we find that the scale independent part of the 1 jet cross-section is given, in the E0 scheme by,

$$
F^{E0} = I_1(z_{\rm cut}, y) \tag{5.39}
$$

where,

$$
y = \min\left(y_{\rm cut}, \frac{1-z_{\rm cut}}{1+z_{\rm cut}}\right).
$$

In the Durham algorithm, for $z_{\rm cut} > 0.5$, we find,

$$
F^D = I_1\left(x, \frac{1-x}{1+x}\right) + \theta\,(z_0 - z_{\rm cut})\,\{I_2(z_0) - I_2(z_{\rm cut})\} \tag{5.40}
$$

with,

$$
x = \max\,(z_0, z_{\rm cut})\,,
$$

and,

$$z_0 = \frac{1-y_0}{1+y_0}.$$

The integral $I_1(a,b)$ has the following form,

$$\begin{aligned} I_1(a,b) &= \left(\frac{\alpha e_q^2}{\pi}\right)\left\{\left(\frac{1-a^2}{2} - 2(1-a) - 2\log(a)\right)\log\left(b(1-a)\right) + \frac{7}{2}(1-a)\right. \\ &+ b\left(\frac{8a-(1-2a)^2}{4}\right) + b^2\left(\frac{4-(1-a)^2}{4}\right) + 2\mathrm{Sp}\left(\frac{(1-a)b}{a}\right) \\ &- 2\mathrm{Sp}(2b) - 2\mathrm{Sp}(1-a) + \left(\frac{7-16b+4b^2}{8}\right)\log(1-2b) - \log^2(a) \\ &+ \left(\frac{a^2}{2(1-a)^2} - \frac{2a}{(1-a)}\right)\log\left(1-\frac{(1-a)b}{a}\right) + \frac{ab}{2(1-a)} \\ &\left. - \left(\frac{b^2}{2} - 2b\right)\log(a-(1-a)b) - \left(\frac{a^2}{2} - 2a\right)\log(a)\right\}, \end{aligned} \tag{5.41}$$

while,

$$\begin{aligned} I_2(z) &= \left(z - \frac{1}{2\,(1-z)^2} + \frac{2}{1-z}\right) y_{\mathrm{cut}}\left(1 + \frac{y_{\mathrm{cut}}}{2}\right) + \left(\frac{(z-4)\,z}{2} + 2\,\log(z)\right)\log(y_{\mathrm{cut}}) \\ &+ \frac{z^2 y_{\mathrm{cut}}\,(y_{\mathrm{cut}}-4)}{4} + \frac{y_{\mathrm{cut}}}{1-z} + y_{\mathrm{cut}}\,(3+y_{\mathrm{cut}})\log(1-z) + 4\,z + (z-4)\,z\log(z) \\ &+ \left(2\,\log(\frac{1-z}{z}) + \frac{5-6\,z}{2\,(1-z)^2}\right)\log(1-y_{\mathrm{cut}}) + 2\,\log^2(z). \end{aligned} \tag{5.42}$$

Chapter 6

Soft Gluon Radiation in Photon plus Single Jet Events at LEP

'Isolated' photon events at LEP have been defined using either a cone algorithm (where the photon is isolated in a cone and the remaining particles clustered with a jet algorithm) or a democratic algorithm (where all particles are clustered and the cluster containing the photon is identified as the photon). By studying the flow of soft gluon radiation in 'isolated' photon + single jet events at LEP we give a qualitative explanation of the size of radiative corrections in the different schemes.

6.1 Introduction

Recently e^+e^- annihilation events with hadronic final states containing an 'isolated' photon have attracted both experimental [40, 41, 42, 43] and theoretical interest [35, 38, 37, 39]. The physics motivation for studying such events is that the photon preferentially couples to up-type quarks, and therefore this event sample is enriched in up-type quarks. A measurement of the quark couplings to the Z boson [36] is thus possible. However, since a perfectly isolated photon is not an infrared safe quantity, it is necessary to discuss exactly what is meant by 'isolation'.

Experimentally, the photon candidate has been defined in two ways. In the CONE algorithm, the photon and all particles in a cone of half-angle θ_c are removed from the event to form the photon cluster. The remaining particles are then scanned for jets using a jet algorithm such as the JADE/E0 [44] or Durham [45] schemes with a jet resolution parameter $y_{\rm cut}$. In the democratic (DEMO) algorithm, the jet finding algorithm is applied to all particles in the event. The 'jet' containing the photon is then interpreted as the photon candidate. In both cases, in order to reduce the background from π^0 decay, the photon cluster is required to contain little or no hadronic contamination and the variable

$$z = \frac{E_\gamma}{E_\gamma + E_h}, \tag{6.1}$$

where E_h is the hadronic energy in the cluster, is constrained to be close to unity. Since it is very hard to detect very low energy particles, for practical purposes an 'isolated' photon may be accompanied by $O(500$ MeV) of hadronic energy.

Theoretical calculations have used both the democratic [35] and cone-type [38, 37, 39] algorithms. In order to cancel the infrared singularities associated with soft gluons, the soft

gluon must be allowed within the photon cluster. However, if all coloured partons are to be treated equally, then the quarks within the event should also be allowed inside the photon cluster and may be collinear with the photon. The quark-photon collinear singularity is regulated by the photon fragmentation function. To eliminate the uncertainty due to this fragmentation function, the theoretical calculations have compromised by allowing a small amount of gluonic energy into the photon cluster, but not allowing quarks to cluster with the photon. Since different calculations allow different amounts of gluon energy inside the photon cluster, the calculations are not in complete agreement [54]. To reconcile these differences it is necessary to treat the quark and gluon equally and to involve the fragmentation function properly [39, 55]. Even then, the region around $z = 1$ is problematic since radiating additional soft gluons may change z significantly.

6.2 Radiative corrections to the one jet rate

The issue we wish to address in this chapter is the size of radiative corrections in the different photon algorithms for photon + 1 jet events. It has been noted [35] that in a democratic scheme the corrections are small. In other words, the ratio of next-to-leading to leading order cross sections ($\mathcal{K}$ factor) is close to unity. On the other hand, in the cone type scheme, the corrections are quite large and negative [38, 37], $\mathcal{K} < 1$. Clearly the absolute size of the correction is determined by how the soft gluon region is treated, nevertheless, the relative size of the correction is determined by how the isolation cuts affect gluons with an energy above the energy allowed within the photon cluster. The $\mathcal{K}$ factors in both CONE and DEMO schemes for both the E0 and Durham jet algorithms are shown in Figure 6.1 using the theoretical definition of 'isolation' as described in ref. [37]. We see that for all $y_{\rm cut}$ and

for both jet algorithms,

$$\mathcal{K}_{DEMO} > \mathcal{K}_{CONE}.$$

By dressing the lowest order $e^+e^- \to q\bar{q}\gamma$ matrix elements with a soft gluon and examining the radiation pattern, we hope to show why this is so.

6.3 Lowest order events

The leading order contribution from the $e^+e^- \to q\bar{q}\gamma$ process to the photon + 1 jet rate is given by integrating the differential cross section (for massless quarks of charge e_q), (Eqn. (5.15))

$$\frac{1}{\sigma_0}\frac{d^2\sigma}{dx\,dx'} = \left(\frac{\alpha e_q^2}{2\pi}\right)\frac{x^2 + x'^2}{(1-x)(1-x')},$$

over the allowed region of the Dalitz plot. Here x and x' are the quark energy-fractions given by $x = 2E_q/\sqrt{s}$, $x' = 2E_{\bar{q}}/\sqrt{s}$ and $x_\gamma = 2 - x - x'$. In terms of these energy fractions, the scaled pair invariant masses are given by,

$$y_{q\gamma} = 1 - x', \quad y_{\bar{q}\gamma} = 1 - x, \quad y_{q\bar{q}} = 1 - x_\gamma, \tag{6.2}$$

where $y_{ij} = (p_i + p_j)^2/s = s_{ij}/s = 2E_iE_j(1 - \cos\theta_{ij})/s$.

The Dalitz plots for "isolated" photons with the CONE and DEMO schemes are shown in Fig. 6.2 for both the E0 and Durham algorithms. In the CONE scheme, the quark-photon singularities at $\theta_{q\gamma} = 0$ and $\theta_{\bar{q}\gamma} = 0$ which lie along the sides of the Dalitz plot are regulated by the photon isolation cut θ_c. In the DEMO scheme, the effective cone size for the photon cluster is much larger and consequently the cross section, for $\theta_c \ll 90°$, is much smaller [37]. Note that as is the case for pure jet analysis the Durham scheme [45] affords more phase

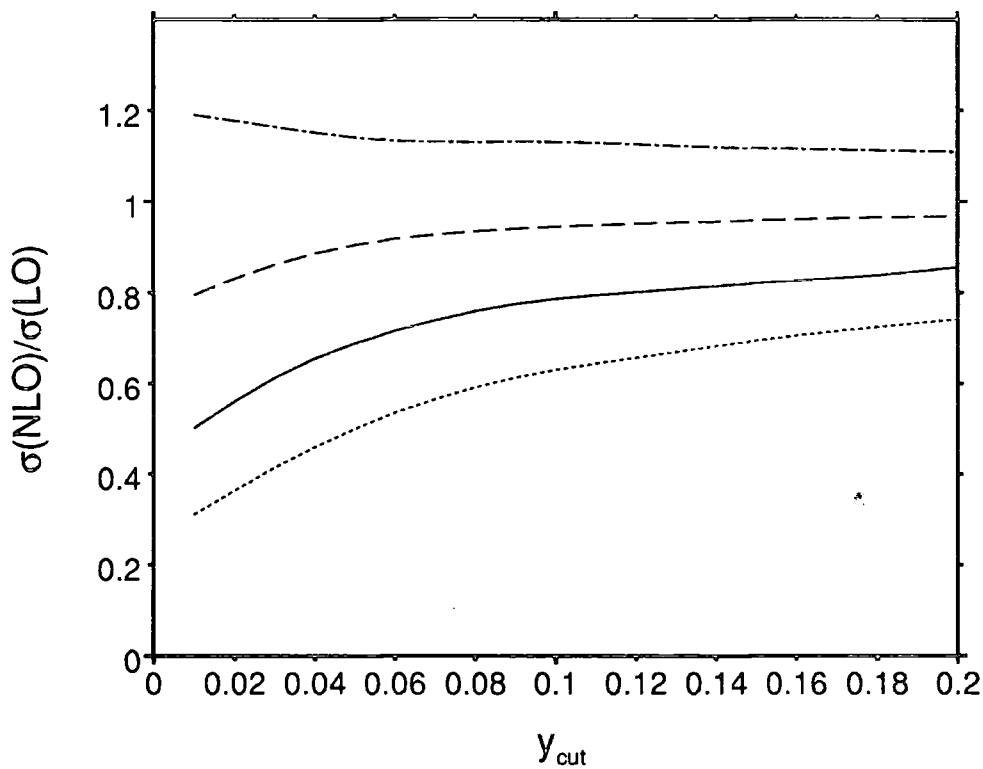

Figure 6.1: The ratio of next-to-leading order to leading-order cross sections for $e^+e^- \rightarrow$ 1-jet + 'isolated' photon production at LEP energies in the CONE scheme (with $\theta_c = 15°$) for the Durham (solid) and E0 (dotted) jet algorithms and in the DEMO scheme also for the Durham (dashed) and E0 (dash-dotted) jet algorithms.

Scheme	$E_\gamma/\sqrt{s}$	$E_{q\,\mathrm{hard}}/\sqrt{s}$	$E_{q\,\mathrm{soft}}/\sqrt{s}$	$\theta_{\gamma q\,\mathrm{hard}}$	$\theta_{\gamma q\,\mathrm{soft}}$	$\theta_{q\bar{q}}$
CONE Durham	.448	.475	.077	173	61	126
CONE E0	.486	.468	.047	176	81	103
DEMO Durham	.475	.419	.106	169	126	65
DEMO E0	.487	.427	.085	173	132	55

Table 6.1: The average value of energies and angles for 1 jet + 'isolated' photon events with $y_{\mathrm{cut}} = 0.06$ and $\theta_c = 15°$ for the different schemes. All angles are in degrees.

space to the analysis for a given y_{cut} than that of the E0 scheme.

The topology of the average (planar) event in the CONE and DEMO algorithms are quite different. As shown in Table 6.1, in the DEMO scheme, the average energy of the softest quark is larger than in the CONE scheme while the average angle between the quark and antiquark is much smaller. In the CONE algorithm, the softest quark typically lies relatively close to the isolation cone so that $y_{\gamma q\,\mathrm{soft}}$ is minimised. Momentum conservation then requires $\theta_{q\bar{q}}$ to be large while the requirement that the q and $\bar{q}$ coalesce to form a jet forces $E_{q\,\mathrm{soft}}$ to be relatively small. On the other hand, in the DEMO scheme, because the photon is in principle allowed to cluster with the quark/antiquark, the isolation criterion forces the $\theta_{\gamma q\,\mathrm{soft}}$ to be large. As a consequence, $\theta_{q\bar{q}}$ is much smaller and $E_{q\,\mathrm{soft}}$ somewhat larger. Within a given scheme, we see that $\theta_{q\bar{q}}$ is smaller with the E0 jet algorithm than in the Durham scheme. This reflects the extra phase space admitted by the Durham algorithm which is principally at large angles. The difference in the average angle between quark and antiquark will influence the colour flow in the event at higher orders.

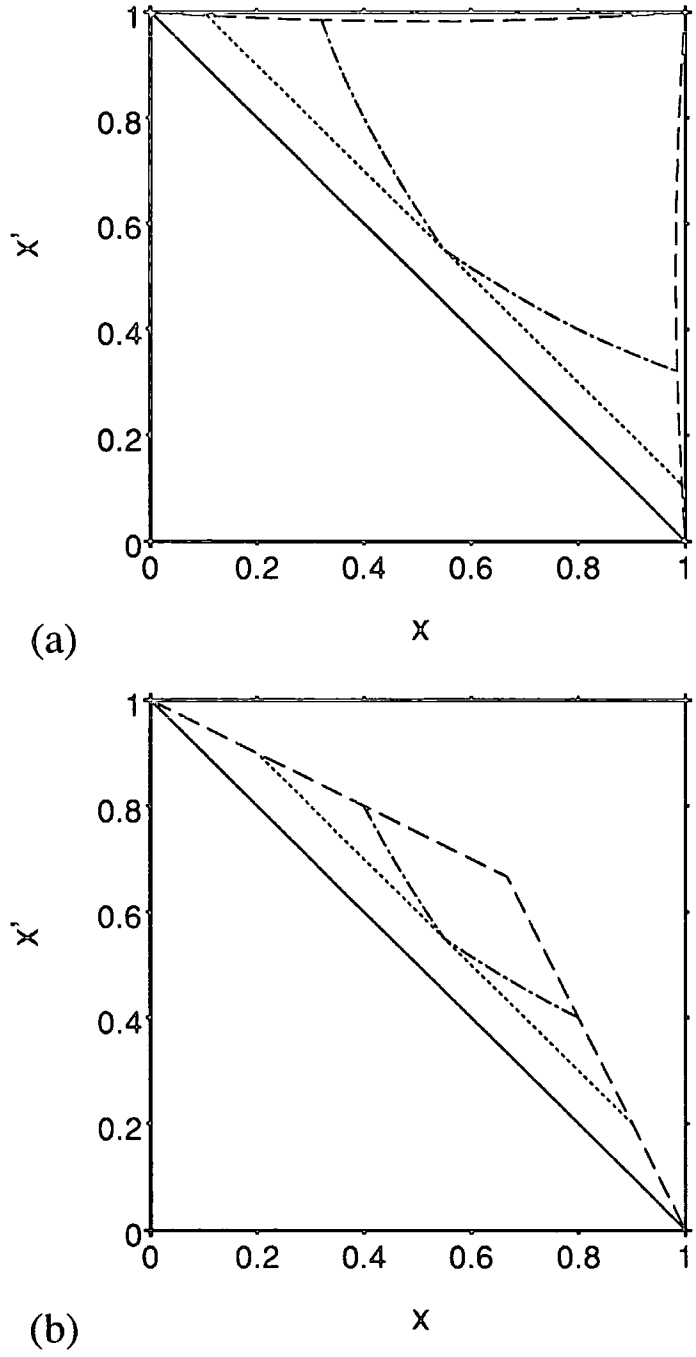

Figure 6.2: The Dalitz plots of isolated 1-jet + photon events with $y_{\rm cut} = 0.1$ for (a) the CONE algorithm with $\theta_c = 30°$ and (b) the DEMO algorithm. The 1-jet phase space is the region enclosed by the main diagonal, the isolation cut (dashed line) and the clustering algorithm - dotted line for E0 clustering and the dash-dotted line for the Durham algorithm.

6.4 The soft gluon distribution

The next-to-leading order corrections involve the addition of a gluon to the event in its real and virtual forms. The physical cross section is the result of a cancellation between the divergent (and positive) bremsstrahlung process and the divergent (and negative) virtual process (cf. Eqn. (4.57)). The isolation cuts will play an important role in determining the size of the bremsstrahlung process since they will veto the allowed configuration of the $q\bar{q}\gamma g$ final state. The radiative cross section is largest when the gluon is soft. In this case, the matrix elements undergo the usual soft factorisation in the limit $E_g \to 0$,

$$|M_{q\bar{q}\gamma g}|^2 \to S_F |M_{q\bar{q}\gamma}|^2, \tag{6.3}$$

where the soft eikonal factor S_F is given by,

$$S_F \sim \frac{y_{q\bar{q}}}{y_{qg} y_{g\bar{q}}}. \tag{6.4}$$

One can therefore study the effect of the isolation cuts on the bremsstrahlung process by fixing the energy of the gluon to be soft and examining the colour flow with respect to the partons of the underlying $q\bar{q}\gamma$ event. The more that the isolation cuts restrict the allowed phase space for the soft gluon to be *outside* the photon cone, the smaller the radiative contribution will be. The $\mathcal{K}$ factor will be correspondingly smaller.

In Fig. 6.3 we show radial plots, in the plane of the underlying event, of the soft eikonal factor, S_F, The $q\bar{q}\gamma$ configurations chosen are the average final state energies and angles, appropriate to (a) the CONE scheme and (b) the DEMO scheme for both the E0 and Durham algorithms as given in Table 6.1. The shaded regions of the plots indicate the forbidden region for gluon emission as dictated by the isolation cuts of the different schemes.

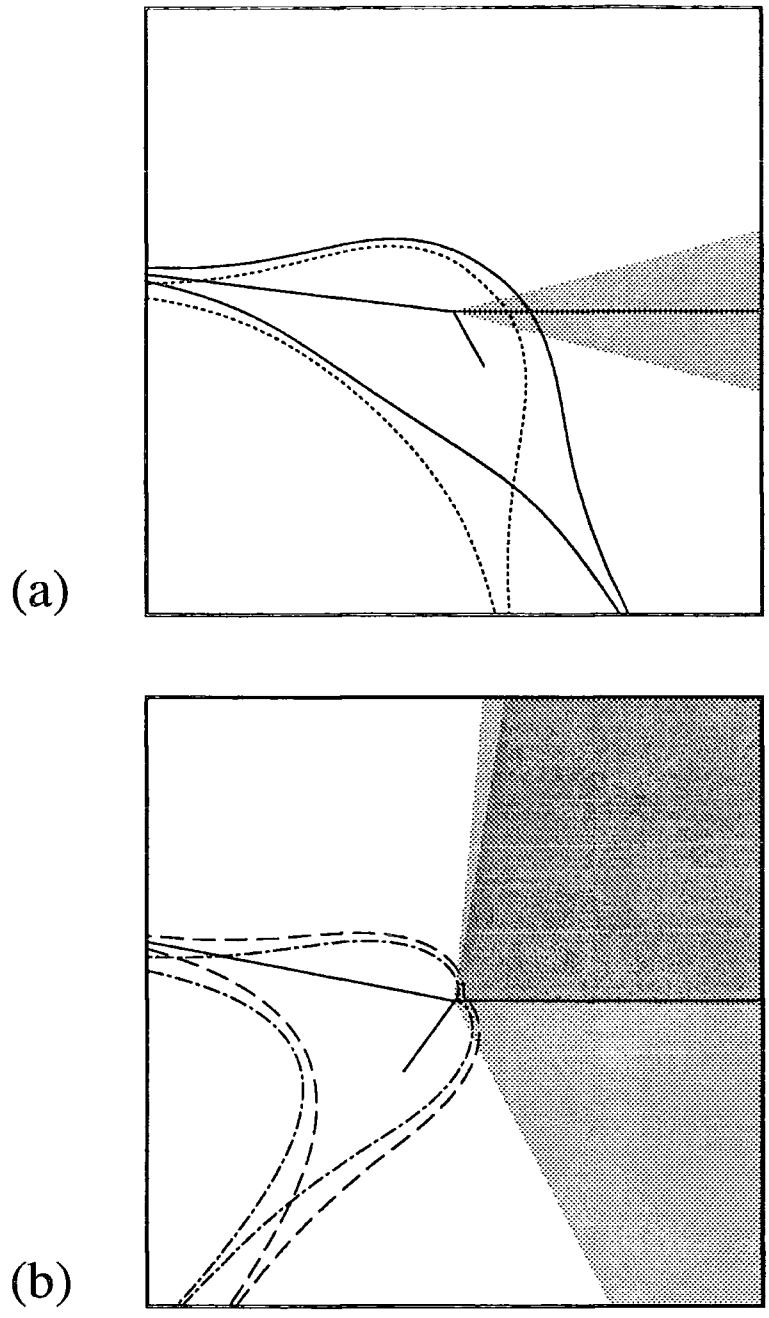

Figure 6.3: Eikonal factor plots for a soft gluon lying in the plane of the underlying 1-jet + photon event for $y_{\rm cut} = 0.06$ in (a) the CONE scheme (with $\theta_c = 15°$) for the Durham (solid) and E0 (dotted) jet algorithms and (b) the DEMO scheme for the Durham (dashed) and E0 (dash-dotted) jet algorithms. The $q\bar{q}\gamma$ configuration represents the average configuration as described in Table 1. For reference, the energy vectors for the Durham scheme are also plotted. The scale is radially logarithmic and normalised to the minimum value of the eikonal factor in the DEMO E0 scheme. The shaded regions indicate the appropriate photon isolation cut for each scheme. In (b) the darker shaded region corresponds to the E0 isolation cut.

The quark and antiquark form a coloured antenna that radiates gluons [56]. The radiation is greatest in the direction of the quark (antiquark) corresponding to the singularity in $1/s_{qg}$ ($1/s_{g\bar{q}}$). Nevertheless, there is significant soft gluon radiation at other angles. The radiation patterns clearly reflect the differences between the CONE and DEMO schemes. In the CONE scheme, the antenna is bent to one side of the exclusion cone surrounding the photon. As a result, the radiation pattern is stretched on the side opposite the soft quark and compressed between the quark and antiquark. The colour flow in such events is still relatively spread out, and soft gluons are able to identify sources of colour flow all around phase space. In the E0 scheme the average angle between quark and antiquark is smaller and this effect is slightly enhanced relative to the CONE Durham scheme.

In contrast, in the DEMO scheme, the antenna has been bent much more—the average angle between quark and antiquark is less than 90° and the compression/stretching of the radiation pattern is much more significant. Together the quark and antiquark form a colour singlet antenna out of which only hard gluons, with a small wavelength, are able to radiate; i.e. soft gluons are unable to resolve the macroscopic dimensions of the jet. The physical consequence of this is that the soft gluons are radiated in the region *between* the two quarks where they can see two colour sources. In the limit that $y_{\rm cut} \to 0$, $\theta_{q\bar{q}} \to 0$ and the antenna closes up. The jet has no net colour and there should be no soft gluon radiation outside of the jet. This is precisely what we are seeing in Fig. 6.3. As is true in the CONE case, the effect is more marked with the E0 jet algorithm than the Durham scheme.

We can now interpret these radiation plots in terms of the photon isolation cuts. Whenever there is a significant overlap in the energy flow of soft gluons into the isolation cone, those events will be vetoed by the isolation criterion. We can see that in the CONE algorithm, there is a significant overlap in the energy flow of soft gluons into the isolation cone. In contrast to this the soft gluon flow in the democratic events is almost exclusively *away*

from the photon and relatively few soft gluon events will be eliminated by the isolation cuts. We therefore expect that

$$\mathcal{K}^{DEMO} > \mathcal{K}^{CONE}.$$

We would also expect that hadronisation effects (and their influence on isolation) would be relatively smaller in the DEMO scheme precisely because the colour flow is largely contained within the jet. Experimentally, jet + photon events in the DEMO scheme should look rather clean in the hemisphere containing the photon. Indeed, it would be an interesting test of QCD to compare the energy flow (particle multiplicity) in ordinary two jet events where each jet is nominally a colour triplet with the energy flow (particle multiplicity) in democratic jet + photon events where the jet is almost a colour singlet.

Finally, we can make some comments about the jet algorithm dependence of the $\mathcal{K}$ factors within a given photon definition. In the democratic analysis, we see that (a) $\theta_{q\bar{q}}$ is smaller and (b) the angular region excluded by the isolation cuts is smaller in the E0 scheme compared to the Durham scheme. Crudely speaking, the E0 scheme is better at reaching into the wrong hemisphere to pull the gluon away from the photon and combine it with the quark-antiquark pair. This is precisely the feature that made the E0 scheme unattractive for purely hadronic final states. These arguments indicate that the E0 scheme will be more stable to radiative corrections so that,

$$\mathcal{K}^{DEMO}_{E0} > \mathcal{K}^{DEMO}_{D}, \tag{6.5}$$

as is seen in Figure 6.1. In fact, unlike ordinary purely hadronic jet events (and the CONE type photon + jet events where the colour antenna is relatively straight and the colour flow is more spread out), as $y_{\rm cut} \to 0$, we do not resolve more jets because the radiation is largely within the jet and the $\mathcal{K}$ factor does not diminish for small $y_{\rm cut}$. This is more marked in the DEMO E0 scheme because the average value of $\theta_{q\bar{q}}$ is smaller than in the DEMO Durham scheme.

In the CONE type algorithm, these simple arguments do not tell the whole story. We see in Figure 6.3 that isolation cuts do play a more significant role in the Durham scheme, however, contrary to our naive expectations, we see from Figure 6.1 that,

$$\mathcal{K}_D^{CONE} > \mathcal{K}_{E0}^{CONE}.$$

The reason for this discrepancy is that the typical energy of the soft quark is much lower in the CONE E0 scheme than in all the other schemes. This is shown in Figure 6.4 as a function of the jet resolution parameter $y_{\rm cut}$. Typically, the soft quark in this scheme has an energy of only a few GeV, significantly less than in the other schemes. To understand how the isolation cuts affect the isolated photon cross section, we have focused on soft gluon radiation with an energy that is in principle resolvable by an experiment, which is typically of $O(1$ GeV). This is not much less than the average energy of the softest quark in the CONE E0 scheme. Therefore, we might expect that the soft gluon approximation is not very reliable in this case and, although the gross features are correct, the radiation pattern does not accurately describe the distribution of soft gluons for this particular scheme. Consequently, the detailed ordering of $\mathcal{K}$-factors in the CONE scheme cannot be not explained by the rather qualitative discussion presented here.

6.5 Summary

In this chapter we have attempted to understand the relative sizes of QCD corrections to 'isolated' photon + 1 jet events at LEP which depend quite dramatically upon the scheme used to define the 'isolated' photon. To do this we have examined the colour flow of soft gluons with respect to the underlying hard scattering and how the isolation cuts restrict the

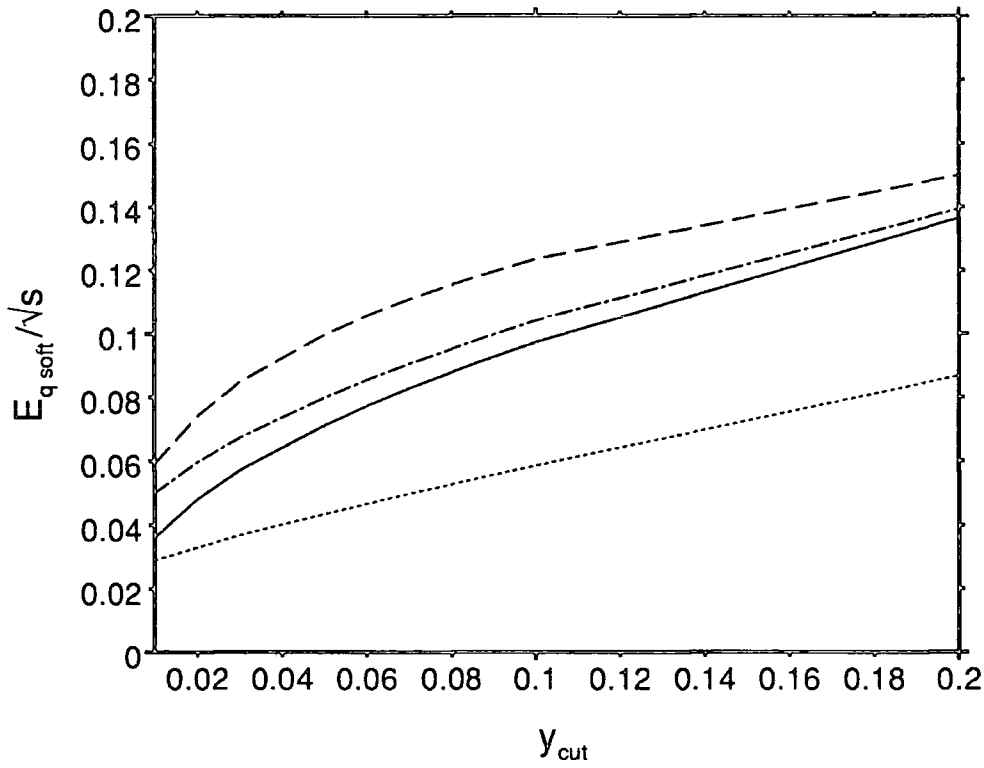

Figure 6.4: The average energy of the softest quark at leading order for $e^+e^- \rightarrow$ 1-jet + 'isolated' photon production at LEP energies as a function of $y_{\rm cut}$ in the CONE scheme (with $\theta_c = 15°$) for the Durham (solid) and E0 (dotted) jet algorithms and in the DEMO scheme also for the Durham (dashed) and E0 (dash-dotted) jet algorithms.

allowed phase space of the soft gluon. While these arguments are rather qualitative, they do describe the more quantitative results of Figure 6.1, namely,

$$\mathcal{K}^{DEMO} > \mathcal{K}^{CONE}.$$

At the same time, we can understand the hierarchy of radiative corrections in the DEMO scheme.

6.6 Postscript

Courtesy of the ALEPH collaboration, we include an example of a $z = 1$ isolated Durham DEMO 1-jet + photon event, Figure 6.5. In accordance with the expectations of this chapter, we note the extremely clean hemisphere associated with the photon. In addition, we note that the event as a whole only contains 6 hadrons—which can be compared with the more *normal* $\sim$ 20+ for a purely hadronic event. This is consistent with notion of a *colour confining antenna* of the form in Figure 6.3b.

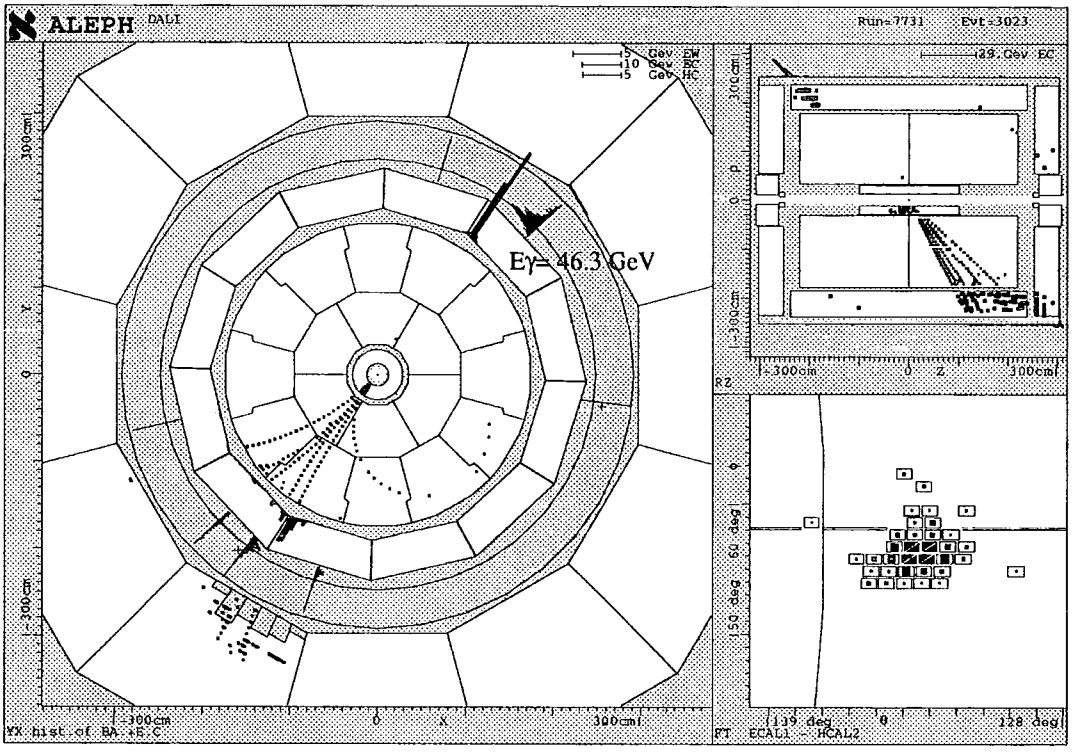

Figure 6.5: Courtesy of the ALEPH collaboration we present a $z = 1$ Durham DEMO 1-jet event. Note that all of the hadrons are confined to the hemisphere not containing the photon.

Chapter 7

The photon + 1 jet event rate with the cone algorithm in hadronic events at LEP

Using the recently measured photon fragmentation function, we make predictions for 'isolated' photon + 1 jet events using a cone type algorithm at LEP energies. For small cone half-angles, perturbation theory breaks down due to the presence of large logarithms. Furthermore, large hadronisation corrections are present. We suggest a definition of an 'isolated' photon which avoids these problems at small cone sizes and can be extrapolated to the reliably calculated large cone region.

7.1 Introduction

As noted in the previous two chapters, there has been some recent interest in studying 'isolated' and non-isolated photon production in hadronic final states in e^+e^- annihilation at LEP energies, $\sqrt{s} \sim M_Z$ [57, 41, 42, 43, 35, 37, 38, 39]. An 'isolated' photon is accompanied by essentially no hadronic energy, while a non-isolated photon cluster is characterised by the fraction z of electromagnetic energy compared with the total energy of the cluster, (Eqn. (5.11))

$$z = \frac{E_{EM}}{E_{EM} + E_{HAD}}.$$

The original motivation for making this distinction was to try to measure the electroweak couplings of the quarks using 'isolated' photons where the background from $\pi^0 \to \gamma\gamma$ was not severe [36]. It is difficult to resolve the two photons from an energetic π^0 and the pion can appear as a single electromagnetic shower in the calorimeter. Since a π^0 is usually accompanied by other hadronic debris, to reduce this background, it was required that few (or no) tracks occurred close to the electromagnetic shower. In non-isolated language, this corresponds to $z \sim 1$. From the theoretical standpoint, perfectly isolated photons are not infra-red safe since the isolation is spoiled by the emission of soft gluons and consequently soft hadrons into the photon direction. Provided that the non-trivial experimental problems in removing π^0 background can be overcome[1], it makes more sense theoretically to study the production of non-isolated photons and subsequently define an 'isolated' photon cluster as having z larger than some cutoff, $z_{\rm iso}$. However, in allowing some hadronic energy to accompany the photon, we admit the *perturbatively* divergent possibility that the photon was emitted from a collinear massless quark. In reality, this happens at large times, $c\tau \sim 1/\sqrt{s_{q\gamma}}$, so that in practice the quark has already hadronised and this final state collinear

[1]The ALEPH collaboration claims to be able to remove the π^0 background for $z > 0.7$ [58] and it may prove possible to extend this to $z > 0.5$

divergence can be factorised into a *non-perturbative* quark to photon fragmentation function at factorisation scale μ_F in much the same way that initial state collinear divergences are factorised into parton distributions [34]. The μ_F independent cross section then contains two components,

$$\sigma \sim \sigma(\gamma + \text{partons})(\mu_F) + \sum_{a=\text{quarks}} \sigma(\text{partons})\ D_{a\to\gamma}(z, \mu_F), \tag{7.1}$$

often denoted 'direct' and 'resolved' respectively which individually depend on μ_F. It is important to note that in order to correctly absorb the infra-red divergence, each contribution should be evaluated at the same order in perturbation theory [59, 55], i.e. if $\sigma(\gamma + \text{partons})(\mu_F)$ is evaluated at $\mathcal{O}(\alpha\alpha_s^n)$, then $\sigma(\text{partons})$ should be evaluated at $\mathcal{O}(\alpha_s^n)$ since $D_{q\to\gamma}(z, \mu_F)$ is $\mathcal{O}(\alpha)$ in the presence of isolation [39] (and *not* $\mathcal{O}(\alpha/\alpha_s)$ as commonly quoted in the literature). Once measured, the parton to photon fragmentation function, $D_{parton\to\gamma}(z, \mu_F)$, can be applied to a wide range of processes just as the proton parton densities are extracted from deep inelastic scattering experiments and used in hadron hadron collisions.

Previously (see Chapter 5 [55]), we described how the quark to photon fragmentation function could be measured in 'photon' + 1 jet events at LEP using a democratic algorithm to define the photon cluster: all particles (including the photon) are subjected to a clustering algorithm and the cluster containing the photon is designated the photon cluster provided that $z > z_{\text{cut}}$. This 'photon' + 1 jet rate is especially sensitive to the fragmentation function since the lowest order process, $e^+e^- \to \gamma + \text{parton}$, vanishes, while the next-to-leading order $\mathcal{O}(\alpha^3)$ 'photon' + 1 jet cross section, schematically given by,

$$\sigma \sim \sigma(q\bar{q}\gamma) + \sum_{a=q,\bar{q}} \sigma(q\bar{q})\ D_{a\to\gamma}(z, \mu_F), \tag{7.2}$$

does depend on the fragmentation function.

Following the ALEPH measurement of this function using a democratic photon definition with the Durham clustering algorithm in the region $0.7 < z < 0.95$ [58], one finds that the 'photon' + 1 jet data (after subtraction of the rather large π^0 background) can be described by a fragmentation function of the form, (Eqn. (5.36))

$$D^{\aleph}_{q\to\gamma}(z,\mu_F) = \left(\frac{\alpha e_q^2}{2\pi}\right)\left\{\frac{1+(1-z)^2}{z}\log\left(\frac{\mu_F^2}{\mu_0^2(1-z)^2}\right)+B\right\}, \tag{7.3}$$

where $\mu_0 = 0.20$ GeV and $B = -12.40$. The particular form of the fitting function is motivated by requiring that (a) the cross section is independent of μ_F and (b) the cross section is well behaved as $z \to 1$. This latter point requires some further clarification: the 'direct' contribution acquires one factor of $(1-z)$ in the logarithm from using dimensional regularisation and the $\overline{\rm MS}$ scheme to isolate the divergence as $s_{q\gamma} \to 0$. The second factor of $(1-z)$ comes from the boundary between the phase space regions where either the quark and antiquark combine to form the jet or the quark(antiquark) and photon combine to form the photon cluster. By explicitly removing these factors with this form of fragmentation function we ensure that the differential distribution is well behaved as $z \to 1$. In this chapter, we wish to make predictions for the 'photon' + 1 jet rate using the cone type photon definition currently in use for 'isolated' photon studies at LEP. The fragmentation function as measured by ALEPH should enable this quantity to be reliably predicted.

7.2 Photons defined with respect to a cone

The CONE algorithm for 'isolated' photon production [57, 41, 42, 43] can be straightforwardly carried over into the non-isolated case. First, a cone of half angle δ is placed around the photon and all hadrons inside the cone are clustered with the photon to form the photon

cluster such that $z > z_{\rm cut}$. Second, all hadrons outside the cone are subjected to a jet-finding algorithm, typically the E0/JADE [44] or the Durham [45] algorithms, with a jet resolution parameter $y_{\rm cut}$. Third, the photon cluster is resolved from the jets according to a resolution parameter $y^{\gamma}_{\rm cut}$.

As discussed above, the first non trivial contribution to the 'photon' + 1 jet rate comes from $e^+e^- \to q\overline{q}\gamma$ and $e^+e^- \to q\overline{q}$ where one of the quarks fragments into a photon. The Dalitz plot for the $q\overline{q}\gamma$ final state is shown in Figure 7.1 for the Durham and E0 jet algorithms with $\delta = 60°$, $y_{\rm cut} = y^{\gamma}_{\rm cut} = 0.1$ and $z_{\rm cut} = 0.8$ in terms of the quark and antiquark energy fractions,

$$x = \frac{2E_q}{\sqrt{s}} = 1 - y_{\overline{q}\gamma}, \qquad x' = \frac{2E_{\overline{q}}}{\sqrt{s}} = 1 - y_{q\gamma}, \tag{7.4}$$

where $y_{ij} = s_{ij}/s = (p_i + p_j)^2/s$ and $x_\gamma = 2E_\gamma/\sqrt{s} = 2 - x - x'$. This plot is basically the same as that of Figure 6.2b, the only difference is that here we indicate a non-unity $z_{\rm cut}$ value. In region 1, the quark and antiquark coalesce to form the jet and the photon cluster has $z = 1$, while in region 2 (3), the quark (antiquark) combines with the photon to form a mixed cluster with $z < 1$. The dashed line separating regions 1 and 2, shows the effect of the cone size in determining whether the quark combines with the photon or the antiquark. The collinear divergence occurs at $x' = 1$ and $x = 1$ respectively and lies along the edge of regions 2 and 3. This singularity can be absorbed into the 'resolved' photon contribution from $q\overline{q}$ final states where one of the quarks fragments into a photon. The 1 jet + 'photon' cross section (for massless quarks of charge e_q) as a function of z in scheme $S = E0$, D is then given by (Eqn. (5.20)),

$$\begin{aligned}\frac{1}{\sigma_0}\frac{d\sigma^S(1\text{ jet} + \text{“}\gamma\text{”})}{dz} &= 2\,D_{q\to\gamma}(z,\mu_F) + \left(\frac{\alpha e_q^2}{\pi}\right)\left[\frac{\left(1+(1-z)^2\right)}{z}\log\left(\frac{s}{\mu_F^2}\right)\right] \\ &+ \frac{1}{\sigma_0}\frac{d\hat{\sigma}(1\text{ jet} + \text{“}\gamma\text{”})}{dz} + R^S_\Delta\,\delta(1-z).\end{aligned} \tag{7.5}$$

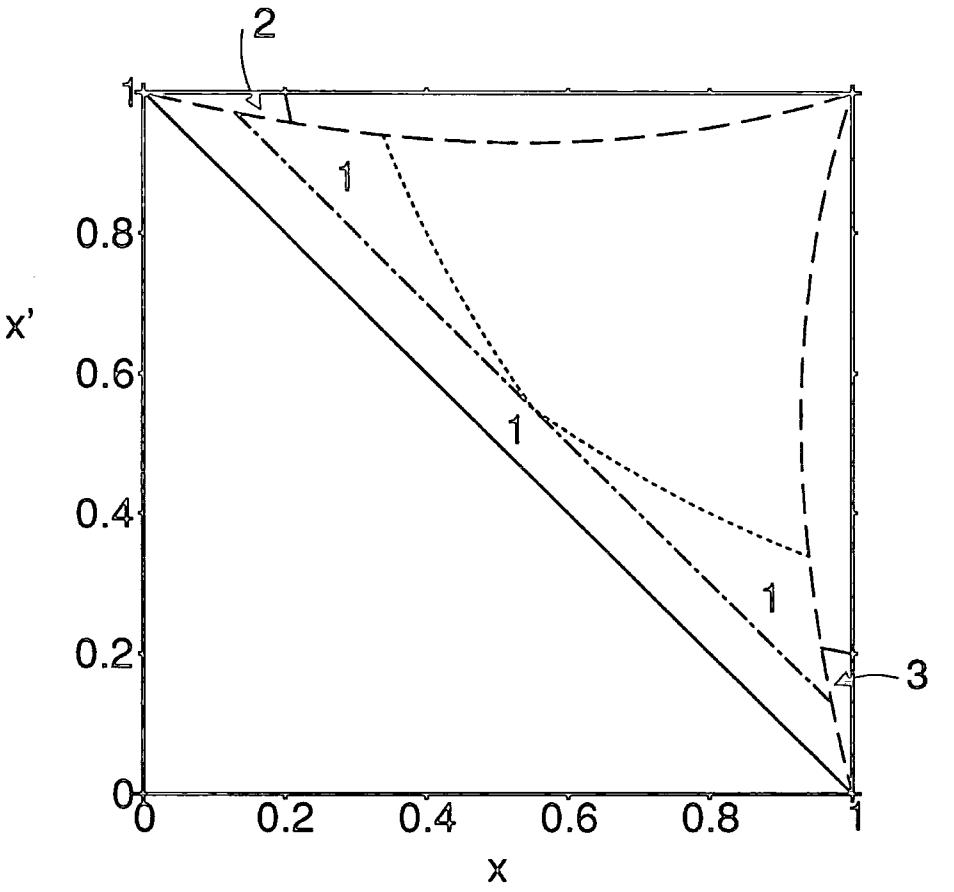

Figure 7.1: Dalitz plot for the $q\bar{q}+\gamma$ final state in terms of the quark and antiquark energy fractions x and x'. The dotted and dash-dotted lines show the 'photon' + one and two jet regions for $\delta = 60°$, $y_{\rm cut} = y^{\gamma}_{\rm cut} = 0.1$ in the Durham and E0 schemes respectively. The regions where the quark-antiquark combine to form a jet are separated from the region where the quark (antiquark) combines with the photon by a dashed line. The boundary in z for $z_{\rm cut} = 0.8$ curtailing regions 2 and 3 is shown solid.

Here the dependence on the scale μ_F has been made explicit, while the quantity R_Δ^S represents the jet algorithm dependent contribution to the cross section where quark and anti-quark combine, thus leaving the photon completely isolated. In this case, the photon cluster has $z = 1$. Unlike the democratic algorithms, R_Δ is the only scheme dependent contribution. The factorisation scale independent (but cone size dependent) contribution is given by, (Eqn. (5.21))

$$\begin{aligned}\frac{1}{\sigma_0}\frac{d\hat{\sigma}(1\text{ jet} + \text{“}\gamma\text{”})}{dz} = \left(\frac{\alpha e_q^2}{\pi}\right)\Bigg[&\frac{\left(1+(1-z)^2\right)}{z}\log\left(yz(1-z)\right) + z \\ &- \frac{1+(1-z)^2}{1-z}\left(\frac{zy}{1-z} + \frac{y(y-2)}{2} + \frac{(1-2z)^2}{z(1-z)^2}\log\left(\frac{z(1+y)-y}{z}\right)\right) \\ &- 4(1-z)y - 4\log\left(\frac{z(1+y)-y}{z}\right)\Bigg].\end{aligned} \tag{7.6}$$

Here y is the maximum value of $y_{q\gamma}$ allowed when the photon and quark combine,

$$y = \frac{1}{v}\left(1 - \sqrt{1-2v}\right) - 1 \quad \text{where} \quad v = z(1-z)(1-\cos\delta). \tag{7.7}$$

In the limit $z \to 1$ this boundary is given by,

$$y \to \frac{1}{2}(1-z)(1-\cos\delta), \tag{7.8}$$

which is to be compared with the analogous large z boundaries in the democratic Durham and E0 schemes of $y = (1-z)/(1+z)$ (see Eqn. (5.23) [55]). We see that in both cases, the boundary contains the same $(1-z)$ factor, so that with the choice of fragmentation function given in Eqn. (5.36), the cross section should in principle be well behaved as $z \to 1$. Furthermore, for $\delta = 90°$, the large z limits for the cone and democratic algorithms are identical.

There is a slight subtlety since there is a discontinuity in z across this boundary - for

$y_{q\gamma} > y$, $z = 1$, while for $y_{q\gamma} < y$, $z < 1$. This causes a problem when hadronisation effects are taken into account—the process of going from the parton level to the hadron level can cause a sizable shift in z. Although this mismatch exists in both democratic and cone algorithms, the problem is most severe when the matrix elements are largest - i.e. when y is small. In the democratic case, analysed by ALEPH [58], this problem is visible in the data as a spillover from the $z = 0.99-1$ bin to the adjoining $z = 0.95-0.99$ bin (see Figure 5.10). To get round this problem and to make a sensible comparison with the parton level predictions, ALEPH have defined an 'isolated' photon as having $z > z_{\rm iso} = 0.95$ and compared that with the parton level prediction for $z > z_{\rm iso}$. Since the $z \neq 1$ contribution (all the terms in Eqn. (7.5) apart from R_Δ) tends to zero at high z in the democratic Durham scheme, the result is dominated by R_Δ. By doing this, the uncertainty in z due to hadronisation effects is reduced where the cross section is largest. Hadronisation corrections can still move events from $z = 1$ to values of $z < z_{\rm iso}$, however, this occurs at larger values of $y_{q\gamma}$ where the cross section is smaller. With this procedure, ALEPH find good agreement between the theoretical predictions for the democratically 'isolated' photon + 1,2 and 3 jet rates [58]. In the cone algorithm, because y is somewhat smaller than in the democratic scheme, we expect that the mismatch between the z measured at the parton and hadron levels where the cross section is significant will extend over a larger range of z and that the corresponding value of $z_{\rm iso}$ should be smaller.

The differential cross section $1/\sigma_0 d\sigma/dz$ for the appropriate combination of light quarks at LEP energies is shown in Figure 7.2 for the CONE algorithm (this contribution is independent of the choice of hadron clustering algorithm) with $y_{\rm cut} = y^\gamma_{\rm cut} = 0.1$ and $\delta = 90°$, $60°$, $30°$ and $15°$. As noted earlier, for $\delta = 90°$, the cone and democratic algorithms merge at large z so that it is no surprise that the z distribution for $\delta = 90°$ is well behaved as $z \to 1$. However, for smaller cone sizes, although finite the distribution is negative for z close to 1. This is balanced by the rapid increase of R_Δ with decreasing cone size.

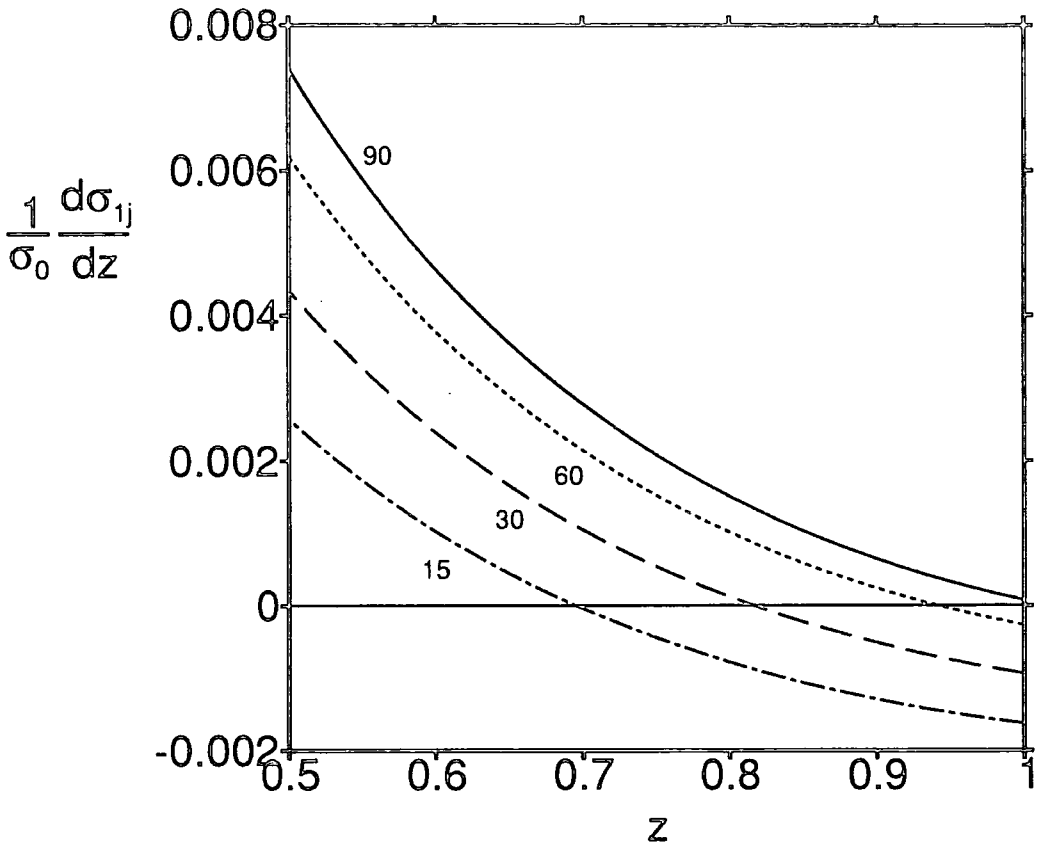

Figure 7.2: The differential cross section $1/\sigma_0 d\sigma/dz$, in the CONE type schemes and $y_{\rm cut} = y^{\gamma}_{\rm cut} = 0.1$ for the appropriate combination of light quarks at LEP energies with the ALEPH determination of the fragmentation function. The cone size is $\delta = 90°$ (solid), $\delta = 60°$ (dotted), $\delta = 30°$ (dashed) and $\delta = 15°$ (dash-dotted).

Based on the previous discussion, we expect that after hadronisation corrections the R_Δ contribution is partially smeared to lower z values, thereby filling in the negative region and creating a physically sensible positive definite distribution. To make a sensible comparison with experiment, it is necessary to introduce a suitable (δ dependent) choice of $z_{\rm iso}$. Clearly, for $\delta = 90°$, the ALEPH choice for the democratic algorithm would be appropriate, $z_{\rm iso} = 0.95$. However, we see that as δ becomes smaller, the negative region rapidly extends to much smaller values of z so that a much smaller value of $z_{\rm iso}$ is required. We can understand this by looking at the small δ limit,

$$\begin{aligned} R_\Delta^S &\rightarrow \left(\frac{\alpha e_q^2}{\pi}\right)\frac{\left(1+(1-z)^2\right)}{z}\log\left(\frac{1}{\delta^2}\right), \\ \frac{1}{\sigma_0}\frac{d\sigma^S(1\text{ jet} + \text{“}\gamma\text{”})}{dz} &\rightarrow \left(\frac{\alpha e_q^2}{\pi}\right)\frac{\left(1+(1-z)^2\right)}{z}\log\left(\delta^2\right). \end{aligned} \tag{7.9}$$

The $z = 1$ contribution (R_Δ) grows logarithmically as $\delta \rightarrow 0$ at the expense of the $z < 1$ fragmentation contribution. This is precisely the region in which perturbation theory breaks down because we try to resolve the collinear region where the fragmentation contribution is important. At small cone angles, the R_Δ contribution alone becomes meaningless. Note that in many studies of 'isolated' photons, the cone size is chosen to be $10° - 20°$ so that it is important to attempt to make a sensible prediction for 'isolated' photon + 1 jet production with small cone angles at LEP energies.

To estimate the cross section in the small δ limit it is vital to include the fragmentation contribution. This can be done in a well defined way, that avoids the large logarithms of the cone angle while simultaneously reducing the hadronisation corrections, by extending the boundary between the 'photon' + two jet region and region 1 (the dotted and dot-dashed lines in Figure 7.1) onto the $x = 1$ or $x' = 1$ axes such that,

$$z_{\rm iso}^D = 1 - \sqrt{y_{\rm cut}},$$

$$z_{\rm iso}^{E0} \;=\; 1 - y_{\rm cut}. \tag{7.10}$$

With this choice, the $\log(1/\delta)$ from R_Δ precisely cancels with a similar logarithm from the fragmentation region so that the cross section is almost independent of the cone size. This is exactly what we would expect; varying the cone size within the fragmentation region should not affect the cross section since we are unable to resolve any structure within this region. Furthermore, hadronisation corrections which slightly change x (x') and move events from region 1 to region 2(3) or vice versa, do not change the cross section. As a consequence, we expect that the cross section for $z > z_{\rm iso}^S$ (where $S = D,\ E0$) is a reliable estimate of the 'isolated' photon + 1 jet rate at *small* cone angles.

Figure 7.3 shows the 'isolated' photon + 1 jet cross section normalised to the total hadronic cross section as a function of the jet resolution parameter $y_{\rm cut}$. In Figure 7.3a, the cone size is 20° and the data is taken from ref. [41], while in Figure 7.3b, $\delta = 15°$ and the data is taken from ref. [57]. In both cases, the solid lines show the lowest order R_Δ contribution. As discussed in the previous chapter [37, 38, 60], the $\mathcal{O}(\alpha_s)$ corrections to R_Δ are large and negative ($\sim -45\%$), so that reasonable agreement with the data can be made for $\alpha_s \sim 0.12$ [57, 41]. These large corrections reflect the confusion over the precise definition of an isolated photon. On the other hand, the δ independent 'isolated' photon + 1 jet cross section for $z > z_{\rm iso}$ defined by Eqn. (7.10) (dotted line) is significantly closer to the data which suggests that (a) the hadronisation effects are modeled better and (b) that the higher order corrections to *both* R_Δ and the fragmentation region are of a more reasonable size.

It is interesting to ask how the 'isolated' photon + 1 jet cross section varies as a function of the cone angle. At large angles, $\delta \sim 90°$, the prediction merges with that for the democratic algorithm used to extract the fragmentation function while at small angles, we see from Figure 7.3 that the prescription described by Eqn. (7.10) is reasonable. By measuring

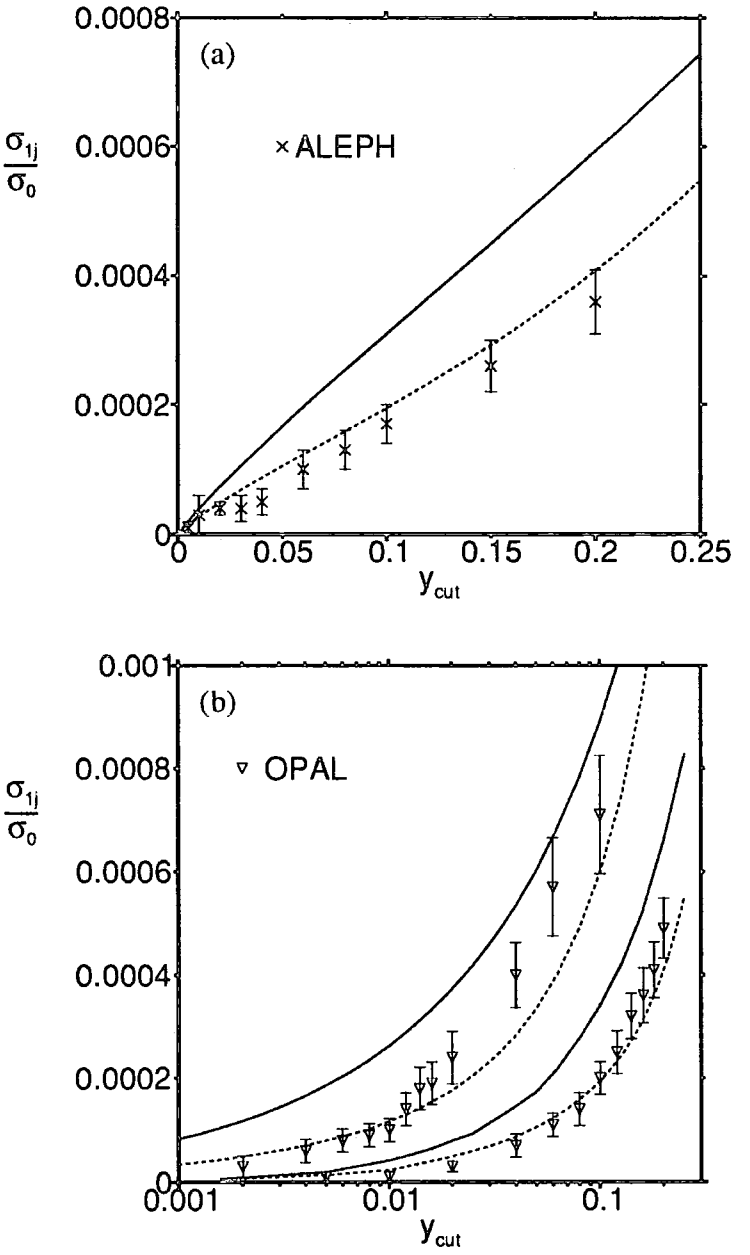

Figure 7.3: The 'isolated' photon + 1 jet cross section R_Δ (solid) and $\int_{z_{iso}}^{1} 1/\sigma_0 d\sigma/dz\ dz$ (dotted) for (a) $\delta = 20°$ in the E0 scheme and (b) $\delta = 15°$ in both Durham and E0 schemes as a function of the jet resolution parameter y_{cut}. z_{iso} is given in the text, whilst the data is taken from Refs. [57, 41]

the cross section as a function of δ, we can hope to extract further information about the fragmentation region. To make a rough estimate of how the cross section varies for intermediate δ, we can adapt the phenomenological ALEPH approach to solving the hadronisation problem and choose the value of z separating 'isolated' from non-isolated photons to be the value of z where the boundary between the fragmentation and quark-antiquark combination region takes the value $y = y_0$ such that for $\delta > \delta_0$,

$$z_0 = \frac{1}{2}\left(1 + \sqrt{1 - \frac{(1-\cos\delta_0)}{(1-\cos\delta)}}\right), \tag{7.11}$$

where,

$$\cos\delta_0 = 1 - \frac{8y_0}{(1+y_0)^2}. \tag{7.12}$$

For $y > y_0$ ($z < z_0$) we can in principle use perturbation theory to examine the fragmentation region, however for $y < y_0$ ($z > z_0$), we cannot reliably resolve the photon from the accompanying hadronic debris and therefore assign the event to the 'isolated' photon category. In the democratic scheme, ALEPH find $z_{\rm iso} = 0.95$ corresponding to $y_0 = 0.025$ to be a suitable choice [58] which corresponds to a cone size of $\delta_0 = 35.9°$, and an apparently *large* invariant mass for the photon quark cluster of $\approx$ 14 GeV. Therefore, as a first estimate of the cone size dependence of the cross section, we define the value of z separating 'isolated' from non-isolated photons to be,

$$z_{\rm iso} = \max\,(z_{\rm iso}^S, z_0). \tag{7.13}$$

This is shown in Figure 7.4 for both the Durham and E0 schemes with $y_{\rm cut} = y_{\rm cut}^\gamma = 0.1$ and $y_0 = 0.025$. The solid lines show the logarithmically increasing R_Δ contribution while the dotted lines represent this approximation. At large values of δ, $z_{\rm iso} \to 0.95$, while for small values of δ ($\delta < 39°$ in the Durham scheme and $\delta < 61°$ in the E0 scheme), $z_{\rm iso} \to 0.68$ and 0.9 respectively. As expected from Eqn. (7.2), at large cone angles, the cross section integrated

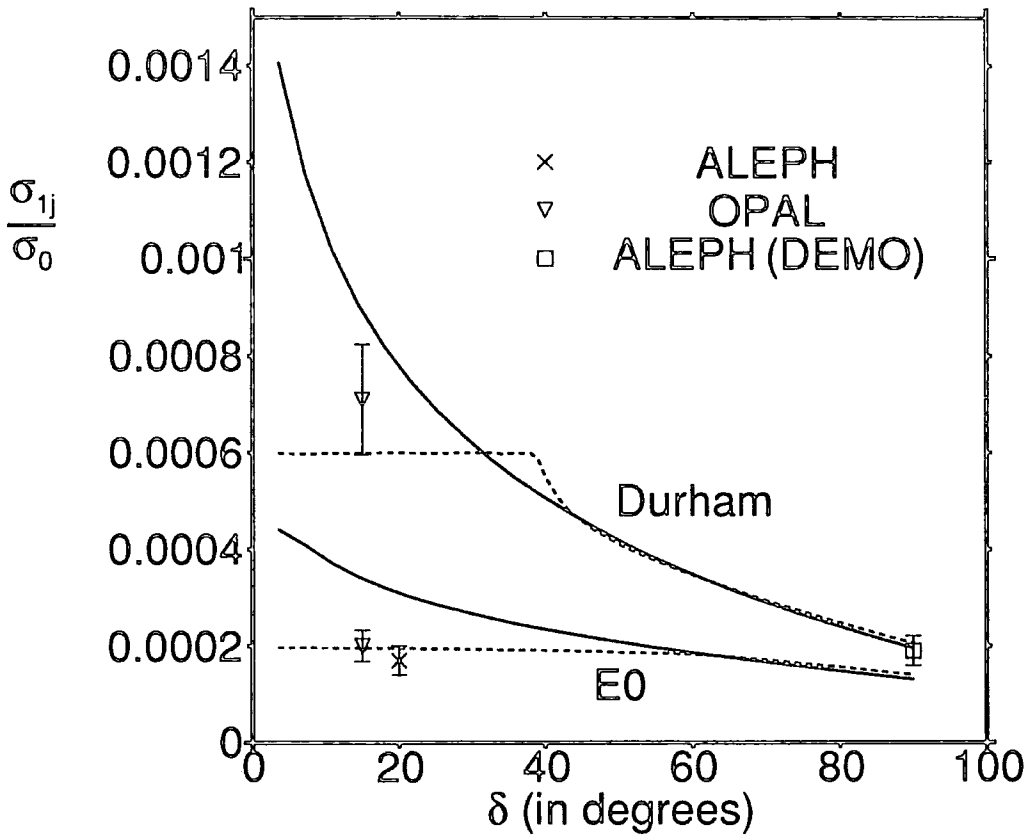

Figure 7.4: The 'isolated' photon + 1 jet cross section R_Δ (solid) and $\int_{z_{\rm iso}}^1 1/\sigma_0 d\sigma/dz\ dz$ (dotted) for $z_{\rm iso}$ given by Eqn. (7.13) in the Durham and E0 schemes as a function of the cone angle δ for $y_{\rm cut} = y_{\rm cut}^\gamma = 0.1$. The data is taken from Refs. [57, 41] and [58]

above $z_{\rm iso}$ and R_Δ are rather close; perturbation theory is working well and the hadronisation corrections are small. The z distribution tends to zero as $z \to 1$ and the contribution from $1 > z > z_{\rm iso}$ is small. On the other hand, for smaller values of δ this is no longer the case and the rapid growth of R_Δ is counterbalanced by the increasingly negative contribution from $1 > z > z_{\rm iso}$. Around $\delta \sim 40°$ in the Durham scheme, the overall contribution from $1 > z > z_{\rm iso}$ is slightly positive resulting in a cross section slightly larger than R_Δ. The available data from OPAL [57] and ALEPH [41] are also shown. For comparison, we also show the $y_{\rm cut} = 0.1$ point from the democratic ALEPH analysis [58] at $\delta = 90°$.

7.3 Summary

In this chapter we have attempted to utilise the recent ALEPH measurement of the photon fragmentation function to predict the 'photon' + 1 jet rate using the cone algorithm. However, at small angles there are large hadronisation corrections and large logarithms of the cone size. To avoid these problems, we have defined an 'isolated' photon as having $z > z_{\rm iso}$ where $z_{\rm iso}$ is given in Eqn. (7.13). At small angles, we find rough agreement between our lowest order prediction and the available data. This is quite remarkable since previously large negative $\mathcal{O}(\alpha_s)$ corrections to the 'perfectly' isolated photon event rate (R_Δ alone) were necessary to describe the data. We expect that the $\mathcal{O}(\alpha_s)$ corrections to the 'isolated' photon + 1 jet rate using our definition will be small.

At large cone sizes, the cone algorithm is very close to the democratic algorithm used to extract the photon fragmentation function. Accordingly, we expect the prediction of the large δ cross section to be reliable. Motivated by the ALEPH data, we have also provided an estimate of how the 'isolated' photon + 1 jet rate depends on the cone size. A measurement

of this dependence should provide yet another probe of the fragmentation region.

Chapter 8

Z boson decay into photons

We perform a complete one-loop $O(\alpha^4)$ calculation of the coupling of the Z-boson to three photons via both fermion and W boson loops keeping the full dependence on the quark and W masses. To evaluate the W boson contribution to the fourth rank polarisation tensor we use the unitary gauge. We find that the contributions from fermion and boson loops are remarkably similar. Expressions for the helicity amplitudes are presented. The results are applied to the decay $Z \to \gamma\gamma\gamma$ where we find a partial width of about 1.35 eV for $m_{\rm top} > 91$ GeV and $\sin^2\theta_W = 0.23$, of which the W boson loops account for approximately 0.3 eV mainly through their interference with the fermion loops.

8.1 Introduction

One interesting aspect of quantum field theories is the generation of interactions that are not present at the classical level. Such interactions occur when a virtual pair of particles is emitted, radiate further particles and are then reabsorbed. The most famous example of this is the scattering of light by light which was first studied in the context of quantum electrodynamics [61]. Since the photon only interacts directly with charged particles, this process first occurs at $\mathcal{O}(\alpha^4)$ when four photons are attached to a charged fermion loop. In other words, at *one-loop* the *effective action* contains terms that couple chargeless fields. Within the $SU(2) \times U(1)$ model of electroweak interactions, there is also a contribution at the same order from charged boson loops. Although it has been shown that the boson contribution is finite for photon-photon scattering [62, 63], as indeed it must be in a renormalisable theory, the effects of the W loops have not been widely studied.

Recently, prompted by experiments at LEP, attention has focused on the decay of the Z boson into photons [64, 65, 66]. The two photon decay is forbidden by Yang's theorem, however the three photon decay is allowed and the fermion contribution is well known [67, 68, 69]. As dictated by the Appelquist-Carrazone decoupling theorem [70], the top quark contribution rapidly decouples for $m_{\rm top} > M_Z/2$ and can essentially be ignored. The remaining light leptons and quarks give a contribution to the amplitude proportional to the vector coupling with the Z boson, v_f and the cube of the electric charge, e_f. A closed form for the light fermion contribution to the partial width can be found [71, 69],

$$\Gamma(Z \to \gamma\gamma\gamma) = \alpha^3 \alpha_Z \left(3 \sum_q e_q^3 v_q + \sum_l e_l^3 v_l\right)^2 \frac{1}{6} \frac{M_Z}{12\pi^3} X, \tag{8.1}$$

where,

$$X = 200\zeta_5 - 8\pi^2\zeta_3 + \frac{7}{15}\pi^4 - 128\zeta_3 + \frac{41}{3}\pi^2 - 124 \sim 14.954, \tag{8.2}$$

and ζ_n is the nth Riemann zeta function. The factor 3 multiplying the quark contribution is due to colour. For five flavours of light quarks, $\alpha(M_Z) = 1/128$, $\alpha_Z = \alpha(M_Z)/\sin^2\theta_W \cos^2\theta_W$ and $\sin^2\theta_W = 0.23$, we find,

$$\Gamma(Z \to \gamma\gamma\gamma) = 1.05 \text{ eV}. \tag{8.3}$$

In addition to the fermion loop contribution, there is also a contribution from $W^{\pm}$ boson loops which probes the non-abelian nature of the electroweak model. Both trilinear ($WW\gamma$ and WWZ) and quartic ($WW\gamma\gamma$ and $WW\gamma Z$) vertices contribute and in principle this provides a test of these couplings. In practice, however, if these couplings deviate from the structure dictated by the $SU(2) \times U(1)$ gauge theory, the W boson loop contribution is incalculable. Three calculations exist in the literature. Baillargeon and Boudjema [64] use a non-linear R_ξ gauge [72], while Pham [65] and Dong et al. [66] use a linear R_ξ gauge. By making an approximation where M_W is large compared to all other scales in the problem, Refs. [64] and [66] find that the W loop alone contributes about 0.02 eV to the Z boson width, approximately 50 times smaller than the fermion contribution. Pham, estimates that the total $Z \to \gamma\gamma\gamma$ width for both fermion and boson loops is about 2 eV. No estimate exists where the exact dependence on both M_W and the unknown top quark mass is kept.

It is worth noting that in all three cases, the 't Hooft-Feynman gauge is chosen so that $\xi = 1$. This gauge has the particular advantage that the $k^\mu k^\nu$ part of the W boson propagator is zero so that individual diagrams do not contain superficial divergences. On the other hand, these gauges do contain many more diagrams than the unitary gauge due to the propagation of the unphysical Goldstone boson and ghost fields. For the purposes of this chapter, we choose to minimise the number of Feynman diagrams and use the unitary gauge. It is straightforward to cancel the superficial divergences before reducing the tensor integral to scalar integrals in the usual way [18].

The organisation of our chapter is as follows. In Section 8.2, we construct the polarisation tensor for the $Z\gamma\gamma\gamma$ coupling. Due to gauge invariance and the possibility of exchanging identical photons, this tensor be described by three independent scalar amplitudes (rather than four [66, 73]). We find that the boson amplitudes are (surprisingly) closely related to the fermion amplitudes. In order to translate the polarisation tensor into a physical decay width, we introduce helicity amplitudes in Section 8.3. Numerical results for the $Z \to \gamma\gamma\gamma$ partial width are given in Section 8.4, while the main results are summarised in Section 8.5.

8.2 The $Z\gamma\gamma\gamma$ polarisation tensor

The matrix element, $\mathcal{T}$, for the scattering of an on-shell Z boson with three on-shell photons can be written as,

$$\mathcal{T} = \epsilon_\alpha(p_4)\epsilon_\mu(p_1)\epsilon_\nu(p_2)\epsilon_\rho(p_3)\mathcal{T}^{\alpha\mu\nu\rho}(p_1, p_2, p_3), \tag{8.4}$$

where we denote the ingoing momenta and Lorentz indices of the photons by p_1^μ, p_2^ν, p_3^ρ while the momentum and Lorentz index for the Z boson is p_4^α. Using momentum conservation, the momentum of the Z boson is related to the photon momenta by,

$$p_4^\alpha = -p_1^\alpha - p_2^\alpha - p_3^\alpha, \tag{8.5}$$

so that the polarisation tensor for the $Z\gamma\gamma\gamma$ coupling, $\mathcal{T}^{\alpha\mu\nu\rho}(p_1, p_2, p_3)$, depends only on the three photon momenta.

The most general fourth rank tensor contains 81 terms of the type $p_i^\mu p_j^\nu p_k^\rho p_l^\alpha$, 54 terms of the type $p_i^\mu p_j^\nu g^{\rho\alpha}$ and 3 terms of the form $g^{\mu\nu}g^{\rho\alpha}$. However, the general tensor must have certain properties which provide relations between the different terms and allow for a

somewhat simpler expression. For example, using the fact that in the matrix element, the tensor is always contracted with physical polarisations for on-shell photons allows us to make the identification,

$$p_1^\mu = p_2^\nu = p_3^\rho = 0. \tag{8.6}$$

This drastically reduces the number of terms to 24 terms of the type $p_i^\mu p_j^\nu p_k^\rho p_l^\alpha$ and 30 terms of the type $p_i^\mu p_j^\nu g^{\rho\alpha}$ while the number of $g^{\mu\nu}g^{\rho\alpha}$ terms remains 3.

We also note that the tensor must be completely symmetric under interchange of the photon momenta and indices,

$$p_1^\mu \leftrightarrow p_2^\nu \leftrightarrow p_3^\rho \leftrightarrow p_1^\mu. \tag{8.7}$$

It is therefore useful to write the tensor in a manifestly symmetric way,

$$\mathcal{T}^{\alpha\mu\nu\rho}(p_1,p_2,p_3) = \sum_{perm} \mathcal{M}^{\alpha\mu\nu\rho}(p_1,p_2,p_3), \tag{8.8}$$

where the sum is over the six possible permutations of the photon four momenta. Gauge invariance requires that the tensor is transverse,

$$p_{1\mu}\,\mathcal{T}^{\alpha\mu\nu\rho}(p_1,p_2,p_3) = p_{2\nu}\,\mathcal{T}^{\alpha\mu\nu\rho}(p_1,p_2,p_3) = p_{3\rho}\,\mathcal{T}^{\alpha\mu\nu\rho}(p_1,p_2,p_3) = 0. \tag{8.9}$$

This reduces the number of independent terms to 3 so that,

$$\begin{aligned}
\mathcal{M}^{\alpha\mu\nu\rho}(p_1,p_2,p_3) = \;& + A_1(p_1,p_2,p_3)\,\frac{1}{p_1\cdot p_3}\left(\frac{p_3^\mu p_1^\rho}{p_1\cdot p_3} - g^{\mu\rho}\right) p_1^\alpha \left(\frac{p_3^\nu}{p_2\cdot p_3} - \frac{p_1^\nu}{p_1\cdot p_2}\right) \\
& + A_2(p_1,p_2,p_3)\left\{\frac{1}{p_2\cdot p_3}\left(\frac{p_1^\alpha p_3^\mu}{p_1\cdot p_3} - g^{\alpha\mu}\right)\left(\frac{p_1^\nu p_2^\rho}{p_1\cdot p_2} - g^{\nu\rho}\right)\right. \\
& \qquad \left. + \frac{1}{p_1\cdot p_3}\left(\frac{p_1^\nu}{p_1\cdot p_2} - \frac{p_3^\nu}{p_2\cdot p_3}\right)\left(p_1^\rho g^{\alpha\mu} - p_1^\alpha g^{\mu\rho}\right)\right\} \\
& + A_3(p_1,p_2,p_3)\,\frac{1}{p_1\cdot p_3}\left(\frac{p_1^\alpha p_3^\mu}{p_1\cdot p_3} - g^{\alpha\mu}\right)\left(\frac{p_3^\nu p_2^\rho}{p_2\cdot p_3} - g^{\nu\rho}\right).
\end{aligned} \tag{8.10}$$

Finally, we note that the tensor is also transversal with respect to the Z boson momentum,

$$p_{4\alpha}\ \mathcal{T}^{\alpha\mu\nu\rho}(p_1,p_2,p_3)=0. \tag{8.11}$$

The three functions, A_i, receive contributions from the fermion and boson loops such that,

$$\begin{aligned} A_i(p_1,p_2,p_3) &= A_i(s,t) \\ &= \frac{ie^4}{16\pi^2}\left(\sum_f Q_f^3 v_f\ A_i^f(s,t,m_f)+\cot\theta_W\ A_i^b(s,t,M_W)\right), \end{aligned} \tag{8.12}$$

where the sum runs over fermions with mass m_f, electric charge Q_f and vector coupling to the Z boson v_f. We have also introduced the Mandelstam variables s, t and u,

$$\begin{aligned} s&=(p_1+p_2)^2=2p_1.p_2, \qquad s_1=s-M_Z^2, \\ t&=(p_2+p_3)^2=2p_2.p_3, \qquad t_1=t-M_Z^2, \\ u&=(p_3+p_1)^2=2p_3.p_1, \qquad u_1=u-M_Z^2. \end{aligned} \tag{8.13}$$

The different photon permutations are obtained by exchanging the Mandelstam variables in the obvious way,

$$A_i(p_3,p_1,p_2)=A_i(u,s), \qquad A_i(p_1,p_3,p_2)=A_i(u,t), \tag{8.14}$$

and so on.

It is straightforward to obtain the scalar functions A_i^f and A_i^b using the standard techniques for one loop integrals of reducing the tensor integral to a combination of scalar integrals ([18] see Sections B.4 and B.4.4). There are three types of boson loop as shown

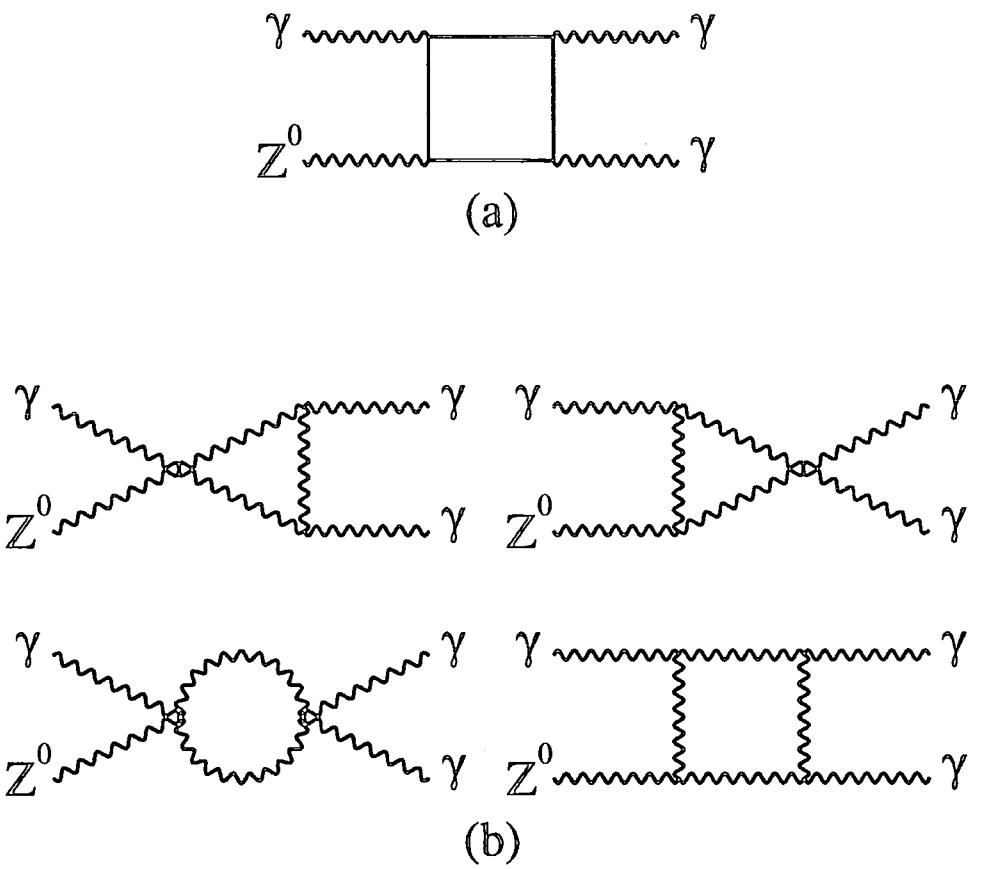

Figure 8.1: Feynman diagrams in the unitary gauge for Z boson decay into three photons (a) via fermion loops and (b) via W boson loops.

in Figure 8.1 containing triple and quartic boson couplings. As mentioned earlier, we use the unitary gauge so that only physical particles can propagate—there are no diagrams containing ghosts or unphysical Goldstone bosons. As a penalty, each diagram is superficially divergent. However, all graphs taken together are finite and we find that,

$$\begin{aligned}
A_1^b(s,t,M_W) &= \frac{1}{4}\left(\frac{M_Z^2}{M_W^2}-6\right)\ A_1^f(s,t,M_W),\\
A_2^b(s,t,M_W) &= \frac{1}{4}\left(\frac{M_Z^2}{M_W^2}-6\right)\ A_2^f(s,t,M_W)\\
&+ \frac{1}{4}\left(\frac{M_Z^2}{M_W^2}+10\right)\left(2M_W^2 ut\ H(M_W)-\frac{ut}{s}\ E(t,u,M_W)\right)-2sut\ F(M_W),\\
A_3^b(s,t,M_W) &= \frac{1}{4}\left(\frac{M_Z^2}{M_W^2}-6\right)\ A_3^f(s,t,M_W)\\
&+ \frac{1}{4t}\left(\frac{M_Z^2}{M_W^2}+10\right)\Big\{t^2\ E(s,t,M_W)-u^2\ E(u,s,M_W)\\
&\qquad +2M_W^2 ut(u-t)\ H(M_W)\Big\},
\end{aligned} \tag{8.15}$$

where the functions E and H are combinations of scalar integrals and are defined below.

As a consistency check, we have constructed the complete tensor to make sure that reinserting the scalar functions into Eqns. (8.8 and 8.10) does indeed regenerate the full tensor which is therefore automatically gauge invariant with respect to the external photons.

It is quite remarkable that the boson contribution is so similar to that of a fermion loop, for which we find,

$$\begin{aligned}
A_1^f(s,t,m_f) &= \frac{4st}{t_1}+\frac{8t}{u}\Big(s\ B_1(s,m_f)-s_1\ B_1(t,m_f)\Big)-\frac{4M_Z^2(s+2u)t}{t_1^2}\ B_1(t,m_f)\\
&+ \frac{2st(2t+u)}{u^2}\ E(s,t,m_f)+\frac{8m_f^2 t}{u}\ E(s,t,m_f)+\frac{4m_f^2 t}{s}\ E(t,u,m_f)\\
&+ 4m_f^2\Big(s\ C(s,m_f)+t\ C(t,m_f)+u_1\ C_1(u,m_f)\Big)\\
&- \frac{8m_f^2(s+2u)t}{t_1}\ C_1(t,m_f)-\frac{4m_f^2 st(u+2t)}{u}\ D(s,t,m_f)
\end{aligned}$$

$$- \quad 2m_f^2\Big(ut\ D(t,u,m_f) + st\ D(s,t,m_f) + us\ D(u,s,m_f)\Big) - 8m_f^4 t\ H(m_f), \tag{8.16}$$

$$\begin{aligned}
A_2^f(s,t,m_f) &= \frac{4(2s-u)t}{3t_1} - \frac{2s(u-8t)}{3u}\ B_1(s,m_f) - \frac{2u(s+4t)}{3s}\ B_1(u,m_f) \\
&+ \frac{2t(3su-4ut+8ts)}{3su}\ B_1(t,m_f) - \frac{4M_Z^2 ut}{t_1^2}\ B_1(t,m_f) \\
&- \frac{4ut^2}{3s^2}\ E(t,u,m_f) - \frac{su}{3t}\ E(s,u,m_f) + \frac{(3stu+8st^2)}{3u^2}\ E(s,t,m_f) \\
&- \frac{8m_f^2 ut}{t_1}\ C_1(t,m_f) + \frac{2m_f^2 t(ut_1-4st)}{u}\ D(s,t,m_f) + 2m_f^2 uu_1\ D(u,s,m_f) \\
&+ \frac{8m_f^2 sut^2}{3}\left(\frac{1}{s^2}\ D(t,u,m_f) + \frac{1}{t^2}\ D(u,s,m_f) + \frac{1}{u^2}\ D(s,t,m_f)\right) \\
&+ \frac{4m_f^2 t}{u}\ E(s,t,m_f) - \frac{8m_f^4 t}{3}\ H(m_f)
\end{aligned} \tag{8.17}$$

and,

$$\begin{aligned}
A_3^f(s,t,m_f) &= \frac{4u}{3} - \frac{4s}{3}\left(\frac{2t-u}{t}\ B_1(s,m_f) + \frac{(2s-u)t}{s^2}\ B_1(t,m_f) + \frac{u_1 u^2}{s^2 t}\ B_1(u,m_f)\right) \\
&- \frac{(s-3t_1)t}{3u}\ E(s,t,m_f) + \frac{(t-2u_1)u^2}{3t^2}\ E(u,s,m_f) + \frac{2u^2 t}{3s^2}\ E(t,u,m_f) \\
&+ \frac{4m_f^2 u}{t}\Big(s\ C(s,m_f) + t\ C(t,m_f) + u_1\ C_1(u,m_f)\Big) \\
&+ \frac{2m_f^2(4st+6tu-3M_Z^2 u)}{3}\ D(s,t,m_f) + \frac{2m_f^2 ut(3s-2u)}{3s}\ D(t,u,m_f) \\
&+ \frac{2m_f^2 u(3t^2-3tu-5su)}{3t}\ D(u,s,m_f) - \frac{8m_f^4 u}{3}\ H(m_f),
\end{aligned} \tag{8.18}$$

where the scalar integrals B_1, C, C_1, and D are defined as follows. The finite function B_1 is defined,

$$B_1(p^2,m) = -i16\pi^2\left(B_0(p,m,m) - B_0(M_Z,m,m)\right) \tag{8.19}$$

with respect to Section D.2.2. The function C is defined as $-i16\pi^2\times$ Eqn. (D.16). The

function C_1 follows from this definition as,

$$C_1(s,m) = \frac{sC(s,m) - M_Z^2 C(M_Z^2,m)}{s - M_Z^2}. \tag{8.20}$$

$D(s,t,m)$, like C above, is defined to be $-i16\pi^2\times$ Eqn. (D.18). As auxiliary functions we also define,

$$E(s,t,m) = s\ C(s,m) + t\ C(t,m) + s_1\ C_1(s,m) + t_1\ C_1(t,m) - st\ D(s,t,m), \tag{8.21}$$

and,

$$H(m) = D(s,t,m) + D(t,u,m) + D(u,s,m). \tag{8.22}$$

We have checked that this reproduces the result for the vector coupling of the Z boson with three gluons given in ref. [68].

8.3 The $Z\gamma\gamma\gamma$ helicity amplitudes

Using the $Z\gamma\gamma\gamma$ polarisation tensor given in the previous section, we can construct the corresponding helicity amplitudes. For simplicity, we work in the rest frame of the p_1 and p_2 system where the momenta are given in (E,p_x,p_y,p_z) notation by,

$$\begin{aligned} p_1^\mu &= (-p,0,0,-p), \\ p_2^\mu &= (-p,0,0,p), \\ p_3^\mu &= (q,q\sin\theta,0,q\cos\theta), \\ p_4^\mu &= (E,-q\sin\theta,0,-q\cos\theta), \end{aligned} \tag{8.23}$$

where all momenta are ingoing and where $E = \sqrt{q^2 + m_Z^2}$. The appropriate helicity vectors are then,

$$\begin{aligned}
e_1^{+\mu} = e_2^{-\mu} &= \frac{1}{\sqrt{2}}\,(0,-i,1,0), \\
e_1^{-\mu} = e_2^{+\mu} &= \frac{1}{\sqrt{2}}\,(0,i,1,0), \\
e_3^{+\mu} = e_4^{-\mu} &= \frac{1}{\sqrt{2}}\,(0,i\cos\theta,1,-i\sin\theta), \\
e_3^{-\mu} = e_4^{+\mu} &= \frac{1}{\sqrt{2}}\,(0,-i\cos\theta,1,i\sin\theta), \\
e_0 &= \frac{1}{m_Z}\,(q,-E\sin\theta,0,-E\cos\theta).
\end{aligned} \tag{8.24}$$

Here $e_i^{\pm}$ represents the $\lambda_i = \pm$ polarisation vector of particle i while e_0 represents a Z boson that is longitudinally polarised. It is useful to define the quantity,

$$\Delta = \sqrt{\frac{-M_Z^2}{2stu}}, \tag{8.25}$$

which occurs in all helicity amplitudes associated with a longitudinally polarised Z boson.

In terms of the three independent functions given in Eqns. (8.10 and 8.12) we find that there are nine independent helicity amplitudes, $\mathcal{T}_{\lambda_1\lambda_2\lambda_3\lambda_Z}$, with $\lambda_1 = +$ which are given by,

$$\begin{aligned}
\mathcal{T}_{++++} &= 2\left(\frac{A_1(t,u)}{s_1} + \frac{A_2(s,t)+A_2(u,t)+A_3(u,s)}{t} + (t \leftrightarrow u)\right), \\
\mathcal{T}_{+++-} &= -2\left(\frac{A_1(t,u)+A_1(u,t)}{s_1}\right), \\
\mathcal{T}_{++-+} &= 2\left(\frac{A_1(s,t)-A_1(u,t)-A_2(s,t)+A_2(u,t)}{s_1} + \frac{A_3(s,t)}{u} - \frac{u\,A_3(u,t)}{ss_1} + (t \leftrightarrow u)\right), \\
\mathcal{T}_{++--} &= 2\left(\frac{-A_1(s,t)+A_1(u,t)+A_2(s,t)-A_2(u,t)}{s_1} + \frac{A_3(t,s)}{u} - \frac{t\,A_3(u,t)}{ss_1} + (t \leftrightarrow u)\right), \\
\mathcal{T}_{+-++} &= 2\left(\frac{A_1(s,u)-A_2(s,u)-A_2(t,u)}{s_1} + \frac{A_2(t,s)+A_2(u,s)}{s} + \frac{A_3(s,t)}{u} - \frac{u\,A_3(u,t)}{ss_1}\right),
\end{aligned}$$

$$\mathcal{T}_{+-+-} = -2\left(\frac{A_1(s,u)}{s_1} + \frac{t\,(A_2(s,u)+A_2(t,u))}{us_1} + \frac{t\,A_3(u,t)}{ss_1}\right), \tag{8.26}$$

while for the amplitudes where the Z boson is longitudinally polarised,

$$\begin{aligned}
\mathcal{T}_{+++0} &= \frac{2\Delta}{M_Z^2}\left(\frac{su-tM_Z^2}{s_1}\,A_1(t,u) + s\,(A_2(s,u)+A_2(t,u)) + \frac{su\,A_3(u,s)}{t} - (t\leftrightarrow u)\right)\\
\mathcal{T}_{++-0} &= \frac{2\Delta}{M_Z^2}\left(\frac{su-tM_Z^2}{s_1}\,(A_1(s,u)-A_1(t,u)+A_2(t,u)-A_2(s,u)) + s_1\,(A_1(t,s)-A_2(t,s))\right.\\
&\qquad \left. -\frac{st}{u}\,(A_3(s,t)-A_3(t,s)) + \frac{ut(s+M_Z^2)}{ss_1}\,A_3(u,t) - (t\leftrightarrow u)\right),\\
\mathcal{T}_{+-+0} &= \frac{2\Delta}{M_Z^2}\left(\frac{su-tM_Z^2}{s_1}\,A_1(s,u) - s_1\,A_1(u,s) + \frac{t(s+M_Z^2)}{s_1}\,(A_2(s,u)+A_2(t,u))\right.\\
&\qquad \left. -t\,(A_2(t,s)+A_2(u,s)) - \frac{st}{u}\,A_3(s,t) + \frac{ut(s+M_Z^2)}{ss_1}\,A_3(u,t)\right).
\end{aligned} \tag{8.27}$$

The other three helicity amplitudes with $\lambda_1 = +$ are obtained by exchanging u and t,[1]

$$\begin{aligned}
\mathcal{T}_{+--+} &= \mathcal{T}_{+-+-}\,(t\leftrightarrow u),\\
\mathcal{T}_{+---} &= \mathcal{T}_{+-++}\,(t\leftrightarrow u),\\
\mathcal{T}_{+--0} &= \mathcal{T}_{+-+0}\,(t\leftrightarrow u),
\end{aligned} \tag{8.28}$$

while the amplitudes with $\lambda_1 = -$ are obtained by the parity relations,

$$\mathcal{T}_{-\lambda_2\lambda_3\lambda_Z} = \mathcal{T}_{+\,-\lambda_2\,-\lambda_3\,-\lambda_Z}, \tag{8.29}$$

for $\lambda_Z = \pm$, and,

$$\mathcal{T}_{-\lambda_2\lambda_30} = -\mathcal{T}_{+\,-\lambda_2\,-\lambda_30}, \tag{8.30}$$

for longitudinally polarised Z bosons.

[1]Note that in Appendix B of ref. [68], the amplitude V_{+---} is incorrectly given and should read $V_{+---}(s,t,u) = V_{+-++}(s,u,t)$.

8.4 Numerical results

Using the helicity amplitudes, from the previous section and the explicit forms for the scalar integrals given above, it is straightforward to calculate the $Z \to \gamma\gamma\gamma$ decay rate,

$$\Gamma(Z \to \gamma\gamma\gamma) = \frac{1}{3! \cdot 384\pi^3 M_Z^3} \int \sum_{\lambda_1 \ldots \lambda_Z} |\mathcal{T}_{\lambda_1\lambda_2\lambda_3\lambda_4}|^2 ds\ dt\ du\ \delta(M_Z^2 - s - t - u). \qquad (8.31)$$

The factor 1/3! is the identical particle factor for the photons. The coupling constants and the masses of the particles in the loop are contained in the definition of the A_i in Eqn. (8.12).

For the numerical results, we take $M_Z = 91.175$ GeV, $\alpha(M_Z) = e^2/(4\pi) = 1/128$ and $\sin^2\theta_W = 0.23$ while the W boson mass is given by the relation, $M_W = M_Z \cos\theta_W = 80.0$ GeV. The vector couplings, v_f, are defined in Eqns. (3.31 and 3.32) and are listed in Table 4.1. For very light fermions, the amplitudes are essentially independent of the precise value of the fermion mass. For computational reasons we choose $m_u = m_d = m_s = m_c = m_e = m_\mu = m_\tau = 100$ eV. Varying this mass between 100 eV and 2 GeV does not change the results by more than the monte-carlo error on the integration, which is less than 1%. For the bottom quark, we take $m_b = 5$ GeV.

The only unknown parameter is the top quark mass, $m_{\rm top}$, and in Figure 8.2, we show $\Gamma(Z \to \gamma\gamma\gamma)$ in the interval $0 < m_{\rm top} < 200$ GeV. The latest experimental bound on the mass of the top quark from CDF is $174 \pm 10^{+12}_{-12}$ GeV and from LEP is $177 \pm 11^{+18}_{-19}$ GeV [9]. Nevertheless, we show the whole range of $m_{\rm top}$ in order to exhibit the threshold behaviour around $m_{\rm top} = M_Z/2$ where the possibility of making two on-shell top quarks vanishes. Above the threshold, the top quark rapidly decouples as is well known [71].

At small $m_{\rm top}$, the top quark makes a sizable contribution. This is because each quarks contribution is proportional to the cube of the quark charge and therefore quarks with

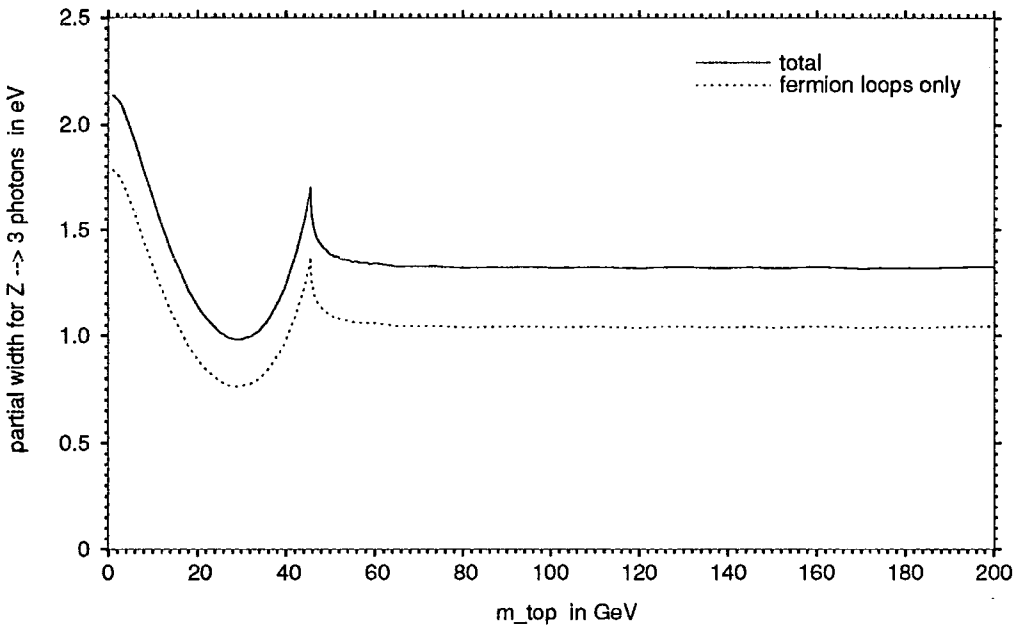

Figure 8.2: The partial width for $Z \to \gamma\gamma\gamma$ in eV as a function of the top quark mass m_{top}. The total (fermion + boson) width is shown as a solid line, while the fermion contribution alone is shown dotted.

$Q_f = +2/3$ dominate. The lepton contribution is suppressed both by colour and by the fact that v_f is small for charged leptons. The rate at small $m_{\rm top}$ is therefore approximately 50% larger than at large $m_{\rm top}$ where the up and charm quark contribution dominates. The monte-carlo estimate of the partial width at small $m_{\rm top}$ agrees with the analytic formula of Eqn. (8.1).

Figure 8.3 shows both the total $Z \to \gamma\gamma\gamma$ partial width (including both fermion and boson loops) and the fermion contribution alone. On its own, the W loop contribution is 0.026 eV, in rough agreement with the estimates of [64, 66], however, the interference with the larger fermion loop contribution is significant and increases the width by about 27% or 0.3 eV over the whole range of $m_{\rm top}$.

We note that the decay rate does depend quite sensitively on the precise choice of $\sin^2\theta_W$ through the vector couplings of the Z boson with the fermions. Allowing $\sin^2\theta_W = 1 - M_W^2/M_Z^2$ to vary between 0.20 and 0.25 (i.e. 81.5 GeV $> M_W >$ 78.9 GeV) causes the total three photon decay width to vary up or downwards by a factor of about 2. The W loop contribution alone remains almost constant at 0.026 eV.

8.5 Summary

In summary, we have computed the polarisation tensor for the $Z\gamma\gamma\gamma$ coupling including both fermion and W boson loops using the unitary gauge. The three independent amplitudes describing this tensor have not appeared in the literature before. It is remarkable that the boson and fermion contributions are so similar, bearing in mind the non-supersymmetric nature of the standard model. By projecting out the different helicity amplitudes we have obtained the $Z \to \gamma\gamma\gamma$ decay width keeping the full dependence on the top quark and W

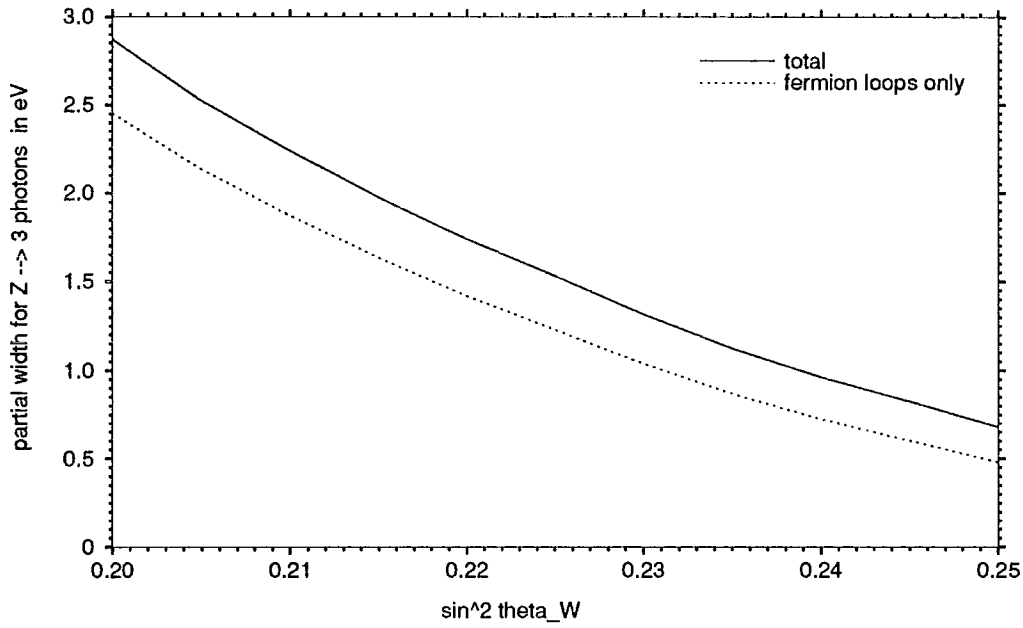

Figure 8.3: The partial width for $Z \rightarrow \gamma\gamma\gamma$ in eV as a function of $\sin^2\theta_W$ for $m_{\rm top} = 120$ GeV. The total (fermion + boson) width is shown as a solid line, while the fermion contribution alone is shown dotted.

boson masses. For the allowed range of $m_{\rm top}$, the entire one-loop standard model contribution to the $Z \to \gamma\gamma\gamma$ decay is 1.35 eV. In other words, one such decay would occur for every 10^9 hadronic Z boson events. Such a rate is clearly beyond even the high luminosity option at LEP. It is interesting to compare this rate with that for the two loop process $Z \to \gamma H \to \gamma\gamma\gamma$, which is heavily dependent on the mass of the Higgs particle, H. The product of the branching ratios for these two processes are: 2×10^{-10} for a Higgs mass of $m_H = 60$ GeV; and 7×10^{-11} for $m_H = 70$ GeV [76]. The current limit on the mass of the Higgs is $m_H > 62.5$ GeV [77] so our calculation represents the majority of the SM signal.

In fact, three photon events have already been observed at LEP [78, 79, 80], however, they are completely consistent with the purely QED process,

$$e^+e^- \to \gamma\gamma\gamma. \tag{8.32}$$

This tree level process provides an irreducible background to the rare decay discussed here. Expressed as an *effective* partial width at the Z-pole, this has a value of about 10 keV [81] and makes the observation of the standard model process described here completely unlikely. Nevertheless, many extensions to the Standard Model such as models where the Z boson is a bound state of charged constituents do allow an anomalously large three photon decay rate [82, 81] analogous to the decay of the J/ψ into photons. Any disagreement with the QED prediction cannot be due to standard model processes and must indicate some new physics.

Chapter 9

The 2nd Order Formalism

Here we describe, in two distinct ways, a re-interpretation of the Dirac algebra of interaction in QED; the 2nd Order Formalism.

9.1 Introduction

Fermionic calculations, at their most elementary, are just strings of γ_μ (Appendix E) matrices over which we must eventually perform a trace. The *2nd Order Formalism* is in essence a re-writing of the conventional *1st Order* Feynman rules for the calculation of processes involving gauge bosons coupled to fermions that form a closed loop. A general property of complete perturbative calculations at any fixed order in the coupling is that they are gauge invariant. These rules ensure that explicit gauge invariance is present at the level of small subsets of

diagrams and not just when *all* of the diagrams for a given process are summed.

The discussion of Section 9.2 will show that this approach does generalise to non-abelian theories, indeed from its *string* inspired origins [83, 84] it was originally directed at problems in QCD, but for the purposes of this thesis (namely the content of Chapter 10) all that is required is an abelian analysis.

The calculation of fermion processes in quantum field theories necessitates the extensive manipulation of Dirac algebra. Specifically, we are required to manipulate so called *gamma matrices*, γ_μ. Section 9.3 will explicitly relate the *2nd Order* Feynman rules to the more conventional *1st Order* ones.

9.2 A formal approach

The contribution to Z (of Eqn. (2.7)) from a fermion coupled to an abelian field is a factor,

$$\sim \int \mathcal{D}\psi\mathcal{D}\overline{\psi}\ldots\exp\left[i\int\overline{\psi}\left(i\not{D}-m_\psi\right)\psi\right] \tag{9.1}$$

which, with reference to Eqn. (2.40), may be formally re-written as,

$$\det\left(i\not{D}-m_\psi\right)=\det\left[\left(i\not{D}-m_\psi\right)\left(i\not{D}+m_\psi\right)\right]^{1/2}=\left[\det\left(-\not{D}^2-m_\psi^2\right)\right]^{1/2}. \tag{9.2}$$

We recall that the vertex functions of a theory are generated from the Effective Action Eqn. (2.20). So in calculating amplitudes for a theory containing this determinant we should expect the power of $1/2$ to reveal itself as an overall factor. With this in mind we *discard* it—only to divide by two when we finish an amplitude calculation. Using Eqn. (2.40) again,

we raise the operator to obtain,

$$\det\left(-\not{D}^2 - m_\psi^2\right)\ldots = \int \mathcal{D}\Psi\mathcal{D}\overline{\Psi}\ldots\exp\left[-i\int\overline{\Psi}\left(\not{D}^2 + m_\psi^2\right)\Psi\right]. \tag{9.3}$$

Note, that these Ψ fields are clearly not the same as the ψ fields since $\mathcal{L}$ by definition must have dimension $[M]^4$. Indeed, they bare a closer resemblance to regular *scalar* fields, fermionic ones.

This exponent may be re-written (see Eqns. (E.1, E.3 and 2.32)),

$$\begin{aligned}\not{D}^2 + m_\psi^2 &= \frac{1}{2}\left\{\gamma^\mu,\gamma^\nu\right\}D_\mu D_\nu + m_\psi^2 + \frac{i}{2i}\left[\gamma^\mu,\gamma^\nu\right]D_\mu D_\nu \\ &= D^2 + m_\psi^2 + \frac{1}{2i}\sigma^{\mu\nu}\left[D_\mu, D_\nu\right] \\ &= D^2 + m_\psi^2 + \frac{gQ_\psi}{2}\sigma^{\mu\nu}F_{\mu\nu}.\end{aligned} \tag{9.4}$$

Provided we do not forget the factor of $-1/2$, from the log det(...) of the Effective Action, we can deduce a set of *2nd Order* Feynman rules (from Eqn. (9.4)) for closed fermion loops—the minus sign being the conventional fermion loop factor. The fact that the fermions are in *closed loops* ensures that we need not address the question of how Ψ is physically manifest.

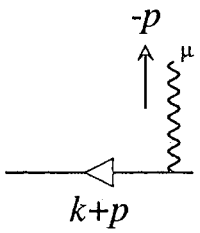

Figure 9.1: The basic unit of contribution to a gauge boson-fermion calculation; $A^{\mu}_{k,p}$.

9.3 A hands on approach

On close inspection we see that all gauge field-fermion interaction calculations are built from sequences of the following form[1],

$$\frac{i}{\not k + \not p - m_f}\ (-igQ_f\gamma^{\mu}) = -gQ_f\frac{A^{\mu}_{k,p}}{D_{k+p}} \tag{9.5}$$

with

$$D_k = -\left(k^2 - m_f^2\right) \tag{9.6}$$

Here, we define $A^{\mu}_{k,p}$ to be the lorentz structure carrying part and D_{k+p} the denominator of the normal (*1st Order*) product of a fermion propagator, and a gauge vertex. Here g is the coupling and Q_f is the charge of the fermion, f, with respect to the gauge field that carries $-p$ from the vertex. This is shown explicitly in Figure 9.1. In QED $g = e$ and $Q_f = -1$.

We can manipulate this expression into the following useful form,

$$\begin{aligned} A^{\mu}_{k,p} &= \left(\not k + \not p + m_f\right)\gamma^{\mu} \\ &= \frac{1}{2}\left(2\left(2k^{\mu} + p^{\mu}\right) + \not p\gamma^{\mu} - \gamma^{\mu}\left(2\not k + \not p - 2m_f\right)\right) \end{aligned} \tag{9.7}$$

[1] We are considering only those processes not involving the γ_5 matrix.

$$= (k^\mu + p^\mu) - (-k^\mu) - \frac{1}{2}\left[\gamma^\mu, \not{p}\right] - \gamma^\mu\left(\not{k} - m_f\right) \tag{9.8}$$

We note that the contracted γ matrices, $\not{p}$ and $\not{k}$, are now separated. The first is present in a conveniently minimal form, i.e. for massless, or massive, gauge bosons it identically obeys the gauge invariance condition for externally polarised gauge fields, namely,

$$(\epsilon_\mu + \lambda p_\mu)[\gamma^\mu, \not{p}] = \epsilon_\mu[\gamma^\mu, \not{p}]. \tag{9.9}$$

As we shall see, the second gives rise to a different simplification when it is followed by another A.

For transparency we define $B^\mu_{k,p}$, C^μ_k and $E^{\mu\nu}$ for this fermion (with Eqn. (E.3)),

$$B^\mu_{k,p} = (k^\mu + p^\mu) - (-k^\mu) + i\sigma^{\mu\nu}p_\nu \tag{9.10}$$

$$C^\mu_k = +\gamma^\mu\left(\not{k} - m_f\right) \tag{9.11}$$

$$E^{\mu\nu} = \gamma^\mu\gamma^\nu \tag{9.12}$$

such that,

$$A^\mu_{k,p} = B^\mu_{k,p} - C^\mu_k \tag{9.13}$$

and,

$$C^\mu_{k+p}A^\nu_{k,p} = -E^{\mu\nu}D_{k+p}. \tag{9.14}$$

We shall now consider the consequences of partially expanding two or more consecutive As in terms of these new objects, (see Figure 9.2a)

$$A^\nu_{k+p,q}\,A^\mu_{k,p}\,\ldots = \left(B^\nu_{k+p,q} - C^\nu_{k+p}\right)A^\mu_{k,p}\,\ldots$$

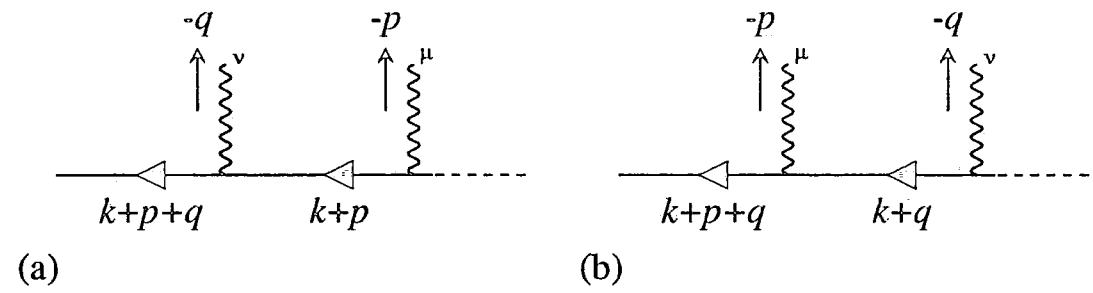

Figure 9.2: A consecutive pair of $A^{\mu}_{k,p}$ type objects; generalising to a fermion spin line connected to a number of gauge bosons. (a) and (b) correspond to the two "orderings" of coupling the fermion to the bosons.

$$\begin{aligned} &= \left(B^{\nu}_{k+p,q}B^{\mu}_{k,p} - C^{\nu}_{k+p}A^{\mu}_{k,p} - B^{\nu}_{k+p,q}C^{\mu}_{k}\right)\ldots \\ &= \left(B^{\nu}_{k+p,q}B^{\mu}_{k,p} + E^{\nu\mu}D_{k+p} - B^{\nu}_{k+p,q}C^{\mu}_{k}\right)\ldots \end{aligned} \tag{9.15}$$

where we have used the property Eqn. (9.14). We note that only the last term in the numerator contains the object C.

The above process of exchanging As for Bs, Es and Ds generalises immediately for n consecutive As. The obvious complication, however, is that we do require a C factor to truncate a fraction of the terms. We note that such terms are always preceded by a minus sign.

In the case that the fermion line is *closed* (i.e. a fermion loop) the string of As is actually *traced* over. For this reason we are permitted to move a trailing C to come at the left of the sequence (the cyclic property of the trace operation). It is then possible to all but completely remove the Cs from the trace, by simply replacing all Bs that are to the immediate right of a C with the appropriate $A + C$ and then using Eqn. (9.14) to remove the A. The only offending term that remains after exhaustively repeating such a replacement is a single sequence of Cs. For example, in the simple case of two As in a closed loop (the vacuum

polarisation cf. Eqn. (4.17) and Figure 4.6) we have,

$$\begin{aligned} -\mathrm{Tr}\left\{A^{\mu}_{k,q}\ A^{\nu}_{k+q,-q}\right\} &= -\mathrm{Tr}\left\{B^{\mu}_{k,q}\, B_{k+q,-q} + E^{\mu\nu}\, D_k - B^{\mu}_{k,q}\, C^{\nu}_{k+q}\right\} \\ &= -\mathrm{Tr}\left\{B^{\mu}_{k,q}\, B_{k+q,-q} + E^{\mu\nu}\, D_k - C^{\nu}_{k+q}\left(A^{\mu}_{k,q} + C^{\mu}_{k}\right)\right\} \\ &= -\mathrm{Tr}\left\{B^{\mu}_{k,q}\, B_{k+q,-q} + E^{\mu\nu}\, D_k + E^{\nu\mu}\, D_{k+q} - C^{\nu}_{k+q}\, C^{\mu}_{k}\right\}. \end{aligned} \tag{9.16}$$

The minus sign accompanying the sequence of Cs is the one noted after Eqn. (9.15). This form solves the problem of removing the Cs completely, see Eqns. (9.7 and 9.11), since

$$\mathrm{Tr}\left\{C_n C_1 C_2 C_3 \ldots\right\} = \mathrm{Tr}\left\{A_1 A_2 A_3 \ldots A_n\right\} \tag{9.17}$$

where again we have used the cyclic property of the trace. Accordingly, Eqn. (9.16) may be written,

$$-\mathrm{Tr}\left\{A^{\mu}_{k,q}\ A^{\nu}_{k+q,-q}\right\} = -\frac{1}{2}\mathrm{Tr}\left\{B^{\mu}_{k,q}\, B_{k+q,-q} + E^{\mu\nu}\, D_k + E^{\nu\mu}\, D_{k+q}\right\}. \tag{9.18}$$

The effect of *removing* the Cs can be seen as simply pinching the first and last As to give an ED term and an overall factor of $1/2$ outside the trace. We find that compared with the conventional -1 for the *1st Order* fermion rules the *2nd Order* rules require a factor of $-1/2$ for a fermion loop.

In this simple case we can perform a change of loop momentum (change the variable of integration in Eqn. (4.17)) $k \rightarrow -k - q$ in the third term (of Eqn. (9.18)) to make the coefficients of the E terms the same.

In the more general case (for a larger loop) some more analysis is required. Returning to

the level of Eqn. (9.15) we write the spinor line where the gauge couplings are reversed (see Figure 9.2b) as

$$A^{\mu}_{k+q,p}\, A^{\nu}_{k,q}\, \ldots = \left(B^{\mu}_{k+q,p} B^{\nu}_{k,q} + E^{\mu\nu} D_{k+q} - B^{\mu}_{k+q,p} C^{\nu}_{k}\right) \ldots \tag{9.19}$$

In any physical (gauge invariant) process, diagrams of both this and Eqn. (9.15) forms must be included when calculating the associated observable. Accordingly, we are at liberty, in an attempt to rewrite the Feynman rules, to immediately sum these two contributions. Including the associated propagators (Ds), the E parts of the two orderings of As sum to give,

$$\frac{A^{\nu}_{k+p,q}\, A^{\mu}_{k,p}}{D_{k+p+q} D_{k+p}} + \frac{A^{\mu}_{k+q,p}\, A^{\nu}_{k,q}}{D_{k+p+q} D_{k+q}} = \ldots + \frac{E^{\nu\mu} + E^{\mu\nu}}{D_{k+p+q}} + \ldots = \ldots + \frac{2g^{\nu\mu}}{D_{k+p+q}} + \ldots \tag{9.20}$$

The effect of this combination of terms is then to *pinch* the fermion propagator between the two gauge couplings and invoke a *four* point interaction type term—since the only surviving propagator is that which is common to both diagrams. Thus, in a gauge invariant set of diagrams with all possible orderings of the gauge bosons, all pairs of bosons will give rise to *pinched* four point terms. More generally, with a factor of $-gQ_f$ for each gauge coupling, the objects B, D and $2g^{\mu\nu}$ provide a complete set of Feynman rules for fermion loop calculations.

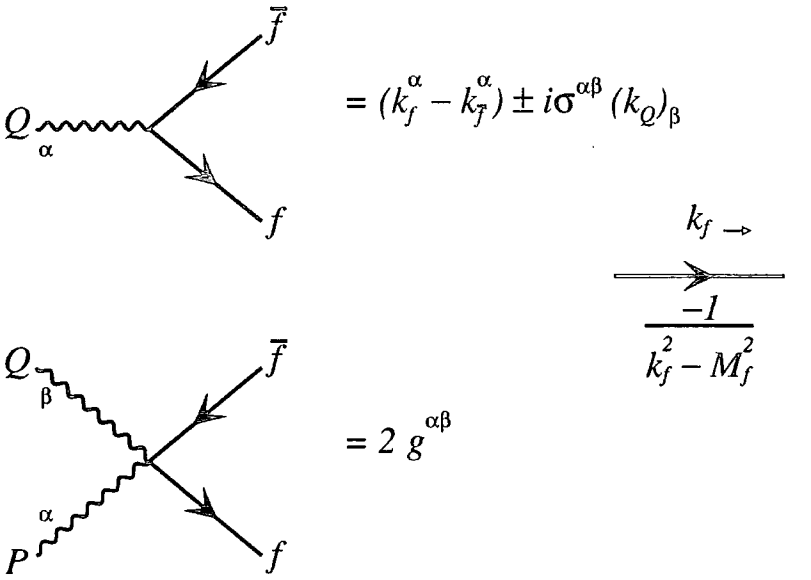

Figure 9.3: The Feynman rules for QED type interactions—all momenta are directed outwards. In addition to the rules given here a factor of $-1/2$ is required for a closed fermion loop. Care should be taken to remember the implicit unit matrix (say ${\gamma_0}^2$) present in those parts of the rules not containing an explicit $\sigma^{\alpha\beta}$ matrix.

9.4 Summary

In summary, a closed spinor line may be computed from a 2nd order set of Feynman rules namely those given in Figure 9.3. These rules, although equivalent to, are significantly different from the standard ones. Notably they only include the anti-symmetric object $\sigma^{\mu\nu}$ and no individual γ matrices.

In the figure the $\pm$ sign accompanying the $\sigma^{\alpha\beta}$ contribution to the 3-point interaction term is the *discrepancy* between the two derivations of Sections 9.2(+) and 9.3(−). At first sight this might appear to be an inconsistency, but it actually highlights a curious and currently *empirical*, subtlety in the rules. Namely, that all terms in a traced fermion loop that contain an odd number of σ's are canceled in the complete amplitude. We have checked

this is the case up to the level of a fermion box.

Chapter 10

Supersymmmetry Relations Between Contributions To One-Loop Gauge Boson Amplitudes

We apply ideas motivated by string theory to improve the calculational efficiency of one-loop weak interaction processes with massive external gauge bosons. In certain cases "supersymmetry" relations between diagrams with a fermion loop and with a gauge boson loop hold. This is explicitly illustrated for a particular one-loop standard model process with four-external gauge bosons. The supersymmetry relations can be used to provide further significant improvements in calculational efficiency.

10.1 Introduction

Even the simplest one-loop gauge boson amplitudes can be rather formidable to compute. Recently, an advance in the calculation of one-loop gauge boson amplitudes has been made based on string theory [85, 83]. Using this technique, the first calculation of the one-loop five-gluon amplitude has been performed [21, 22]. As another example, one-loop graviton scattering calculations have been shown to be relatively simple once the corresponding QCD calculations have been performed [86].

In the case of QCD, the string-based rules have been interpreted in terms of a particular set of vertices and organisations whose main feature is that they lead to relatively efficient computations. As a bonus, the various contributions to the one-loop amplitude exhibit simple relations between the gluon and fermion contributions at the level of the integrands.

In the usual Feynman diagram approach, the initial lorentz structure of the various diagrams bear little resemblance to each other. Each of the different types of Feynman diagrams are then separately evaluated. This may be contrasted to string theory, where the various particle states are treated more uniformly, making relationships between the various types of contributions apparent. In the calculation of the five-gluon amplitude [21], a striking manifestation of this is that the gluon loop contribution is rather easy to obtain from the fermion loop contribution since the two calculations are almost identical. These relations between fermion and boson loop contributions are connected to the remarkable simplicity of one-loop amplitudes in $N = 4$ super-Yang-Mills, which was first pointed out with the aid of string theory [87]. Supersymmetry relations have become a standard tool in QCD calculations [88]. The conventional supersymmetry relations are between amplitudes with differing numbers of external fermions. The relations we discuss here are between diagrams with the same type of external particles but with differing internal particles.

Here we explain how to reorganise one-loop gauge boson amplitudes involving W's and Z's to mimic the efficient reorganisation for gluons. As an added bonus in certain cases the manifest relations between gauge boson and fermion loops are preserved. These relations can then be used to provide further significant reductions in the amount of work involved in a computation. To do this, we will make direct use of the field theory lessons obtained from string theory [84, 89]. The approach presented here is helpful whenever a one-loop diagram contains a non-abelian vertex.

As a particular example, we will discuss the calculation of the process $Z \to 3\gamma$ [90, 91] (which is of some interest for compositeness searches). From the results of a unitary gauge calculation (Chapter 8 [91]) the striking relationship between the boson and fermion contributions to the amplitude has already been noted. Here we explicitly show how to make use of this supersymmetry relationship to significantly improve calculational efficiency for this process. With the superstring-motivated reorganisation nearly the entire result for the W-loop contributions can be obtained from the fermion loop contribution. In processes such as $2\gamma \to 2Z$ [92] (which is of some interest for searches for ultra-heavy fermions at future photon-photon colliders) there are additional mixed scalar and gauge-boson loops. However, one can still use the supersymmetry relations to significantly reduce the computational difficulty of the gauge-boson loop contributions. For processes with external W's, one loses simple supersymmetry relations due to the flavour changing in the loop, but there are still significant advantages to the gauge choices which we describe.

In Section 10.2, we review the supersymmetry relations for the diagrams that appear in one-loop gauge boson scattering calculations and describe the application to spontaneously broken theories such as the standard model. In Section 10.3, we present the calculation of $Z \to 3\gamma$ as an explicit example. In Section 10.4, we comment on other processes such as $2\gamma \to 2Z$ and provide tables containing the coupling constants for the various vertices.

10.2 $N = 4$ supersymmetry relations

Although derived from string theory, the string-based organisation, can be understood in ordinary field theory [84, 83]. Besides the inherent advantage of obtaining simpler diagrams with an efficient organisation, as an added bonus one obtains relations, connected to the simplicity of $N = 4$ super-Yang-Mills amplitudes, between gauge-boson and fermion loop diagrams. The use of these $N = 4$ supersymmetry relations as a computational tool was pointed out in ref. [21] for the one-loop five-gluon amplitude. With the string-based organisation the relations are manifest at the level of the integrands of diagrams and can be effectively used as a computational tool to obtain most of the gauge boson loop contribution from the fermion loop contribution.

Following the discussion of refs. [84, 83] the key field theory ingredients for obtaining a good fraction of the gluon amplitude simplifications of the string-based approach are:

- The Feynman rules should be colour ordered [93, 83]. To a large extent this simply amounts to rewriting the Yang-Mills structure constants in terms of traces of commutators of fundamental representation matrices and considering only one colour structure at a time (see Appendix F). This concept is useful in QCD because it reduces the number of diagrams to be considered.

- The background field Feynman gauge [94] should be used in calculations where a non-abelian vertex appears in the loop. This gauge is used to construct the one particle irreducible diagrams describing a *gauge invariant* effective action (see Section 2.4). The background field Feynman gauge is advantageous to use because the propagators are the normal ones but the vertices are more simple than in the conventional Feynman gauge. For the $N = 4$ supersymmetry identities to be manifest it is essential for all

vertices of the one-particle irreducible diagrams to be background field gauge vertices.

- The second order formalism should be used for the vector part (no γ_5) of one particle irreducible diagrams with fermion loops (see Chapter 9 and ref. [84]). This formalism amounts to rewriting the usual Dirac determinant with Eqn. (9.2). With this formalism, the fermion loop contributions are very similar to those of the gauge bosons. Additionally, there is considerable overlap with the calculation of ghost or scalar loop contributions.

- The scattering amplitudes are constructed by sewing trees onto the one-particle irreducible diagrams. One can use standard Feynman gauge for the trees if one desires. For gluons, a particularly convenient gauge for the trees is the non-linear Gervais-Neveu gauge [95, 84] because of the simple vertices. It is obviously advantageous to use different gauges for the tree and loop parts of the computation since one can optimise the gauge choices to minimise the computations required in the different parts of the diagrams. (Although it might seem strange that two different gauge choices are used for the loop and tree parts of the Feynman diagrams, in the background field method this has been justified by Abbott, Grisaru and Schaeffer [94]).

- With the background field Feynman gauge and second order fermion formalism for the one-particle irreducible diagrams, virtually the entire calculation of a gauge boson loop is contained in the fermion loop calculation. This can be used to avoid pointless duplication of significant portions of the calculation.

- Finally, a decomposition into gauge invariant tensors [96, 91] or spinor helicity methods [97] can be used. In this paper we use the former method. With the tensor decomposition method one can use the usual Passarino-Veltman technique for performing tensor integrals ([18] see Section B.4). To use the spinor helicity technique, one first performs those spinor simplifications which are not obstructed by the presence of loop

momentum. Then a Feynman parameterisation is performed to eliminate the loop momentum; the remaining spinor helicity simplifications can then be performed. (One can use an electric circuit analogy [98] to arrive at the same integrand if one desires.) The Feynman parameter integrals can then be evaluated using the integration method of ref. [22].

Here we apply the latter five ideas to weak interactions and demonstrate that the gain in computational efficiency is quite significant. The application of these ideas is straightforward since it mainly involves using a different set of Feynman rules than the conventional ones and then observing a set of relationships between the integrands of certain diagrams. In the string-based approach of refs. [85, 84] these relations are an inherent property of the string-based rules. In the above field theory approach, the relations are found after the trace over γ-matrices has been performed and the integrands of the various loop contributions are compared. We now present the application of the above ideas to weak interactions.

First consider the case of no fermions. In the background field Feynman gauge [94] this sector of the $SU(2) \times U(1)$ Lagrangian is given by $\mathcal{L}_1 + \mathcal{L}_2 + \mathcal{L}_{gf} + \mathcal{L}_{ghost}$ where,

$$\mathcal{L}_1 = -\frac{1}{4}(F_i^{\mu\nu}(\tilde{W}+W))^2 - \frac{1}{4}(F^{\mu\nu}(\tilde{B}+B))^2 \tag{10.1}$$

$$\mathcal{L}_2 = (D_\mu\phi)^\dagger(D^\mu\phi) - \lambda(\phi^\dagger\phi)^2 + \mu^2\phi^\dagger\phi \tag{10.2}$$

$$\begin{aligned}\mathcal{L}_{gf} = & -\frac{1}{2}(\partial_\mu W^{i\,\mu} + g\epsilon^{ijk}\tilde{W}_{j\,\mu}W_k^\mu + \frac{ig}{2}(\phi'^\dagger\tau^i\phi_0 - \phi_0^\dagger\tau^i\phi'))^2 \\ & -\frac{1}{2}(\partial_\mu B^\mu + \frac{ig'}{2}(\phi'^\dagger\phi_0 - \phi_0^\dagger\phi'))^2\end{aligned} \tag{10.3}$$

$$\begin{aligned}\mathcal{L}_{ghost} = & -\omega_i^\dagger\Big(\partial^2\delta^{il} - g\overleftarrow{\partial}_\mu\epsilon^{ijl}(W_j^\mu + \tilde{W}_j^\mu) + g\epsilon^{ijl}\tilde{W}_j^\mu\overrightarrow{\partial}_\mu + g^2\tilde{W}_j^\mu(W_m^\mu + \tilde{W}_m^\mu)\epsilon^{ijk}\epsilon^{kml} \\ & + \frac{g^2}{4}(\phi^\dagger\tau^l\tau^i\phi_0 + \phi_0^\dagger\tau^i\tau^l\phi)\Big)\omega_l - b^\dagger\Big(\partial^2 + \frac{g'^2}{4}(\phi^\dagger\phi_0 + \phi_0^\dagger\phi)\Big)b \\ & -\omega_i\frac{gg'}{4}(\phi^\dagger\tau^i\phi_0 + \phi_0\tau^i\phi)b - b^\dagger\frac{gg'}{4}(\phi^\dagger\tau^l\phi_0 + \phi_0^\dagger\tau^l\phi)\omega_l\end{aligned} \tag{10.4}$$

where τ^i are the Pauli spin matrices and $\tilde{W}^i$ and $\tilde{B}$ are respectively the $SU(2)$ and $U(1)$ hypercharge background fields and W^i and B are the corresponding quantum fields. The covariant derivatives appearing in $\mathcal{L}_2$ are covariant with respect to both quantum and background fields. The field tensor, $F^{\mu\nu}(\tilde{A}+A)$ is that of Eqn. (2.32), for the appropriate gauge group, where we have explicitly replaced the single field A^μ with the sum of *quantum* field, A^μ and *background* field, $\tilde{A}^\mu$ [94]. The ghost Lagrangian may be obtained by the usual Faddeev-Popov technique. In order to obtain the usual fields of the standard model we shift the Higgs field as in Section 3.2. We transform the $\tilde{B}$ and $\tilde{W}$ background fields,

$$\begin{aligned}
\tilde{B}_\mu &= \tilde{A}_\mu \cos\theta_W - \tilde{Z}_\mu \sin\theta_W \\
\tilde{W}^3_\mu &= \tilde{A}_\mu \sin\theta_W + \tilde{Z}_\mu \cos\theta_W \\
\tilde{W}^1_\mu &= \tfrac{1}{\sqrt{2}}\left(\tilde{W}^+ + \tilde{W}^-\right) \\
\tilde{W}^2_\mu &= \tfrac{i}{\sqrt{2}}\left(\tilde{W}^+ - \tilde{W}^-\right)
\end{aligned} \tag{10.5}$$

with similar equations for the quantum and ghost fields (cf. Eqn. (3.13)).

After performing the above shifts of field variables in the various Lagrangian terms, we obtain the gauge sector of the standard model Lagrangian in background field Feynman gauge. The Feynman rules generated by this Lagrangian relevant for the calculation of $Z \to 3\gamma$ are depicted in Figure 10.1. Only those vertices with two quantum fields attached are given since those are the only contributing ones at one loop. These Feynman rules satisfy the property that there is no $\tilde{A}\phi W^\pm$ coupling, considerably reducing the number of diagrams which must be considered in the $Z \to 3\gamma$ calculation, since diagrams with mixed ϕ-W loops do not appear. (This is similar to the absence of such couplings in the *non-linear* R_ξ gauges discussed in refs. [99].) For generality the coupling constants in the rules of Figure 10.1 have been removed since the various types of gauge bosons couple with different strengths. The various coupling constants required for the calculation of $Z \to 3\gamma$ are given in Table 10.1.

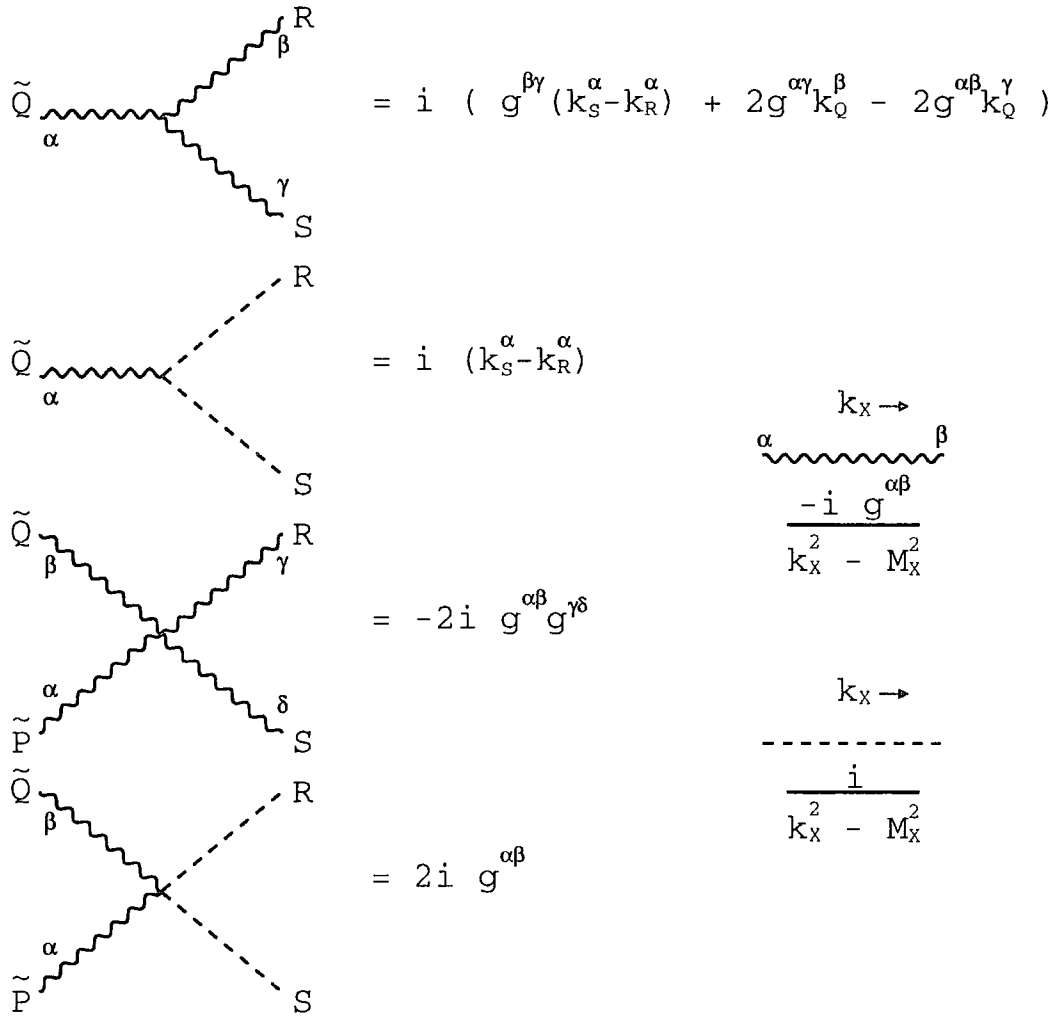

Figure 10.1: The vertices, with coupling constants removed, needed for the calculation of the boson loop contributions to $Z \to \gamma\gamma\gamma$.

Vertex	Coefficient
$\check{A}W^-W^+$	e
$\check{Z}W^-W^+$	$e/\tan\theta_W$
$\check{A}\phi^-\phi^+$, $\check{A}\omega^{+\dagger}\omega^+$, $\check{A}\omega^-\omega^{-\dagger}$	$-e$
$\check{Z}\phi^-\phi^+$	$-e/\tan 2\theta_W$
$\check{Z}\omega^{+\dagger}\omega^+$, $\check{Z}\omega^-\omega^{-\dagger}$	$-e/\tan\theta_W$
$\check{A}\check{A}\phi^+\phi^-$, $\check{A}\check{A}\omega^{\pm\dagger}\omega^\pm$	e^2
$\check{A}\check{Z}\phi^+\phi^-$	$e^2/\tan 2\theta_W$
$\check{A}\check{Z}\omega^{\pm\dagger}\omega^\pm$	$e^2/\tan\theta_W$
$\check{A}\check{A}W^-W^+$,	e^2
$\check{A}\check{Z}W^-W^+$,	$e^2/\tan\theta_W$

Table 10.1: The coupling constants of the vertices needed for the calculation of $Z \to 3\gamma$.

Now consider the inclusion of internal fermions with no flavour changing in the loop. Because the relationship between the fermion and boson loop that we are interested in does not involve the γ_5 in the fermion coupling, we divide the fermion loop computation into a part which contains a γ_5 and a part which does not contain a γ_5. This can be done by considering the one-particle irreducible diagrams in the conventional (first order) formalism; one then collects all the γ_5's together so that the fermion trace contains no more than a single γ_5. This is then split into the axial part containing the γ_5 and the vector part which does not contain the γ_5. The axial part may be evaluated in the usual way since this part does not play a role in the supersymmetry identities. The diagrams of the vector part of the one-loop effective action may be described by the familiar Dirac determinant which is rewritten in the second order form Eqn. (9.2). It is this form which makes the relationship of the fermion loop to the gauge boson loop manifest in the integrands. For the case where there is flavour changing within the loop, and necessarily different masses appear inside it, the relationship to the gauge boson loop is more obscure and one loses the added bonus of simple supersymmetry relations; the advantage of simpler background field vertices is, of course, not lost.

In particular, for the case of $Z \to 3\gamma$, the γ_5 contributions all drop out because of cancellations between diagrams where the fermion circulates in one direction and diagrams where the fermion circulates in the opposite direction. This means that for this process, the relevant fermion loop can calculated with the rules of the 2nd order formalism depicted in Figure 9.3. The coupling associated with each background field is the same as the appropriate effective vector coupling of the first order formalism with an accompanying loop factor $-1/2$, where the minus sign is the familiar one for a fermion loop. One obvious feature of these second order fermion rules is that they bear a much greater resemblance to the boson rules than the conventional (1st order formalism) Feynman rules for fermions; this is important for making the supersymmetry relations hold diagram-by-diagram.

With the rules given in Figures 10.1 and 9.3 the *integrands* of diagrams for one-loop n gauge boson scattering satisfy a $N = 4$ supersymmetry constraint [21, 83]. This relationship between diagrams with fermions in the loop and gauge bosons (and associated ghosts) in the loop is depicted in Figure 10.2 and is given by

$$\begin{aligned} D^{\text{scalar}}(m_s) &= C_s S(m_s) \\ D^{\text{fermion}}(m_f) &= -C_f(2S(m_f) + F(m_f)) \\ D^{\text{gauge boson}}(m_g) &= C_g((1-\delta_R\epsilon)2S(m_g) + 4F(m_g) + G(m_g)) \end{aligned} \tag{10.6}$$

where the particle labels refer to the states circulating in the loop, the m_x are the masses of the particles circulating in the loop and the C_i are coupling constant factors which depend on the processes under consideration. The D all refer to the same diagram types, but with different particles circulating in the loops. For two or three legs attached to the loop the simple quantity G vanishes at the level of the integrand. (The dimensional regularisation parameter is $\delta_R = 1$ for either conventional dimensional regularisation or for the 't Hooft-Veltman scheme [16] while $\delta_R = 0$ for either the dimensional reduction [100]

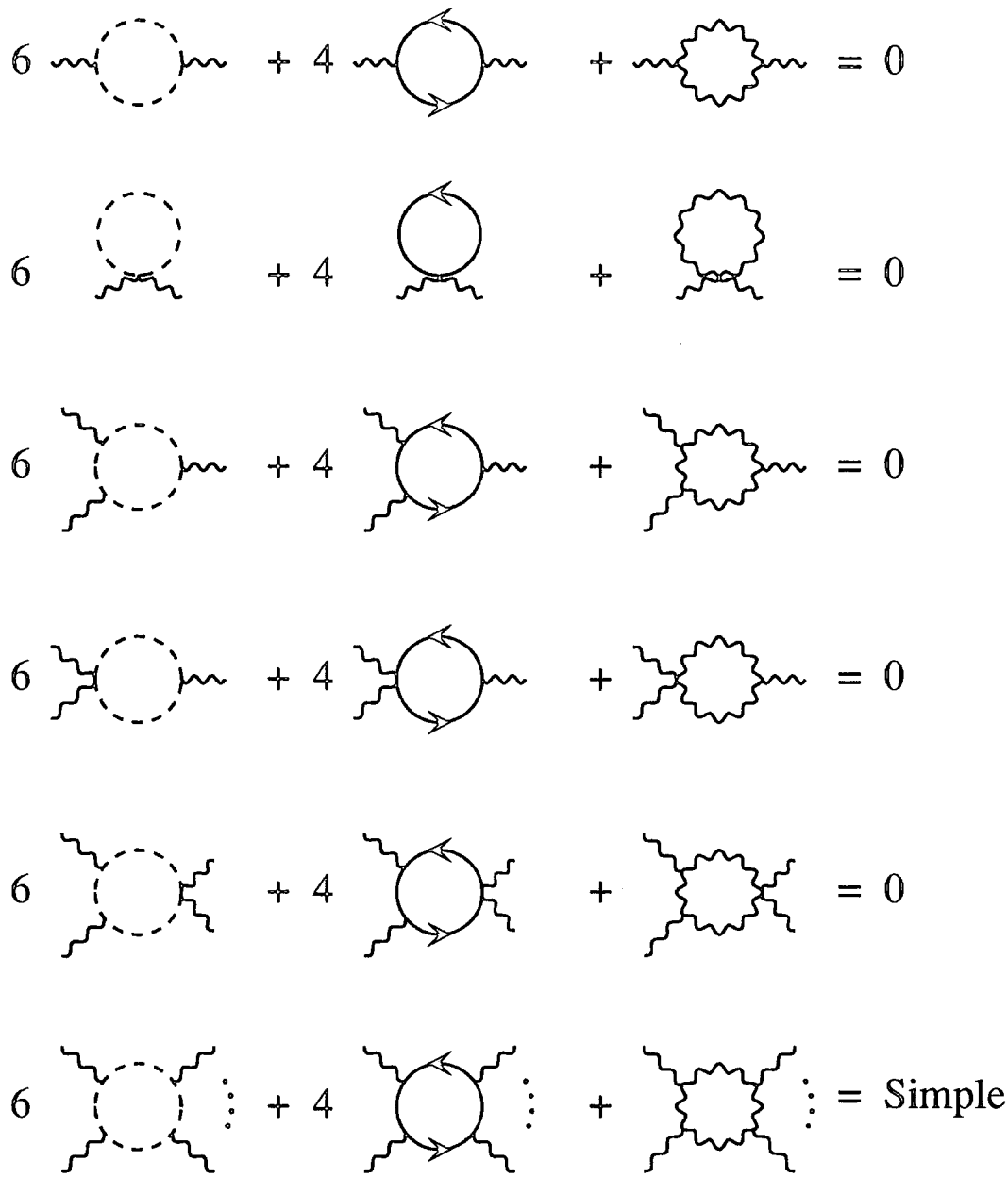

Figure 10.2: The $N = 4$ supersymmetry relations. These relations hold in the integrands of the diagrams. (For simplicity the ghost loop is implicitly included in the gauge boson loop.)

or four-dimensional helicity [85] schemes.) In cases where all types of diagrams satisfy the supersymmetry identities Eqn. (10.6) (such as $Z \to 3\gamma$), the sum over all diagrams – namely the amplitude – also satisfies this identity.

The connection of these identities to $N = 4$ supersymmetry is that for $N = 4$ super-Yang-Mills (one gluon, four Weyl fermions, and 6 real scalars) everything but G *cancels* after summing over the various loop contributions. (The regulator factor $\delta_R = 0$ is necessary so that supersymmetry is not broken). That is,

$$D^{N=4 \text{ susy}} = g^4 G \tag{10.7}$$

where g is the coupling. The other terms all cancel.

In performing the calculation, instead of calculating the diagrams directly it is more efficient to calculate S, F and G. The importance of the above identities is that each part of the calculation is successively easier to perform; S is the most complicated part, F is the next most complicated part and G is by far the easiest part of the calculation. In a conventional approach one would effectively be recomputing the S and F parts since one computes the gauge boson loop directly. This leads to a significant computational advantage for the gauge boson loop beyond the already large simplifications of Feynman background field gauge. (With conventional gauge choices, like 't Hooft-Feynman or unitary gauge, the unnecessary re-computation of S and F is actually significantly more complicated than the direct computation of these quantities from scalar and fermion loops.)

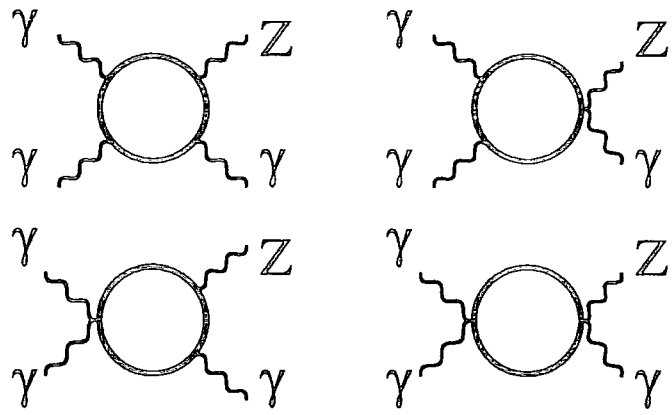

Figure 10.3: The diagrams needed for the calculation of $Z \to 3\gamma$: the loops can be either fermions, gauge bosons or scalars.

10.3 Explicit example

Consider the process $Z \to 3\gamma$. This process has already been discussed in refs. [90, 91] (see Chapter 8) using more conventional techniques. We show here how to reduce the W-loop computation to a very simple one once the fermion loop is calculated. The four one-loop diagram types required for calculating $Z \to 3\gamma$ are depicted in Figure 10.3. The complete amplitude is obtained by summing over the six permutations of external legs.

From ref. [91] we have the general tensor consistent with gauge invariance and crossing symmetry for the three photons as Eqn. (8.10). The amplitude is obtained from this tensor by *dotting* it into the external polarisation vectors. In this method one only computes the scalar quantities A_1, A_2, A_3 thereby eliminating the redundant information contained in a gauge invariant expression, in a way analogous to what happens with spinor helicity methods. Factoring out the coupling constants we obtain an expression for the A_i's in terms of the

scalar, fermionic and gauge boson Feynman rules of Figures 10.1 and 9.3,

$$A_i(p_1,p_2,p_3) = \frac{ie^4}{16\pi^2}\Big(\sum_f Q_f^3 v_f A_i^f(s,t,m_f) + \cot\theta_W A_i^W(s,t,M_W) + \cot 2\theta_W A_i^\phi(s,t,M_W)\Big) \qquad (10.8)$$

cf. Eqn. (8.12). Here the fermionic A_i's are defined to include their overall minus sign. For the gauge loop, A_i^W, we note that the inclusion of both ghosts, $\omega^\pm$ and $\omega^{\pm\dagger}$, is straightforward since they are just (fermionic) complex scalar fields. In fact, in background field gauge, $A_i^{\omega^\pm}(s,t,M_W) = -A_i^\phi(s,t,M_W)$, and thus A_i^W, which we take to include both the W and Faddeev-Popov ghost contributions, is obtained by application of the Feynman rules of Figure 10.1 minus twice the scalar A_i^ϕ result. We therefore only need to compute the three separate contributions A_i^ϕ, A_i^f and A_i^W. Further discussion of the tensor decomposition method can be found in ref. [96].

In order to minimise the duplication of effort, we make use of the supersymmetry relations Eqn. (10.6) to systematise our evaluation of the above scalar A_i functions. Since all of the diagram types in this calculation satisfy the supersymmetry relation Eqn. (10.6), the sum over the diagrams or amplitude will satisfy the relation. As mentioned previously, it is not difficult to verify that the γ_5 contribution in the fermion loop drops out because of cancellations between diagrams where the fermion circulates in one direction and diagrams where the fermion circulates in the opposite direction. This means that the entire fermion loop contribution is of the vector type and therefore included in the supersymmetry identity.

The first step is to compute the scalar loop contribution. After summing over diagrams and reducing the tensor integral down to scalar ones (see Section B.4) the result is

$$A_1^\phi(s,t,m) = \mathcal{S}_1(s,t,m) = -\frac{1}{2}A_1^f(s,t,m),$$

$$
\begin{aligned}
A_2^{\phi}(s,t,m) &= \mathcal{S}_2(s,t,m) = -\frac{1}{2}A_2^f(s,t,m) - \frac{tu}{2}\Big(2m^2H(m) - \frac{1}{s}E(t,u,m)\Big), \quad (10.9)\\
A_3^{\phi}(s,t,m) &= \mathcal{S}_3(s,t,m) = -\frac{1}{2}A_3^f(s,t,m) - \frac{1}{2t}\Big\{t^2E(s,t,m) - u^2E(u,s,m)\\
&\qquad +2m^2ut(u-t)H(m)\Big\}
\end{aligned}
$$

where the functions A_i^f, etc. are defined in Chapter 8. The mass, m, is that of the scalar going around the loop and the arguments s, etc. are defined in Eqn. (8.13).

The scalar loop is the most complicated piece to integrate since the graphs contain the most powers of loop momentum in the numerator. In general, because of the explosion of terms which occurs in the evaluation of tensor integrals [18, 22], factors of loop momenta cause the largest complications; this is reflected in the complexity of this result, see Eqns. (8.16-8.18).

The next stage of the computation is to subtract out the part of the fermion loop proportional to the scalar loop in the integrand of each diagram; after integration this yields the $\mathcal{F}_i$ which after summing over diagrams are as follows

$$
\begin{aligned}
\mathcal{F}_1(s,t,m) &= -A_1^f(s,t,m) - 2\mathcal{S}_1(s,t,m) = 0,\\
\mathcal{F}_2(s,t,m) &= -A_2^f(s,t,m) - 2\mathcal{S}_2(s,t,m) = tu\Big(2m^2H(m) - \frac{1}{s}E(t,u,m)\Big), \quad (10.10)\\
\mathcal{F}_3(s,t,m) &= -A_3^f(s,t,m) - 2\mathcal{S}_3(s,t,m) = \frac{1}{t}\Big\{t^2E(s,t,m) - u^2E(u,s,m)\\
&\qquad +2m^2ut(u-t)H(m)\Big\}.
\end{aligned}
$$

The required integrals are much simpler quantities than for $\mathcal{S}_i$ since the integrands contain at most two powers of loop momentum instead of four. The relative simplicity of the computation as compared to the scalar loop calculation is reflected in the relative simplicity of the results. Plugging the $\mathcal{S}_i$ and $\mathcal{F}_i$ into the second of the supersymmetry relations in Eqn. (10.6) reproduces the results for fermion loops of ref. [91].

To obtain the $W^{\pm}$ loop contribution in each diagram we subtract the integrands associated with $2\mathcal{S}(s,t,M_W)+4\mathcal{F}(s,t,M_W)$ from the full expression for the $W^{\pm}$ loop (including Faddeev-Popov ghosts); this leaves only box diagrams to be evaluated since all other integrands cancel by the supersymmetry relations given in Figure 10.2. Furthermore, the only terms in the vertices which contribute are those which contain no loop momentum. The ones containing loop momentum manifestly cancel in the calculation of $\mathcal{G}(s,t,M_W)$. This cancellation is a direct consequence of the $N=4$ supersymmetry relations. Since the terms with loop momentum cancel, $\mathcal{G}$ is reduced to a relatively simple algebraic expression times a scalar box integral, which may be obtained from ref. [101]. Since there is no need to evaluate a tensor integral, this part of the computation is relatively trivial. (Indeed, by using rules of the string based type [85, 83] it is possible to write down the answer without calculation.) For the diagrams with a 1,2,3,4 and reversed ordering of legs the remaining kinematic tensor is simple and given by

$$\begin{aligned} G^{\alpha\mu\nu\rho}(1234) &= -D(s,t)\Big(8\Big(g^{\alpha\mu}g^{\nu\rho}su+g^{\alpha\nu}g^{\mu\rho}st+g^{\alpha\rho}g^{\mu\nu}ut\Big) \\ &+ 16s\Big(g^{\alpha\rho}p_3^{\mu}p_3^{\nu}+p_3^{\mu}(g^{\nu\rho}p_2^{\alpha}-g^{\alpha\nu}p_2^{\rho})+p_3^{\nu}(g^{\mu\rho}p_1^{\alpha}-g^{\alpha\mu}p_1^{\rho})\Big) \\ &+ 16t\Big(g^{\alpha\mu}p_1^{\nu}p_1^{\rho}+p_1^{\nu}(g^{\mu\rho}p_3^{\alpha}-g^{\alpha\rho}p_3^{\mu})+p_1^{\rho}(g^{\mu\nu}p_2^{\alpha}-g^{\alpha\nu}p_2^{\mu})\Big) \\ &+ 16u\Big(g^{\alpha\nu}p_2^{\mu}p_2^{\rho}+p_2^{\rho}(g^{\mu\nu}p_1^{\alpha}-g^{\alpha\mu}p_1^{\nu})+p_2^{\mu}(g^{\nu\rho}p_3^{\alpha}-g^{\alpha\rho}p_3^{\nu})\Big)\Big) \end{aligned} \tag{10.11}$$

where we have organised the terms to exhibit manifest gauge invariance. The other orderings of external legs are obtained by a relabeling of legs. After summing over the independent orderings, comparing to the kinematic tensor Eqn. (8.10) and using

$$\mathcal{G}_i(s,t,M_W)=A_i^W(s,t,M_W)-(2\mathcal{S}_i(s,t,M_W)+4\mathcal{F}_i(s,t,M_W))$$

the result can be summarized in terms of the three scalar functions

$$\begin{aligned} \mathcal{G}_1(s,t,M_W) &= 0, \\ \mathcal{G}_2(s,t,M_W) &= -2stuH(M_W), \\ \mathcal{G}_3(s,t,M_W) &= 0\,. \end{aligned} \tag{10.12}$$

Again the simplicity of the calculation is reflected in the simplicity of the result. Inserting these functions into the supersymmetry identities Eqn. (10.6), reproduces the results of Chapter 8 for the gauge boson loop. In particular, eliminating for $\mathcal{S}_i$ in favour of A_i^f, and using the following SM identity,

$$\cot 2\theta_W = \frac{1}{2}\cot\theta_W(2 - M_Z^2/M_W^2), \tag{10.13}$$

(cf. Eqn. (3.15)) we find that the non-fermionic contribution to the $Z\gamma\gamma\gamma$ scattering tensor

$$A_i^b = A_i^W + \frac{\cos 2\theta_W}{2}A_i^\phi \tag{10.14}$$

$$= \frac{1}{4}\Big(\frac{M_Z^2}{M_W^2} - 6\Big)A_i^f + \frac{1}{4}\Big(\frac{M_Z^2}{M_W^2} + 10\Big)\mathcal{F}_i + \mathcal{G}_i. \tag{10.15}$$

This then provides an explanation for the empirically observed relations Eqn. (8.15) of Chapter 8: namely that they are supersymmetry identities.

As a simple check on the results for $\mathcal{G}$, we have verified that for external mass $M_Z \to 0$ the kinematic coefficient of the box diagram given in Eqn. (10.11) is proportional to the colour ordered Yang-Mills tree. This is in agreement with expectations from superstring theory with $N = 4$ space-time supersymmetry [87] where the one-loop four-point amplitude is also proportional to the tree.

The calculation we have presented for the W loop may be compared to the unitary gauge

calculation presented in ref. [91]. In that paper, the unitary gauge was used because of the significant reduction in the number of diagrams as compared to the standard 't Hooft-Feynman gauge. In the string-motivated organisation presented here we have retained all the diagrammatic advantages of the unitary gauge. In addition, since it has been possible to use a simple Feynman type background field gauge it has not been necessary at any stage to cancel superficial ultra-violet divergences arising from the extra powers of momentum in the unitary gauge propagator. (This was the most time consuming part of the tensor reduction of ref. [91]). Furthermore, the vertices of background field 't Hooft-Feynman gauge are simpler than those of the unitary gauge. Finally, by making use of the $N = 4$ supersymmetry relations we have reduced the W-loop calculation to that of simple scalar box integrals which are given in refs. [101]. The reorganisation we have presented therefore represents a clear computational advantage.

What about the fermion loop part of the calculation? Superficially it might seem that, since there are *four* diagram types in the second order formalism (Figures 9.3 and 10.3) instead of a single diagram type in the more usual spinor based (first order) formalism, this represents a retrograde step in the calculational technique. In fact, the use of the second order formalism significantly improves the calculational efficiency of the fermion loops since most of the calculation can be directly obtained from the calculation of scalars or ghosts in the loop. The similarity in structure of the fermion to scalar vertices (Figures 10.1 and 9.3) ensures that when calculating the $\mathcal{F}_i$, the cancellations between the scalar and fermion loops implied by the supersymmetry equations of Eqn. (10.6), occur *on the first line* at the level of the integrand and before the evaluation of any tensor integrals. (Even if one were not interested in scalar or gauge boson loop contributions, it is generally still advantageous to break the fermion loop contribution into two separate pieces since it is usually easier to handle smaller physical pieces in a large calculation.) The second order formalism therefore also represents a considerable advance in calculational efficiency for the vector part of fermion

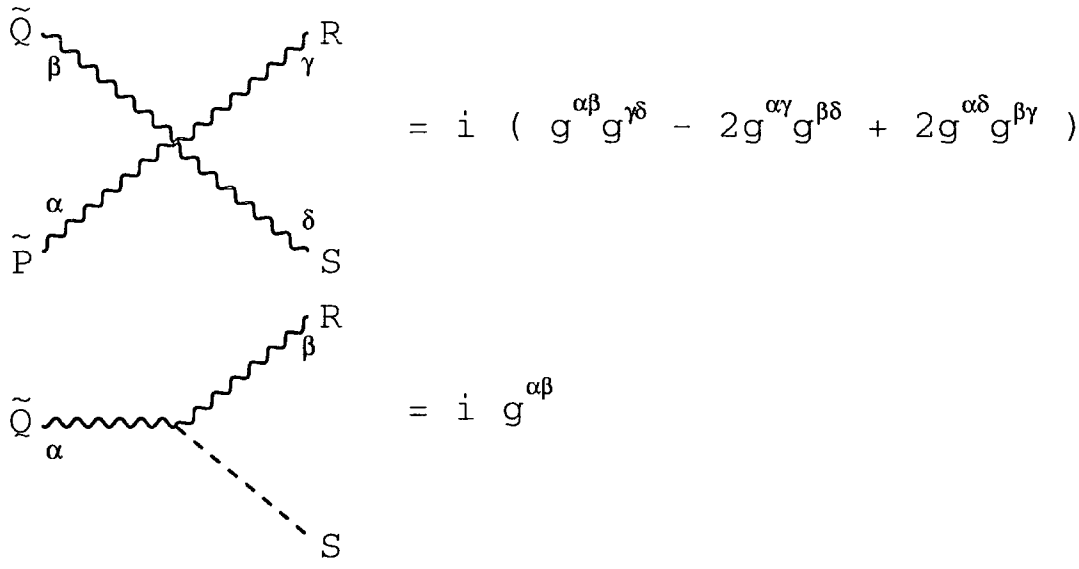

Figure 10.4: Two extra rules. The three point rule for a mixed scalar gauge boson internal loop and the non-abelian four-point vertex where the internal fields are not interchangeable.

loops (with no flavour changing).

10.4 Other processes

The string-motivated reorganisation discussed above is useful for other amplitudes. For completeness the coupling constants for the various other vertices with external gauge bosons are presented in Tables 10.2-10.4.

Table 10.2 contains the coupling constants associated with other three point vertices. Those involving an odd number of gauge fields may be found in Figure 10.1 and the remaining vertices that involve only two gauge fields are to be found in Figure 10.4.

Table 10.3 contains the remaining four-point couplings that obey the rules of Figure 10.1.

Vertex	Coefficient
$\tilde{W}^+AW^-$, $\tilde{W}^-W^+A$	e
$\tilde{W}^+ZW^-$, $\tilde{W}^-W^+Z$	$e/\tan\theta_W$
$\tilde{Z}W^\pm\phi^\mp$	$-e^2v/\sin\theta_W\sin 2\theta_W$
$\tilde{Z}ZH$	$2e^2v/\sin^2 2\theta_W$
$\tilde{W}^\pm W^\mp H$	$e^2v/2\sin^2\theta_W$
$\tilde{W}^\pm W^\mp\chi$	$\mp ie^2v/2\sin^2\theta_W$
$\tilde{W}^\pm A\phi^\mp$	$e^2v/\sin\theta_W$
$\tilde{W}^\pm Z\phi^\mp$	$e^2v/\tan 2\theta_W\sin\theta_W$
$\tilde{W}^+H\phi^-$, $\tilde{W}^-\phi^+H$	$e/2\sin\theta_W$
$\tilde{W}^\pm\chi\phi^\mp$	$ie/2\sin\theta_W$
$\tilde{Z}\chi H$	$-ie/\sin 2\theta_W$

Table 10.2: The coupling constants associated with other three point vertices as represented in Figures 10.1 and 10.4.

Vertex	Coefficient
$\tilde{W}^+\tilde{W}^-AA$	e^2
$\tilde{W}^+\tilde{W}^-AZ$	$e^2/\tan\theta_W$
$\tilde{Z}\tilde{Z}W^-W^+$, $\tilde{W}^+\tilde{W}^-ZZ$	$e^2/\tan^2\theta_W$
$\tilde{W}^\pm\tilde{W}^\pm W^\mp W^\mp$	$-e^2/\sin^2\theta_W$
$\tilde{W}^+\tilde{W}^-\omega^{A\dagger}\omega^A$	e^2
$\tilde{W}^\pm\tilde{A}\omega^{\pm\dagger}\omega^A$, $\tilde{W}^\pm\tilde{A}\omega^{A\dagger}\omega^\mp$	$-e^2$
$\tilde{W}^+\tilde{W}^-\omega^{\pm\dagger}\omega^\pm$,	$e^2/\sin^2\theta_W$
$\tilde{W}^\pm\tilde{W}^\pm\omega^{\pm\dagger}\omega^\mp$	$-e^2/\sin^2\theta_W$
$\tilde{W}^\pm\tilde{Z}\omega^{\pm\dagger}\omega^A$, $\tilde{W}^\pm\tilde{Z}\omega^{A\dagger}\omega^\mp$,	
$\tilde{W}^\pm\tilde{A}\omega^{\pm\dagger}\omega^Z$, $\tilde{W}^\pm\tilde{A}\omega^{Z\dagger}\omega^\mp$	$-e^2/\tan\theta_W$
$\tilde{Z}\tilde{Z}HH$, $\tilde{Z}\tilde{Z}\chi\chi$	$e^2/\sin^2 2\theta_W$
$\tilde{Z}\tilde{Z}\phi^+\phi^-$	$e^2/\tan^2 2\theta_W$
$\tilde{W}^+\tilde{W}^-\phi^+\phi^-$, $\tilde{W}^+\tilde{W}^-HH$, $\tilde{W}^+\tilde{W}^-\chi\chi$	$e^2/4\sin^2\theta_W$
$\tilde{W}^\pm\tilde{A}H\phi^\mp$	$e^2/4\sin\theta_W$
$\tilde{W}^\pm\tilde{Z}H\phi^\mp$	$-e^2/4\cos\theta_W$
$\tilde{W}^\pm\tilde{A}\chi\phi^\mp$	$\pm ie^2/4\sin\theta_W$
$\tilde{W}^\pm\tilde{Z}\chi\phi^\mp$	$\mp ie^2/4\cos\theta_W$
$\tilde{W}^+\tilde{W}^-\omega^{Z\dagger}\omega^A$, $\tilde{W}^+\tilde{W}^-\omega^{A\dagger}\omega^Z$	$e^2/\tan\theta_W$
$\tilde{W}^+\tilde{W}^-\omega^{Z\dagger}\omega^Z$, $\tilde{Z}\tilde{Z}\omega^{\pm\dagger}\omega^\pm$	$e^2/\tan^2\theta_W$
$\tilde{W}^\pm\tilde{Z}\omega^{\pm\dagger}\omega^Z$, $\tilde{W}^\pm\tilde{Z}\omega^{Z\dagger}\omega^\mp$,	$-e^2/\tan^2\theta_W$

Table 10.3: The remaining four-point vertices represented by Figure 10.1.

Vertex	Coefficient
$\tilde{W}^{\pm}\tilde{A}W^{\mp}A$	e^2
$\tilde{W}^{\pm}\tilde{Z}W^{\mp}A$, $\tilde{W}^{\pm}\tilde{A}W^{\mp}Z$	$e^2/\tan\theta_W$
$\tilde{W}^{\pm}\tilde{Z}W^{\mp}Z$	$e^2/\tan^2\theta_W$
$\tilde{W}^{+}\tilde{W}^{-}W^{+}W^{-}$	$-e^2/\sin^2\theta_W$

Table 10.4: The coupling constants associated with non-abelian four-point vertex as represented by Figure 10.4.

Besides the vertex structures already encountered in Figure 10.1 there is an additional non-abelian vertex given in Figure 10.4; the coupling constants associated with this vertex are presented in Table 10.4.

Using these tables, one could for example consider the one-loop process $2\gamma \to 2Z$ [92] (which is of some interest to future photon-photon colliders). In this process one can again use the $N = 4$ supersymmetry relations of Figure 10.2 to relate the diagrams with the W going around the loop to the diagrams with fermions going around the loop. In this case, however, there are mixed diagrams with both W's and ϕ's in the loop. Although such diagrams are apparently not simply related to fermion loop diagrams they are simpler to evaluate since they have a maximum of two powers of loop momentum in the numerator.

Due to the simplicity of the background field vertices as well as the supersymmetry relations Eqn. (10.6), one can expect a significant efficiency over previous calculations of $2\gamma \to 2Z$ [92]. For example in the one performed by Berger in standard 't Hooft-Feynman gauge, there were 188 diagrams to evaluate for the boson loop contributions. Since each of the vertices is relatively complicated compared to background field vertices, this calculation is significantly more complicated than one which follows the above strategy. Indeed, Bajc in his paper states that there are 608 terms in the W box diagram alone. We may also contrast the above strategy to the non-linear gauge used by Jikia in his calculation; we retain the advantage of eliminating the $\tilde{A}\phi^{\pm}W^{\mp}$ vertex and have the additional advantages of having

simpler vertices and supersymmetry relations between diagrams. A third alternative is the non-linear gauge used by Dicus and Kao which has the advantage of eliminating all remaining diagrams with mixed W-ϕ loops, but then the vertices are more complicated and one loses the supersymmetry relations for the un-mixed diagrams. Due to the supersymmetry relations, the main part of each of these calculations only reproduces pieces already computed for the fermion loops.

The ideas discussed above can also be applied to the case of external fermions. In particular, background field Feynman gauge is still advantageous to use even when some external legs are fermions. As for the purely external gauge boson case it is also useful to identify parts of the calculation which are duplicated in the various diagrams. This type of strategy has already been successfully applied in the calculation of the one-loop corrections to four- [102] and five-parton [103] processes.

10.5 Summary

Various contributions to gauge boson amplitudes have relations between them connected to the fact that amplitudes in $N = 4$ super-Yang-Mills have extremely simple forms. These relations were first applied in the string-based calculation of gluon amplitudes [21, 83]. In order to make practical use of the supersymmetry relations one needs a formalism where the relations hold between the integrands of diagrams. The guidance for constructing such a formalism is provided by string theory and amounts to special gauge choices and organisations of the diagrams.

In this chapter we have described the supersymmetry relations in weak interaction processes which involve gauge bosons. These types of relationships were observed to hold in the

explicitly computed weak interaction process $Z \to 3\gamma$ [91], although in the unitary gauge where the calculation was performed the relations seem *mysterious*. We have shown how to reorganise this calculation as well as other processes so that the supersymmetry relations are manifest in all stages of the calculation. Important ingredients for making the relationships manifest in the diagrams are the background field Feynman gauge for the gauge-boson loops and the second order formalism for fermion loops. In this way the gauge boson and fermion loop computations have considerable overlap. The parts of the calculation which overlap do not need to be recomputed for the gauge boson loop contributions.

A practical consequence of the reorganised calculation and the manifest supersymmetry relations is that instead of the W-loop contribution being the most complicated part of the calculation it is relatively easy to obtain it using results from the fermion loop contribution.

Chapter 11

Conclusions

11.1 Summary

In this thesis we have reviewed the path integral approach to Quantum Field Theory, the Standard Model of Particle Physics and some simple phenomenology appropriate for the Large Electron-Positron Collider (LEP). The remainder of the text has been devoted to a study of final state photon radiation at LEP.

Firstly, we have discussed photons produced in association with hadrons. We have established that fixed order perturbation theory is unreliable in describing photon radiation collinear to its partonic radiator. We have invoked the mechanism of factorisation to remove the divergence associated with a perturbative collinear emission. To do this we have had to introduce a *non-perturbative* contribution to photon production. This photon frag-

mentation function accounts for the hadronic component to photon emission—necessarily in the collinear region. It is irrevokably (via factorisation and the regularisation scheme) tied to the perturbative divergence it is required to absorb. By itself it has little physical meaning, much like the single diagram of virtual gluon emission in Figure 4.10b. Indeed, it contains a divergence! Only when it is combined with an appropriately regulated perturbative calculation does it make possible a good description of prompt and non-prompt photon emission. Following this work, the ALEPH collaboration have succeeded in measuring the fragmentation function at LEP, and we have seen that our approach satisfactorily describes the observed data, both isolated and non-isolated.

Struck by the apparent sensitivity of calculations to the different methods of isolating photon in photon+1 jet rate at LEP (see Figure 6.1), we have investigated the flow of soft gluons in such events. The collinear photon/gluon region does not contribute a divergence to the calculation. In spite of this, we find that depending upon which photon definition is chosen, a large fraction of the gluon radiation can reside inside the photon's effective cone of isolation. This naturally leads to large radiative corrections, and in the least, signals a need for a more complete calculation. This is especially acute for the cone-type photon definitions. The 'democratically' defined photon events, however, have smaller and generally more stable radiative corrections. The cuts tend to favour more energetic photons and consequently the quarks are forced into a more confined configuration. Such a configuration leads to a suppression in soft gluon radiation in the direction of the photon because here the quarks appear as a colour singlet. This tendency can be seen clearly in actual hadronic events and also apparently leads to a suppression in the *number* of emerging hadrons (see Figure 6.5).

We have used the ALEPH measurement of the photon fragmentation function to make non-isolated cone predictions. In studying this result, we have uncovered an extreme break-

down in the *isolated* perturbative photon prediction: a breakdown that previously required large and negative $\mathcal{O}(\alpha_s)$ radiative corrections to agree with data. Motivated by ALEPH's observation of apparently large *hadronisation corrections* at the high photon energy end of the fragmentation region, we have made a *pseudo-isolated* prediction for the 1-jet rate that coincide with the *democratic* isolated rate for 90° and the fully non-isolated 1-jet rate for small cone angles. This prescription agrees with existing *isolated* data.

Secondly, we have made a study of the rare Z-decay to three photons within the Standard Model. Initially motivated by disagreements in the literature over the observability of such a process at LEP, we have calculated it and found it to be unobservable. In the process of calculation, however, we found that there was a striking similarity in the analytic form of the boson and fermion amplitudes (Eqn. (8.15)). This observation has stimulated much further study.

Following a *string theory* inspired rewriting of the Dirac determinant, we have derived a set of *2nd Order Fermionic* Feynman rules that are valid for gauge invariant effective one-loop vertex functions. We have found a derivation of these same rules from a manipulation of the conventional Feynman rules that has suggested a further symmetry within them. We have applied the *Background Field Method* to the Electroweak sector of the Standard Model to obtain a gauge invariant Effective Action. From which we have obtained a set of Feynman rules for the calculation of gauge invariant vertex functions.

Using these calculational improvements, we are able to see the sorts of symmetry observed in the above calculation at the level of individual diagrams, and not just at the level of the complete amplitude. The symmetry observed above is inherent in all field theories involving fermions and gauge fields, but was first noted in a supersymmetric theory with the aid of string theory. We have sketched a method of calculation based on these principles which removes the redundant parts of calculations at an early stage.

11.2 Outlook

This thesis has two aspects: a phenomenological one and a more formal field theoretic one. The results of both lead naturally to further questions and topics for further study.

Having an ideal test-bed of high statistics at LEP, there is sufficient reason for extending the Measurement of the photon fragmentation function to a higher order calculation. This necessitates the inclusion of *doubly collinear* radiation into the formulation, to extend the calculation to next-to-next-to-leading order. This may provide an explanation for the shoulder observed at high photon energy, in the ALEPH data. Furthermore it may give an insight into the possibility of resumming the collinear region. Also of interest, is the prospect of using the measured fragmentation function at other colliders, such as the Tevatron at Fermilab. Following the appropriate calculation it may prove possible to measure the gluon structure function from non-isolated photon data, where the statistics are higher and, if our observations about 'isolated' photons carry over from LEP, *more reliable.*

With regard to the Fermion methods developed in this thesis, there is some prospect for extending them to general fermion calculations. In doing this it may prove possible to calculate internal loops of mixed fermions and gauge bosons in a more transparent and interchangeable manner.

In conclusion, it is the opinion of the author that there has been, and will continue to be, more to the photon than meets the eye!

Bibliography

[1] As quoted in,

J. Gleick, "GENIUS. Richard Feynman and modern physics", Abacus (1984) 373.

[2] see for example:

C. Itzykson and J-B. Zuber, "Quantum Field Theory", McGraw Hill (1980).

L.H. Ryder, "QUANTUM FIELD THEORY", Wiley (1984).

F. Mandl and G. Shaw, "QUANTUM FIELD THEORY", Cambridge (1985).

[3] see for example:

P.A.M. Dirac, "The Principles of Quantum Mechanics" *fourth edition*, Oxford (1958),

L.I. Schiff, "QUANTUM MECHANICS" *3rd edition*, McGraw-Hill (1968).

[4] P.A.M. Dirac, Phys. Zeit. der Sov. 2:64 (1933);

reprinted in J. Schwinger (ed.) "Selected Papers on Quantum Electrodynamics", New York: Denver (1958).

[5] R.P. Feynman and A.R. Hibbs, "Quantum Mechanics and Path Integrals", McGraw-Hill, New York (1965).

[6] see for example:

"The Feynman Lectures on Physics" vol 2, Addison Wesley (1964)

T.W.R. Kibble, "Classical Mechanics" 3rd Edition, Longman (1986).

[7] T-P. Cheng and L-F. Li, "Gauge theory of elementary particle physics", Oxford (1984).
I.J.R. Aitchison and A.J.G. Hey, "Gauge Theories in Particle Physics" *second edition*, Adam Hilger (1989).

[8] L.D. Faddeev and V.N. Popov, Phys. Lett. **B25** (1967) 29.

[9] F. Abe et al., FERMILAB-PUB-94-097-E (1994).
R. Jacobsen, CERN-PPE/94-97 (1994)
The CDF collaboration have recently released a preprint entitled "Evidence for Top Quark Production in $\overline{p}p$ Collisions at $\sqrt{s} = 1.8$ TeV". With various cuts they observe a larger cross-section than QCD theory suggests in the absence of a top quark, which they claim is consistent with a top mass of $174 \pm 10^{+12}_{-12}$ GeV. The evidence is, however, not conclusive because current theory with this mass suggests a smaller cross-section than is actually observed. It remains to be seen, with more analysis and increased data, whether QCD and experiment will converge. More recently, estimates of the Top mass based on their indirect effect on Electroweak physics have lead to consistent bounds from LEP of $177 \pm 11^{+18}_{-19}$ GeV.

[10] P.W. Higgs, Phys. Rev. Lett. **12** (1964) 132.
P.W. Higgs, Phys. Rev. **145** (1966) 1156.

[11] K. Fujikawa, B.W. Lee and A.I. Sanda, Phys. Rev. **D6** (1972) 2923.

[12] S.L. Glashow, Nucl. Phys. **22** (1967) 579,
S. Weingerg, Phys. Rev. Lett. **19** (1967) 1264,
A. Salam, Proceedings of the 8th Nobel Symposium, ed. N Svatholm, Amqvist and Wiksell (1968).

[13] N. Cabbibo, Phys. Rev. Lett. **10** (1963) 531.
M. Kobayashi and M. Maskawa, Prog. Theor. Phys. **49** (1973) 652.

[14] S.L. Glashow, J. Iliopoulos and L. Maianim, Phys. Rev. **D2** (1970) 1287.

[15] K. Hikasa et. al., Particle Data Group, Phys. Rev. **D45**:11 (1992).

[16] C.G. Bollini and J.J. Giambiagi, il Nuovo Cimento **12B** (1972) 20,
G. 't Hooft and M. Veltman, Nucl. Phys. **B44** (1972) 189.
For a review
G. Leibbrandt, Rev. Mod. Phys. **47** (1975) 849,
J.C. Collins, "Renormalization", Cambridge (1989).

[17] W. Pauli and F. Villars, Rev. Mod. Phys. **21** (1949) 434.
D.Z. Freedman, K. Johnson, R. Muñoz-Tapia and X. Vilasís-Cardona, Nucl. Phys. **B395** (1993) 454;
R. Muñoz-Tapia, Phys. Lett. **B295** (1992) 95.

[18] G. Passarino and M. Veltman, Nucl. Phys. **B161** (1979) 151.

[19] M. Nowakowski, A. Pilaftsis and U. Karlsruhe, Z.Phys **C60** (1993) 121.

[20] M.R. Pennington, Rep. Prog. Phys. **46** (1983) 393.

[21] Z. Bern, L. Dixon and D.A. Kosower, Phys. Rev. Lett. **70** (1993) 2677.

[22] Z. Bern, L. Dixon and D.A. Kosower, Phys. Lett. **B302** (1993) 299
Z. Bern, L. Dixon and D.A. Kosower, Nucl. Phys. **B412** (1994) 751

[23] Z. Kunszt, A. Signer and Z. Trocsanyi, ETH-TH-94-14 (1994).

[24] T. Sjostrand and M. Bengtson, Comput. Phys. Comm. **43** (1987) 367
G. Marchesini et. al., Comput. Phys. Comm. **67** (1992) 465
L. Lonnblad, Comput. Phys. Comm. **71** (1992) 15.

[25] A.D. Martin, R.G. Roberts and W.J. Stirling, DTP/94/34 and hep-ph9406315 (1994).

[26] J.H. Da Luz Vieira and J.K. Storrow, Z. Phys. **C51** (1991) 241.

[27] Z. Kunszt and P. Nason, "Z Physics at LEP", CERN yellow report CERN 89-08 vol. 1, ed. G. Altarelli, R. Kleiss and C. Verzegrassi (1989) 373.

[28] W.T. Giele and E.W.N. Glover, Phys. Rev, **D46** (1992) 1980.

[29] T. Kinoshita, J. Math. Phys. **3** (1962) 650;
T.D. Lee and M. Nauenberg, Phys. Rev. **133** (1964) 1549.

[30] See for example:
S. Catani, L. Trentadue, G. Turnock and B.R. Webber, Nucl. Phys. **B407** (1993) 3.
N.S. Craigie and H.F. Jones, Nucl. Phys. **B172** (1980) 59.

[31] D. J. Summers, MAD-PH-833 (1994).

[32] K. Koller, T.F. Walsh and P.M. Zerwas, Z. Phys. **C2** (1979) 197.

[33] E. Laermann, T.F. Walsh, I. Schmitt and P.M. Zerwas, Nucl. Phys. **B207** (1982) 205.

[34] G. Altarelli, R.K. Ellis, G. Martinelli and S.-Y. Pi, Nucl. Phys. **B160** (1979) 301.

[35] G. Kramer and B. Lampe, Phys. Lett. **B269** (1991) 401.

[36] P. Mättig and W. Zeuner, Z. Phys. **C52** (1991) 31.

[37] E.W.N. Glover and W.J. Stirling, Phys. Lett. **B295** (1992) 128.

[38] G. Kramer and H. Spiesberger, DESY preprint DESY 92-022 (1992).

[39] Z. Kunzst and Z. Trocsanyi, Nucl. Phys. **B394** (1993) 139.

[40] OPAL Collaboration, P.D. Acton et al., Z. Phys. **C54** (1992) 193.

[41] ALEPH Collaboration, D. Buskulic et al., Z. Phys. **C57** (1992) 17.

[42] DELPHI Collaboration, P. Abreu et al., Z. Phys. **C53** (1992) 555.

[43] L3 Collaboration, O. Adriani et al., Phys. Lett. **B292** (1992) 463.

[44] JADE Collaboration, S.Bethke et al., Phys. Lett. **B213** (1988) 235.

[45] Y. Dokshitzer, Contribution to the Workshop on Jets at LEP and HERA, J. Phys. **G17** (1991) 1441.

[46] H. Baer, J. Ohnemus and J. F. Owens, Phys. Lett. **B234** (1990) 127.

[47] B. Bailey, J. Ohnemus and J. F. Owens, Phys. Rev. **D42** (1990) 61.

[48] CDF Collaboration, F. Abe et al., Phys. Rev. Lett. **68** (1992) 2734.

[49] CDF Collaboration, F. Abe et al., Phys. Rev. Lett. **70** (1993) 2232.

[50] F. Bloch and A. Nordsieck, Phys. Rev. **52** (1937) 54.

[51] M. Glück, E. Reya and A. Vogt, Phys. Rev, **D48** (1993) 116.

[52] N. Brown and W.J. Stirling, Z. Phys. **C53** (1992) 629.

[53] D.W. Duke and J.F. Owens, Phys. Rev. **D26** (1982) 1600.

[54] P. Mättig, H. Spiesberger and W. Zeuner, Z. Phys. **C60** (1993) 613.

[55] E.W.N. Glover and A.G. Morgan, Z. Phys. **C62** (1994) 311.

[56] Yu L Dokshitzer, V A Khoze, A H Meuller and S I Troyan, "Basics of Perturbative QCD." Editions Frontières (1991).

[57] OPAL Collaboration, P.D. Acton et al., Z. Phys. **C58** (1993) 405.

[58] ALEPH Collaboration, presented by J.C. Thompson, 29th Rencontres de Moriond, Meribel, March 1994.

ALEPH Collaboration, contribution to 27th International Conference on High Energy Physics, Glasgow Scotland, July 1994.

[59] J. Chyla, Phys. Lett. **B320** (1994) 186.

[60] E.W.N. Glover and A.G. Morgan, Phys. Lett. **B324** (1994) 487.

[61] R. Karplus and M. Neuman, Phys. Rev. **80** (1950) 380;
R. Karplus and M. Neuman, Phys. Rev. **83** (1951) 776;
V. Constantini, B. De Tollis and G. Pistoni, Nuovo Cimento **A2** (1971) 733.

[62] H. Fanchiotti, H.O. Girotti and A. Sirlin, Lett. al Nuovo Cimento **4** (1972) 826.

[63] F. Boudjema, Phys. Lett. **B187** (1987) 362.

[64] M. Baillargeon and F. Boudjema, Phys. Lett. **B272** (1991) 158.

[65] X.Y. Pham, Phys. Lett. **B272** (1991) 373.

[66] F.-X. Dong, X.-D. Jiang and X.-J. Zhou, Phys. Rev. **D46** (1992) 5074.

[67] M.L. Laursen, K.O. Mikaelian and M.A. Samuel, Phys. Rev. **D13** (1981) 2795.

[68] E.W.N. Glover and J.J. van der Bij, Nucl. Phys. **B313** (1989) 237.

[69] E.W.N. Glover, J.J. van der Bij et al, Proc. Workshop on Z Physics at LEP1, eds. G. Altarelli, R. Kleiss and C. Verzegnassi, CERN report CERN 89-08, Vol. 2 (1989) 1.

[70] T. Appelquist and J Carazzone, Phys. Rev. **D11** (1975) 2856.

[71] V.N. Baier, E.A. Kurayev and V.S. Fadin, Sov. J. Nucl. Phys. **31** (1980) 364.

[72] M.B. Gavela, G. Girardi, C. Malleville and P. Sorba, Nucl. Phys. **B193** (1981) 257.

[73] X.-D. Jiang and X.-J. Zhou, Phys. Rev. **D47** (1993) 214.

[74] F. Abe et al., CDF Collaboration, Phys. Rev. Lett. **68** (1992) 447.

[75] J. Ellis, G.L. Fogli and E. Lisi, Phys. Lett. **B292** (1992) 427.

[76] We are grateful to David Summers for providing us with these numbers.

[77] A.A. Carter, Institute of Physics Conference on Nuclear and Particle Physics, Glasgow, March 1993.

[78] OPAL Collaboration, Phys. Lett. **B257** (1991) 531.

[79] DELPHI Collaboration, Phys. Lett. **B268** (1991) 296.

[80] L3 Collaboration, Phys. Lett. **B288** (1992) 404.

[81] F. Boudjema, F.M. Renard et al, Proc. Workshop on Z Physics at LEP1, eds. G. Altarelli, R. Kleiss and C. Verzegnassi, CERN report CERN 89-08, Vol. 2 (1989) 182.

[82] F.M. Renard, Phys. Lett. **B116** (1982) 264.

[83] Z. Bern, UCLA/93/TEP/5, hep-ph/9304249, proceedings of TASI (1992).

[84] Z. Bern and D.C. Dunbar, Nucl. Phys. **B379** (1992) 562.

[85] Z. Bern and D.A. Kosower, Phys. Rev. Lett. **66** (1991) 1669
Z. Bern and D.A. Kosower, Nucl. Phys. **B379** (1992) 451
Z. Bern and D.A. Kosower, in *Proceedings of the PASCOS-91 Symposium*, eds. P. Nath and S. Reucroft
Z. Bern, Phys. Lett. **B296** (1992) 85

[86] Z. Bern, D.C. Dunbar, and T. Shimada, Phys. Lett. **B312** (1993) 277.

[87] M.B. Green, J.H. Schwarz and L. Brink, Nucl. Phys. **B198** (1982) 472.

[88] M.T. Grisaru, H.N. Pendleton and P. van Nieuwenhuizen, Phys. Rev. **D15** (1977) 996
M.T. Grisaru and H.N. Pendleton, Nucl. Phys. **B124** (1977) 81
S.J. Parke and T. Taylor, Phys. Lett. **B157** (1985) 81
Z. Kunszt, Nucl. Phys. **B271** (1986) 333
M.L. Mangano and S.J. Parke, Phys. Rep. **200** (1991) 301

[89] M.J. Strassler, Nucl. Phys. **B385** (1992) 145

M.G. Schmidt and C. Schubert, Phys. Lett. **B318** (1993) 438

[90] M. Baillargeon and F. Boudjema, Phys. Lett. **B272** (1991) 158

X.Y. Pham, Phys. Lett. **B272** (1991) 373

F.-X. Dong, X.-D. Jiang and X.-J. Zhou, Phys. Rev. **D46** (1992) 5074

[91] E.W.N. Glover and A.G. Morgan, Z. Phys. **C60** (1993) 175

[92] M. Chanowitz, Phys. Rev. Lett. **69** (1992) 2037

G.V. Jikia, Phys. Lett. **B298** (1993) 224

Nucl. Phys. **B405** (1993) 24

B. Bajc, Phys. Rev. **D48** (1993) 1907

M.S. Berger, Phys. Rev. **D48** (1993) 5121

D. A. Dicus and C. Kao, Phys. Rev. **D49** (1994) 1265

A. Abbasabadi, D. Bowser-Chao, D.A. Dicus and W.W. Repko, Phys. Rev. **D49** (1994) 547

[93] J.E. Paton and H.M. Chan, Nucl. Phys. **B10** (1969) 516

F.A. Berends and W.T. Giele, Nucl. Phys. **B294** (1987) 700

M. Mangano and S.J. Parke, Nucl. Phys. **B299** (1988) 673

M. Mangano, Nucl. Phys. **B309** (1988) 461

Z. Bern and D.A. Kosower, Nucl. Phys. **B362** (1991) 389

[94] G. 't Hooft, Acta Universitatis Wratislavensis no. 38, 12th Winter School of Theoretical Physics in Karpacz; *Functional and Probabilistic Methods in Quantum Field Theory*, Vol. 1 (1975)

B.S. DeWitt, in *Quantum Gravity II*, eds. C. Isham, R. Penrose and D. Sciama (Oxford, 1981)

L.F. Abbott, Nucl. Phys. **B185** (1981) 189

L.F Abbott, M.T. Grisaru and R.K. Schaeffer, Nucl. Phys. **B229** (1983) 372

[95] J.L. Gervais and A. Neveu, Nucl. Phys. **B46** (1972) 381

D.A. Kosower, Nucl. Phys. **B335** (1990) 23

[96] R. Karplus and M. Neuman, Phys. Rev. **80** (1950) 380

[97] F. A. Berends, R. Kleiss, P. De Causmaecker, R. Gastmans and T. T. Wu, Phys. Lett. **B103** (1981) 124

P. De Causmaeker, R. Gastmans, W. Troost and T. T. Wu, Nucl. Phys. **B206** (1982) 53

R. Kleiss and W. J. Stirling, Nucl. Phys. **B262** (1985) 235

J. F. Gunion and Z. Kunszt, Phys. Lett. **B161** (1985) 333

R. Gastmans and T.T. Wu, "The Ubiquitous Photon: Helicity Method for QED and QCD", Clarendon Press (1990)

Z. Xu, D.-H. Zhang and L. Chang, Nucl. Phys. **B291** (1987) 392

[98] J.D. Bjorken, Stanford Ph.D. thesis (1958)

J.D. Bjorken and S.D. Drell, *Relativistic Quantum Fields* (McGraw-Hill, 1965)

J. Mathews, Phys. Rev. **113** (1959) 381

S. Coleman and R. Norton, Nuovo Cimento **38** (1965) 438

C.S. Lam and J.P. Lebrun, Nuovo Cimento **59A** (1969) 397

C.S. Lam, Nucl. Phys. **B397** (1993) 143

[99] K. Fujikawa, Phys. Rev. **D7** (1973) 393

M. Base and N.D. Hari Dass, Ann. Phys. **94** (1975) 349

(See also [72])

N.G. Deshpande and M. Nazerimonfared, Nucl. Phys. **B213** (1983) 390

F. Boudjema, Phys. Lett. **B187** (1987) 362

[100] W. Siegel, Phys. Lett. **84B** (1979) 193

[101] G. 't Hooft and M. Veltman, Nucl. Phys. **B153** (1979) 365

A. Denner, U. Nierste, and R. Scharf, Nucl. Phys. **B367** (1991) 637

A. Davydychev and N.Ussyukina, Phys. Lett. **B298** (1993) 363

[102] Z. Kunszt, A. Signer and Z. Trocsanyi, Nucl. Phys. **B411** (1994) 397

[103] Z. Bern, L. Dixon, and D.A. Kosower, in preparation

[104] L. Lewin, "Dilogarithms and Associated Functions", MacDonald (1958).

[105] J. Vermaseren, "FORM User's Guide" (1990).

[106] E. Byckling and K. Kajantie, "Particle Kinematics", Wiley (1972)

Appendix A

Useful Functions

A.1 The Gamma function, $\Gamma(z)$

The Gamma Function, $\Gamma(z)$, is defined in the following way,

$$\Gamma(z) = \int_0^1 dt\, e^{-t}\, t^{z-1}. \tag{A.1}$$

The function $\Gamma(z)$ is defined to satisfy the following identity,

$$z\Gamma(z) = \Gamma(z+1). \tag{A.2}$$

It can be seen to be a natural extension to the factorial function since for integer arguments,

$n \geq 0$,

$$\Gamma(n+1) \;=\; n!. \tag{A.3}$$

It follows from the gaussian integral that,

$$\Gamma\left(\frac{1}{2}\right) = \sqrt{\pi}. \tag{A.4}$$

A useful identity is,

$$\frac{\Gamma\left(\frac{1}{2}\right)}{\Gamma(z)} = \frac{2^{2z-1}\Gamma\left(z+\frac{1}{2}\right)}{\Gamma(2z)}. \tag{A.5}$$

An alternative, but equivalent, definition for this function is the so called Euler Representation:

$$\Gamma(z) = \lim_{n\to\infty} \frac{1\cdot 2\cdot 3\cdots n}{z(1+z)(2+z)\ldots(n+z)} n^z. \tag{A.6}$$

The advantage of this definition is that it enables one to write the gamma function in exponential form,

$$\Gamma(1+z) = \exp\left\{-z\gamma_E + \sum_{j=2}^{\infty} \frac{(-z)^j}{j}\zeta(j)\right\} \tag{A.7}$$

where $\zeta(j)$ is the j th Riemann-Zeta function and γ_E the Euler constant. The Gamma Function is a fundamental tool in the application of Dimensional Regulation, where it is used to generalise the notion of $n!$.

A.2 The Beta function, $B(x, y)$

The Beta Function is defined as follows,

$$B(x,y) = \frac{\Gamma(x)\Gamma(y)}{\Gamma(x+y)} \tag{A.8}$$

As for the Gamma function this combination is useful in the evaluation of non-integer dimension integrals.

From a manipulation of Eqn. (A.1) we obtain,

$$\int_0^{\pi/2} d\theta \, \cos^m\theta \sin^n\theta = \frac{1}{2} B\left(\frac{m+1}{2}, \frac{n+1}{2}\right). \tag{A.9}$$

With respect to this integral form and a change of variables to $z = \cos^2\theta$, we obtain an alternative integral form,

$$\int_0^1 dz \, z^i (1-z)^j = B(i+1, j+1). \tag{A.10}$$

From this identity with the change of variable, $t = u/(1+u)$, we obtain

$$\int_0^\infty \frac{u^m}{(u+a)^n} \equiv \frac{1}{a^{n-m-1}} B(m+1, n-m-1) \tag{A.11}$$

A.3 The symmetric Gram determinant, $\Delta(a, b, \ldots c)$

The Gram Determinant, Δ, is defined,

$$\Delta(a, b, \ldots c) = \det \begin{pmatrix} a \cdot a & a \cdot b & \cdots & a \cdot c \\ b \cdot a & b \cdot b & \cdots & b \cdot c \\ \vdots & \vdots & & \vdots \\ c \cdot a & c \cdot b & \ldots & c \cdot c \end{pmatrix} \tag{A.12}$$

Three of its most useful properties are immediately apparent,

$$\begin{aligned} \Delta(a, b, \ldots) &= \Delta(b, a, \ldots) \\ \Delta(a, b + \lambda a, \ldots) &= \Delta(a, b, \ldots) \\ \Delta(-a, b, \ldots) &= \Delta(a, b, \ldots) \end{aligned} \tag{A.13}$$

A.4 The Spence function, $\mathrm{Sp}(x)$

The *Spence Function* (or dilogarithm) [104, 101] is defined,

$$\mathrm{Sp}(x) = -\int_0^1 \frac{dz}{z} \log(1 - xz). \tag{A.14}$$

It is a frequently recurring function in high energy physics calculations, and is used extensively in this thesis. The following two identities are found to be useful,

$$\mathrm{Sp}(x) = -\mathrm{Sp}(1 - x) + \frac{\pi^2}{6} - \log(x) \log(1 - x) \tag{A.15}$$

and

$$\mathrm{Sp}(x) = -\mathrm{Sp}\left(\frac{1}{x}\right) - \frac{\pi^2}{6} - \frac{1}{2}\log^2(-x). \tag{A.16}$$

Appendix B

Integration Tools and Techniques

In this appendix we have collected a number of integration tools and techniques that we have referred to in the text and cross-referenced in other appendices.

B.1 The Wick rotation

The Wick Rotation is a technique used to turn four dimensional Minkowski space integrals into four dimensional Euclidean space integrals. This procedure has the effect of making coordinate transformations more transparent, and consequently simplifies the method of solution for the following class of integrals,

$$\int \frac{d^d k}{(2\pi)^d} \frac{1}{(k^2 - m^2 + i\varepsilon)^\alpha}. \tag{B.1}$$

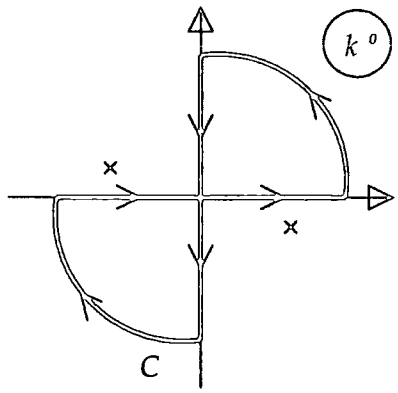

Figure B.1: The contour of integration used in performing the wick rotation. The poles are indicated by crosses and lie outside the contour.

We note the positions of potential poles in the integrand. These poles satisfy, $(k^0)^2 = \mathbf{k}^2 + m^2 - i\varepsilon$;

$$k^0 = \pm(\mathbf{k}^2 + m^2)^{\frac{1}{2}} \mp i\delta \tag{B.2}$$

($\delta \equiv \varepsilon/2\,|k^0| > 0$) and thus (see Figure B.1),

$$\oint_C dk^0 \frac{1}{(k^2 - m^2 + i\varepsilon)^\alpha} = 0 \tag{B.3}$$

hence (for a real mass m),

$$\int_\infty^\infty dk^0 \frac{1}{(k^2 - m^2 + i\varepsilon)^\alpha} = \int_{-i\infty}^{i\infty} dk^0 \frac{1}{(k^2 - m^2 + i\varepsilon)^\alpha}. \tag{B.4}$$

For a moment we define the quantity $k^{-0} \equiv ik^0$ such that

$$k^2 = -(k^{-0})^2 - \mathbf{k}^2 \equiv -\underline{k}^2 \tag{B.5}$$

(where $\underline{k}$ is an Euclidean d-vector). Changing variable from k^0 to k^{-0} we can write (B.1) as an integral over Euclidean space:

$$i\int \frac{d^d\underline{k}}{(2\pi)^d}\frac{1}{(-\underline{k}^2-m^2)^\alpha} \tag{B.6}$$

We are free to drop the $i\varepsilon$ because the potential poles do not lie close to the real (k^{-0}) axis.

In summary then, for real m,

$$\int \frac{d^dk}{(2\pi)^d}\frac{1}{(k^2-m^2+i\varepsilon)^\alpha} = i(-1)^\alpha \int \frac{d^d\underline{k}}{(2\pi)^d}\frac{1}{(\underline{k}^2+m^2)^\alpha}. \tag{B.7}$$

B.2 Dimensional regularisation

We find that the following result is very useful [16]. We consider the following integral,

$$\int \frac{d^dk}{(2\pi)^d}\frac{1}{(k^2+2k\cdot p+C+i\varepsilon)^\alpha}. \tag{B.8}$$

Completing the square and making the substitutions $q \equiv k+p$ and $a^2 \equiv p^2-C^2$ this integral takes the form,

$$\int \frac{d^dq}{(2\pi)^d}\frac{1}{(q^2-a^2+i\varepsilon)^\alpha} \tag{B.9}$$

performing a Wick Rotation (B.7) and noting that the integrand becomes symmetric about $q=0$ we separate out the radial and angular integrals;

$$\begin{aligned} & i(-1)^\alpha \int \frac{dq}{(2\pi)^d}\frac{q^{d-1}}{(q^2+a^2)^\alpha}d\Omega_{d-1} \\ \text{with,} \quad & \int d\Omega_d \equiv \int_0^{2\pi} d\theta_1 \int_0^\pi d\theta_2 \sin\theta_2 \ldots \int_0^\pi d\theta_d \sin^{d-1}\theta_d \end{aligned} \tag{B.10}$$

Using the identity (cf. Eqn. (A.9))

$$\int_0^{\frac{\pi}{2}} d\theta \sin^n \theta = B\left(\frac{1}{2}, \frac{n+1}{2}\right) = \frac{\sqrt{\pi}\Gamma(\frac{n+1}{2})}{\Gamma(\frac{n+2}{2})} \tag{B.11}$$

we have

$$\int d\Omega_d = \frac{2\pi^{\frac{d+1}{2}}}{\Gamma\left(\frac{d+1}{2}\right)} \tag{B.12}$$

and making the substitution $u \equiv q^2$ (B.8) becomes

$$\frac{i(-1)^\alpha}{(4\pi)^{\frac{d}{2}}\Gamma(\frac{d}{2})} \int_0^\infty du \frac{u^{\frac{d}{2}-1}}{(u+a^2)^\alpha} \tag{B.13}$$

Finally, we use Eqn. (A.11) to obtain the result,

$$\int \frac{d^dk}{(2\pi)^d} \frac{1}{(k^2+2k\cdot p+C+i\varepsilon)^\alpha} = i\left(\frac{-1}{4\pi}\right)^{\frac{d}{2}} \frac{\Gamma(\alpha-\frac{d}{2})}{\Gamma(\alpha)} (C-p^2)^{\frac{d}{2}-\alpha}. \tag{B.14}$$

B.3 Feynman Parameters

It is often the case in loop calculations that one must integrate over a string of denominators each of which is quadratic in the loop momentum. A favourite method for dealing with such calculations is to employ *Feynman Parameters.*

We note that (by simply integrating out x and y),

$$\frac{1}{A_1A_2} \equiv \int_0^1 dx \int_0^1 dy \frac{\delta(1-x-y)}{(xA_1+yA_2)^2}. \tag{B.15}$$

The general case, for any positive integer N, is

$$\frac{1}{A_1 A_2 \ldots A_N} \equiv \Gamma(N) \int_0^1 dx_1 \int_0^1 dx_2 \ldots \int_0^1 dx_N \frac{\delta(1 - x_1 - x_2 \ldots - x_N)}{(x_1 A_1 + x_2 A_2 + \ldots x_N A_N)^N}. \tag{B.16}$$

We can show this to be so by induction. The x_N integral is trivial giving,

$$\begin{aligned} \frac{1}{A_1 A_2 \ldots A_N} &\equiv \Gamma(N) \int_0^1 dx_1 \int_0^{1-x_1} dx_2 \ldots \int_0^{1-x_1-x_2\ldots-x_{N-2}} dx_{N-1} \\ &\times \frac{1}{(x_1(A_1 - A_N) + \ldots x_{N-1}(A_{N-1} - A_N) + A_N)^N} \end{aligned} \tag{B.17}$$

and the x_{N-1} integration is simply performed to yield

$$\begin{aligned} & \Gamma(N) \int_0^1 dx_1 \int_0^{1-x_1} dx_2 \ldots \int_0^{1-x_1-x_2\ldots-x_{N-3}} dx_{N-2} \frac{-1}{(N-1)(A_{N-1} - A_N)} \times \\ \times & \left[\frac{1}{(x_1(A_1 - A_N) + \ldots x_{N-1}(A_{N-1} - A_N) + A_N)^N - 1} \right]_0^{1-x_1-x_2\ldots-x_{N-2}} \\ = & \frac{\Gamma(N-1)}{A_{N-1} - A_N} \int_0^1 dx_1 \int_0^{1-x_1} dx_2 \ldots \int_0^{1-x_1-x_2\ldots-x_{N-3}} dx_{N-2} \times \\ \times & \left\{ + \frac{1}{(x_1(A_1 - A_N) + \ldots + x_{N-2}(A_{N-2} - A_N) + A_N)^N - 1} \right. \\ & \left. - \frac{1}{(x_1(A_1 - A_{N-1}) + \ldots + x_{N-2}(A_{N-2} - A_{N-1}) + A_{N-1})^N - 1} \right\}. \end{aligned}$$

Comparison of these two terms with the form of B.17 reveals that we may write this result as,

$$\begin{aligned} & \frac{\Gamma(N-1)}{A_{N-1} - A_N} \int_0^1 dx_1 \int_0^1 dx_2 \ldots \int_0^1 dx_{N-1} \delta(1 - x_1 - x_2 \ldots - x_{N-1}) \\ & \times \left\{ \frac{1}{(x_1 A_1 \ldots + x_{N-2} A_{N-2} + x_{N-1} A_N)^N - 1} \right. \\ & \left. - \frac{1}{(x_1 A_1 \ldots + x_{N-2} A_{N-2} + x_{N-1} A_{N-1})^N - 1} \right\}. \end{aligned}$$

In the case $N = 3$ both of these terms have the form of B.15 and this expression reduces to

$$\frac{1}{A_2 - A_3}\left\{\frac{1}{A_1 A_3} - \frac{1}{A_1 A_2}\right\} = \frac{1}{A_1 A_2 A_3} \tag{B.18}$$

and hence by induction we conclude that B.16 is true.

B.4 Form Factor Reduction

This technique is essentially a method of reducing loop integrals which possess a lorentz structure to a sum of scalar integrals with tensor coefficients.

Firstly we make some definitions, (for brevity we have made the infinitesimal transformations $m_n^2 = m_n^2 - i\varepsilon$ —see for example (D.14))

$$A_0(m_0) = \int \frac{d^d k}{(2\pi)^d} \frac{1}{k^2 - m_0^2} \tag{B.19}$$

$$B_{0;\mu;\mu\nu}(p_1, m_0, m_1) = \int \frac{d^d k}{(2\pi)^d} \frac{1; k_\mu; k_\mu k_\nu}{(k^2 - m_0^2)\left((k+p_1)^2 - m_1^2\right)} \tag{B.20}$$

$$C_{0;\mu;\mu\nu;\mu\nu\rho}(p_1, p_2, m_0, m_1, m_2) =$$

$$\int \frac{d^d k}{(2\pi)^d} \frac{1; k_\mu; k_\mu k_\nu; k_\mu k_\nu k_\rho}{(k^2 - m_0^2)\left((k+p_1)^2 - m_1^2\right)\left((k+p_1+p_2)^2 - m_2^2\right)} \tag{B.21}$$

$$D_{0;\mu;\mu\nu;\mu\nu\rho;\mu\nu\rho\sigma}(p_1, p_2, p_3, m_0, m_1, m_2, m_3) =$$

$$\int \frac{d^d k}{(2\pi)^d} \frac{1; k_\mu; k_\mu k_\nu; k_\mu k_\nu k_\rho; k_\mu k_\nu k_\rho k_\sigma}{(k^2 - m_0^2)\left((k+p_1)^2 - m_1^2\right)\left((k+p_1+p_2)^2 - m_2^2\right)\left((k+p_1+p_2+p_3)^2 - m_3^2\right)} \tag{B.22}$$

B.4.1 Reduction of the As

As indicated by the exclusion of the fermion-type tadpole integral from the above set of definitions the following integral,

$$\int \frac{d^d k}{(2\pi)^d} \frac{k_\mu}{k^2 - m_0^2} \equiv 0 \tag{B.23}$$

simply because the integrand is antisymmetric about $k = 0$.

B.4.2 Reduction of the Bs

Whilst the C case is more representative we shall first consider the B form factor reduction.

The only vector available to provide the tensor structure of B_μ is its argument momentum p_1^μ. We may write,

$$B^\mu(p_1, m_0, m_1) = p_1^\mu B_1(p_1, m_0, m_1) \tag{B.24}$$

Further if we consider the identity,

$$k \cdot p_1 \equiv \frac{1}{2}\left(\left[(k+p1)^2 - m_1^2\right] - \left[k^2 - m_0^2\right] - \left[p_1^2 - m_1^2 + m_0^2\right]\right) \tag{B.25}$$

and contract B_μ with p_1 then the result can be obtained in two ways. Firstly as $p_1^2 B_1(\ldots)$ and secondly, by canceling the denominators occurring in B_μ (B.20) against the alternative form of the contracted numerator (B.25), as

$$p_1^\mu B_\mu(p_1, m_0, m_1) = \frac{1}{2}\left(A_0(m_0) - A_0(m_1) - (p_1^2 - m_1^2 + m_0^2) B_0(p_1, m_0, m_1)\right) \tag{B.26}$$

In the case that $p_1^2 \neq 0$ we can use this observation to write B_1 in terms of the scalar integrals A_0 and B_0 (see Appendix D). Expanding $B_{\mu\nu}$;

$$B^{\mu\nu} = p_1^\mu p_1^\nu B_{22} + g^{\mu\nu} B_{20} \tag{B.27}$$

and contracting in d dimensions with $p_{1\mu}$ and $g_{\mu\nu}$ we obtain a new set of relations for B_{22} and B_{20}. A summary of the relations concerning these scalar coefficients is:

$$\begin{aligned}
B_{20}(p_1, m_0, m_1) &= \frac{1}{2(d-1)} \\
&\quad \times \Big(A_0(m_1) + 2B_0(p_1, m_0, m_1)m_0^2 + (p_1^2 + m_0^2 - m_1^2)B_1(p_1, m_0, m_1)\Big) \\
p_1^2 B_{22}(p_1, m_0, m_1) &= \frac{1}{2(d-1)} \\
&\quad \times \Big((d-2)A_0(m_1) - d(p_1^2 + m_0^2 - m_1^2)B_1(p_1, m_0, m_1) - 2m_0^2 B_0(p_1, m_0, m_1)\Big) \\
p_1^2 B_1(p_1, m_0, m_1) &= \frac{1}{2}\Big(A_0(m_0) - A0(m_1) - (p_1^2 + m_0^2 - m_1^2)B_0(p_1, m_0, m_1)\Big)
\end{aligned} \tag{B.28}$$

For massless external particles these equations become insufficient to reduce all of the Bs to B_0 and the distinction between B_0 and A_0 is blurred. A new set of relations emerges; if $m_1^2 = m_0^2$,

$$\begin{aligned}
B_1(p_1, m_0, m_0) &= -\frac{1}{2}B_0(p_1, m_0, m_0) \\
B_{20}(p_1, m_0, m_0) &= \frac{1}{2}A_0(m_0) \\
B_0(p_1, m_0, m_0) &= \frac{d-2}{2m_0^2}A_0(m_0)
\end{aligned} \tag{B.29}$$

We note that the first of these three relations also holds in the $m_0^2 = m_1^2$, $p_1^2 \neq 0$ case.

B.4.3 Reduction of the Cs and Ds

The masslessness of external particles does not affect the form factor reduction of C and higher integrals. The two simultaneous equations that arise from contraction with p_1^μ, p_2^μ, etc. and (where appropriate) $g^{\mu\nu}$ form a matrix equation, for example[1]

$$\begin{pmatrix} R_1 \\ R_2 \end{pmatrix} = \begin{pmatrix} p_1^2 & p_1 \cdot p_2 \\ p_1 \cdot p_2 & p_1^2 \end{pmatrix} \begin{pmatrix} C_{220} \\ C_{211} \end{pmatrix} \tag{B.31}$$

with,

$$\begin{aligned}
R_1 &= \frac{1}{2}\left(-2C_{200} + B_0(p_2, m_1, m_2) - \left(p_1^2 + m_0^2 - m_1^2\right) C_{110} + B_1(p_1 + p_2, m_0, m_2)\right) \\
R_2 &= -\frac{1}{2}\left(\left(p_2^2 + 2p_1 \cdot p_2 + m_1^2 - m_2^2\right) C_{110} - B_1(p_1 + p_2, m_0, m_2) + B_1(p_1, m_0, m_1)\right) \\
C_{200} &= \frac{1}{2(d-2)}\left(+\left(p_1^2 + m_0^2 - m_1^2\right) C_{110} + \left(p_2^2 + 2p_1 \cdot p_2 + m_1^2 - m_2^2\right) C_{101}\right. \\
&\quad \left. + B_0(p_2, m_1, m_2) + 2m_0^2 C_0\right)
\end{aligned}$$

Inverting the matrix we do not encounter a problem when an external invariant mass goes to zero because the inverse of the matrix (B.31) is not identically singular here. Indeed when the associated Gram determinant (see appendix A.3) goes to zero we encounter the IR poles that are dealt with by our regularisation procedure.

In a very mechanical way we can reduce each of the integrals of Eqns. (B.20 to B.22)

[1]The adopted convention for labeling the expansion coefficients associated with each tensor integral is as follows.

$$C^{\mu\nu\rho} = \ldots + C_{n\,ab} p_i{}^\mu p_j{}^\nu p_k{}^\rho + \ldots \tag{B.30}$$

where n is the number of ks appearing in the numerator of the corresponding integral, i, j and k take the values 1 or 2 and a is the number of p_1's multiplying the scalar coefficient; b is that for p_2 (this convention is also obeyed by the B_2s of the previous section—although B_1 one might argue should be written as B_{11}). For example,

$$C^{\mu\nu} = C_{220} p_1^\mu p_1^\nu + C_{202} p_2^\mu p_2^\nu + C_{211}(p_1^\mu p_2^\nu + p_2^\mu p_1^\nu) + C_{200} g^{\mu\nu}.$$

This is not the same notation as employed in Ref. [18].

down to a sum of D_0, C_0, B_0 and A_0 integrals. Using the symbolic manipulation language FORM [105] this process has been automated.

B.4.4 A note on simplifications

We note the following property of general integrals with an odd power of loop momenta in the numerator. Consider the following integral,

$$I = \int \frac{d^d k}{(2\pi)^d} \frac{k^\alpha k^\beta k^\gamma}{(k^2 - m^2)\left((k+p_1)^2 - m^2\right)}. \tag{B.32}$$

The method given above would have to be extended beyond the integrals B.20 in order to handle this form. Instead we can consider the effect of making the momentum transformation, $k \to -k - p_1$. After such a change we have,

$$I = -\int \frac{d^d k}{(2\pi)^d} \frac{(k+p_1)^\alpha (k+p_1)^\beta (k+p_1)^\gamma}{(k^2 - m^2)\left((k+p_1)^2 - m^2\right)}, \tag{B.33}$$

where the denominators have effectively swapped over and the leading term in numerator powers of k has changed sign. By taking this contribution to the left hand side we obtain an expression for $2I$ in terms of integrals with only 2 powers of k in the numerator. This technique generalises to the higher point integrals, and was used extensively in the unitary gauge calculation of Chapter 8, where there were initially 12 powers of k in some *box* numerators! It should be noted that this technique fails to work if the masses of the internal propagators of the loop differ.

Appendix C

Analytic Phase Space Integrals

For many of the calculations in this thesis it is required that we integrate over the two and three particle phase space [106] of our out going particles. The derivations of the relevant integrations in terms of invariants are presented here.

C.1 Two particle phase space

We present the $1 \to 2$ particle phase spaces for massless particles in d-dimensions and that for massive particles in 4-dimensions.

C.1.1 Massless two particle phase space in d-dimensions

The basic integral for massless out going particles is

$$\int Dlips_{1\to 2}\ldots = \int \frac{d^d p_1}{(2\pi)^d}\int \frac{d^d p_2}{(2\pi)^d}(2\pi)\delta(p_1^2)(2\pi)\delta(p_2^2)(2\pi)^d\delta^d(p_0-p_1-p_2)\ldots \qquad \text{(C.1)}$$

Where p_0 is the in going d-momentum and p_1 and p_2 are the out going d-momenta.

Performing the p_2 integral using the δ^d function, integrating over ${p_1}^0$ and rewriting the remaining $d^{d-1}p_1$ integral as a radial-angular integral we have that

$$\int Dlips_{1\to 2}\ldots = \frac{1}{(2\pi)^{d-2}}\int dE_1 E_1^{d-3} d\Omega_{d-2}\frac{\delta(p_2^2)}{2}\ldots\Big|_{p_2=p_0-p_1} \qquad \text{(C.2)}$$

where we have chosen a particular frame in which to do our integral, namely one in which $p_0^\mu = (M,0,0,\ldots)$ and E_1 is the magnitude of the energy of the out going particle.

We have that

$$p_2^2 = (p_0-p_1)^2 \equiv S_{01} = M^2 - 2ME_1 \qquad \text{i.e.} \qquad E_1 = \frac{M^2-S_{01}}{2M} \qquad \text{(C.3)}$$

and thus (see Eqn. (B.10)),

$$\int Dlips_{1\to 2}\ldots = \frac{1}{4M(2\pi)^{d-2}}\int_0^{M^2} dS_{01}\left(\frac{M^2-S_{01}}{2M}\right)^{d-3} d\Omega_{d-2}\delta(S_{01})\ldots \qquad \text{(C.4)}$$

We use the identity of Eqn. (A.5) to write (see Eqn. (B.12)),

$$\int d\Omega_{d-2} = \frac{(4\pi)^{\frac{d-2}{2}}\,\Gamma\left(\frac{d-2}{2}\right)}{\Gamma(d-2)}. \qquad \text{(C.5)}$$

In the case that the integrand $(\ldots)$ is independent of S_{01}, the integration becomes a pre-

factor, expanding about 4 *physical* dimensions $d = 4 - 2\epsilon$, it has the form,

$$\int Dlips_{1\to 2}\ldots = \frac{1}{8\pi}\frac{\Gamma(1-\epsilon)}{\Gamma(1-2\epsilon)}\left(\frac{4\pi}{M^2}\right)^{\epsilon}\frac{1}{1-2\epsilon}\ldots \tag{C.6}$$

C.1.2 Massive Particles in 4-Dimensions

For massive out-going particles the two particle phase space integral (cf. Eqn. (C.1)) generalises to

$$\begin{aligned}\int Dlips_{1\to 2}\ldots &= \int\frac{d^4p_1}{(2\pi)^d}\int\frac{d^4p_2}{(2\pi)^d}(2\pi)\delta(p_1^2-m_1^2)(2\pi)\delta(p_2^2-m_2^2)(2\pi)^d\delta^d(p_0-p_1-p_2)\ldots \\ &= \int\frac{d^4p_1}{(2\pi)^d}\int\frac{d^4p_2}{(2\pi)^d}(2\pi)\delta(p_1^2-m_1^2)(2\pi)\delta((p_0-p_1)^2-m_2^2)\ldots \end{aligned}\tag{C.7}$$

We choose the centre of mass frame to evaluate this integral, $(E > m_1)$

$$p_0 = (M,0,0,0) \qquad p_1 = (E, p\cos\theta, p\sin\theta, 0), \tag{C.8}$$

where it becomes,

$$\int Dlips_{1\to 2} = \frac{1}{(2\pi)^2}\int d\Omega_2\int_{m_1}^{\infty} dE\, dp\, p^2\,\delta(E^2-p^2-m_1^2)\delta(M^2-2ME+m_1^2-m_2^2)\ldots \tag{C.9}$$

In the case of the $2 \to 2$ process we must retain one of the angles of integration from $d\Omega_2$ to correlate the initial and final state directions. Changing the arguments to the delta functions, we obtain,

$$\int Dlips_{1\to 2} = \frac{1}{8\pi M}\int_0^{\pi} d\theta\,\sin\theta\int dE\, dp\, p\,\delta\left(p-\sqrt{E^2-m_1^2}\right)\delta\left(E-\frac{M^2+m_1^2-m_2^2}{2M}\right)\ldots \tag{C.10}$$

In the case of $1 \to 2$ the θ integral may be performed, i.e. it is replaced by a factor 2.

C.2 Three particle phase space

All of the processes involving 3 particles in the final state that are studied in this thesis are for massless ones. Accordingly we give an analytic form for the d-dimensional $1 \to 3$ phase space integral only.

C.2.1 Massless particles in d-dimensions

Having utilised a δ^d function and integrated away the d-momentum of the third particle the integral the massless three particle phase space integral takes the form,

$$\int Dlips_{1\to 3} \ldots = \int \frac{d^{d-1}p_1}{(2\pi)^d} \int \frac{d^{d-2}p_2}{(2\pi)^d} \frac{(2\pi)\delta(p_3^2)}{4E_1E_2} \ldots \Big|_{p_3=p_0-p_1-p_2} \tag{C.11}$$

(we have chosen the special frame of reference in which $p_0^\mu = (M, 0, 0, \ldots)$, $p_1^\mu = (E_1, E_1, 0, \ldots)$ and $p_2^\mu = (E_2, E_2 \cos\theta_{12}, E_2 \sin\theta_{12}, \ldots)$).

Writing this as a radial/angular integral, but singling out the angle between $\mathbf{p}_1$ and $\mathbf{p}_2$; θ_{12}, we obtain

$$\int Dlips_{1\to 3} \ldots = \frac{1}{4(2\pi)^{2d-3}} \int d\Omega_{d-2}^1 d\Omega_{d-3}^2 \int dE_1 dE_2 d\theta_{12} \left(E_1 E_2 \sin\theta_{12}\right)^{d-3} \delta(p_3^2) \tag{C.12}$$

The two solid angle integrals if evaluated become, (see Eqns. (B.12 and A.5))

$$\int d\Omega^1_{d-2} d\Omega^2_{d-3} = \frac{4\pi^{d-\frac{3}{2}}}{\Gamma\left(\frac{d-1}{2}\right)\Gamma\left(\frac{d-2}{2}\right)} = \frac{2(4\pi)^{d-2}}{\Gamma(d-2)}. \tag{C.13}$$

In order to be of use we transform the remaining integral into one over the invariants S_{12}, S_{13} and S_{13} the associated Jacobian, $\mathcal{J}$ for this change of co-ordinates satisfies, (see Eqn. (A.13))

$$\begin{aligned}(8M\mathcal{J})^{-2} &= (ME_1E_2\sin\theta_{12})^2 = \Delta(p_0,p_1,p_2) = \Delta(p_1+p_2+p_3,p_1,p_2) = \Delta(p_1,p_2,p_3) \\ &= \frac{1}{4}S_{12}S_{23}S_{13}. \end{aligned} \tag{C.14}$$

Defining $y_{ij} \equiv \frac{S_{ij}}{M^2}$ and expanding about $d = 4$ the form of the integral is

$$\begin{aligned}\int Dlips_{1\to 3}\ldots &= \frac{M^2}{128\pi^3}\frac{1}{\Gamma(1-2\epsilon)}\left(\frac{4\pi}{M^2}\right)^{2\epsilon}\frac{1}{1-2\epsilon} \\ &\times \int_0^1 dy_{12}dy_{23}dy_{13}\delta(1-y_{12}-y_{23}-y_{31})(y_{12}y_{23}y_{31})^{-\epsilon}\ldots \end{aligned} \tag{C.15}$$

Appendix D

Scalar Loop Integrals

As is shown in Section B.4 the technique of form factor reduction is in essence a method by which one may reduce complicated Lorentz *tensor* loop integrals down into a sum of more elementary *scalar* loop integrals with tensor coefficients. The following sections include the evaluation of the first four scalar loops needed in the main text, in order of increasing complexity; A_0, B_0, C_0 and a selected D_0. [22]

D.1 The Tadpole: A_0

We consider the simplest loop integral,

$$A_0(m) \equiv \int \frac{d^d k}{(2\pi)^d} \frac{1}{k^2 - m^2 + i\varepsilon} \tag{D.1}$$

which is clearly (simply counting powers of momentum) divergent in $d = 2$ and 4 dimensions. As indicated by the use of d we evaluate the loop keeping tabs on the divergences using Dimensional Regularization.

Directly from (B.14) we may write

$$A_0(m) = i\left(\frac{-1}{4\pi}\right)^{\frac{d}{2}}(-m^2)^{\frac{d}{2}-1}\frac{\Gamma(1-\frac{d}{2})}{\Gamma(1)}$$

and expanding about 4-*physical* dimensions $d = 4 - 2\epsilon$ we have that,

$$A_0(m) = \frac{im^2}{16\pi^2}\left(\frac{4\pi}{m^2}\right)^{\epsilon}\frac{\Gamma(1+\epsilon)}{\epsilon(1-\epsilon)}. \tag{D.2}$$

As a special case we observe that in the limit $m \to 0$, $A_0(m) \to 0$.

D.2 The Bubble: B_0

$$B_0(p_1, m_0, m_1) \equiv \int \frac{d^dk}{(2\pi)^d}\frac{1}{(k^2 - m_0^2 + i\varepsilon)\left((k+p_1)^2 - m_1^2 + i\varepsilon\right)} \tag{D.3}$$

This integral is logarithmically divergent in $d = 4$ dimensions. To calculate it we use Feynman parameters (Section B.3) to re-write the integral in the form of (B.8).

$$\begin{aligned} B_0(p_1, m_0, m_1) &= \int \frac{d^dk}{(2\pi)^d}\Gamma(2)\int_0^1 dx\int_0^1 dy\,\delta(1-x-y) \\ &\times \frac{1}{\left(x(k^2 - m_0^2 + i\varepsilon) + y(k^2 + 2k\cdot p_1 + p_1^2 - m_1^2 + i\varepsilon)\right)^2}. \end{aligned}$$

Performing the trivial x integration we obtain,

$$\Gamma(2)\int_0^1 dy \int \frac{d^dk}{(2\pi)^d}\frac{1}{(k^2+2k\cdot p_1 y + y(p_1^2+m_0^2-m_1^2)-m_0^2+i\varepsilon)^2}$$

Following the discussion in Section B.2 and substituting into (B.14) we perform the integral over k to obtain,

$$B_0(p_1,m_0,m_1) = i\,\Gamma\left(\frac{4-d}{2}\right)\left(\frac{-1}{4\pi}\right)^{\frac{d}{2}}\int_0^1 dy\left(y(p_1^2+m_0^2-m_1^2)-m_0^2-y^2p_1^2+i\varepsilon\right)^{\frac{d-4}{2}}$$

and expressing in terms of ϵ ($d \equiv 4-2\epsilon$) this may be written

$$B_0(p_1,m_0,m_1) = i\,\Gamma(\epsilon)\left(\frac{-1}{4\pi}\right)^{2-\epsilon}\int_0^1 dy\left(y(p_1^2+m_0^2-m_1^2)-m_0^2-y^2p_1^2+i\varepsilon\right)^{-\epsilon}. \qquad \text{(D.4)}$$

D.2.1 Massless internal particles

We consider the $m_0^2 = m_1^2 = 0$ limit of Eqn. (D.4). When $p_1^2 \neq 0$ (D.4) becomes,

$$\begin{aligned} B_0(p_1,0,0) &= i\,\Gamma(\epsilon)\left(\frac{-1}{4\pi}\right)^{2-\epsilon}(p_1^2)^{-\epsilon}\int_0^1 dy\,(y(1-y))^{-\epsilon} \\ &= i\left(\frac{-1}{4\pi}\right)^{2-\epsilon}(p_1^2)^{-\epsilon}\Gamma(\epsilon)B(1-\epsilon,1-\epsilon) \\ &= i\left(\frac{1}{4\pi}\right)^2\frac{\Gamma(1+\epsilon)\Gamma^2(1-\epsilon)}{\Gamma(1-2\epsilon)}\frac{1}{\epsilon(1-2\epsilon)}\left(\frac{-4\pi}{p_1^2}\right)^{\epsilon} \end{aligned} \qquad \text{(D.5)}$$

In the case that $p_1^2 = 0$ it is not immediately apparent what the value of this integral is. Considering the associated integral we have,

$$B_0(p_1) = \int \frac{d^dk}{(2\pi)^d}\frac{1}{k^2\,(k+p_1)^2} = \int \frac{d^dk}{(2\pi)^d}\frac{1}{(k-a)^2\,(k+a)^2}$$

where we have made a change of variable $k = k - a$ with $a = \frac{1}{2}p_1$. Using partial fractions this may be written,

$$B_0(p_1) = \int \frac{d^d k}{(2\pi)^d} \frac{1}{(4\, k \cdot a)} \left(\frac{1}{(k-a)^2} - \frac{1}{(k+a)^2} \right)$$

and since, for any λ, $(k + \lambda a) \cdot a = k \cdot a$ we find that both of these integrands become anti-symmetric about $k = 0$. In summary, for $p_1^2 = 0$, $B_0(p_1, 0, 0) = 0$ in dimensional regularization. When we compare this result with (D.5) we see that have made the statement that $(0)^{-\epsilon} \equiv 0$.

D.2.2 Equal Mass Internal Particles

For the case of equally massive internal fields we return to Eqn. (D.4) and make the simplification $m_0^2 = m_1^2 = m^2$. In this limit,

$$B_0(p_1, m, m) = \frac{i}{16\pi^2} \left(\frac{4\pi}{m^2} \right)^{\epsilon} \Gamma(1+\epsilon) \frac{\mathcal{I}_\epsilon}{\epsilon} \tag{D.6}$$

where $\mathcal{I}_\epsilon = \int_0^1 dy (f(y))^{-\epsilon}$

$$\text{for} \quad f(y) = y^2 \frac{p_1^2}{m^2} - y \frac{p_1^2}{m^2} + 1 - i\epsilon \tag{D.7}$$

$$= \frac{p_1^2}{m^2}(y - y_+)(y - y_-) \tag{D.8}$$

$$\text{with} \quad y_\pm = \frac{1}{2}\left(1 \pm \sqrt{1 - \frac{4m^2}{p_1^2} + i\varepsilon} \right) \tag{D.9}$$

Note, that the $i\varepsilon$ term fixes the sign of the imaginary part of the square root for $y_\pm$ to be $\pm ve$. Expanding to $\mathcal{O}(\epsilon^2)$ and performing the integrations we obtain the following result,

$$\mathcal{I}_\epsilon = 1 + \epsilon\left[2 + y_+ \log\left(\frac{1-y_+}{-y_+}\right) + y_- \log\left(\frac{1-y_-}{-y_-}\right)\right] + \mathcal{O}(\epsilon^2). \tag{D.10}$$

We can consider each of the physical regions for $\mathcal{I}_\epsilon$ with respect to the invariant mass squared, p_1^2, of the external particle, being careful to analytically continue where necessary. In terms of the *positive* quantity, $x = |1 - \frac{4m^2}{p_1^2}|^{1/2}$, $\mathcal{I}_\epsilon$ is as follows:

$$p_1^2 < 0 \ \ (x > 1) \qquad \mathcal{I}_\epsilon = 1 + \epsilon\left\{2 + x \log\left(\frac{x-1}{x+1}\right)\right\} + \mathcal{O}(\epsilon^2) \tag{D.11}$$

$$0 < p_1^2 < 4m^2 \ \ (\infty > x > 0) \qquad \mathcal{I}_\epsilon = 1 + \epsilon\left\{2 - x\left(\pi - 2\tan^{-1} x\right)\right\} + \mathcal{O}(\epsilon^2) \tag{D.12}$$

$$4m^2 < p_1^2 < \infty \ \ (0 < x < 1) \qquad \mathcal{I}_\epsilon = 1 + \epsilon\left\{2 + x \log\left(\frac{1-x}{1+x}\right) + i\pi x\right\} + \mathcal{O}(\epsilon^2). \tag{D.13}$$

The quantity $\mathcal{J} = (\mathcal{I}_\epsilon - 1)/\epsilon$, is the finite correction to the divergence of $B_0(p_1, m, m)$.

D.3 The Triangle: C_0

$$C_0(p_1, p_2, m_0, m_1, m_2) \equiv \int \frac{d^d k}{(2\pi)^d} \times \frac{1}{(k^2 - m_0^2 + i\varepsilon)\left((k+p_1)^2 - m_1^2 + i\varepsilon\right)\left((k+p_1+p_2)^2 - m_2^2 + i\varepsilon\right)} \tag{D.14}$$

This integral is not ultra-violet divergent in $d = 4$ dimensions however we evaluate it in $4 - 2\epsilon$ dimensions as before in order to account for the infra-red divergences associated with the soft limit of the loop integration. As before we use Feynman parameters to re-write this

integral in a more straight forward way;

$$
\begin{aligned}
C_0(p_1,p_2,m_0,m_1,m_2) &= \int \frac{d^dk}{(2\pi)^d}\Gamma(3)\int_0^1 dx\int_0^1 dy\int_0^1 dz\delta(1-x-y-z) \\
&\times \frac{1}{\left(x\left(k^2-m_0^2+i\varepsilon\right)+y\left((k+p_1)^2-m_1^2+i\varepsilon\right)+z\left((k+p_1+p_2)^2-m_2^2+i\varepsilon\right)\right)^3} \\
&= \Gamma(3)\int_0^1 dy\int_0^{1-y} dz\int \frac{d^dk}{(2\pi)^d} \\
&\frac{1}{\left(k^2+2k\cdot(p_1y+(p_1+p_2)z)+y\left(p_1^2+m_0^2-m_1^2\right)+z\left((p_1+p_2)^2+m_0^2-m_2^2\right)-m_0^2+i\varepsilon'\right)^3}
\end{aligned}
$$

and then substituting into equation (B.14) we obtain,

$$
\begin{aligned}
C_0(p_1,p_2,m_0,m_1,m_2) &= i\left(\frac{-1}{4\pi}\right)^{\frac{d}{2}}\Gamma\left(3-\frac{d}{2}\right)\int_0^1 dy\int_0^{1-y} dz \\
&\times\left(y\left(p_1^2+m_0^2-m_1^2\right)+z\left((p_1+p_2)^2+m_0^2-m_2^2\right)-m_0^2-(p_1y+(p_1+p_2)z)^2\right)^{\frac{d}{2}-3} \\
&= i\left(\frac{1}{4\pi}\right)^2\Gamma(1+\epsilon)(-4\pi)^\epsilon\int_0^1 dy\int_0^{1-y} dz \\
&\times\left(y\left(p_1^2+m_0^2-m_1^2\right)+z\left((p_1+p_2)^2+m_0^2-m_2^2\right)-m_0^2-(p_1y+(p_1+p_2)z)^2\right)^{-(1+\epsilon)}
\end{aligned}
$$

D.3.1 Massless internal particles

We give the case for $p_1^2=p_2^2=m_0^2=m_1^2=m_2^2=0$. In this limit we have,

$$
\begin{aligned}
&C_0(p_1,p_2,0,0,0) = \\
&\quad i\left(\frac{1}{4\pi}\right)^2\Gamma(1+\epsilon)(-4\pi)^\epsilon(2p_1\cdot p_2)^{-(1+\epsilon)}\int_0^1 dy\int_0^{1-y} dz\left((1-y-z)z\right)^{-(1+\epsilon)}
\end{aligned}
$$

making the change of variable to $x=z/(1-y)$ and the double integral becomes

$$
\ldots\int_0^1 dy\int_0^1 dx(1-y)\left((1-y)^2(1-x)x\right)^{-(1+\epsilon)} =
$$

$$\ldots \int_0^1 dy(1-y)^{-1-2\epsilon} \int_0^1 dx\,((1-x)x)^{-(1+\epsilon)} \;=\; B\,(1,-2\epsilon)\,B\,(-\epsilon,-\epsilon)\,,$$

where B is the Beta function satisfying Eqn. (A.10). Hence we obtain,

$$C_0(p_1,p_2,0,0,0) = i\left(\frac{1}{4\pi}\right)^2 \frac{1}{2p_1\cdot p_2}\frac{\Gamma(1+\epsilon)\Gamma^2(1-\epsilon)}{\Gamma(1-2\epsilon)}\frac{1}{\epsilon^2}\left(\frac{-4\pi}{2p_1\cdot p_2}\right)^{\epsilon}. \tag{D.15}$$

D.3.2 Constant internal masses

We consider Eqn. (D.14) in the limit, $p_1^2 = p_2^2 = 0$ and $m_0 = m_1 = m_2 = m$. This function is finite in four-dimensions so we evaluate it straightforwardly,

$$\begin{aligned} C_0(p_1,p_2,m,m,m) &= \frac{i}{16\pi^2}\int_0^1 \frac{dx}{sx}\,\log\left(1-i\epsilon-\frac{s}{m^2}x(1-x)\right) \\ &= \frac{i}{16\pi^2}\frac{1}{2s}\left[\log\left(\frac{-z}{1-z}\right)\right]^2, \end{aligned} \tag{D.16}$$

where $s=(p_1+p_2)^2$ and,

$$z = \frac{1}{2}\left(1+\sqrt{1-\frac{4m^2}{s}+i\epsilon}\right). \tag{D.17}$$

D.4 The Box: D_0

Finally there is the four-point function with three massless and one massive external line, $p_1^2 = p_2^2 = p_3^2 = 0$, $p_4^2 = M_Z^2$ and an internal mass m, (we suppress the $i\varepsilon$ on the first line)

$$D_0(p_1,p_2,p_3,m,m,m,m) \;=\; \int \frac{d^4q}{(2\pi)^4}\frac{1}{(q^2-m^2)((q+p_1)^2-m^2)((q+p_1+p_2)^2-m^2)((q-p_4)^2-m^2)}$$

$$= i\pi^2 \frac{1}{st} \int_0^1 \frac{dx}{x(1-x) + m^2 u/ts} \Bigg\{ - \log\left(1 - i\varepsilon - \frac{M_Z^2}{m^2} x(1-x)\right)$$
$$+ \log\left(1 - i\varepsilon - \frac{s}{m^2} x(1-x)\right) + \log\left(1 - i\varepsilon - \frac{t}{m^2} x(1-x)\right) \Bigg\}, \tag{D.18}$$

for $s = (p_1 + p_2)^2$, $t = (p_2 + p_3)^2$ and $u = (p_3 + p_1)^2$.

This result can be expressed in terms of Spence functions (see Eqn. (A.14)) via the relation,

$$\int_0^1 \frac{dx}{x(1-x) + m^2 u/ts} \log\left(1 - i\varepsilon - \frac{v}{m_f^2} x(1-x)\right)$$
$$= \frac{2}{\sqrt{1 + 4m^2 u/ts}} \Bigg\{ \mathrm{Sp}\left(\frac{x_-}{x_- - y}\right) - \mathrm{Sp}\left(\frac{x_+}{x_+ - y}\right) + \mathrm{Sp}\left(\frac{x_-}{y - x_+}\right) - \mathrm{Sp}\left(\frac{x_+}{y - x_-}\right)$$
$$- \log\left(\frac{-x_-}{x_+}\right) \log\left(1 - i\varepsilon + \frac{vu}{st}\right) \Bigg\}, \tag{D.19}$$

where,

$$x_\pm = \frac{1}{2}\left(1 \pm \sqrt{1 + 4m^2 u/ts}\,\right), \tag{D.20}$$

and,

$$y = \frac{1}{2}\left(1 + \sqrt{1 - 4(m^2 - i\varepsilon)/v}\,\right). \tag{D.21}$$

Appendix E

Dirac Algebra

E.1 The γ Matrix

The ubiquitous γ matrix is defined by the following two relations,

$$\{\gamma_\mu, \gamma_\nu\} = 2g_{\mu\nu} \tag{E.1}$$

and the hermiticity condition,

$$\gamma^{\mu\dagger} = \gamma^0\gamma^\mu\gamma^0. \tag{E.2}$$

Along with the definition there are a number of conventional constructions that are

referenced throughout the text of this thesis, these are,

$$\sigma_{\mu\nu} = \frac{i}{2}[\gamma_\mu, \gamma_\nu] \tag{E.3}$$

and

$$\gamma_5 = \frac{i}{4!}\epsilon^{\alpha\beta\gamma\delta}\gamma_\alpha\gamma_\beta\gamma_\gamma\gamma_\delta = i\gamma^0\gamma^1\gamma^2\gamma^3 = \gamma_5^\dagger = \gamma^5. \tag{E.4}$$

Further, we frequently use the *Feynman slash* notation,

$$\not{p} = p\cdot\gamma = p^\mu\gamma_\mu \tag{E.5}$$

From these definitions we have the following relations: we list them (where they do not involve γ_5) for d space-time dimensions and also the conventional $d \to 4$ limit.

	d	$d \to 4$
$\gamma^\mu\gamma_\mu$	d	4
$\gamma^\mu\gamma^\alpha\gamma_\mu$	$(2-d)\gamma^\alpha$	$-2\gamma^\alpha$
$\gamma^\mu\gamma^\alpha\gamma^\beta\gamma_\mu$	$4g^{\alpha\beta} - (d-4)\gamma^\alpha\gamma^\beta$	$4g^{\alpha\beta}$
$\gamma^\mu\gamma^\alpha\gamma^\beta\gamma^\gamma\gamma_\mu$	$-2\gamma^\gamma\gamma^\beta\gamma^\alpha + (d-4)\gamma^\alpha\gamma^\beta\gamma^\gamma$	$-2\gamma^\gamma\gamma^\beta\gamma^\alpha$
$\gamma_5\gamma_5$		1
$[\gamma_5, \gamma^\nu]$		0

(E.6)

All Dirac fermion calculations at some level require a trace to be taken over the implicit spinor indices of a string of γ matrices. As for the above table, we give the following results in d dimensions, where we take the dimension for the representation of the gamma matrix to be d.

$\mathrm{Tr}\{\ldots\}$	d	$d=4$
(odd number of γ's)	0	0
$\gamma^\alpha\gamma^\beta$	$dg^{\mu\nu}$	$4g^{\mu\nu}$
$\gamma^\alpha\gamma^\beta\gamma^\gamma\gamma^\delta$	$d\left(g^{\alpha\beta}g^{\gamma\delta}-g^{\alpha\gamma}g^{\beta\delta}+g^{\alpha\beta}g^{\gamma\delta}\right)$	$4\left(g^{\alpha\beta}g^{\gamma\delta}-g^{\alpha\gamma}g^{\beta\delta}+g^{\alpha\beta}g^{\gamma\delta}\right)$
γ_5		0
$\gamma_5\gamma^\alpha\gamma^\beta$		0
$\gamma_5\gamma^\alpha\gamma^\beta\gamma^\gamma\gamma^\delta$		$-4i\epsilon^{\alpha\beta\gamma\delta}$

(E.7)

E.2 The Dirac Equation

The γ-matrix finds its place in high energy formalism through its defining role in the *Dirac Equation*, a relativistic equation for the fermionic wave function [3]. That is to say, free Dirac fermion sates, $|\psi,p\rangle$, obey

$$\left(\hat{\not{p}}-m\right)|\psi,p\rangle=0. \tag{E.8}$$

The observation that such states are on-shell or,

$$\hat{\not{p}}\hat{\not{p}}|\psi,p\rangle=m^2|\psi,p\rangle, \tag{E.9}$$

leads to the definition of γ; Eqn. (E.1). We can expand the *field* operator associated with such states, $\hat{\Psi}$, as a sum over creation and annihilation operators (cf. Eqn. (2.13))

$$\hat{\Psi}(x)=\int\frac{d^4k}{(2\pi)^4}\theta(k^0)\sum_j\left\{e^{-ik\cdot x}\hat{a}_j(k)u_j(k)+e^{ik\cdot x}\hat{b}_j^\dagger(k)v_j(k)\right\}. \tag{E.10}$$

Here, $\hat{a}_j$ $\hat{b}_j^\dagger$ obey *fermionic* statistics, and the *spinors* u_i and v_i define the polarisations of the fermion states. In coordinate space, where $\hat{p_\mu} \rightarrow i\partial_\mu$ the free *field* Dirac Equation is,

$$\left(i\partial\!\!\!/ - m\right)\hat{\Psi}(x) = 0 \tag{E.11}$$

which follows from a Lagrangian term of the form $\hat{\overline{\Psi}}\left(i\partial\!\!\!/ - m\right)\hat{\Psi}$. In terms of the fourier components,

$$\begin{aligned} \left(p\!\!\!/ - m\right)u_j(p)e^{-ip\cdot x}a_j &= 0 \qquad \text{(E.12)} \\ -\left(p\!\!\!/ + m\right)v_j(p)e^{ip\cdot x}b_j^\dagger &= 0. \qquad \text{(E.13)} \end{aligned}$$

With respect to the hermiticity condition of Eqn. (E.2), the hermitian conjugate of these equations in terms of the adjoint field, $\hat{\overline{\Psi}} = \hat{\Psi}^\dagger\gamma^0$, combines with the above to give the following spinor properties,

$$\begin{aligned} \left(p\!\!\!/ - m\right)u_j(p) = \;\; 0 \;\; &= \left(p\!\!\!/ + m\right)v_j(p) \\ \overline{u_j}(p)\left(p\!\!\!/ - m\right) = \;\; 0 \;\; &= \overline{v_j}(p)\left(p\!\!\!/ + m\right). \end{aligned} \tag{E.14}$$

We shall take the normalisation of the spinors to be that defined by,

$$\frac{1}{2m}\overline{u_i}(p)u_j(p) = \delta_{ij} \qquad \text{and} \qquad \frac{1}{2m}\overline{v_i}(p)v_j(p) = -\delta_{ij}, \tag{E.15}$$

where $p^2 = m^2$.

For the summed u spinors in the reverse order, we find that multiplication on the left or right by the operator $(p\!\!\!/ - m)$ must yield zero. This leads to, $\sum_j u_j(p)\overline{u_j} \propto (p\!\!\!/ + m)$. From the

normalisation condition above (and a similar argument for the vs) we obtain the following,

$$\sum_j u_j(p)\overline{u_j}(p) = (\not{p} + m) \qquad \sum_j v_j(p)\overline{v_j}(p) = (\not{p} - m) \tag{E.16}$$

E.3 Coupling Fermions to a Gauge Field

The coupling of a Gauge field, $\hat{A}_\mu$, to a fermionic field is enabled by the replacement of the ∂_μ with the Gauge covariant derivative Eqn. (2.29). The coupled Dirac Equation is thus,

$$\left(i\hat{\not{D}}_\mu - m\right)\hat{\Psi}(x) = \left(i\not{\partial}_\mu - g\hat{\not{A}}_\mu(x) - m\right)\hat{\Psi}(x). \tag{E.17}$$

This leads to the Feynman rule for a fermion-gauge vertex of the general form $-igT^a$, where T^a are the structure constants of the group. Note, that mass terms for a gauge field are gauge invariant, unlike those for the gauge field itself.

E.4 Chiral Fermions

We define the *left* and *right*-handed projection operators,

$$\Lambda_L = \frac{1-\gamma_5}{2} \quad \text{and} \quad \Lambda_R = \frac{1+\gamma_5}{2}. \tag{E.18}$$

With respect to these projection operators ($\Lambda_L\Lambda_L = \Lambda_L$), we define the left and right handed spinors[1],

$$\left.\begin{array}{rcl} u_L &=& \Lambda_L u \\ u_R &=& \Lambda_R u \end{array}\right\} u_L + u_R = u \left\{\begin{array}{rcl} \overline{u_L} &=& \overline{u}\Lambda_R \\ \overline{u_R} &=& \overline{u}\Lambda_L \end{array}\right\}. \tag{E.19}$$

The following *currents* can be written with respect to these component spinors as,

$$\begin{array}{lrcl} \text{scalar:} & \overline{u}u & = & \overline{u_L}u_R + \overline{u_R}u_L \\ \text{pseudo-scalar:} & \overline{u}\gamma_5 u & = & \overline{u_L}\gamma_5 u_R - \overline{u_R}\gamma_5 u_L \\ \text{vector:} & \overline{u}\gamma^\mu u & = & \overline{u_L}\gamma^\mu u_L + \overline{u_R}\gamma^\mu u_R \\ \text{axial-vector:} & \overline{u}\gamma^\mu\gamma_5 u & = & -\overline{u_L}\gamma^\mu\gamma_5 u_L + \overline{u_R}\gamma^\mu\gamma_5 u_R. \end{array} \tag{E.20}$$

From this list we see that the Lagrangian terms that give mass to the fermions are like *chirality-mixing* vertices.

[1] For the remainder of this section the u will stand for either u or v.

Appendix F

Algebra for $SU(2)$ and $SU(3)$

The three gauge groups of the Standard Model are $U(1)$, $SU(2)$ and $SU(3)$. The first of these is an abelian group corresponding to a simple phase symmetry of the Lagrangian fields. The remaining two groups constitute more complex *internal* symmetries of the Standard model Lagrangian.

We note that the number of generators required for the $SU(N)$ groups is $(N^2 - 1)$. In this appendix we review some useful results for these algebras.

F.1 $SU(2)$

The structure constants for the generators of the $SU(2)$ symmetry group are $f^{abc} = \epsilon^{abc}$ so, with reference to Eqn. (2.27), we find that the *Pauli Matrices*, $\tau_i/2$, form a suitable

representation for the generators of this group.

The Pauli Matrices are defined to be hermitian and are as follows,

$$\tau_1 = \begin{pmatrix} 0 & 1 \\ 1 & 0 \end{pmatrix} \quad \tau_2 = \begin{pmatrix} 0 & -i \\ i & 0 \end{pmatrix} \quad \tau_3 = \begin{pmatrix} 1 & 0 \\ 0 & -1 \end{pmatrix}. \tag{F.1}$$

They satisfy the following relation,

$$[\tau_i, \tau_j] = 2i\epsilon_{ijk}\tau_k \tag{F.2}$$

which is sufficient to ensure that $\tau_i/2$ is a generator for $SU(2)$. They also satisfy the following *anti-commutator* relation,

$$\{\tau_i, \tau_j\} = 2\delta_{ij}. \tag{F.3}$$

Combining these two relations we obtain the following useful result,

$$\tau_i\tau_j = i\epsilon_{ijk}\tau_k + \delta_{ij}. \tag{F.4}$$

F.2 $SU(3)$

The algebra of $SU(3)$ is more complex than that of $SU(2)$ it contains 8 instead of 3 generators. It remains an un-broken symmetry of the fields of the Standard Model so it is not necessary to write out an explicit representation for it. Instead, we shall consider some general arguments for fundamental generators of arbitrary groups and use only the dimension of the group as a parameter.

The defining equation for a group is Eqn. (2.27):

$$\left[T^a, T^b\right] = if^{abc}T^c.$$

The normalisation of the fundamental representation (hermitian, $N \times N$ matrices) of this group is given by,

$$\mathrm{Tr}\{T^aT^b\} = \frac{1}{2}\delta^{ab}. \tag{F.5}$$

These two relations are sufficient to calculate the effect of the group structure of $SU(N)$ in all Feynman diagrams. It is conventional to compute *colour factors* for such diagrams: these correspond to an overall factor to accompany the *lorentz* structure associated with general fermions and general gauge bosons.

The members of the $SU(n)$ group have unit determinant from which we can deduce the tracelessness of the generators;

$$\det\left(e^{i\theta^aT^a}\right) = 1 + i\theta^a\mathrm{Tr}\left\{T^a\right\} + \mathcal{O}(\theta^{a\,2}) = 1 \qquad \Rightarrow \mathrm{Tr}\{T^a\} = 0. \tag{F.6}$$

Now, we consider the general form of the product of two identical Ts,

$$T^a_{ij}T^a_{kl} = \alpha\delta_{ij}\delta_{kl} + \beta\delta_{il}\delta_{jk} \tag{F.7}$$

where α and β are to be determined and we implicitly sum over the index a. We exclude the $\delta_{ik}\delta_{jl}$ term from this sum because the first and second indices on T^a_{ij} are *not* interchangeable; they correspond to colour and anti-colour. The neglect of this term simply expresses colour conservation at each vertex, and hence throughout all Feynman diagrams.

Contracting the indices (ij) and using Eqn. (F.6) we obtain,

$$0 = (\alpha N + \beta)\delta_{kl} \qquad \Rightarrow \alpha = -\frac{\beta}{N}. \tag{F.8}$$

Contracting instead the indices (il) and (jk) we obtain $\delta^{ab}\times$ Eqn. (F.5), and in terms of β,

$$-\frac{\beta}{N}N + \beta N^2 = \frac{N^2-1}{2} \qquad \Rightarrow \beta = \frac{1}{2}. \tag{F.9}$$

Thus, we can write Eqn. (F.7) as follows,

$$T^a_{ij}T^a_{kl} = \frac{1}{2}\left\{\delta_{il}\delta_{jk} - \frac{1}{N}\delta_{ij}\delta_{kl}\right\}. \tag{F.10}$$

We can represent the structure constants f^{abc} in terms of the generators too. Multiplying Eqn. (2.27) on the right by T^d we obtain,

$$\left[T^a, T^b\right] T^d = i f^{abc} T^c T^d \tag{F.11}$$

and taking the trace of this expression (with respect to Eqn. (F.5)) we find,

$$f^{abc} = -2i\mathrm{Tr}\left\{\left[T^a, T^b\right] T^c\right\}. \tag{F.12}$$

Relations Eqns. (F.10 and F.12) are sufficient to compute any colour factor, either partially where the free indices are given in terms of the generator indices, a for external gluons, and i for external quarks, or *completely* as for the cases of fully contracted *squared* amplitudes. The terms resulting from the former application of these rules is often termed a *colour decomposition.* It has proved very useful as a tool to break up *large* QCD calculations into

smaller, gauge invariant, sub-amplitudes that can be evaluated more readily. [93, 83]

To keep track of the many indices in the application of these two rules it is both convenient and efficient to represent the two equations in the form of diagrams—this is in the spirit of Feynman diagrams, but rather than as an aide to writing down a colour structure they can be used to *evaluate* a colour factor.

The basic diagram unit is

$T^a_{ij} =$ 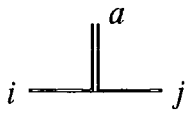

which is an angularly ordered unit. With respect to this unit the relation, Eqn. (F.10), can be written,

$T^a_{ij}T^a_{kl} =$ 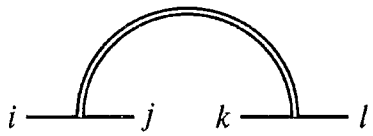

$=$ $\frac{1}{2}\{$ 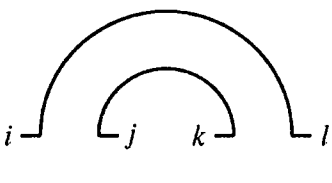

$\frac{-1}{N}$ 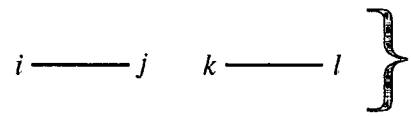

$\}$

We give an example of using this diagrammatic algebra to evaluate the colour factor associated with the virtual correction to the hadronic branching ratio in Figure 4.10b. The

appropriate diagram is as follows,

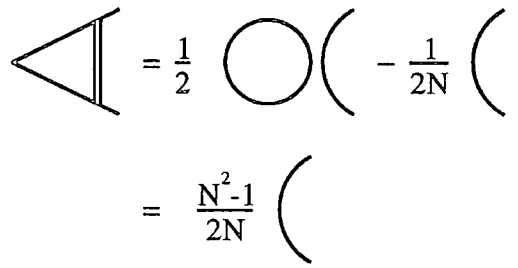

which in terms of the $SU(3)$ generators (a closed loop evaluates to N) is,

$$T^a_{ik}T^a_{kj} = \frac{N^2-1}{2N}\delta_{ij}. \tag{F.13}$$

The structure constants in this diagrammatic representation have the form,